NASA TECHNICAL NOTE

NASA TN D-7149

NASA TN D-7149

WIND-TUNNEL INVESTIGATION OF STATIC LONGITUDINAL AND LATERAL CHARACTERISTICS OF A FULL-SCALE MOCKUP OF A LIGHT SINGLE-ENGINE HIGH-WING AIRPLANE

by

H. Douglas Greer, James P. Shivers, Marvin P. Fink
Langley Research Center

and

C. Robert Carter
Langley Directorate,
U.S. Army Air Mobility R&D Laboratory

NATIONAL AERONAUTICS AND SPACE ADMINISTRATION • WASHINGTON, D. C. • MAY 1973

1. Report No.	2. Government Accession No.	3. Recipient's Catalog No.
NASA TN D-7149		

4. Title and Subtitle	5. Report Date
WIND-TUNNEL INVESTIGATION OF STATIC LONGITUDINAL AND LATERAL CHARACTERISTICS OF A FULL-SCALE MOCKUP OF A LIGHT SINGLE-ENGINE HIGH-WING AIRPLANE	May 1973
	6. Performing Organization Code
7. Author(s) H. Douglas Greer, James P. Shivers, Marvin P. Fink, Langley Research Center; and C. Robert Carter, Langley Directorate, U.S. Army Air Mobility R&D Laboratory	8. Performing Organization Report No. L-8682
	10. Work Unit No. 760-60-01-16
9. Performing Organization Name and Address NASA Langley Research Center Hampton, Va. 23365	11. Contract or Grant No.
	13. Type of Report and Period Covered Technical Note
12. Sponsoring Agency Name and Address National Aeronautics and Space Administration Washington, D.C. 20546	14. Sponsoring Agency Code

15. Supplementary Notes

16. Abstract

The model was a full-scale mockup of a light single-engine high-wing monoplane. Tests were made over an angle-of-attack range of -4° to 24° and over a sideslip range of $\pm 8^{\circ}$ at thrust coefficients of 0, 0.14, and 0.30. Control effectiveness and hinge moments were taken on the aileron, elevator, and rudder for a full range of deflections. Downwash measurements at the tail were obtained for the range of thrust coefficient and flap deflection.

17. Key Words (Suggested by Author(s))	18. Distribution Statement
Light single-engine high-wing airplane Stability and control Tail downwash Hinge moments	Unclassified – Unlimited

19. Security Classif. (of this report)	20. Security Classif. (of this page)	21. No. of Pages	22. Price*
Unclassified	Unclassified	157	$3.00

*For sale by the National Technical Information Service, Springfield, Virginia 22151

WIND-TUNNEL INVESTIGATION OF STATIC LONGITUDINAL AND LATERAL CHARACTERISTICS OF A FULL-SCALE MOCKUP OF A LIGHT SINGLE-ENGINE HIGH-WING AIRPLANE

By H. Douglas Greer, James P. Shivers, Marvin P. Fink,
Langley Research Center

and C. Robert Carter
Langley Directorate, U.S. Army Air Mobility R&D Laboratory

SUMMARY

A force-test investigation has been conducted in the Langley full-scale tunnel to determine the static longitudinal and lateral stability and control characteristics of a full-scale mockup of a light single-engine high-wing airplane. Hinge moments were measured on all control surfaces during the investigation and downwash surveys were made at the horizontal tail. The investigation was made over an angle-of-attack range of -4° to 24° at various angles of sideslip between $\pm 8^{\circ}$ for various power and flap settings. The power conditions were a thrust coefficient T_c' of zero which represents either a low-power or a high-speed condition (where the thrust coefficient approaches zero), $T_c' = 0.14$ which corresponds to a climb condition, and $T_c' = 0.30$ which corresponds to a take-off condition.

The investigation showed that the model has both stick-fixed and stick-free longitudinal stability up to the stall for all configurations tested with the center of gravity located at 13.7 percent of the mean geometric chord. Power generally has a small destabilizing effect, but at worst the model could become no more than neutrally stable with the center of gravity as far aft as 40 percent of the mean geometric chord. The model has positive effective dihedral and directional stability for all test conditions. The aileron and rudder effectiveness was maintained up to the stall and was powerful enough to trim out all model moments up to the stall.

INTRODUCTION

The Langley Research Center has been conducting a program to document the aerodynamic characteristics of a number of general-aviation type aircraft. Full-scale mockups of two single-engine low-wing airplanes, two twin-engine low-wing airplanes, and one low-wing general research model which had several nacelle configurations and modes of

propeller rotation have been tested in the Langley full-scale tunnel and the results have been reported in references 1 to 5. The present investigation was conducted to determine the static longitudinal and lateral stability and control characteristics of a mockup of a light single-engine high-wing airplane. The present tests were made with various power and flap settings over a range of angles of attack from -4° to 24° and over a range of sideslip angles of $\pm 8^{\circ}$. The tests at thrust coefficients of 0 and 0.14 were made at a tunnel speed of about 27.4 m/sec (90 ft/sec) giving a Reynolds number of about 2.8×10^6. The tests at a thrust coefficient of 0.30 were made at 22.8 m/sec (75 ft/sec) giving a Reynolds number of about 2.3×10^6. The Reynolds number is based on a mean geometric chord of 1.50 m (4.91 ft).

SYMBOLS

Figure 1 shows the stability-axis system used in the presentation of the data and the positive direction of forces, moments, and angles. The data are computed about the moment center shown in figure 2 which is at 13.7 percent of the mean geometric chord.

Values are given in both SI and U.S. Customary Units. Measurements and calculations were made in U.S. Customary Units.

b	wing span, 11.20 m (36.75 ft)
C_D	drag coefficient, $\frac{\text{Drag}}{qS}$
$C_{h,a}$	aileron hinge-moment coefficient, $\frac{\text{Hinge moment}}{qS_a\bar{c}_a}$
$C_{h,e}$	elevator hinge-moment coefficient, $\frac{\text{Hinge moment}}{qS_e\bar{c}_e}$
$C_{h,r}$	rudder hinge-moment coefficient, $\frac{\text{Hinge moment}}{qS_r\bar{c}_r}$
C_L	lift coefficient, $\frac{\text{Lift}}{qS}$
C_{L_α}	lift-curve slope
C_l	rolling-moment coefficient, $\frac{\text{Rolling moment}}{qSb}$

C_{l_β} effective-dihedral parameter, $\partial C_l/\partial\beta$, per deg

$C_{l_{\delta_a}}$ aileron effectiveness parameter, $\partial C_l/\partial\delta_a$, per deg

C_m pitching-moment coefficient, $\frac{\text{Pitching moment}}{qS\bar{c}}$

$C_{m_{\delta_e}}$ elevator effectiveness parameter, $\partial C_m/\partial\delta_e$, per deg

C_n yawing-moment coefficient, $\frac{\text{Yawing moment}}{qSb}$

C_{n_β} directional stability parameter, $\partial C_n/\partial\beta$, per deg

$C_{n_{\delta_r}}$ rudder effectiveness parameter, $\partial C_n/\partial\delta_r$, per deg

C_Y side-force coefficient, $\frac{\text{Side force}}{qS}$

$\bar{c}$ mean geometric chord, 1.50 m (4.91 ft)

$\bar{c}_a$ aileron mean chord, 0.37 m (1.20 ft)

$\bar{c}_e$ elevator mean chord, 0.46 m (1.50 ft)

$\bar{c}_r$ rudder mean chord, 0.40 m (1.30 ft)

q free-stream dynamic pressure, N/m^2 (lbf/ft^2)

q_t/q ratio of dynamic pressure at tail to free-stream dynamic pressure

S wing area, 16.25 m^2 (175 ft^2)

S_a area of one aileron, 0.65 m^2 (6.95 ft^2)

S_e area of elevator, 1.63 m^2 (17.50 ft^2)

S_r area of rudder, 0.59 m^2 (6.40 ft^2)

T	effective thrust $\left(\text{at } \alpha = 0^{\circ} \text{ and } \delta_f = 0^{\circ}\right)$, $\text{Drag}_{\text{propeller removed}} - \text{Drag}_{\text{propeller operating}}$
T_c'	thrust coefficient, T/qS
X	longitudinal axis
V	free-stream velocity, m/sec (ft/sec)
α	angle of attack of fuselage reference line, deg
β	angle of sideslip, positive when nose is to left, deg
δ_a	total aileron deflection, positive when right aileron is down, $\delta_{aR} - \delta_{aL}$, deg
δ_e	elevator deflection, positive when trailing edge is down, deg
δ_f	flap deflection, positive when trailing edge is down, deg
δ_r	rudder deflection, positive when trailing edge is to left, deg
ϵ	downwash angle of tail, angle is positive when deflected stream is downward relative to free stream, deg
θ	flow angle in tunnel test section with respect to horizontal plane (downflow is negative), deg

Subscripts:

L	left
max	maximum
R	right

MODEL

The model tested was a full-scale mockup of a light single-engine high-wing monoplane having a maximum take-off weight of 16 900 N (3800 lbf). Figure 2 gives the principal dimensions and figure 3 shows the model mounted in the tunnel test section. The

model, which was of conventional production-line construction, had a wing span of 11.20 m (36.75 ft), a wing area of 16.25 m^2 (175 ft^2), an aspect ratio of 7.7, and a mean geometric chord of 1.50 m (4.91 ft). The wing had airfoil sections of NACA 64_2A215 at the model center line and NACA 64_1A412 at the wing tip. The wing had 1.5° dihedral measured along the upper surface of the main spar, 1.5° incidence at the root, and -1.5° incidence at the tip, resulting in 3° of washout. The thrust axis was in the model center-line plane and was inclined downward 3.5° with respect to the model reference line. The horizontal tail was of the stabilizer-elevator type with an elevator travel of 10° to -20°. The control deflection range of the ailerons and rudder was -20° to 15° and ±25°, respectively. The controls were remotely operated by electromechanical actuators. The pushrod of each control was strain-gaged to provide the hinge moments. The single-slotted trailing-edge flap had a maximum deflection of 30°. The propeller was powered by a 198-kW (266-hp) variable-frequency electric motor.

TESTS

The tests were made to determine the static longitudinal and lateral stability and control characteristics of the model over a wide range of flight conditions. Hinge moments were measured for all control surfaces during the investigation. The model was tested over an angle-of-attack range of -4° to 24°, over a sideslip range of ±8° for the clean condition ($\delta_f = 0°$; gear up), and for flap deflections of 10° and 30° with gear down. A range of elevator deflections of 10° to -15° was investigated at zero sideslip, and the aileron and rudder effectiveness was measured over the sideslip range. The tests were made at thrust coefficients of 0, 0.14, and 0.30 which represent a flight condition of low power or high speed (where the thrust coefficient approaches zero), best climb, and full power as in take-off or wave-off, respectively. The thrust coefficients are equated to an installed 224 kW (300 hp). A propeller blade angle of 20° was used for all tests. Tail downwash surveys were made with a calibrated pitch-yaw head along the elevator hinge axis with the horizontal tail removed at zero sideslip for flap deflections of 0°, 10°, and 30° for $T_C' = 0$, 0.14, and 0.30. The tests at $T_C' = 0$ and 0.14 were conducted at a tunnel speed of 27.4 m/sec (90 ft/sec) which gave a Reynolds number of approximately 2.8×10^6. The tests at $T_C' = 0.30$ were made at 22.8 m/sec (75 ft/sec) giving a Reynolds number of about 2.3×10^6. The Reynolds number is based on a mean geometric chord of 1.50 m (4.91 ft).

PRESENTATION OF DATA

The longitudinal data from these tests have been corrected for blockage, airstream misalinement, buoyancy effects, mounting-strut tares, and wind-tunnel jet-boundary effects. The lift and drag have been corrected for the integrated average airstream

misalinement. The lateral data have not been corrected for the lateral variation of the stream angle. It should be pointed out, however, that at least a part of the positive rolling moment noted at the lower angles of attack for most model conditions can be attributed to lateral variation of the tunnel airstream angle as shown in figure 4. Calculations of section rolling moments using the spanwise variations of stream angle of figure 4 indicated that the total measured out-of-trim rolling moment could be approximately accounted for by the airstream angularity. Similar out-of-trim rolling moments were also noted in references 1 to 5.

The data are presented as follows:

RESULTS AND DISCUSSION

The basic data obtained during the wind-tunnel investigation are presented in figures 5 to 43 without analysis. Summary plots have been prepared from some of these data to illustrate the general static stability and control characteristics of the model. Only the summary plots are discussed.

Longitudinal Characteristics

The longitudinal characteristics of the model with various power conditions are presented in figure 44 for flap deflections of 0°, 10°, and 30°. As might be expected, increasing power results in an increase in lift-curve slope and maximum lift coefficient because of the increased slipstream velocity over the wing. This effect of power on the lift characteristics is summarized in figure 45 where lift-curve slope and maximum lift coefficient are shown as a function of thrust coefficient.

The pitching-moment curves shown in figure 44 are fairly linear up to angles of attack near the stall and do not generally exhibit the nose-down pitching moment at the stall usually associated with a straight-wing airplane. The curves of the pitching moment

against angle of attack indicate that increasing thrust has little effect on the longitudinal characteristics except for a nose-up trim change for the full-flap configuration. These effects of power on the static longitudinal stability are summarized in figures 46 and 47 where variations of the static stability parameter $\partial C_m/\partial C_L$ are plotted against C_L and T_c', respectively. These figures show that, in general, the level of stability increased with an increase in lift coefficient and that increased thrust coefficient caused a decrease in stability particularly for the flap-deflected configurations. It might be pointed out here that the model shows a high level of static longitudinal stability for the forward center-of-gravity location. The data indicate that the model would become no worse than neutrally stable with the center of gravity as far aft as $0.40\bar{c}$.

The stick-free static stability characteristics, determined from the pitching- and hinge-moment curves, are shown in figure 48. The data show that the model had stick-free stability for the flap and power conditions tested. The effect of thrust coefficient on the stick-free longitudinal stability at a lift coefficient of 1.0 is presented in figure 49. These data show power has a more destabilizing effect with a full-flap deflection $(\delta_f = 30^o)$ than with the lower deflections $(\delta_f = 0^o, 10^o)$, and the model would have stick-free stability with the center of gravity as far aft as $0.40\bar{c}$.

The variation of elevator effectiveness with angle of attack is presented in figure 50 for flap deflections of 0^o, 10^o, and 30^o. These data show that the effectiveness is only slightly reduced at the higher angles of attack, and effectiveness is still maintained up to the stall. Presented in figure 51 is the variation of elevator effectiveness with thrust coefficient. These data show that power increased the elevator effectiveness.

Presented in figure 52 is the variation of the average downwash angle and the dynamic pressure ratio at the tail with angle of attack for the flap and power conditions investigated. These data show a large increase in downwash angle with flap deflection. Also, the effects of power on the downwash angle are fairly large, particularly at high angles of attack and full flap deflection.

Lateral Characteristics

The variation of the effective-dihedral parameter C_{l_β} with angle of attack is shown in figure 53 for the various flap and power conditions tested. These data show that the model has positive effective dihedral $(-C_{l_\beta})$ for all conditions to $C_{L,max}$. The values of C_{l_β} vary widely depending upon angle of attack, flap, or power condition which means the response of the airplane to gusts or to rudder inputs to raise a wing could vary with the airplane configuration and flight conditions.

The variation of the directional stability parameter C_{n_β} with angle of attack is shown in figure 54 for the flap and power conditions investigated. These data show that

although the directional stability generally decreases with increasing angle of attack up to the stall, the model is directionally stable for all conditions studied. The effect of power on the directional stability characteristics is presented in figure 55 and the data show that, in general, power did not have a major effect on the directional stability.

The variation of the aileron effectiveness with angle of attack for sideslip angles of 0° and $\pm 8^{\circ}$ is presented in figure 56 for flap deflections of 0° and 30° and $T_c' = 0$, 0.14, and 0.30. These data show that, in general, the aileron effectiveness remains at a fairly constant level throughout the angle-of-attack range and is relatively unaffected by flap deflection, power setting, or angle of sideslip.

The variation of rudder effectiveness with angle of attack for sideslip angles from 8° to -8° is presented in figure 57. These data show that rudder effectiveness is maintained throughout the angle-of-attack range for all test conditions. The effect of power on the rudder effectiveness is shown in figure 58. The data show that power caused an increase in effectiveness with flaps up but had little effect with flaps fully deflected.

The basic lateral characteristics of the model, as shown by the variation of the lateral coefficients C_l and C_n with angle of attack for 0° sideslip, are presented in figure 59 for the flap and power conditions of the test. The data show that below the stall, there is an out-of-trim positive rolling moment for all conditions that gradually reduces with an increase in angle of attack, and also large rolling moments caused by asymmetric wing stall for the $\delta_f = 0^{\circ}$ and 10° configurations with power on. The stall for these configurations occurs at an angle of attack about 2° lower than that for the full-flap configuration. The yawing moments remain fairly linear and at almost a constant level over the angle-of-attack range. The data show an increase in yawing-moment coefficient with increased power.

An attempt has been made to determine whether the controls are powerful enough to overcome the asymmetric moments at the stall, and the results of the analysis are presented in figure 60. In this figure are plotted the variations of the rolling and yawing moments with angle of attack at $\beta = 0^{\circ}$, $T_c' = 0.30$, and $\delta_f = 0^{\circ}$. Also shown are the sums of the rolling and yawing moments for the controls neutral and the rolling and yawing moments produced by full opposite aileron and rudder deflection (including the adverse yaw of the ailerons and roll due to rudder). These data (the dashed curves) show that, based on the static wind-tunnel results, the rolling and yawing moments available from aileron and rudder are more than adequate to trim out the model moments.

CONCLUSIONS

An investigation has been made in the Langley full-scale tunnel to determine the static longitudinal and lateral stability and control characteristics of a full-scale mockup

of a light single-engine high-wing airplane. The following conclusions are drawn from the results of the investigation:

1. The model has stick-fixed and stick-free longitudinal stability up to the stall for all configurations tested with the center of gravity located at 13.7 percent of the mean geometric chord. Power generally has a small destabilizing effect, but the model could become no worse than neutrally stable with the center of gravity as far aft as 40 percent of the mean geometric chord.

2. The model has positive effective dihedral up to the stall for all test conditions, but there are large variations of effective dihedral with angle of attack for different power and flap conditions.

3. The model is directionally stable up to the stall.

4. Aileron and rudder effectiveness is maintained up to the stall.

5. Aileron and rudder controls are powerful enough to trim out all asymmetric moments up to the stall.

Langley Research Center,
National Aeronautics and Space Administration,
Hampton, Va., February 6, 1973.

REFERENCES

1. Fink, Marvin P.; and Freeman, Delma C., Jr.: Full-Scale Wind-Tunnel Investigation of Static Longitudinal and Lateral Characteristics of a Light Twin-Engine Airplane. NASA TN D-4983, 1969.

2. Fink, Marvin P.; Shivers, James P.; and Smith, Charles C., Jr.: A Wind-Tunnel Investigation of Static Longitudinal and Lateral Characteristics of a Full-Scale Mockup of a Light Twin-Engine Airplane. NASA TN D-6238, 1971.

3. Fink, Marvin P.; Freeman, Delma C., Jr.; and Greer, H. Douglas: Full-Scale Wind-Tunnel Investigation of the Static Longitudinal and Lateral Characteristics of a Light Single-Engine Airplane. NASA TN D-5700, 1970.

4. Shivers, James P.; Fink, Marvin P.; and Ware, George M.: Full-Scale Wind-Tunnel Investigation of the Static Longitudinal and Lateral Characteristics of a Light Single-Engine Low-Wing Airplane. NASA TN D-5857, 1970.

5. Fink, Marvin P.; Shivers, James P.; Greer, H. Douglas; and Megrail, James L.: The Effects of Configuration Changes on the Aerodynamic Characteristics of a Full-Scale Mockup of a Light Twin-Engine Airplane. NASA TN D-6896, 1972.

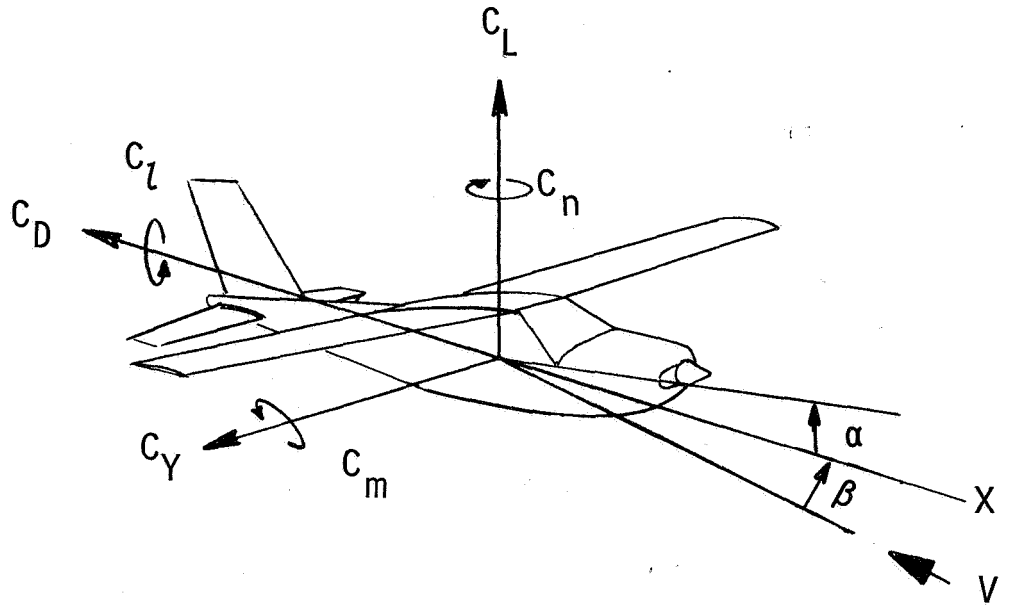

Figure 1.- System of stability axes and positive sense of angles, forces, and moments.

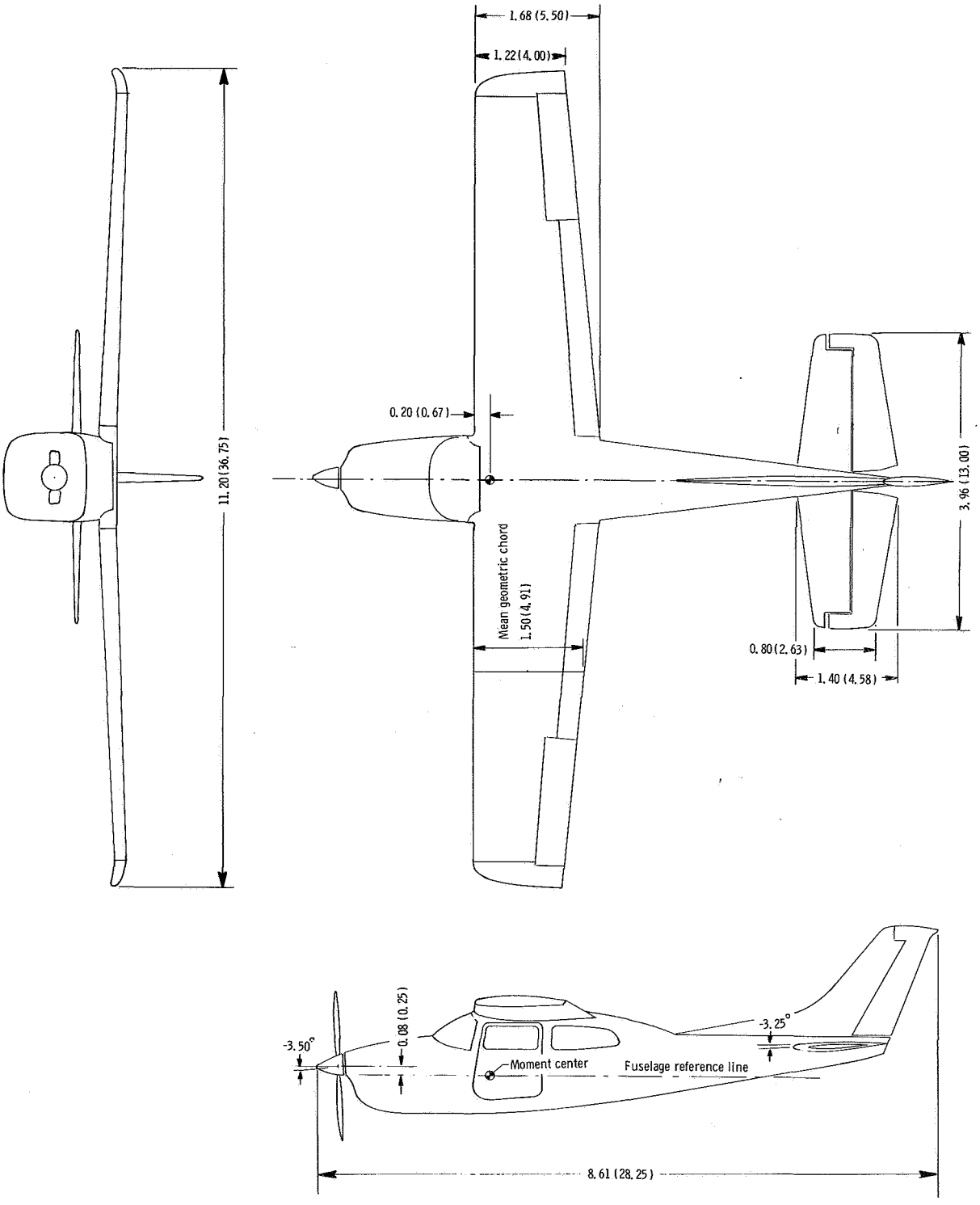

(a) Three-view drawing of the model. All dimensions in meters (ft).

Figure 2.- Three-view drawing of the model and cross-sectional views of the controls.

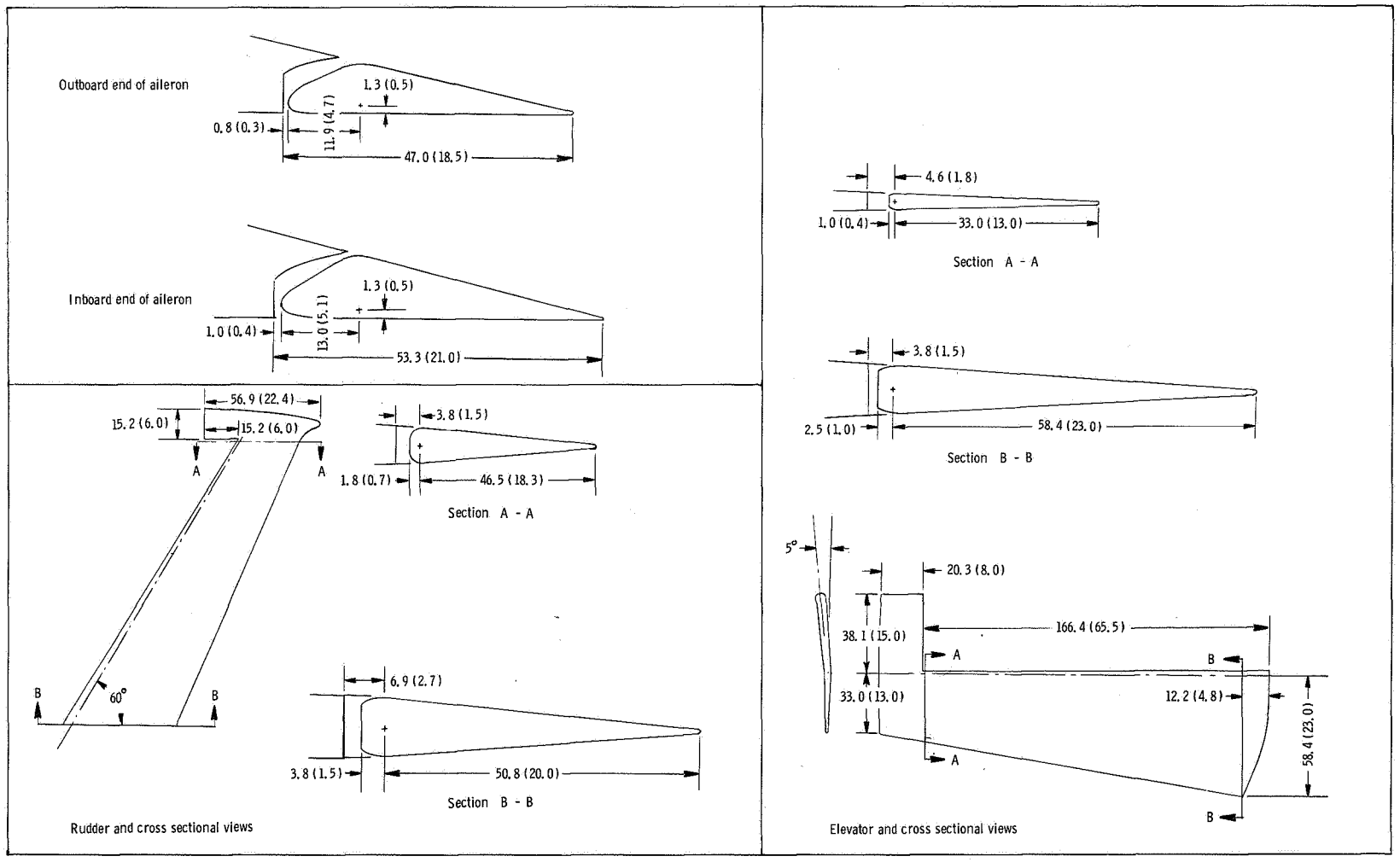

(b) Cross-sectional views of control surfaces. All dimensions are in centimeters (in.).

Figure 2.- Concluded.

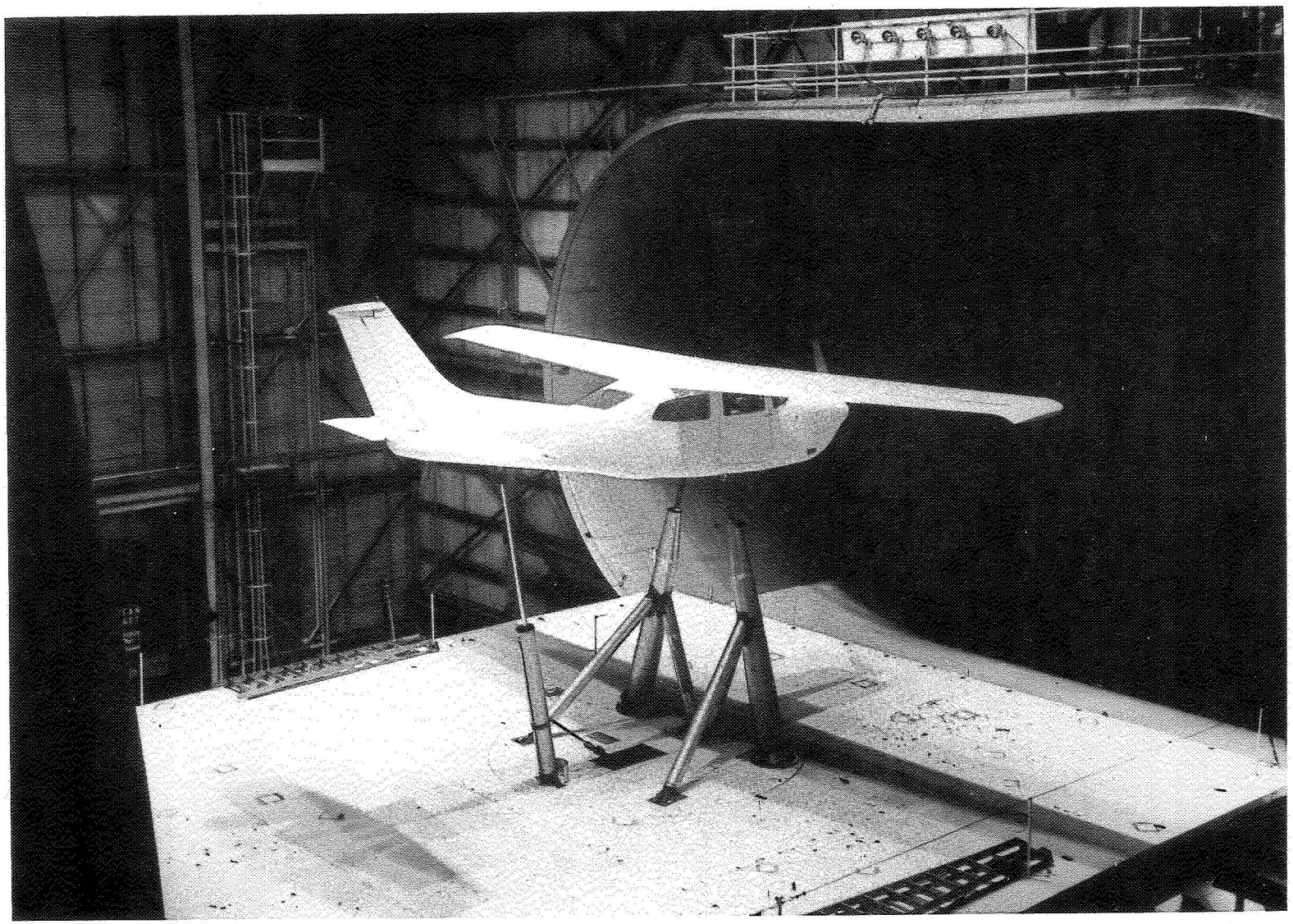

L-72-3552

Figure 3.- Photograph of model mounted in the Langley full-scale tunnel.

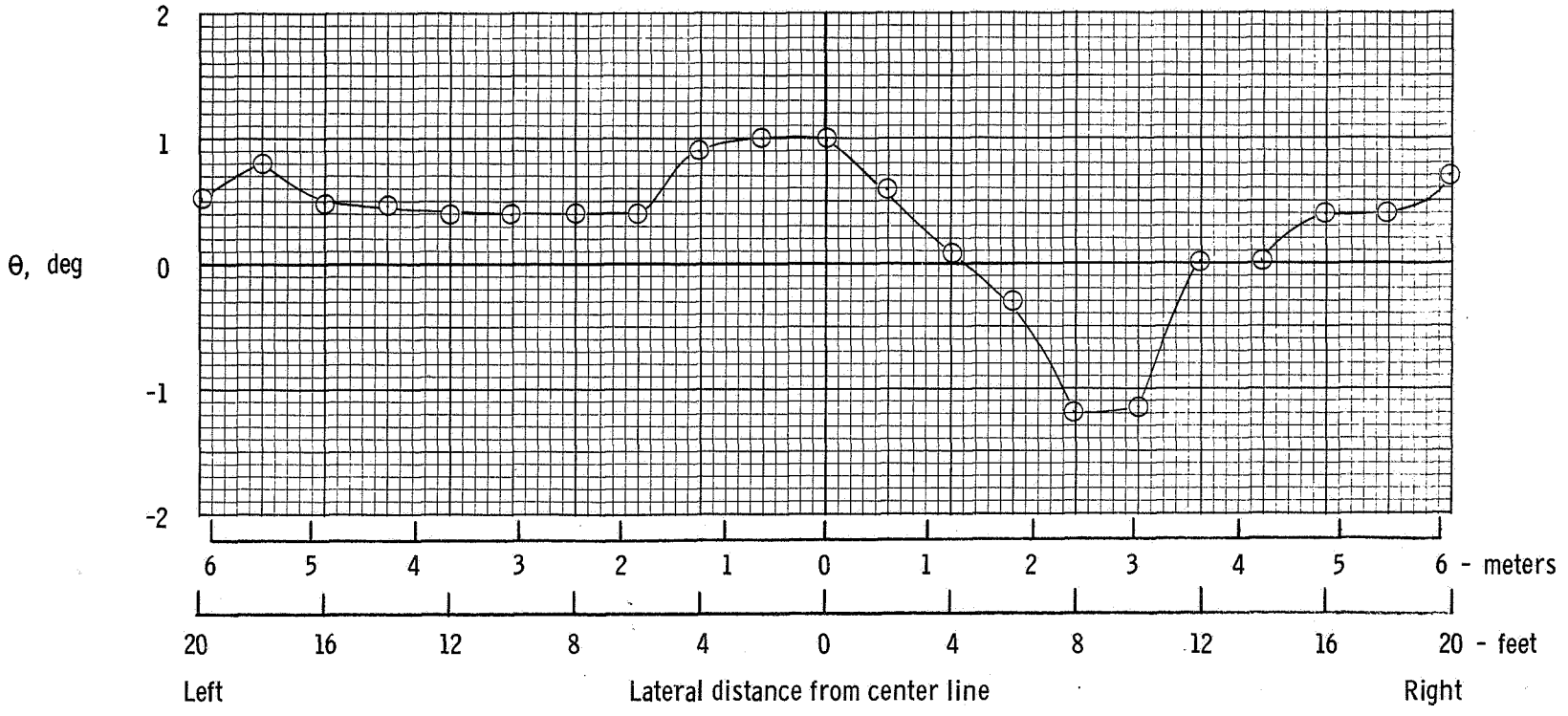

Figure 4.- Lateral variation of airstream angle at the wing location in tunnel.

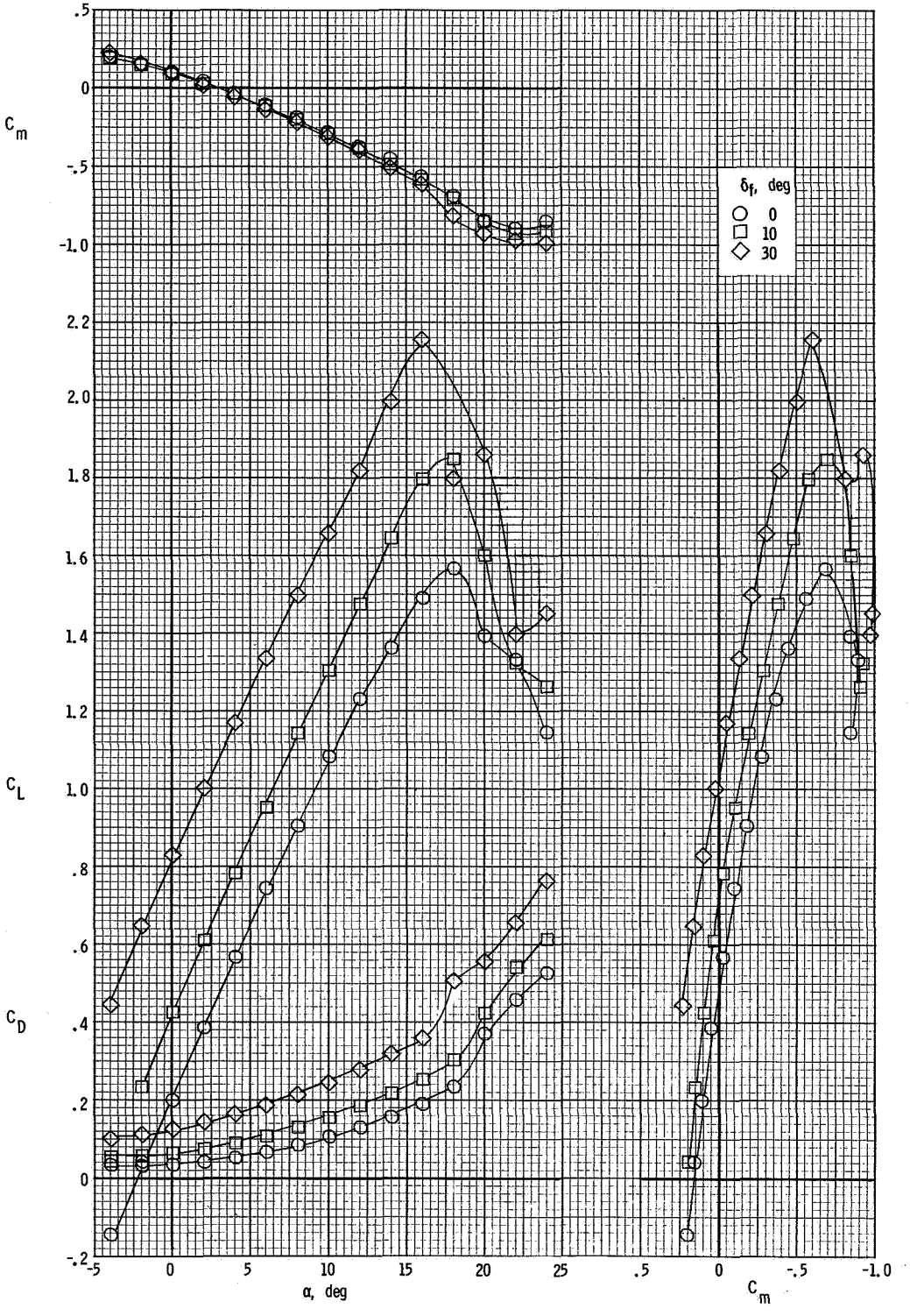

Figure 5.- Longitudinal aerodynamic characteristics of the airplane with propeller removed for several flap deflections.

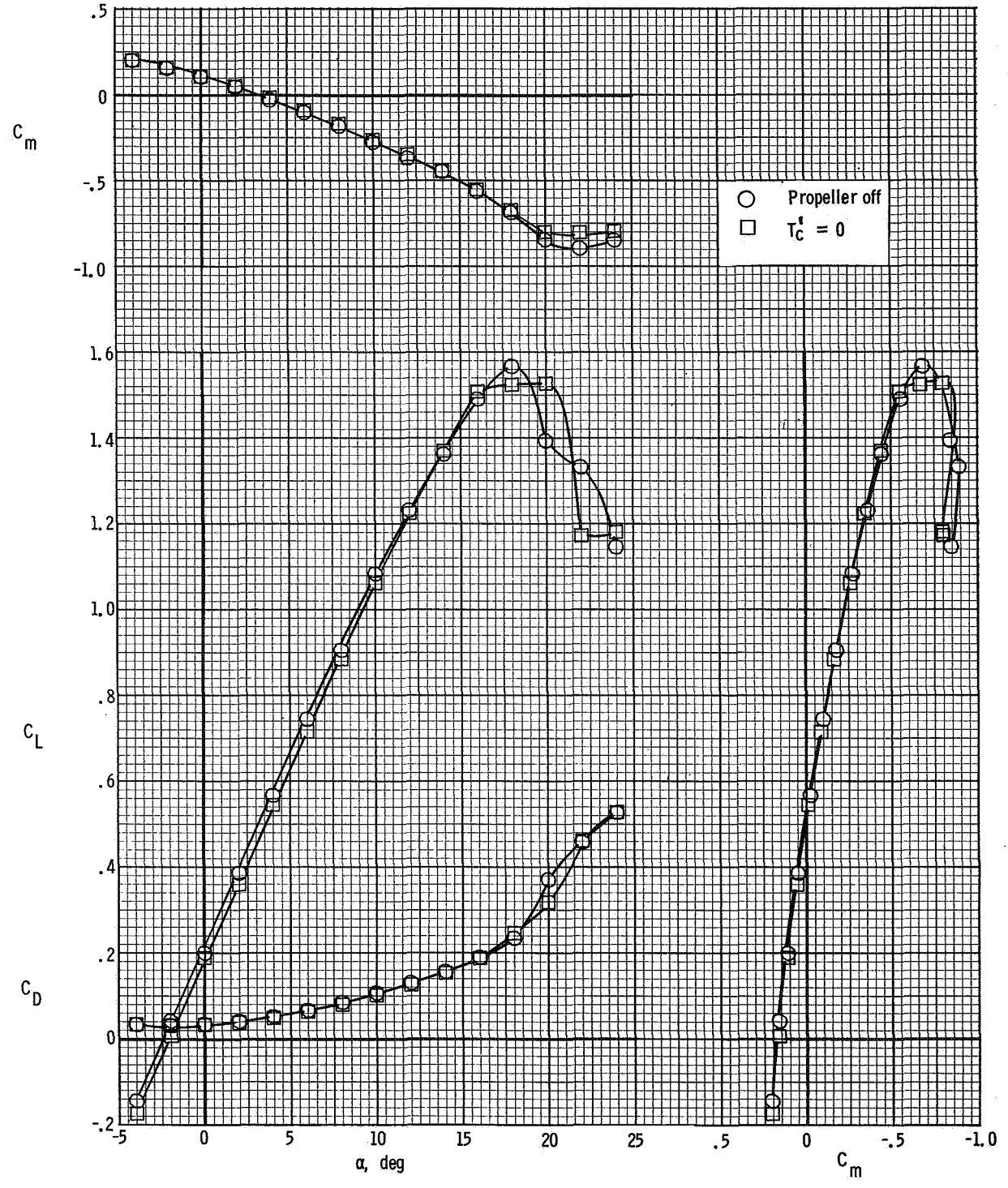

(a) $\delta_f = 0^o$.

Figure 6.- The longitudinal characteristics of the airplane with propeller removed and zero thrust coefficient.

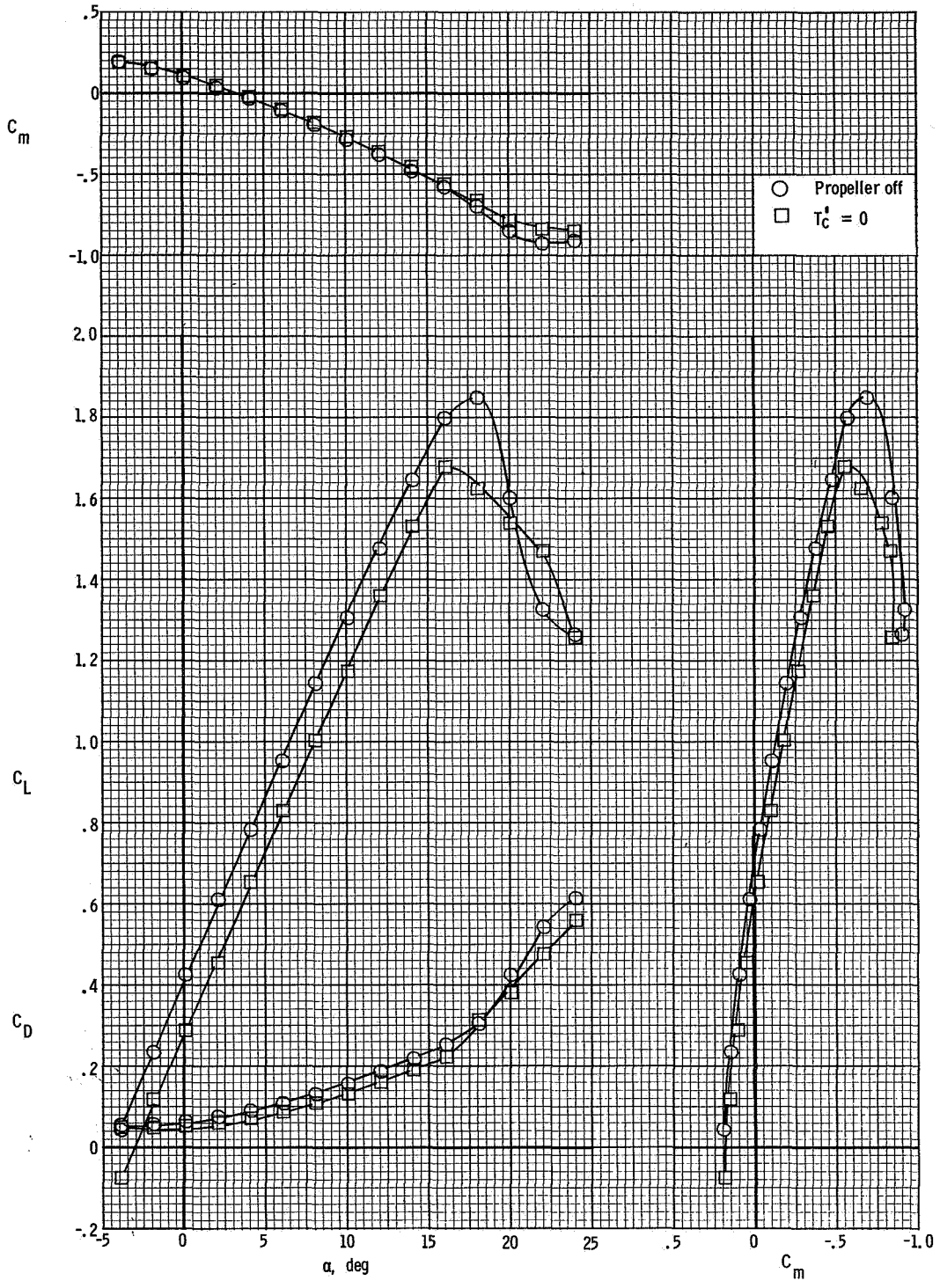

(b) $\delta_f = 10^o$.

Figure 6.- Continued.

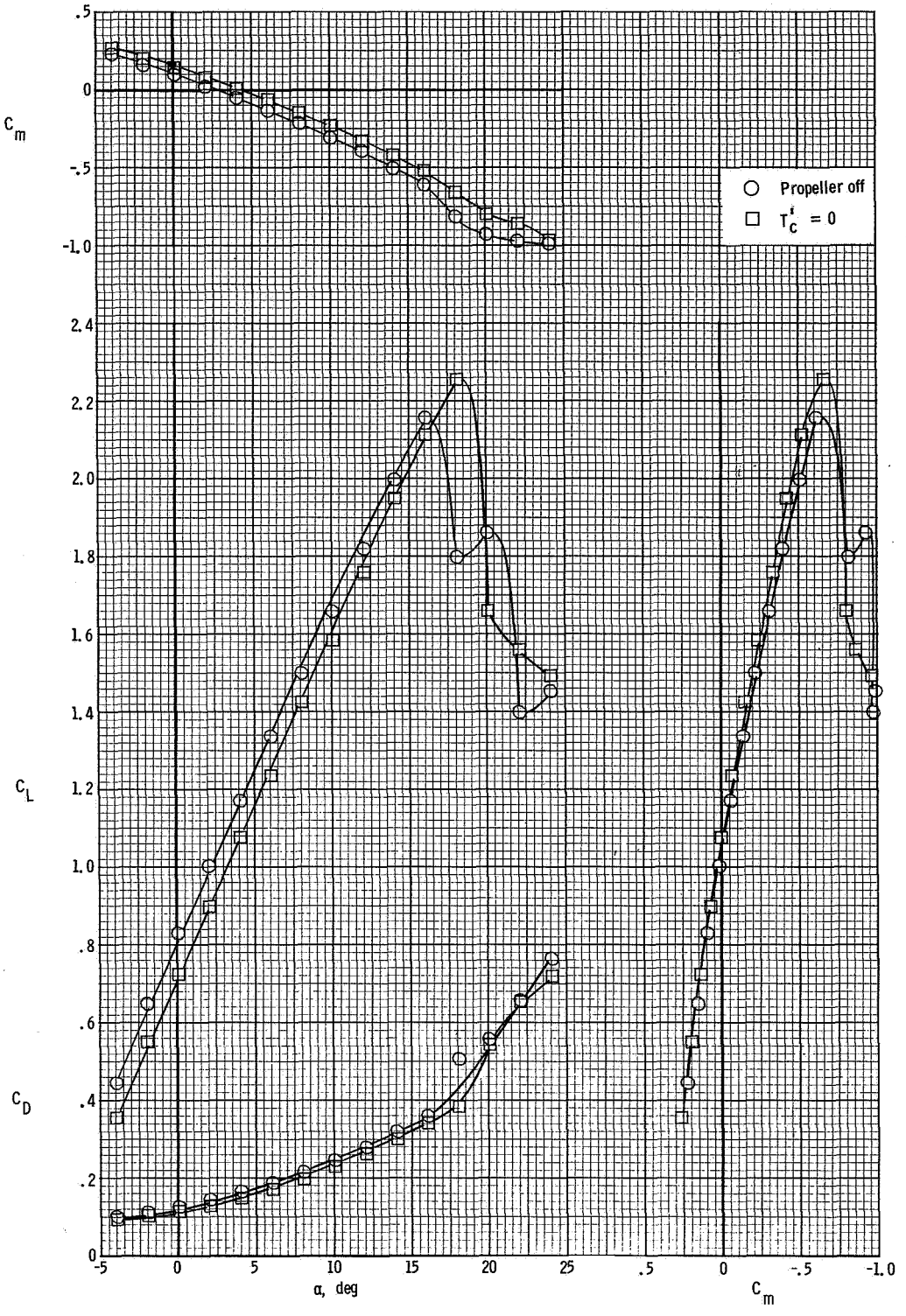

(c) $\delta_f = 30^o$.

Figure 6.- Concluded.

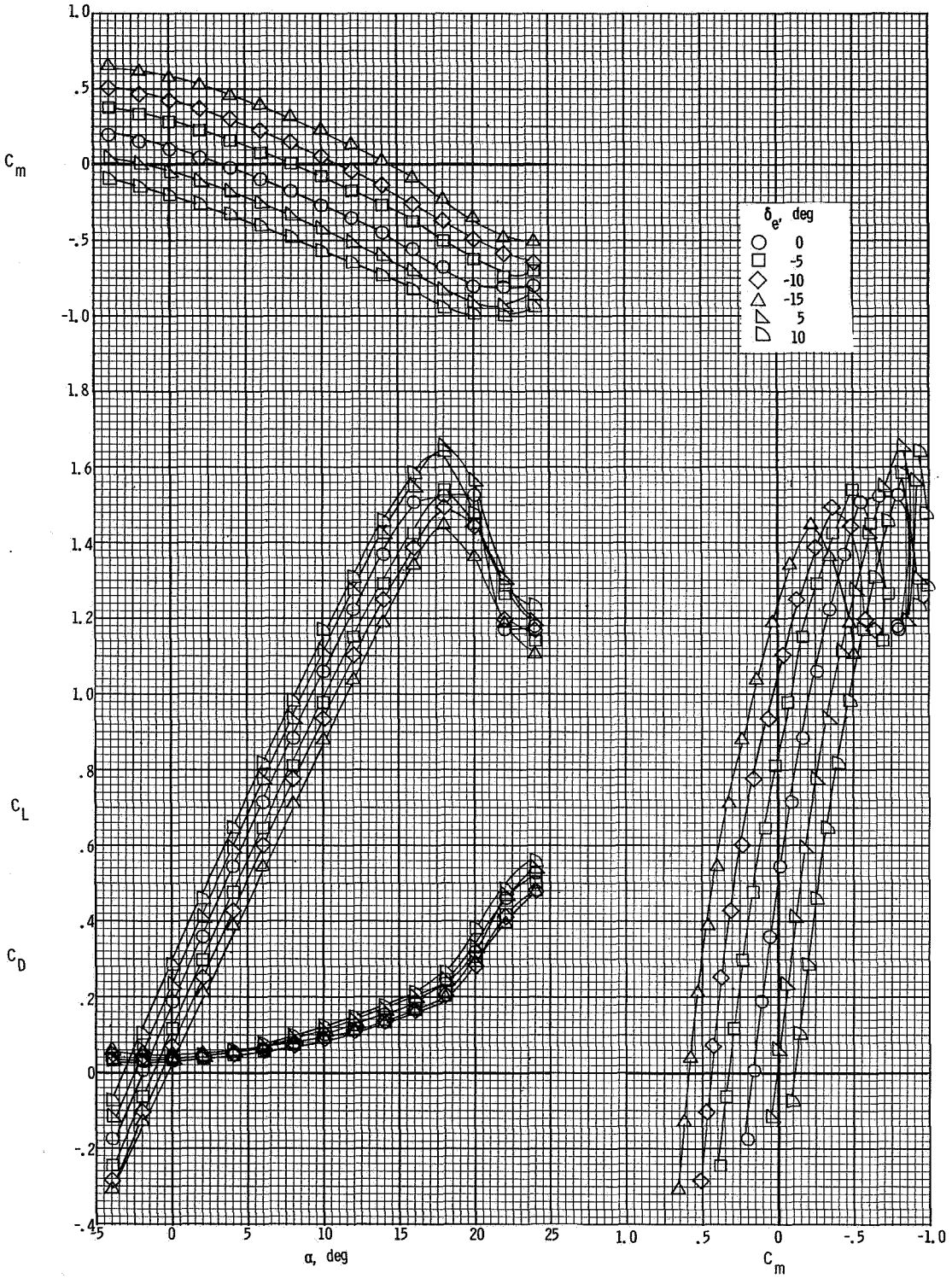

(a) $T_c' = 0$.

Figure 7.- Longitudinal aerodynamic characteristics of the airplane for several thrust coefficients for $\delta_f = 0^o$.

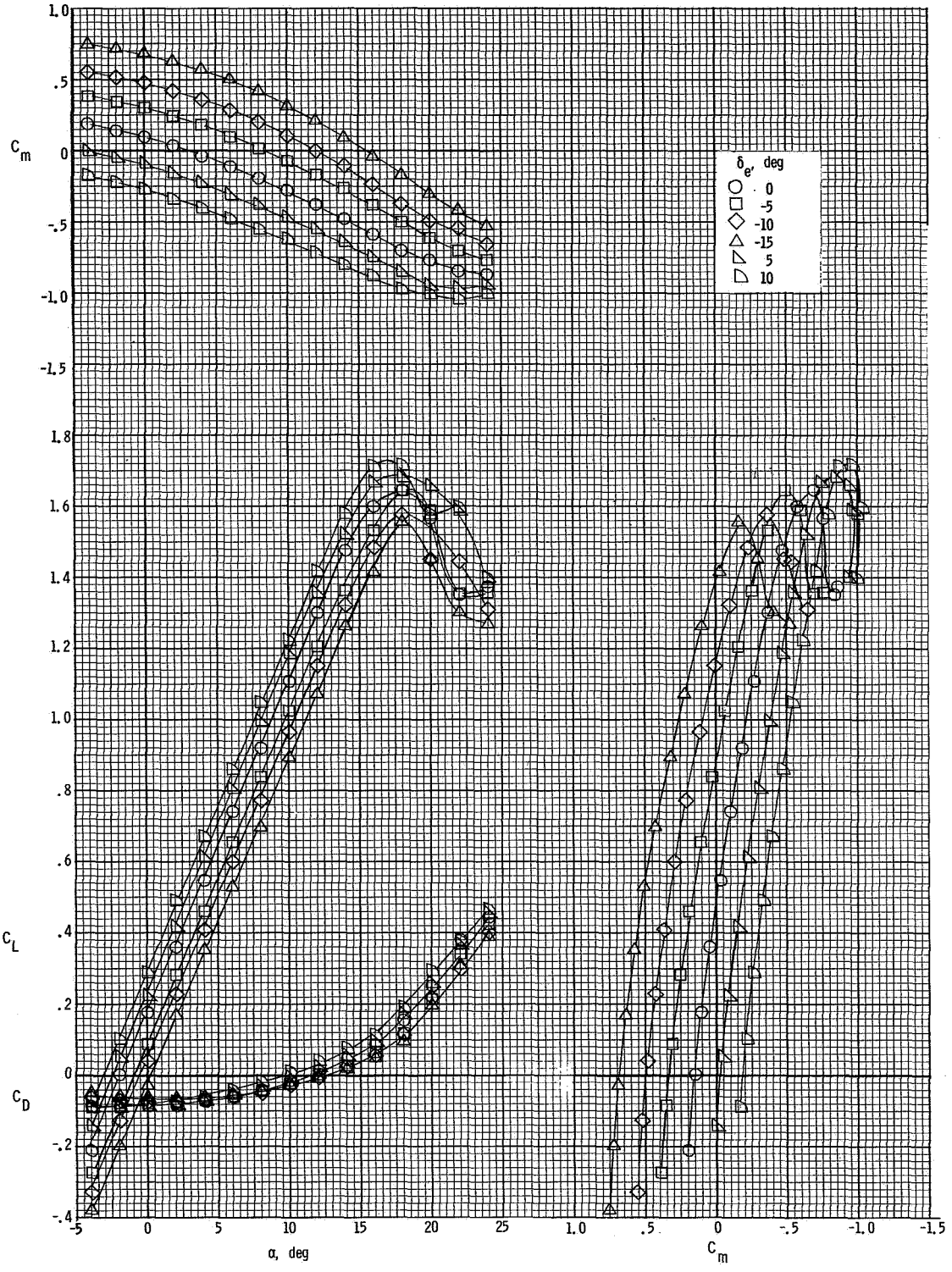

(b) $T'_c = 0.14$.

Figure 7.- Continued.

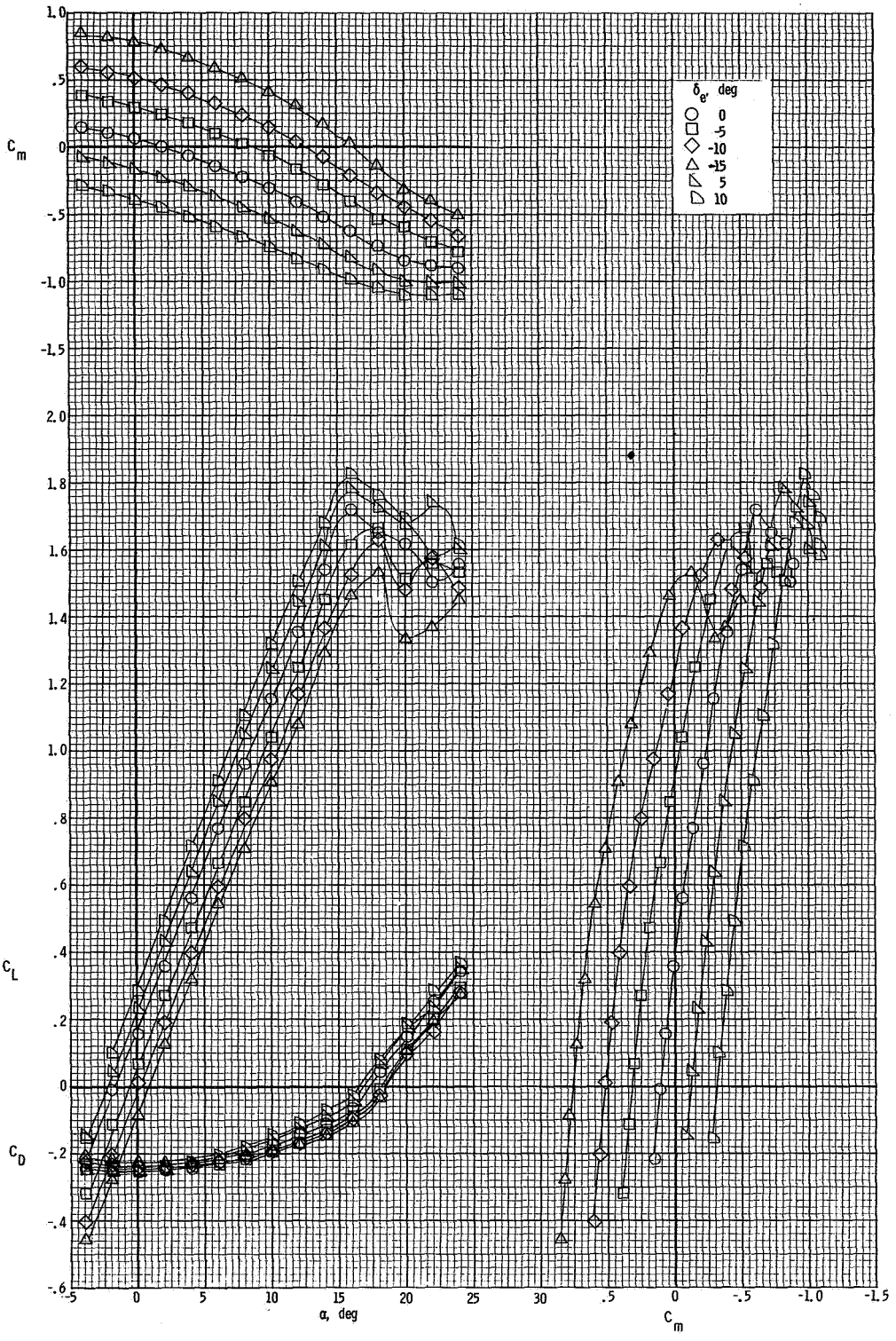

(c) $T'_c = 0.30$.

Figure 7.- Concluded.

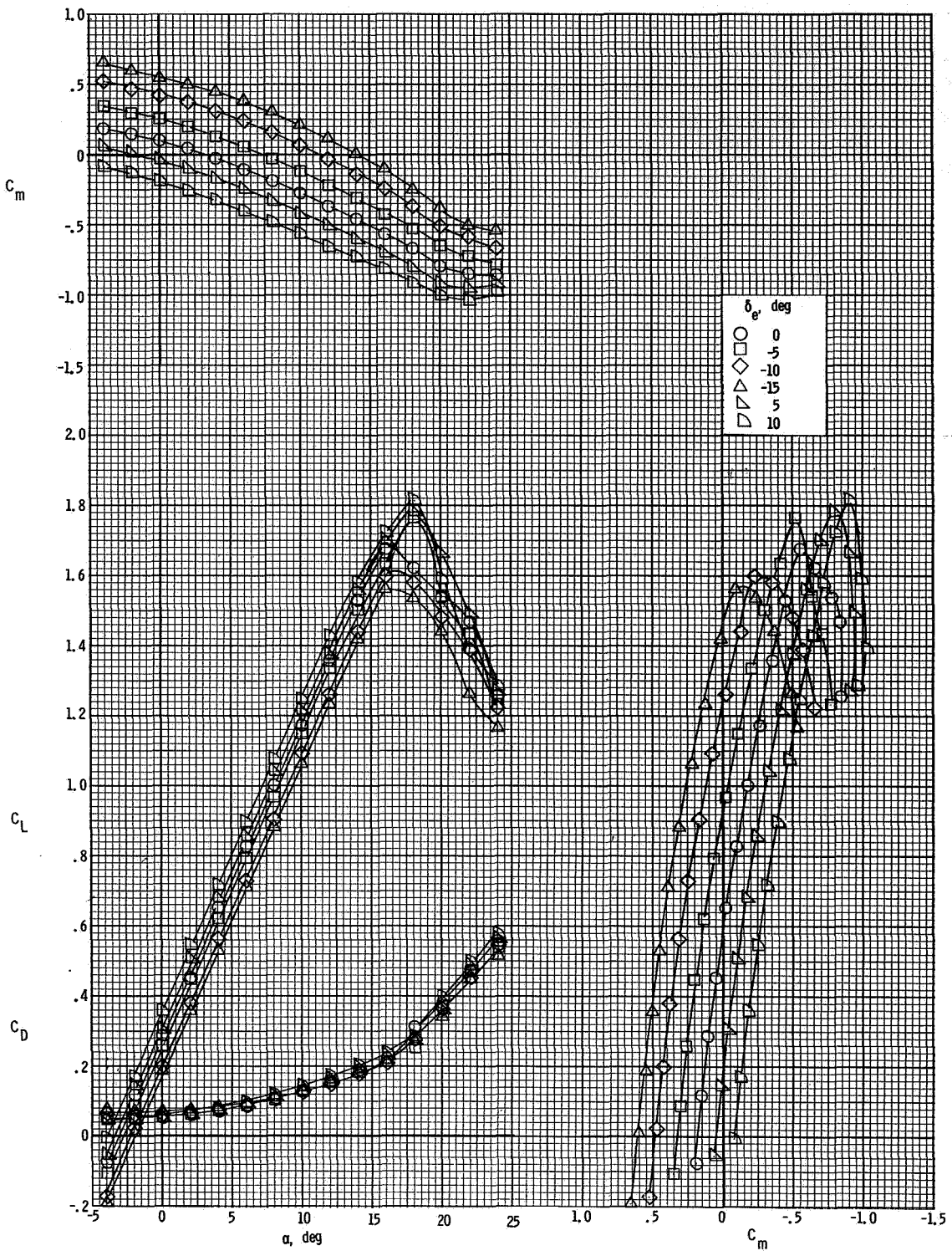

(a) $T_C' = 0$.

Figure 8.- Longitudinal aerodynamic characteristics of the airplane for several thrust coefficients for $\delta_f = 10^o$.

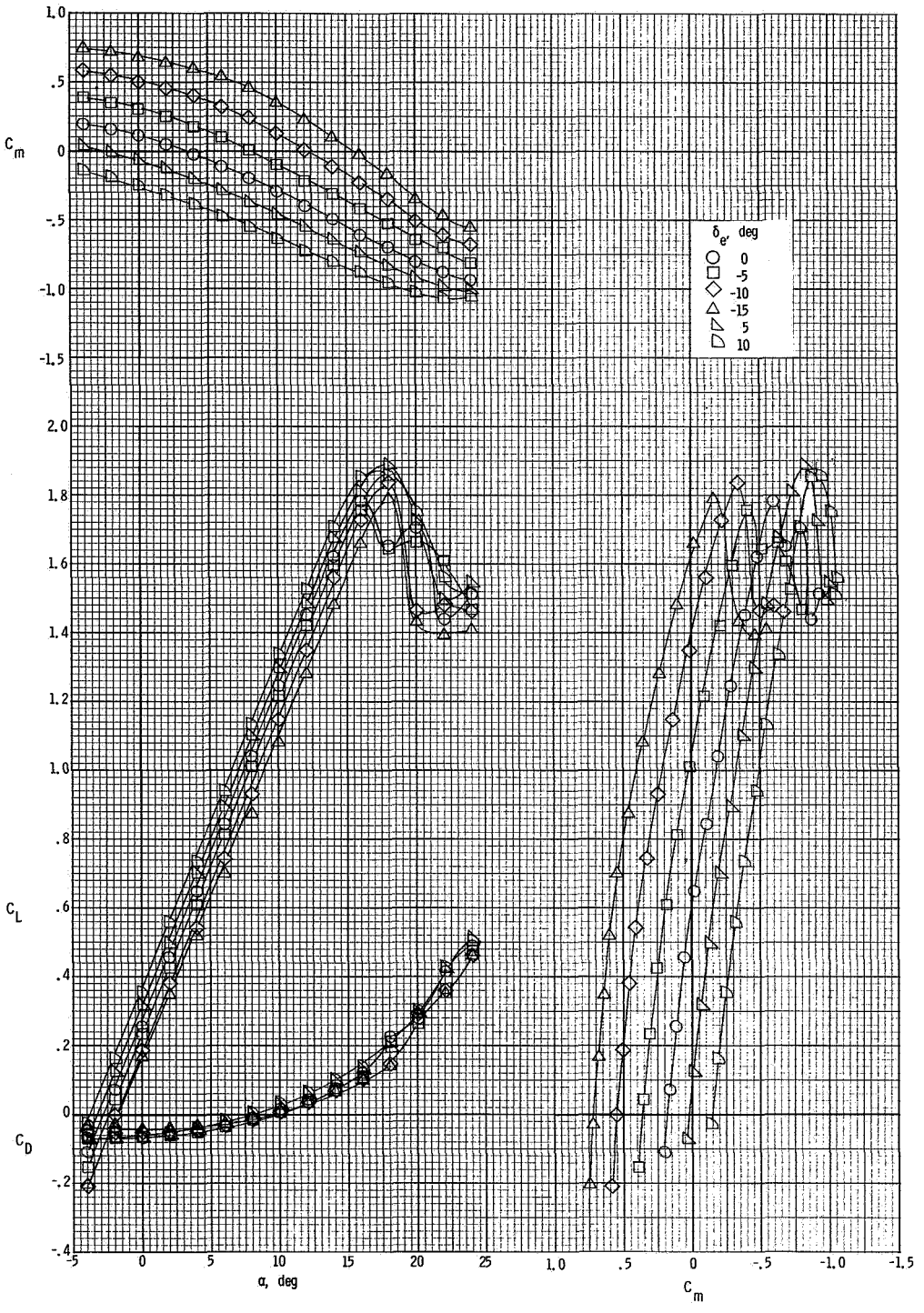

(b) $T'_c = 0.14$.

Figure 8.- Continued.

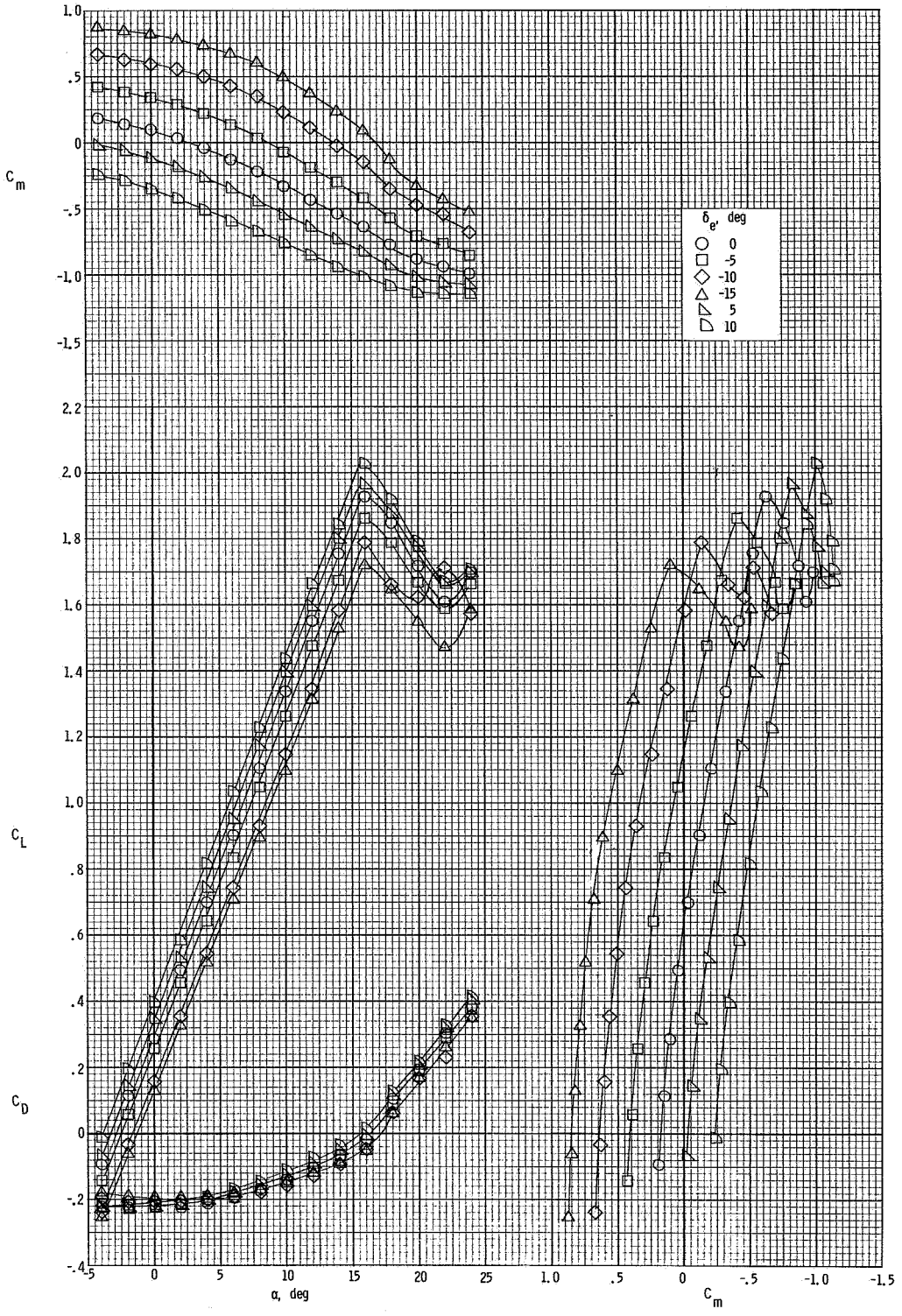

(c) $T_c' = 0.30$.

Figure 8.- Concluded.

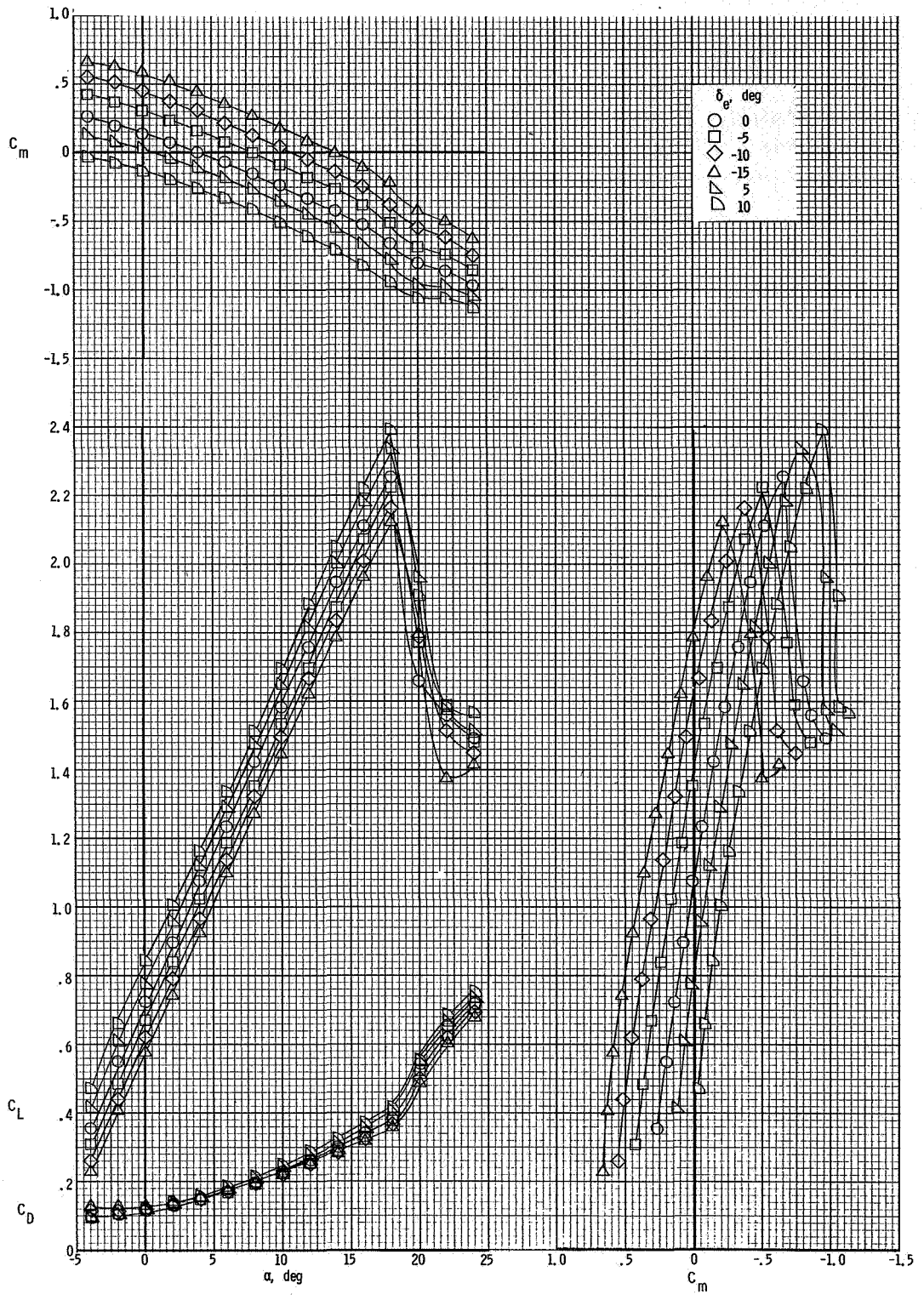

(a) $T_c' = 0$.

Figure 9.- Longitudinal aerodynamic characteristics of the airplane for several thrust coefficients for $\delta_f = 30^o$.

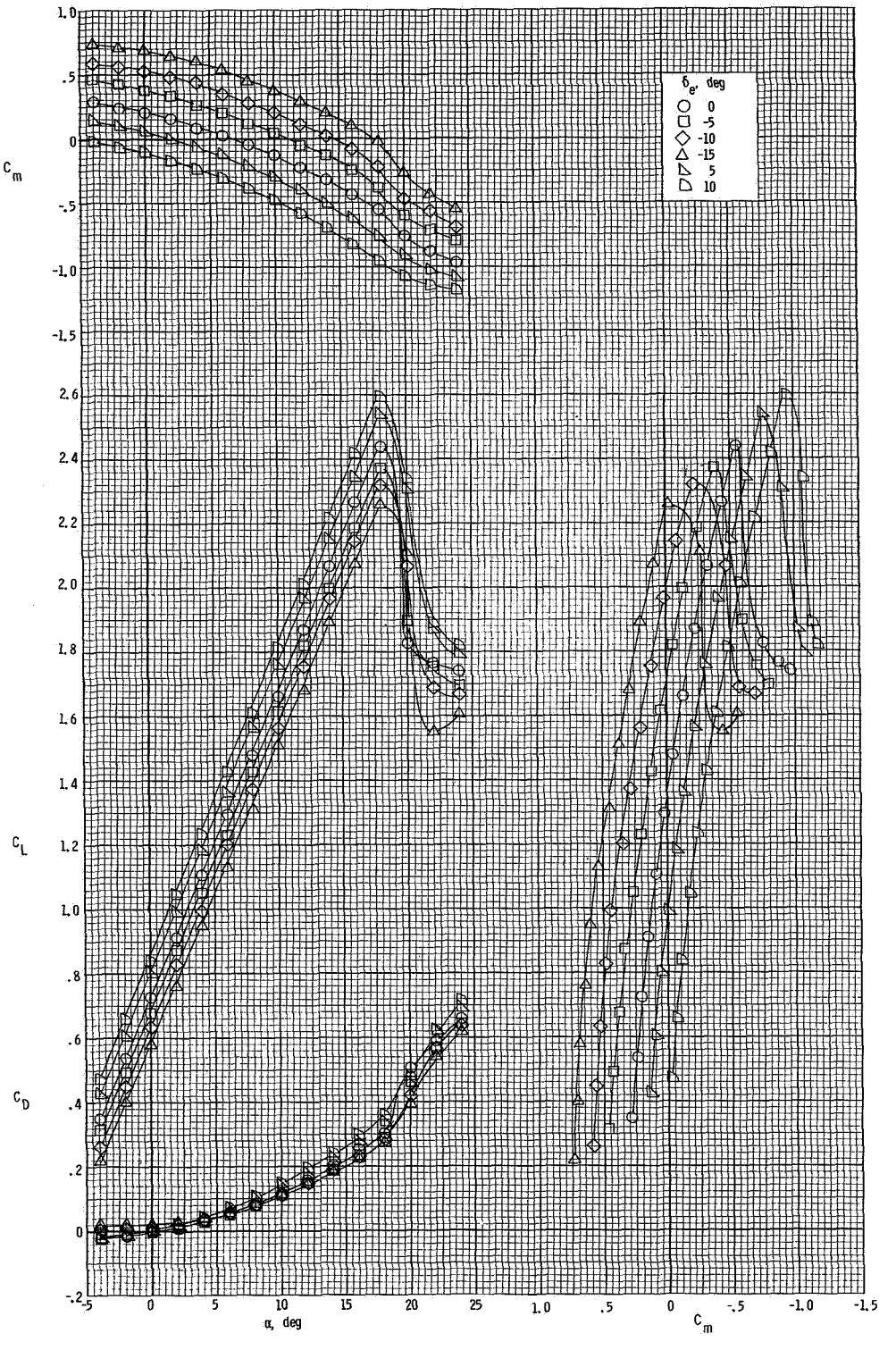

(b) $T_c' = 0.14$.

Figure 9.- Continued.

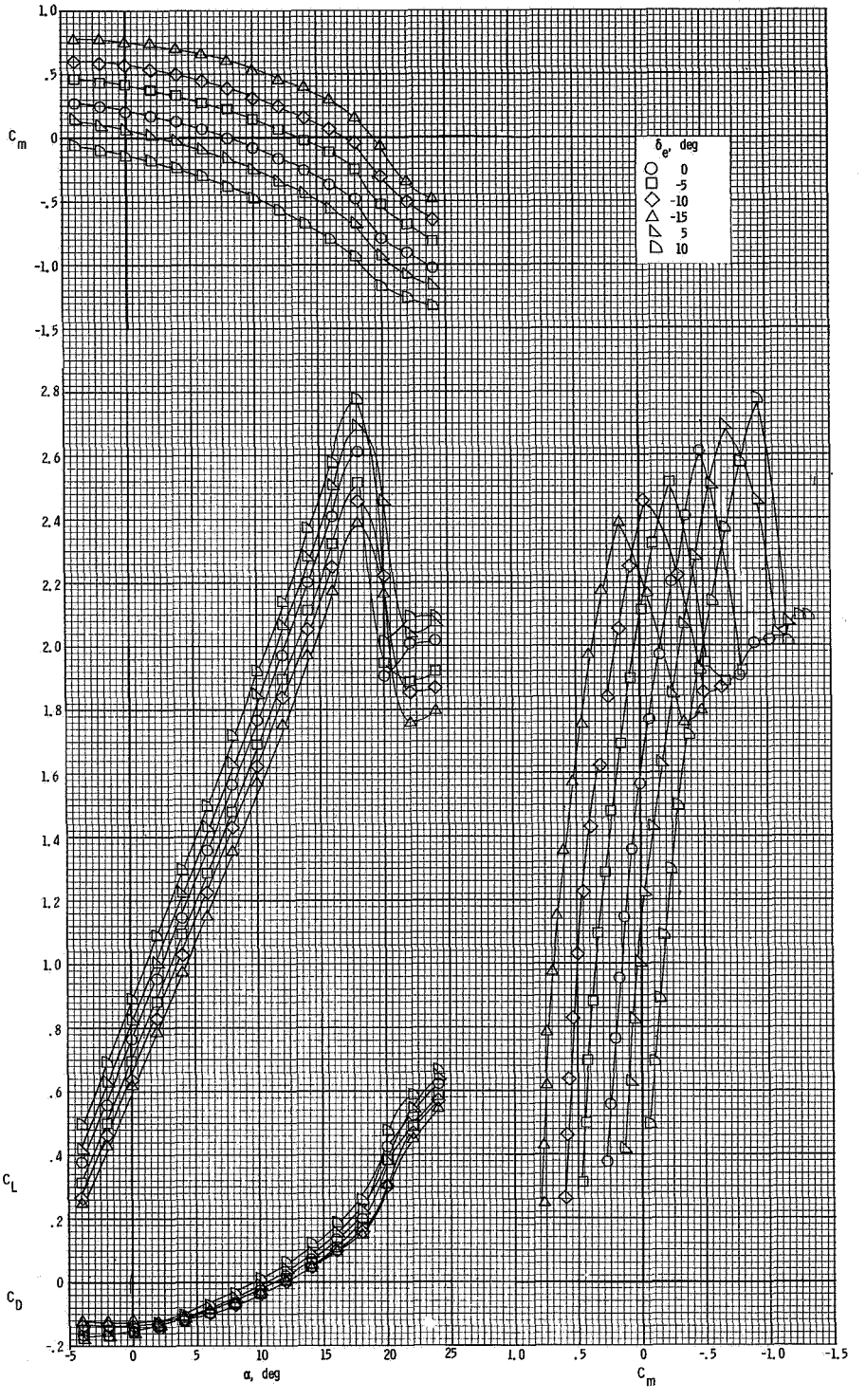

(c) $T'_c = 0.30$.

Figure 9.- Concluded.

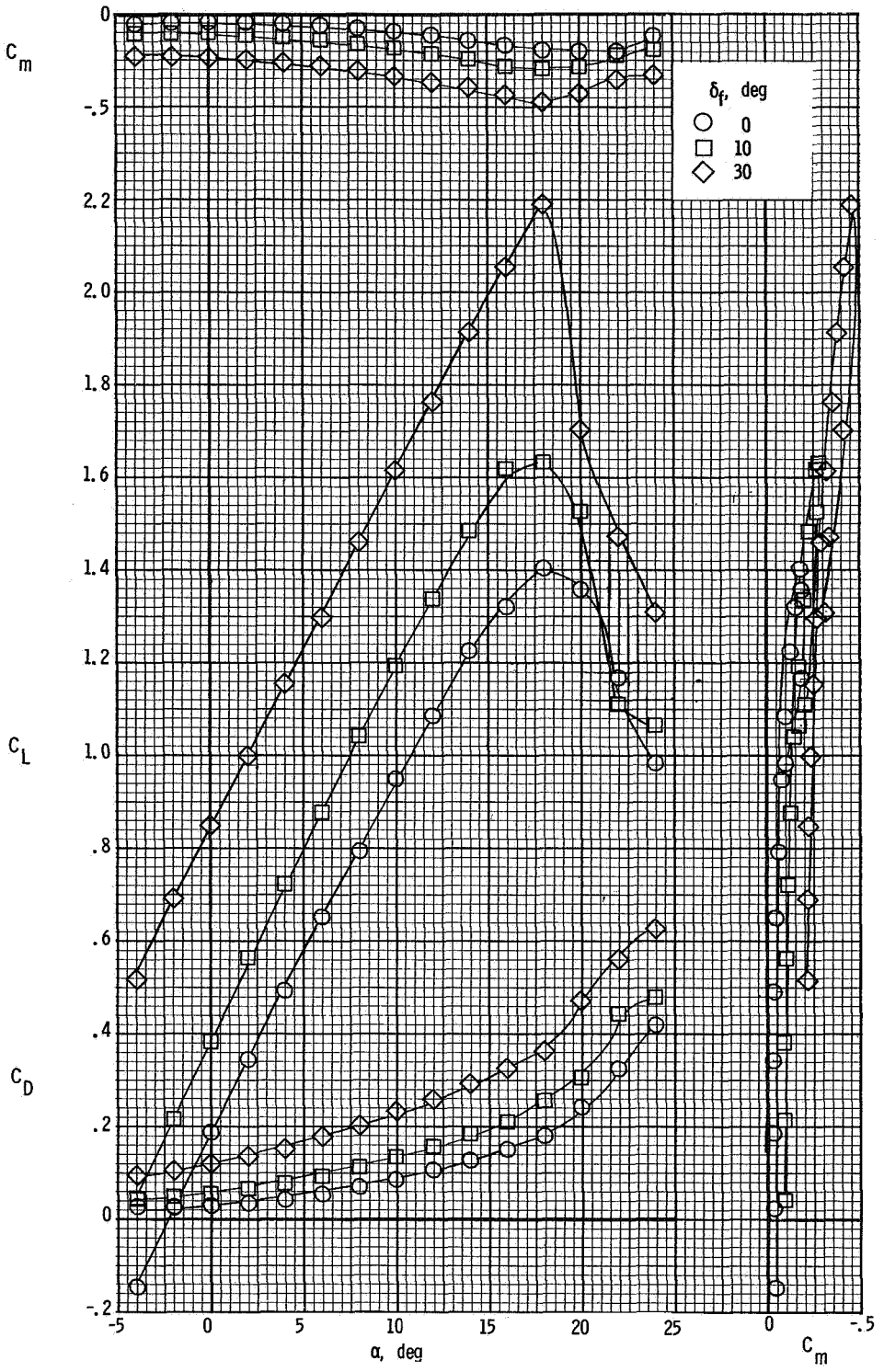

(a) $T_c' = 0$.

Figure 10.- Longitudinal aerodynamic characteristics of the airplane with horizontal tail removed.

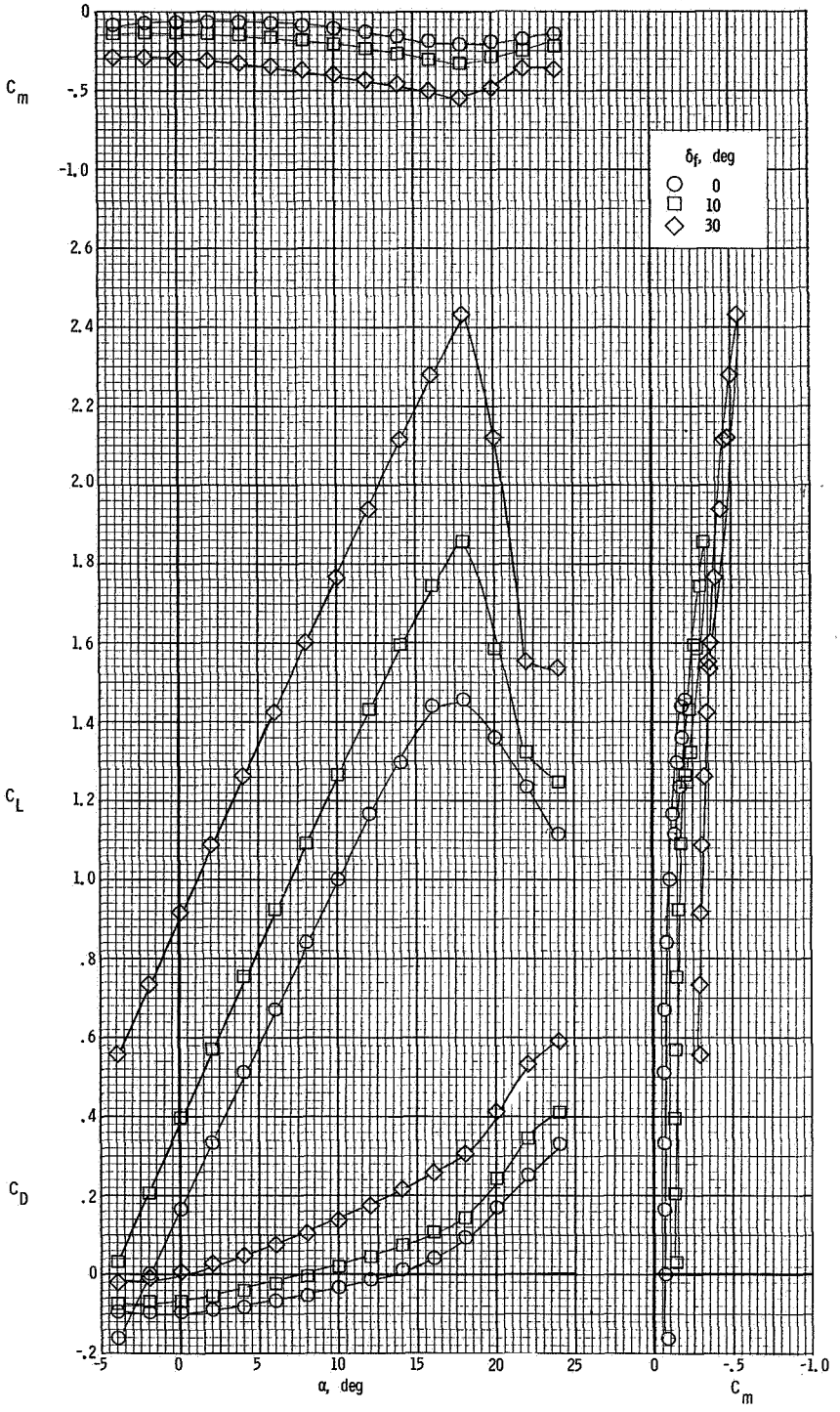

(b) $T_c' = 0.14$.

Figure 10.- Continued.

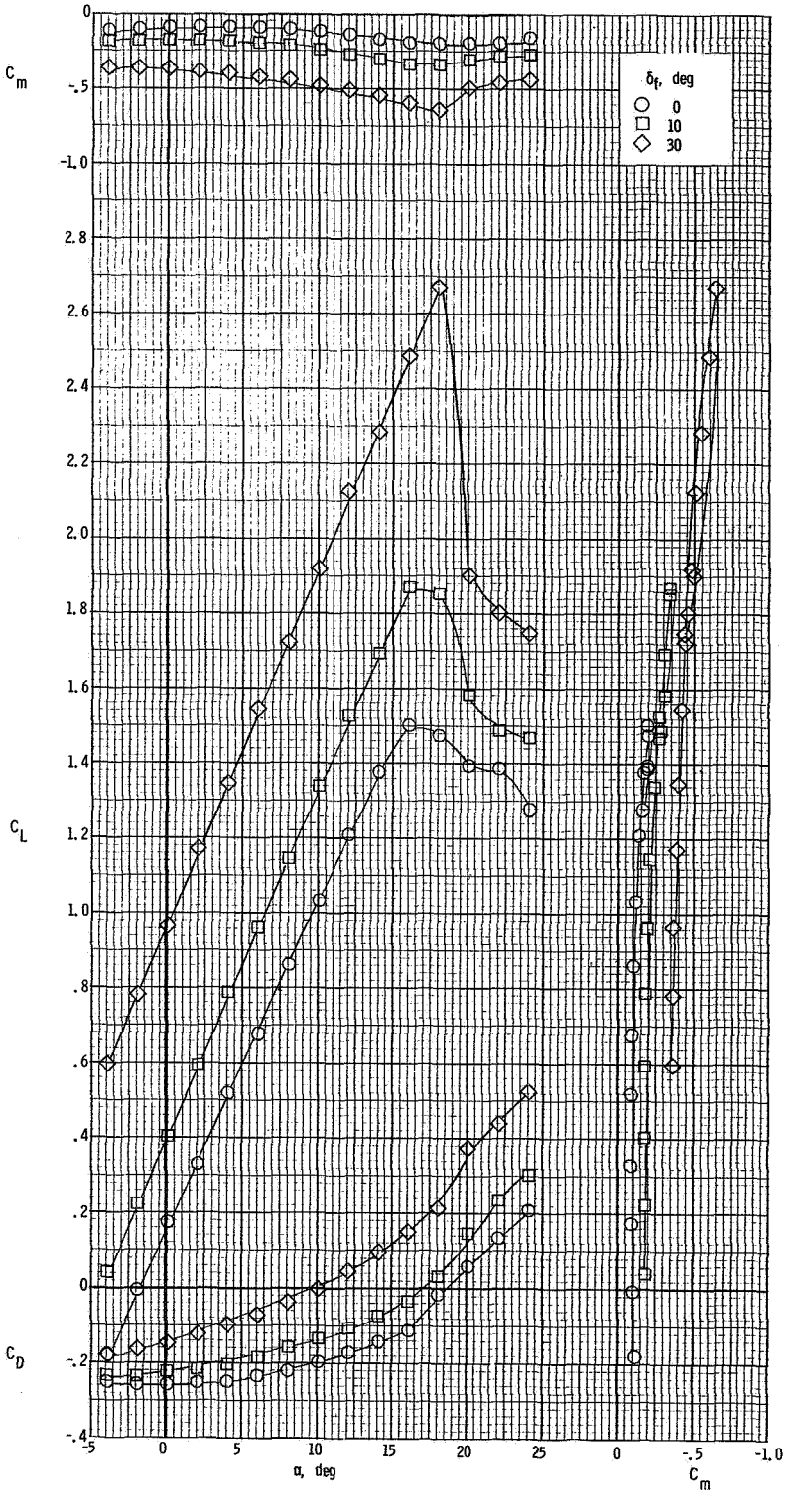

(c) $T'_C = 0.30$.

Figure 10.- Concluded.

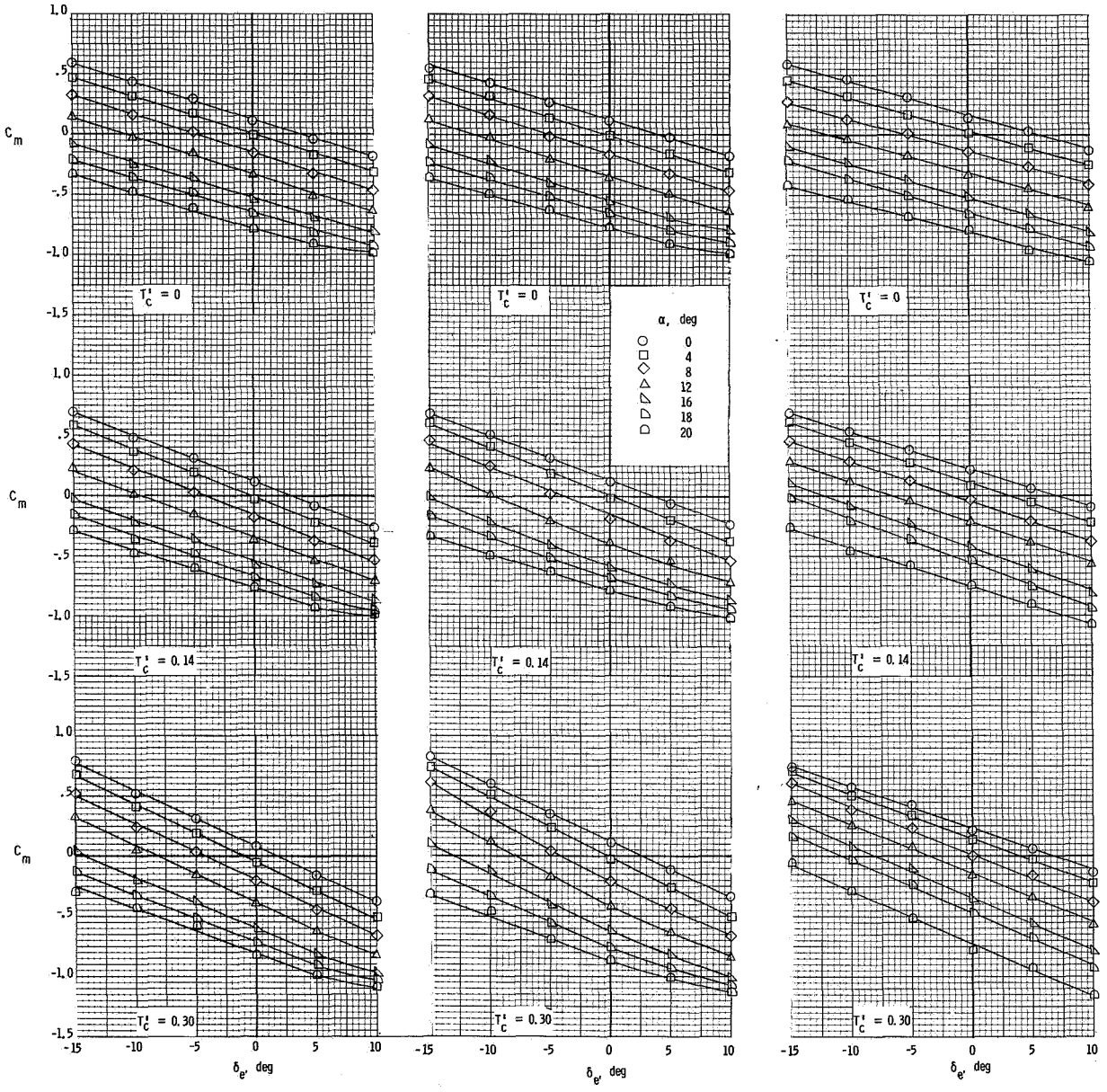

(a) $\delta_f = 0^o$. (b) $\delta_f = 10^o$. (c) $\delta_f = 30^o$.

Figure 11.- Variations of pitching-moment coefficient with elevator deflection for several power and flap deflections.

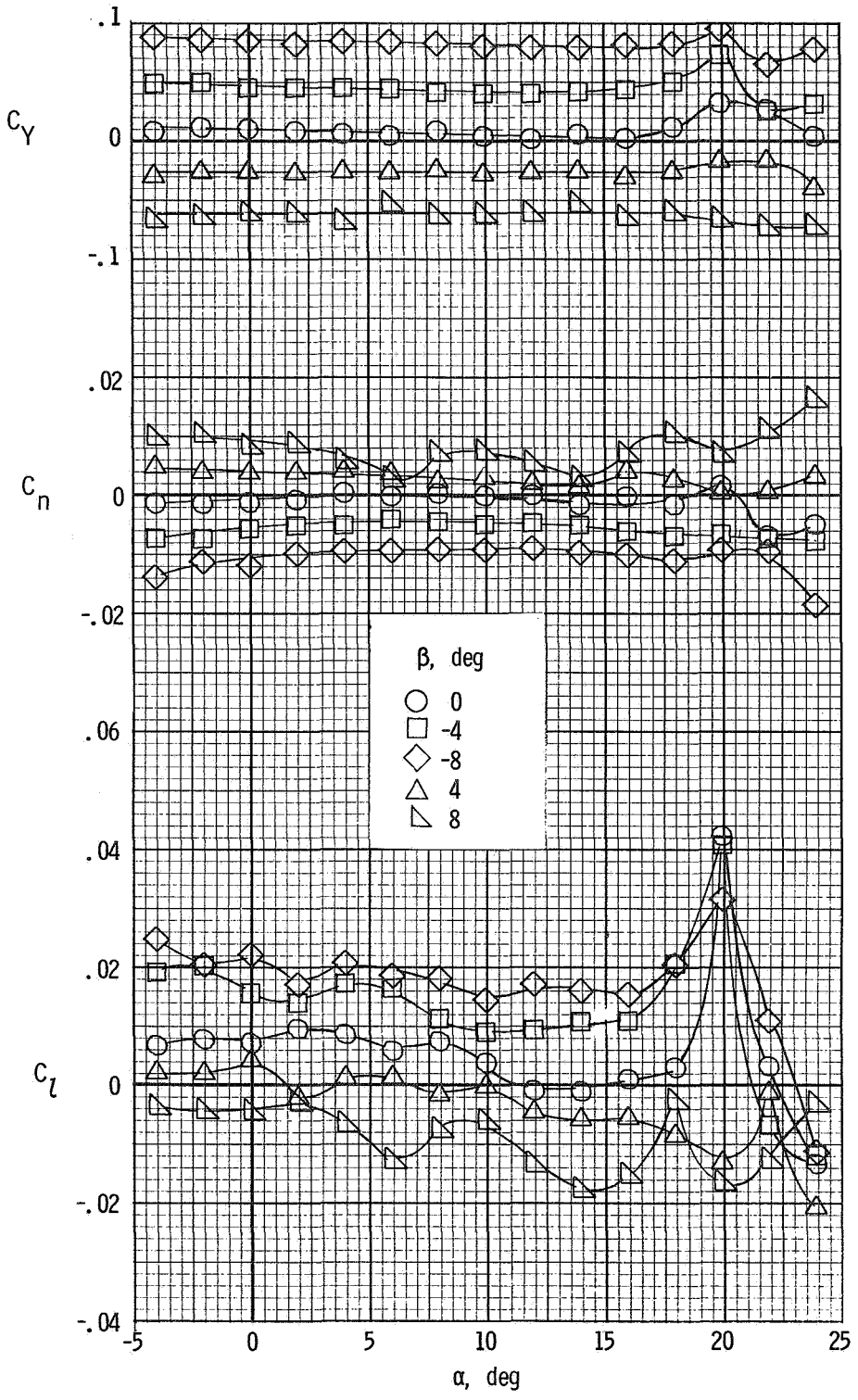

(a) $\delta_f = 0^o$.

Figure 12.- Lateral characteristics of the airplane with propeller removed for several flap deflections.

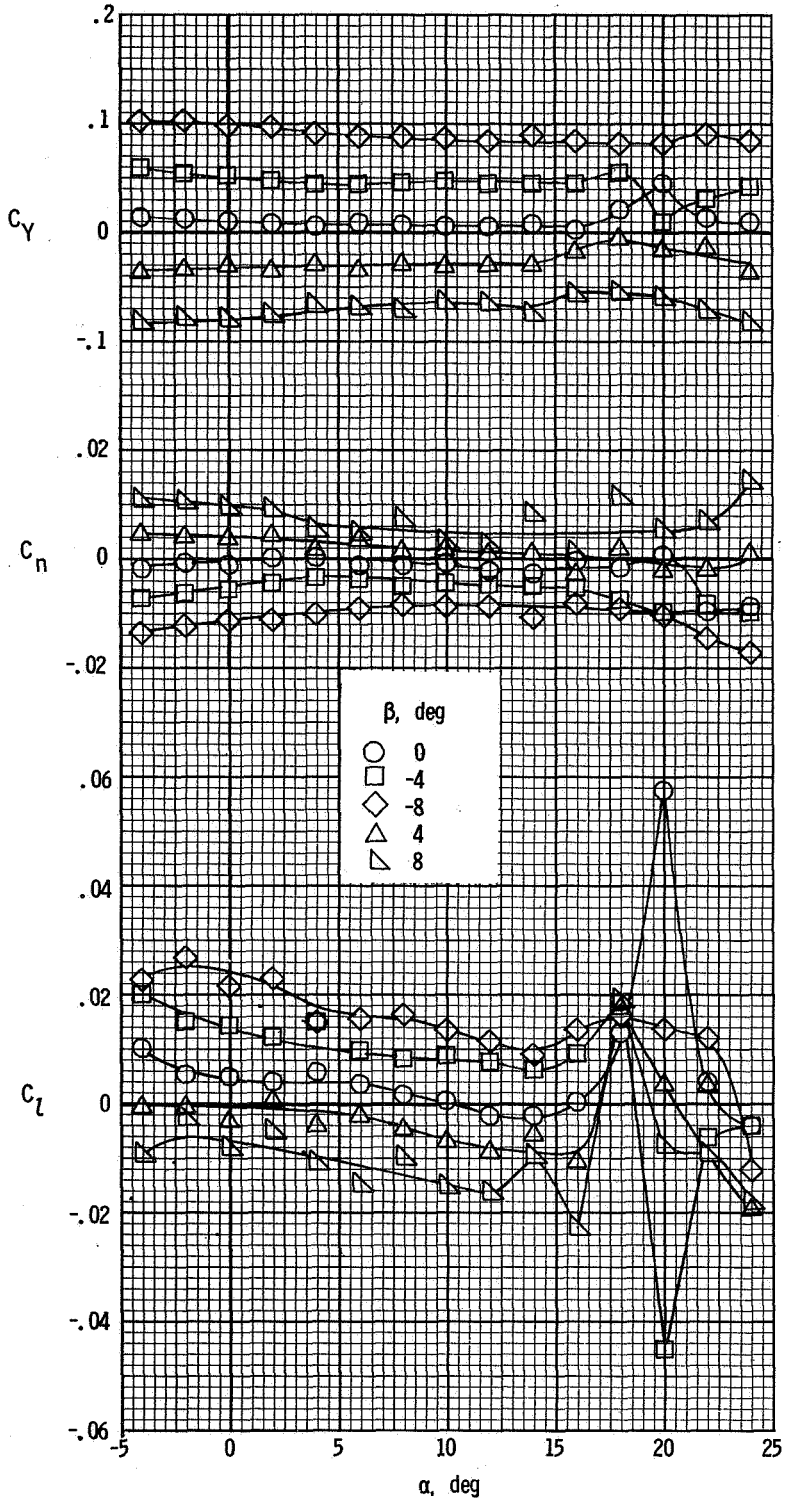

(b) $\delta_f = 10^o$.

Figure 12.- Continued.

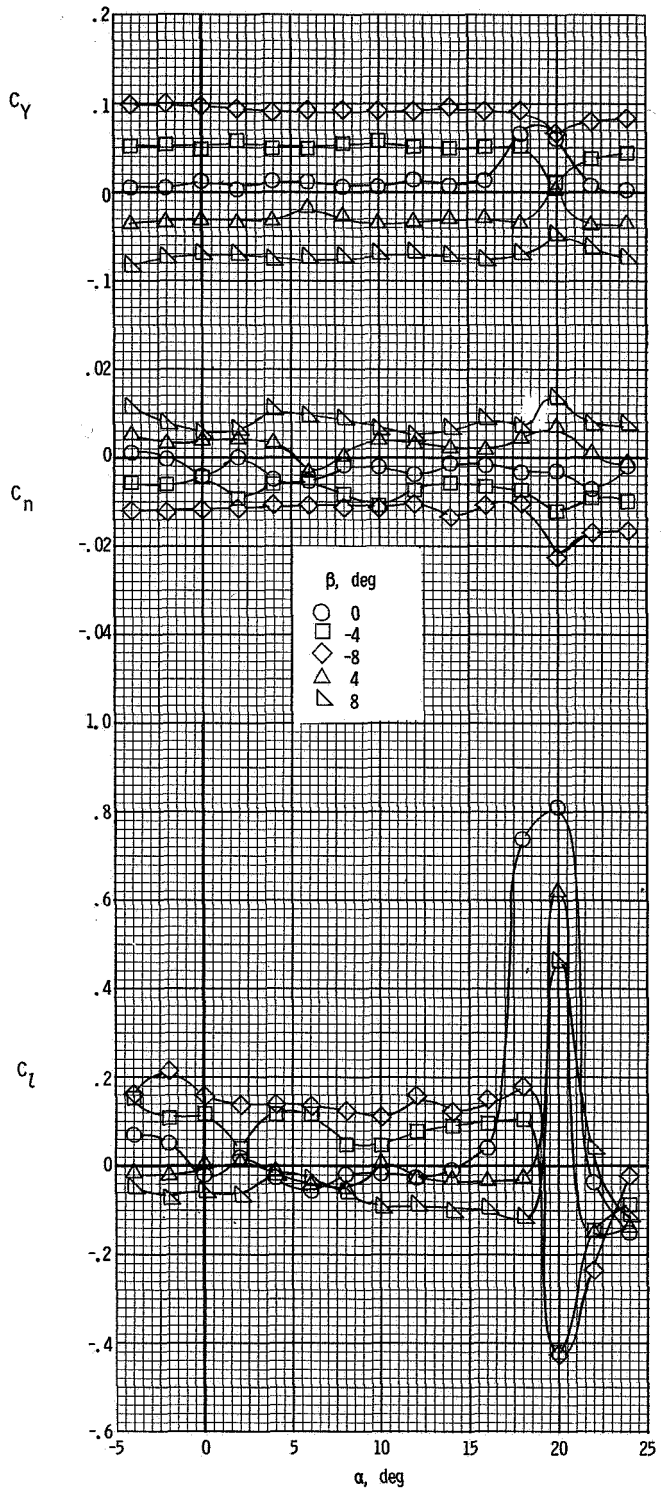

(c) $\delta_f = 30^o$.

Figure 12.- Concluded.

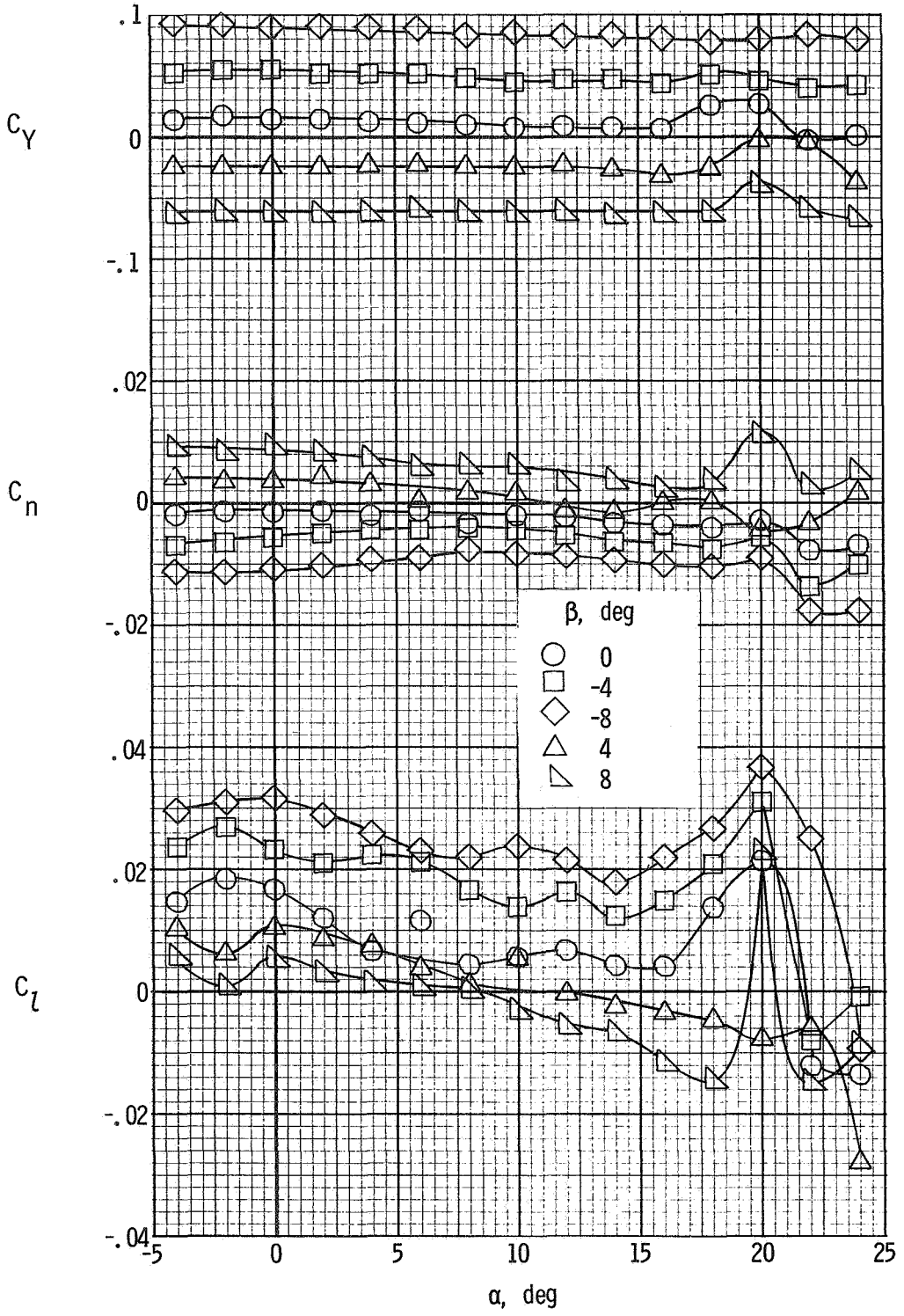

(a) $T_c' = 0$.

Figure 13.- Lateral characteristics of the airplane for several sideslip angles and thrust coefficients for $\delta_f = 0^o$.

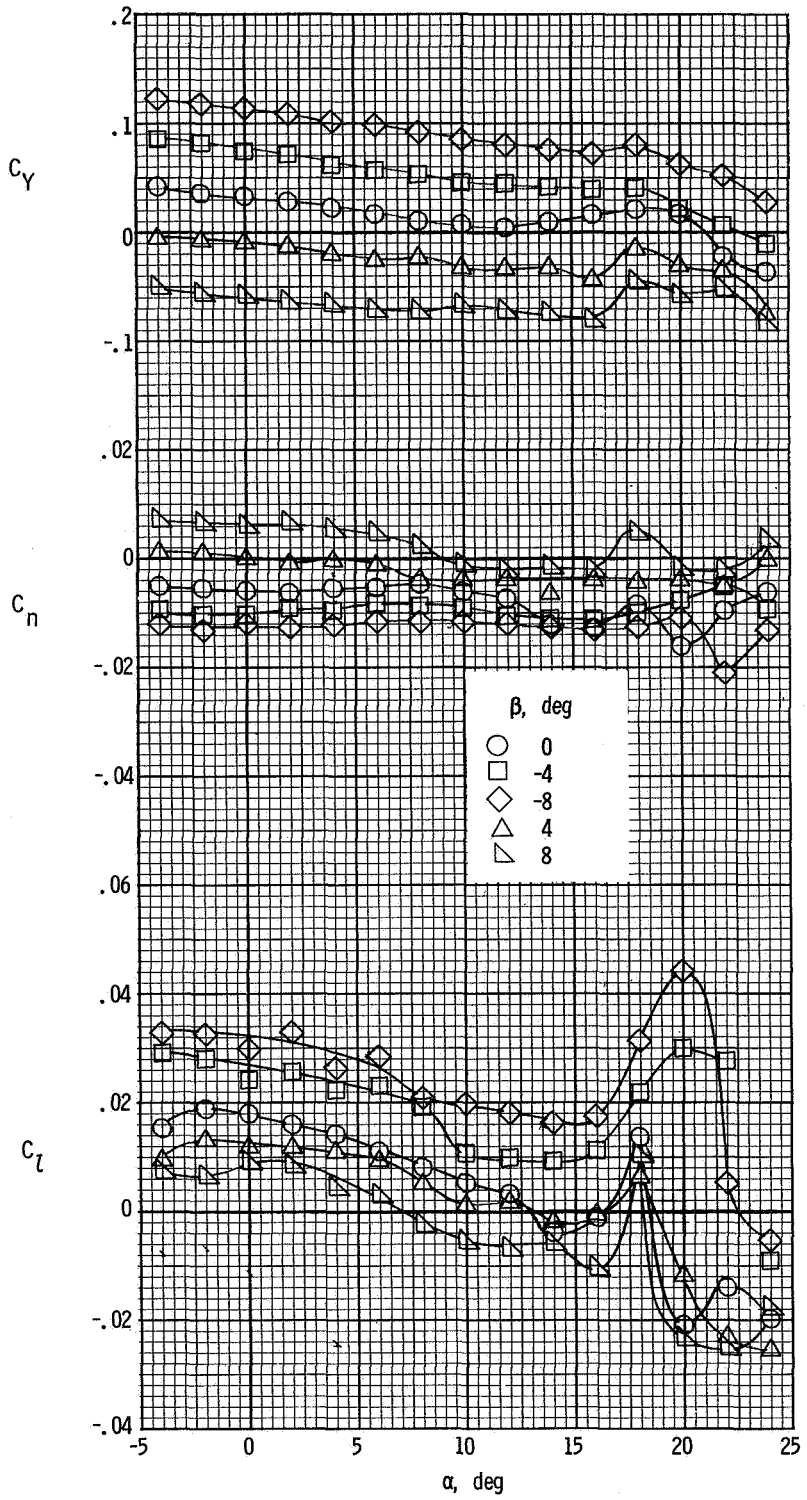

(b) $T_c' = 0.14$.

Figure 13.- Continued.

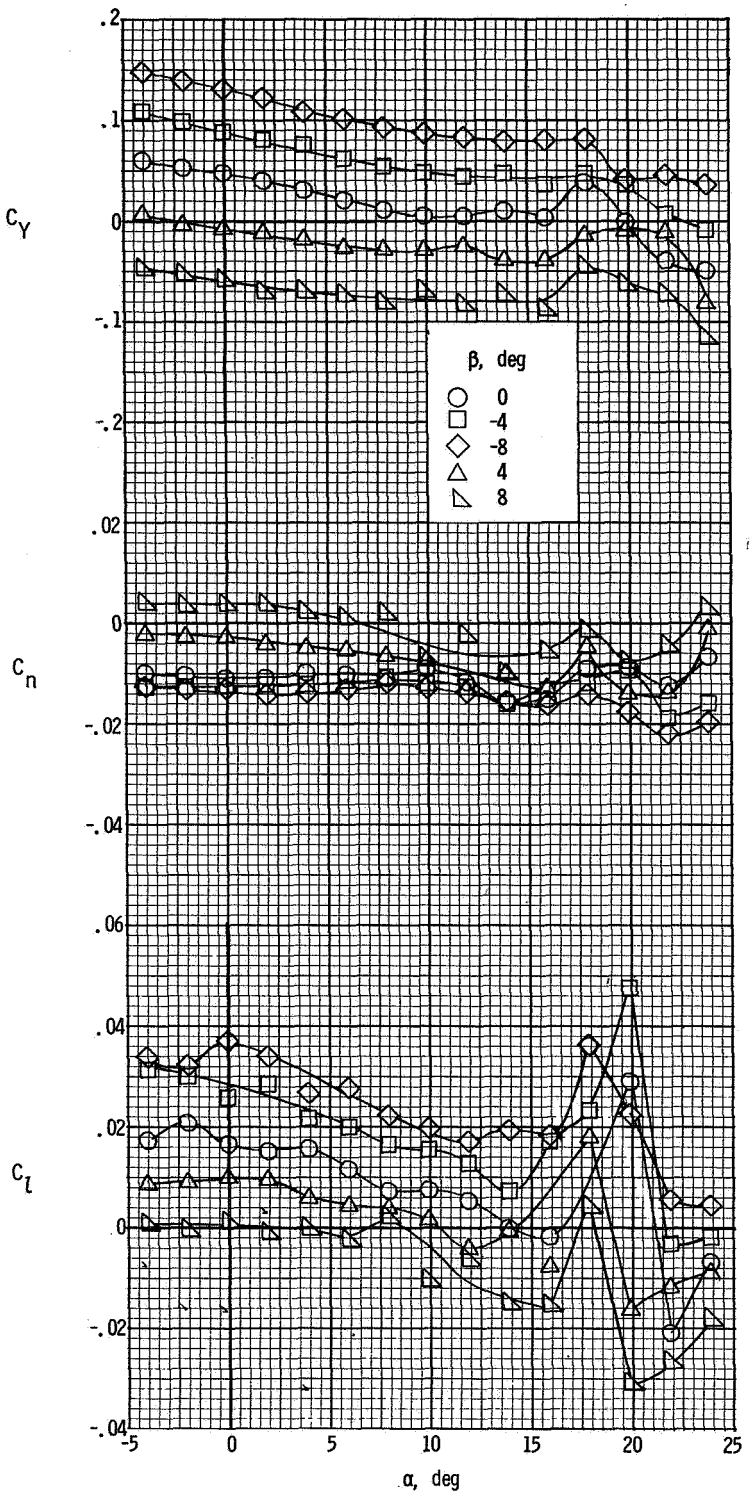

(c) $T'_C = 0.30$.

Figure 13.- Concluded.

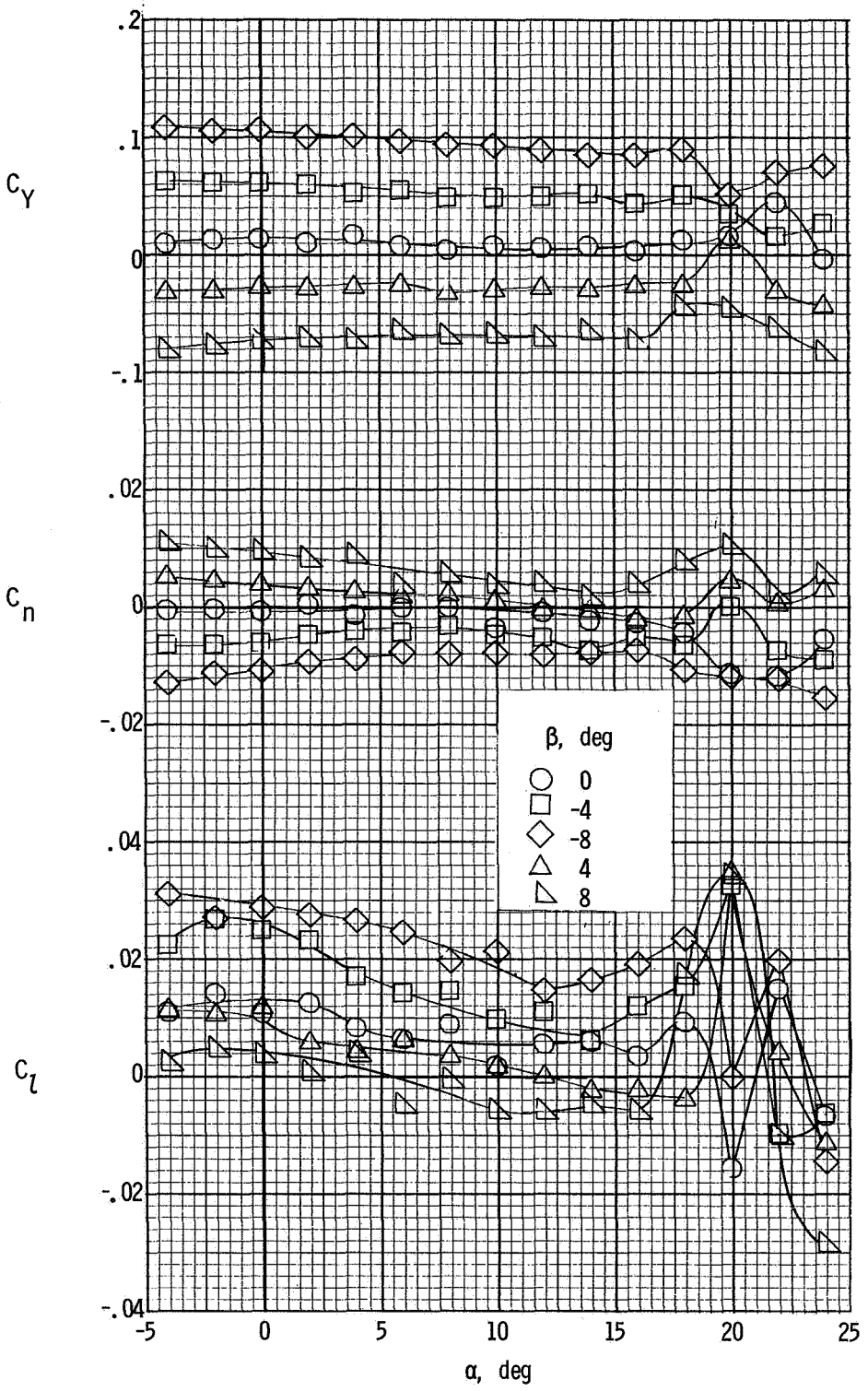

(a) $T_c' = 0$.

Figure 14.- Lateral characteristics of the airplane for several sideslip angles and thrust coefficients for $\delta_f = 10^o$.

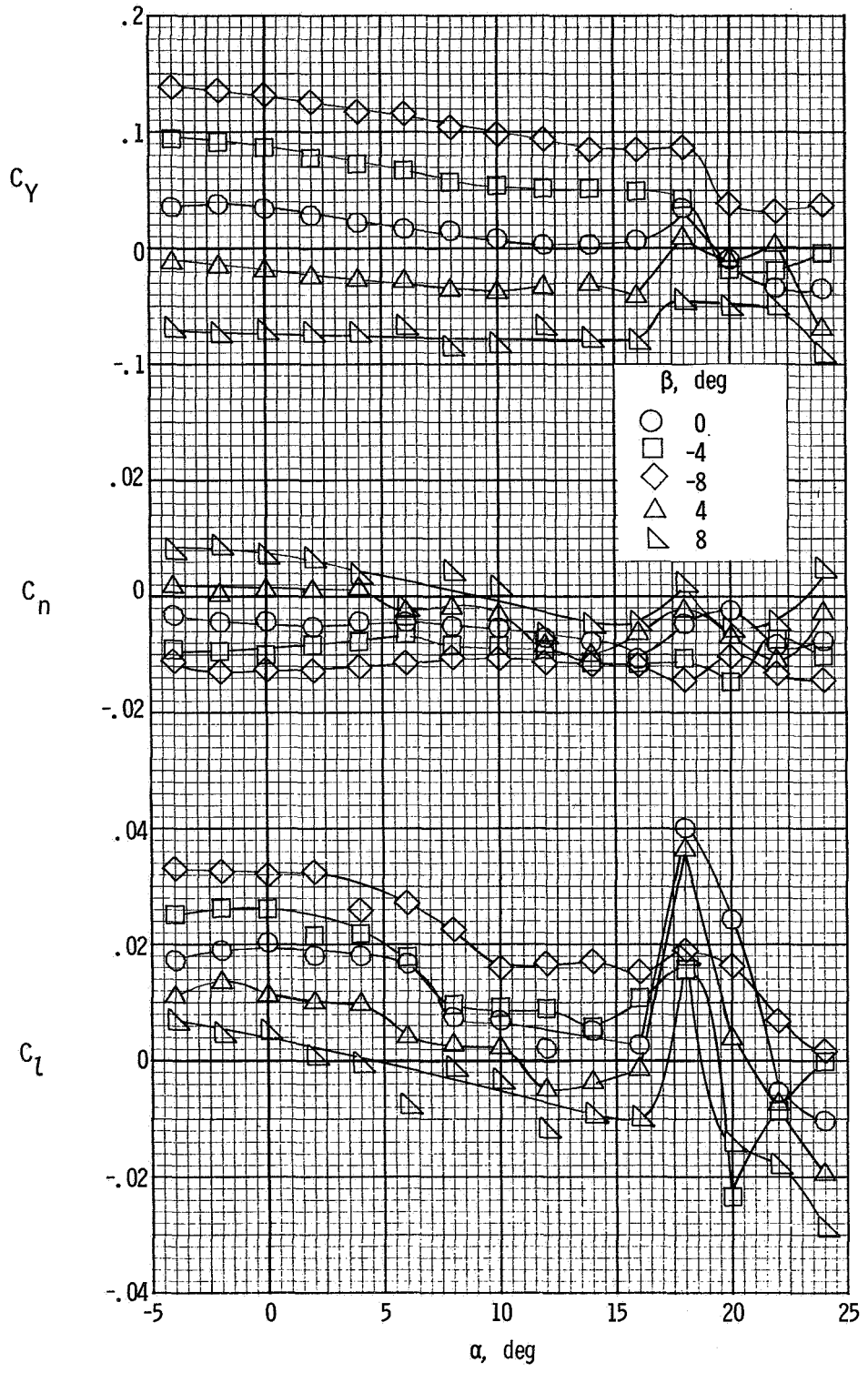

(b) $T'_c = 0.14$.

Figure 14.- Continued.

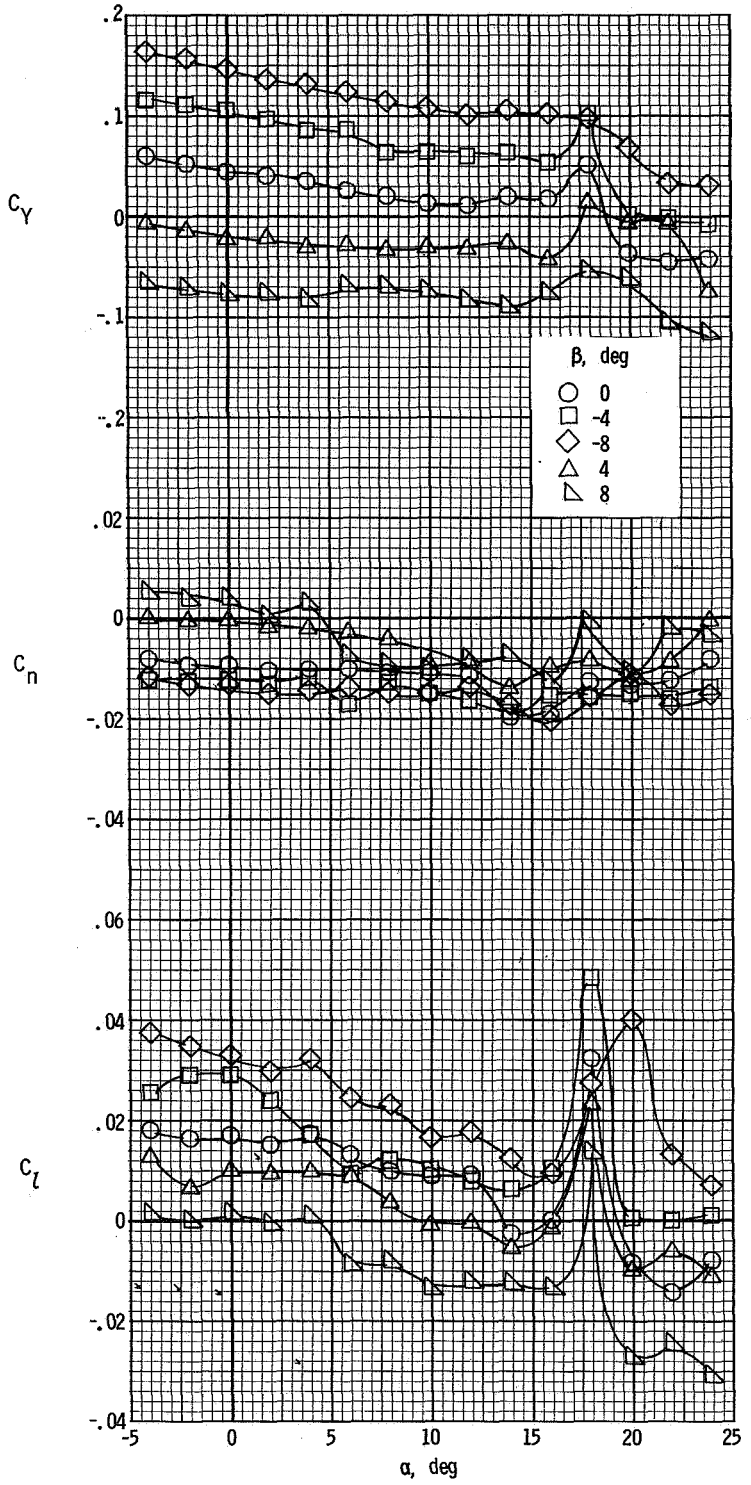

(c) $T'_c = 0.30$.

Figure 14.- Concluded.

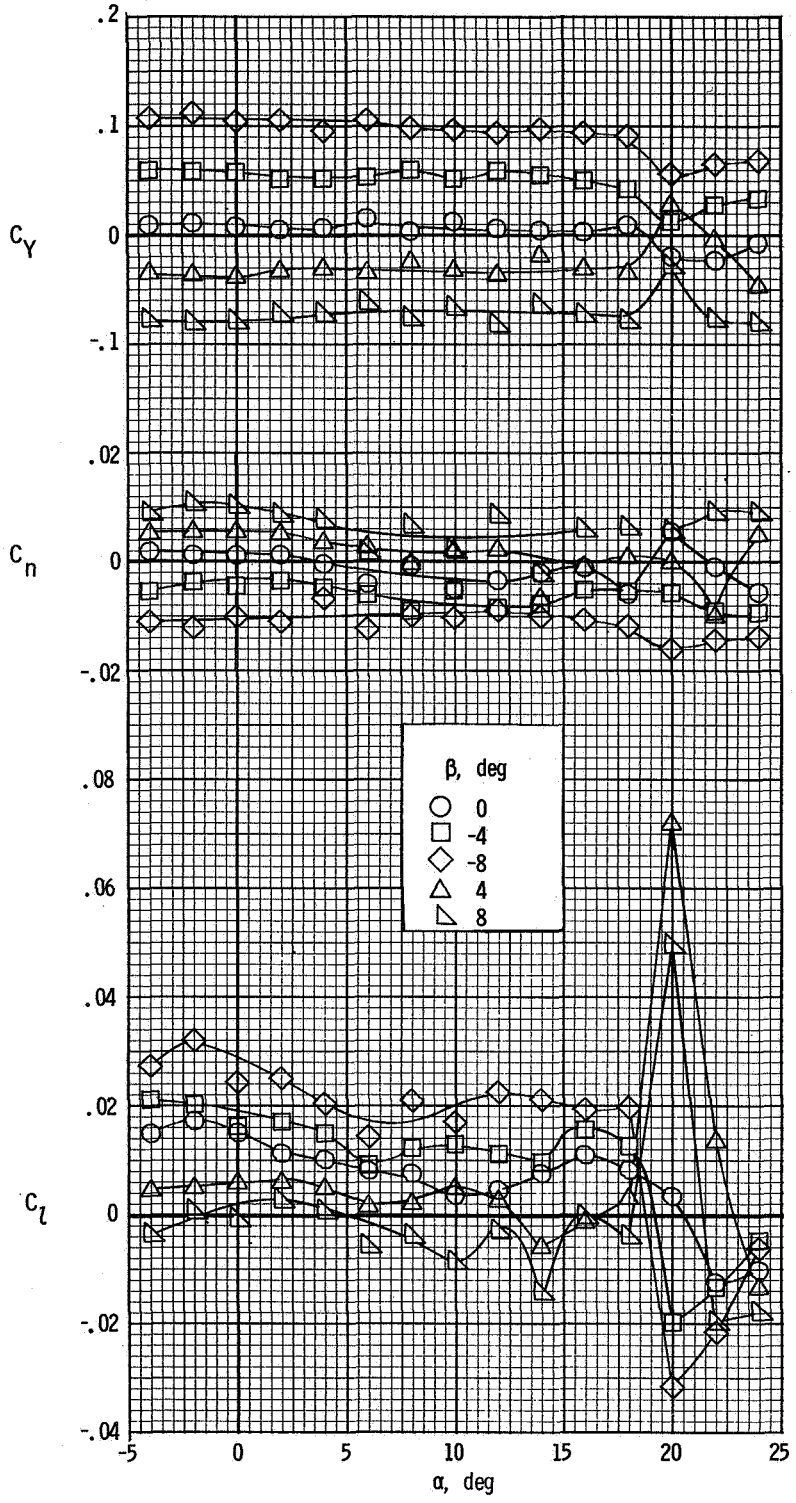

(a) $T_c' = 0$.

Figure 15.- Lateral characteristics of the airplane for several sideslip angles and thrust coefficients for $\delta_f = 30^o$.

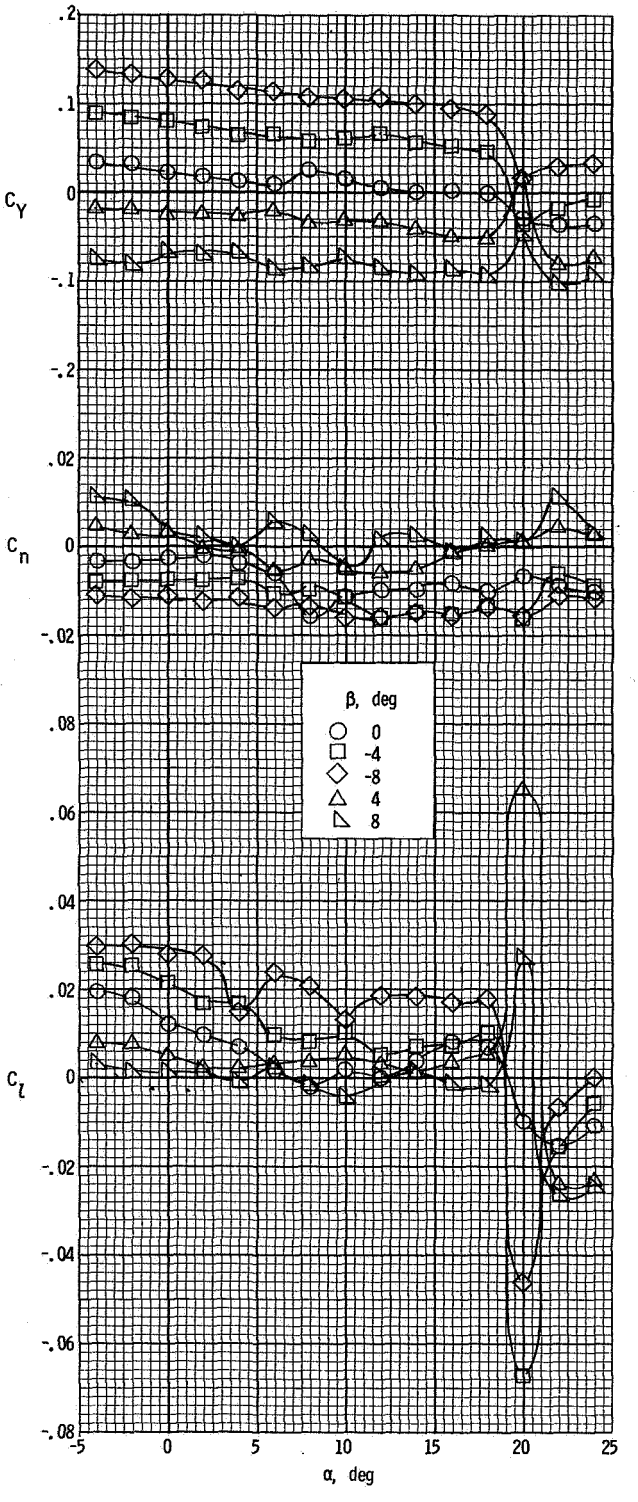

(b) $T'_c = 0.14$.

Figure 15.- Continued.

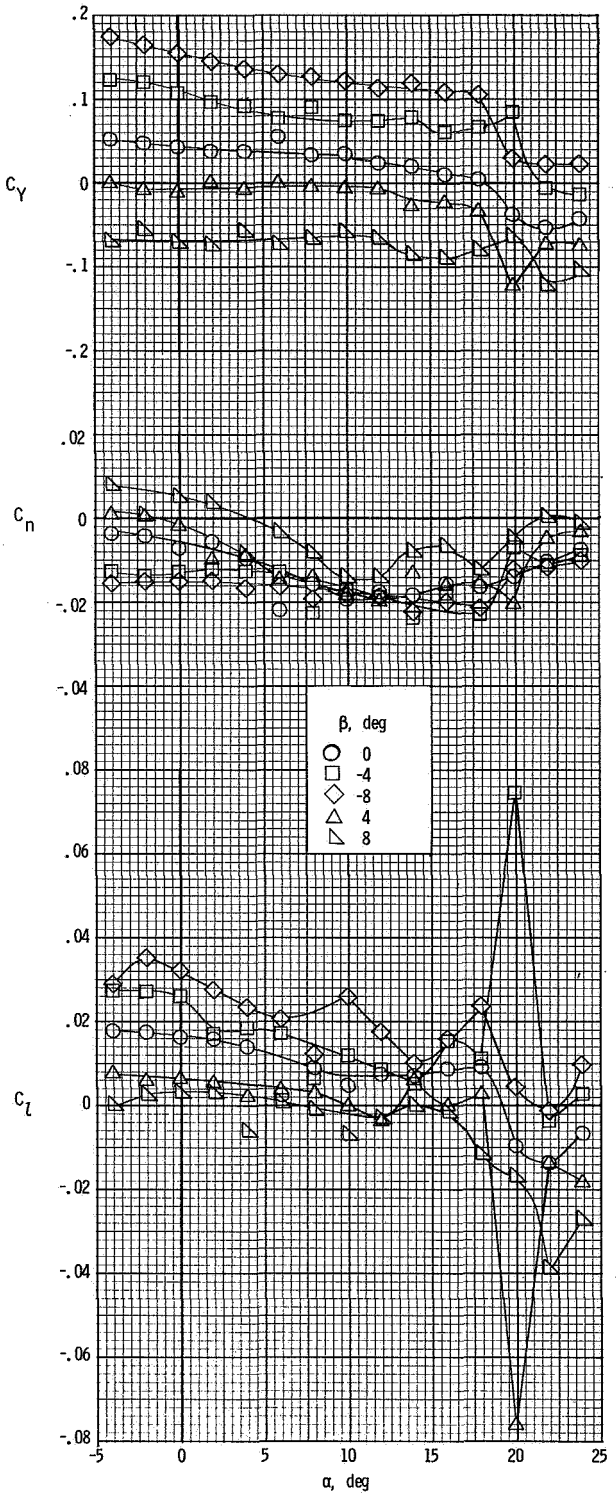

(c) $T'_c = 0.30$.

Figure 15.- Concluded.

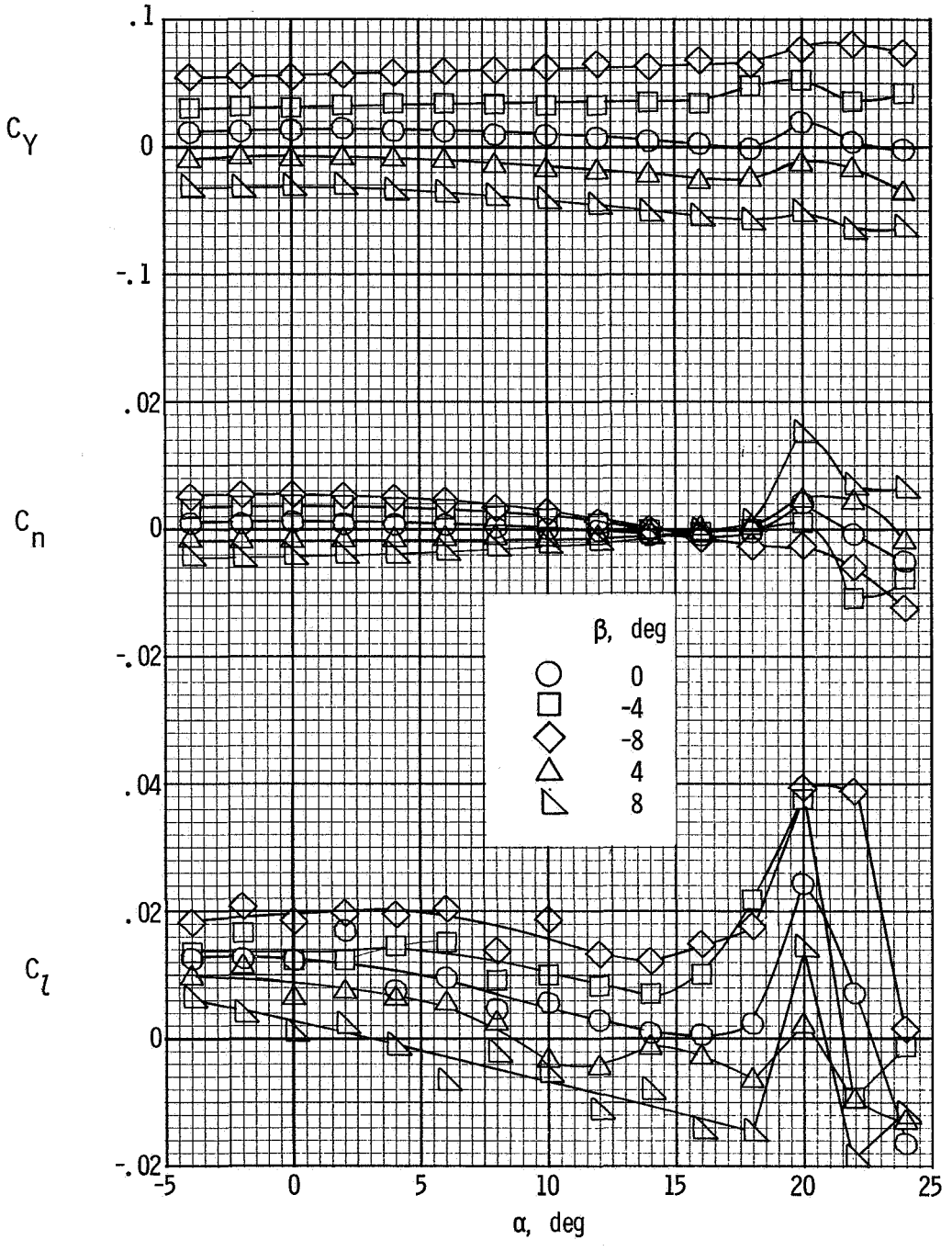

(a) $T'_c = 0$.

Figure 16.- Lateral characteristics of the airplane with the vertical tail removed for $\delta_f = 0^o$.

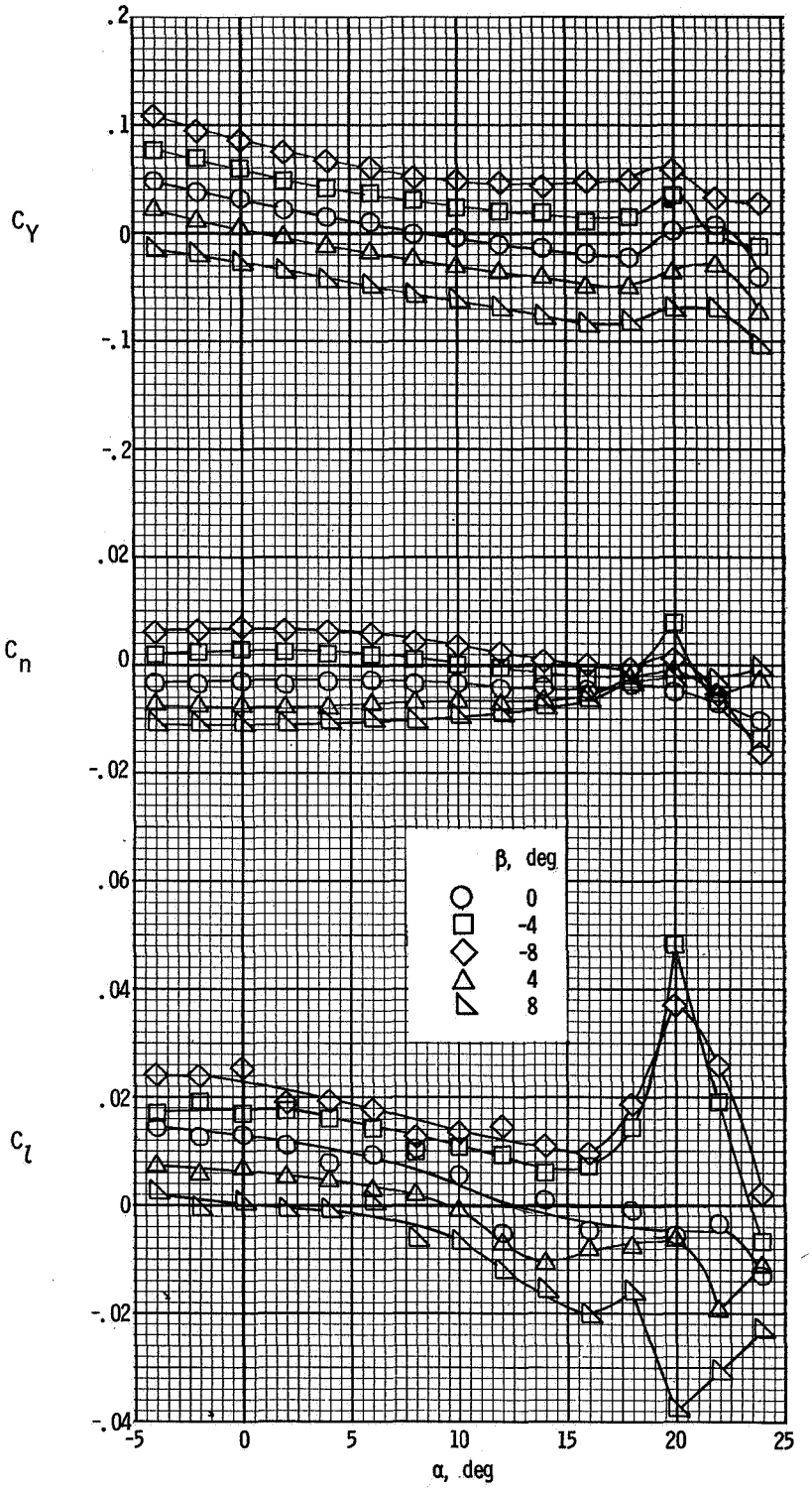

(b) $T_c' = 0.30$.

Figure 16.- Concluded.

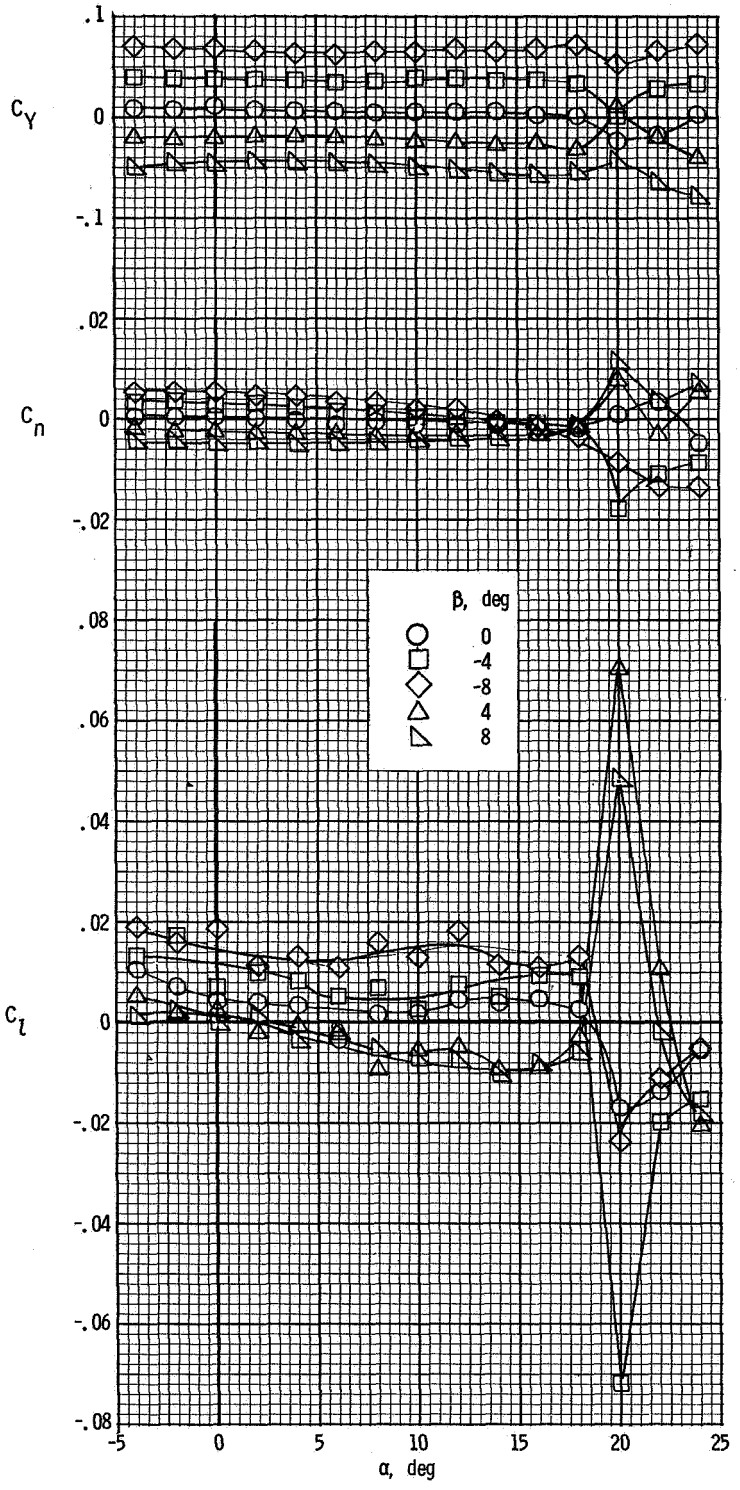

(a) $T'_c = 0$.

Figure 17.- Lateral characteristics of the airplane with the vertical tail removed for $\delta_f = 30^o$.

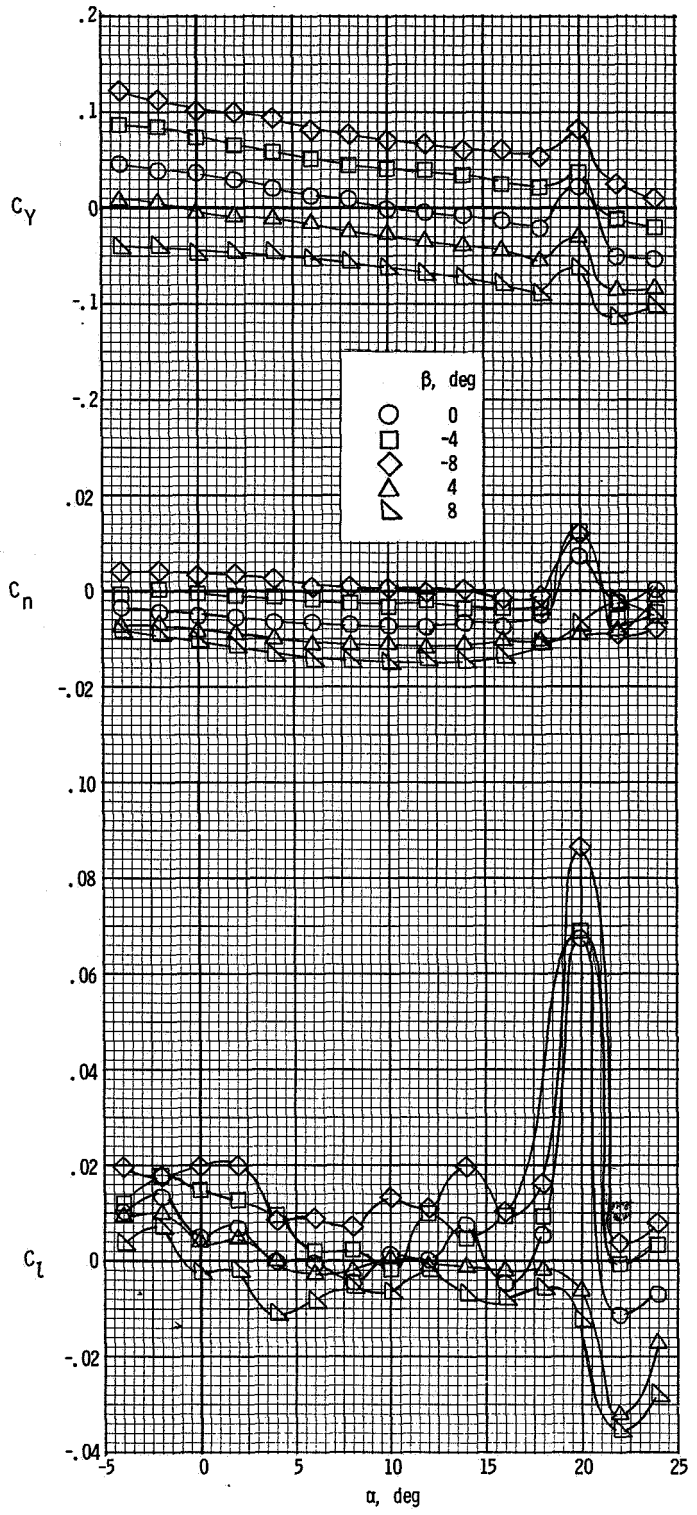

(b) $T_c' = 0.30$.

Figure 17.- Concluded.

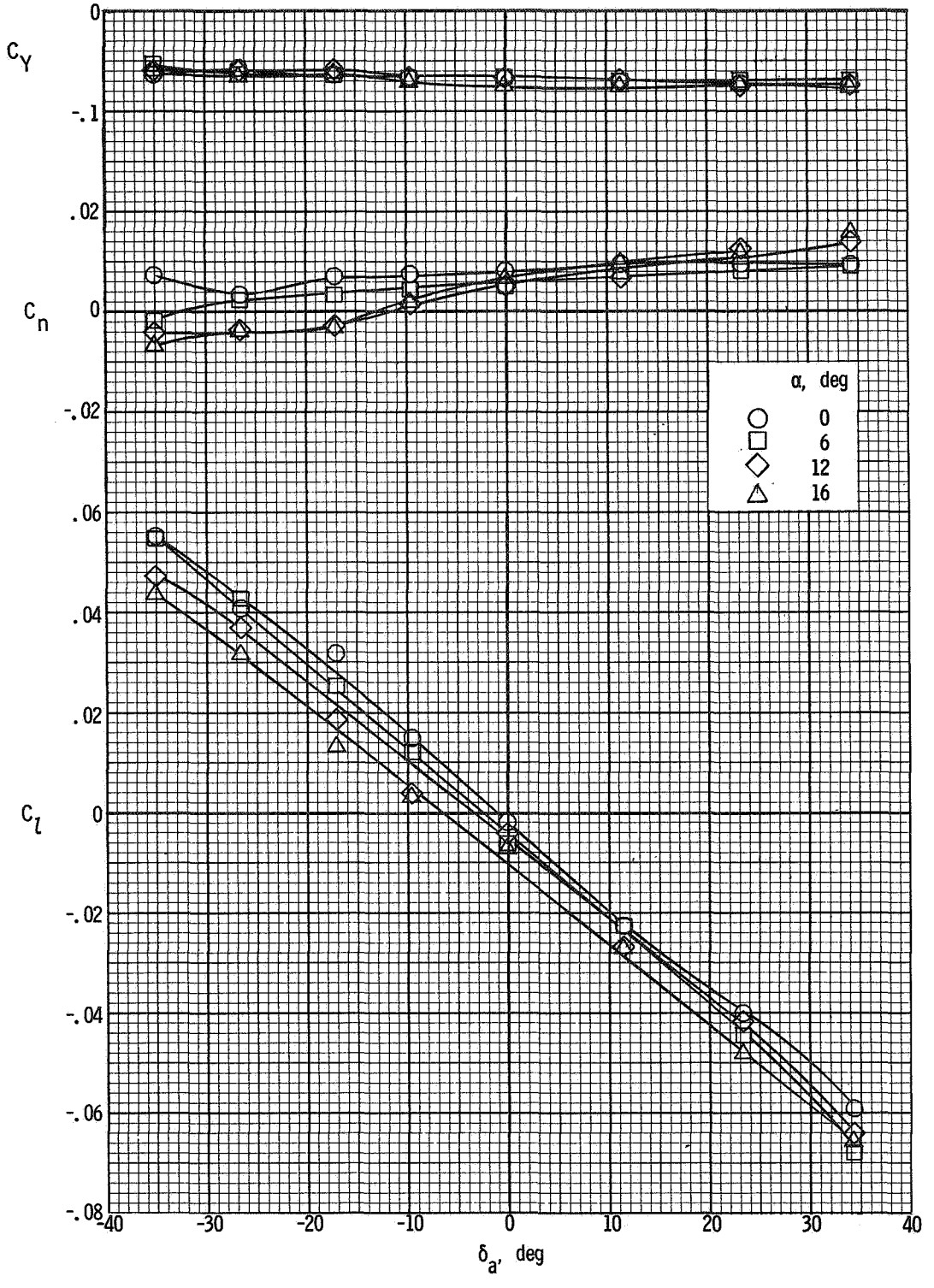

(a) $\beta = 8^{o}$.

Figure 18.- Variation of the lateral characteristics of the airplane with aileron deflection. $\delta_f = 0^{o}$; $T_c' = 0$.

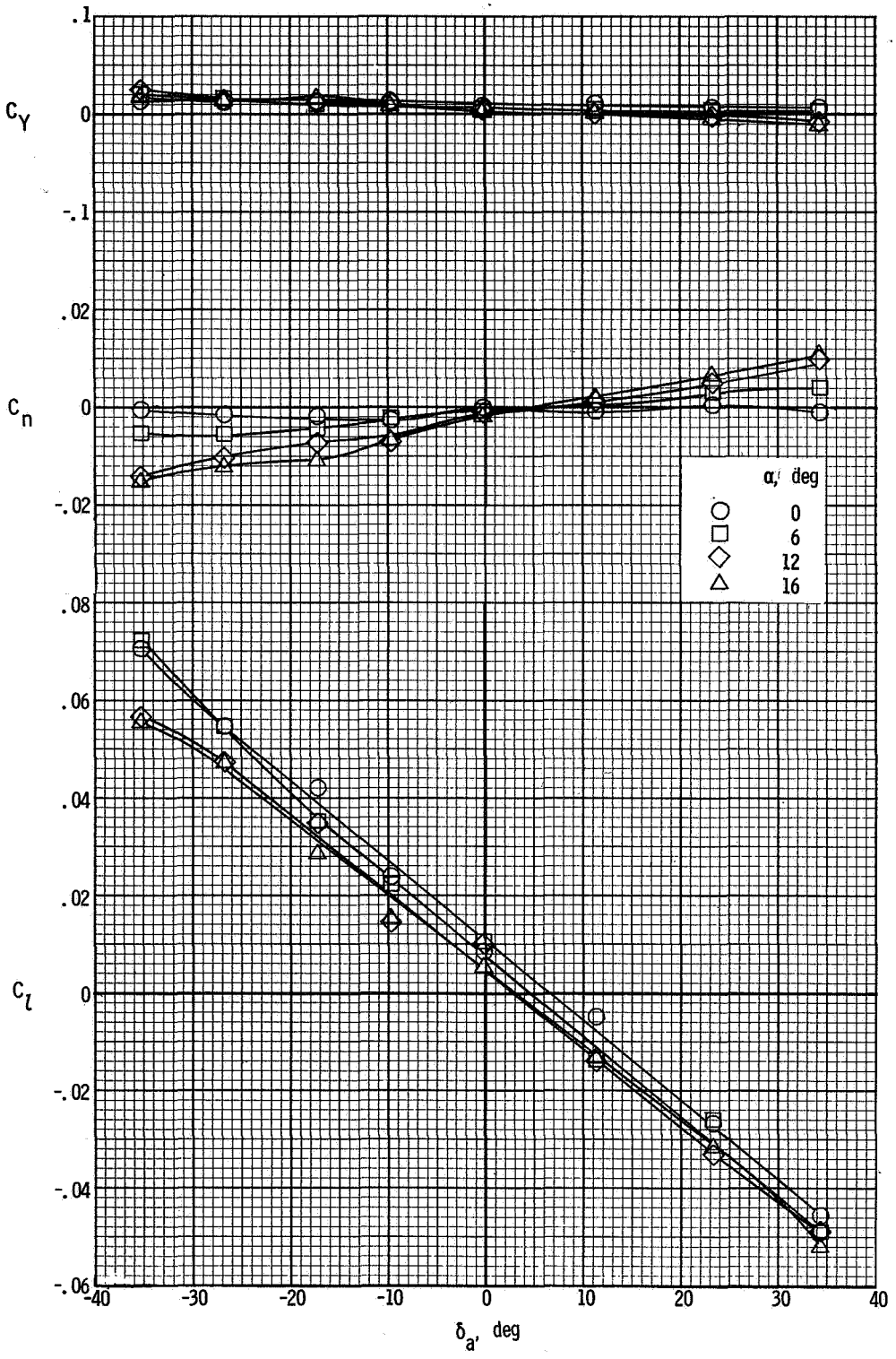

(b) $\beta = 0^o$.

Figure 18.- Continued.

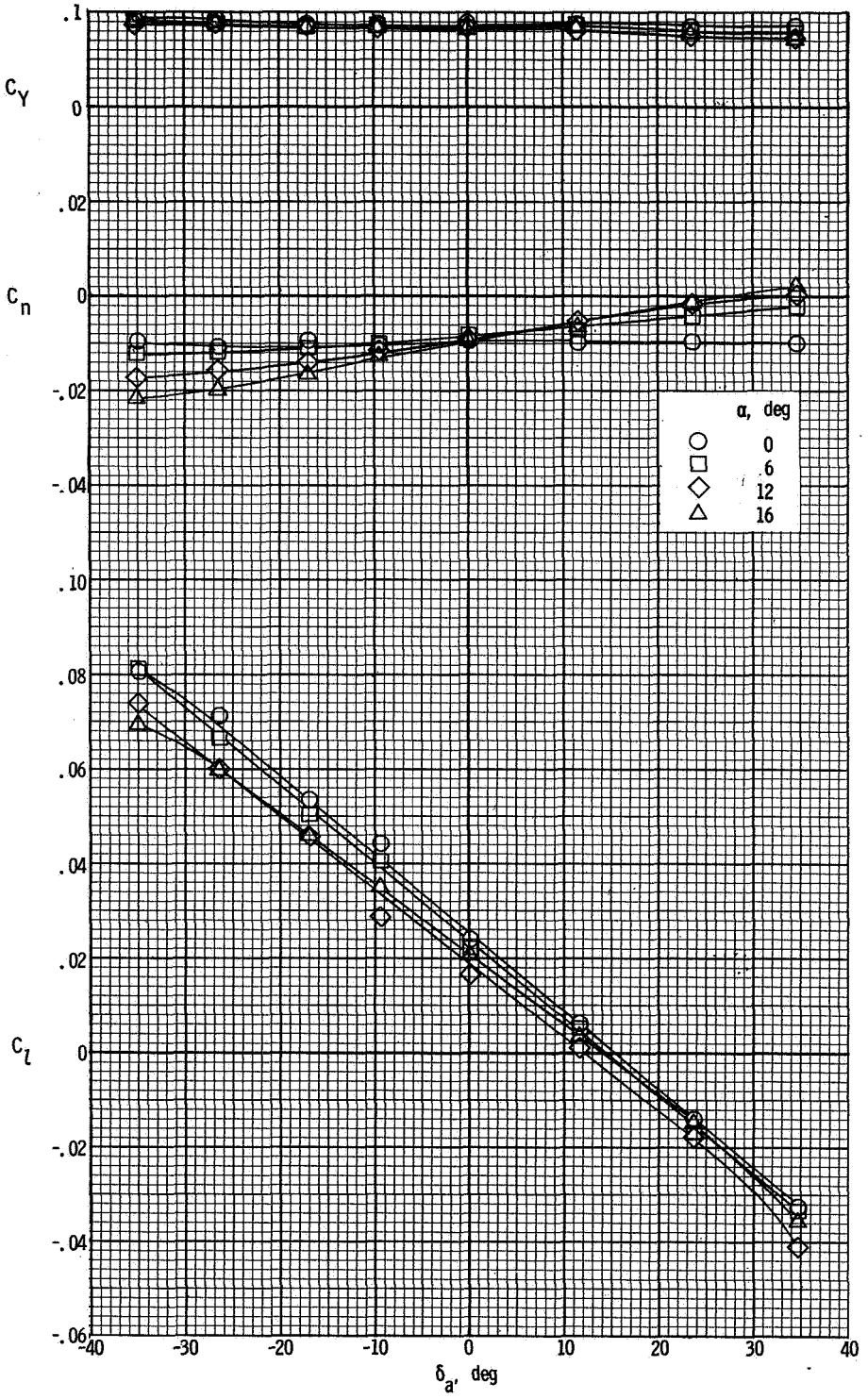

(c) $\beta = -8^{o}$.

Figure 18.- Concluded.

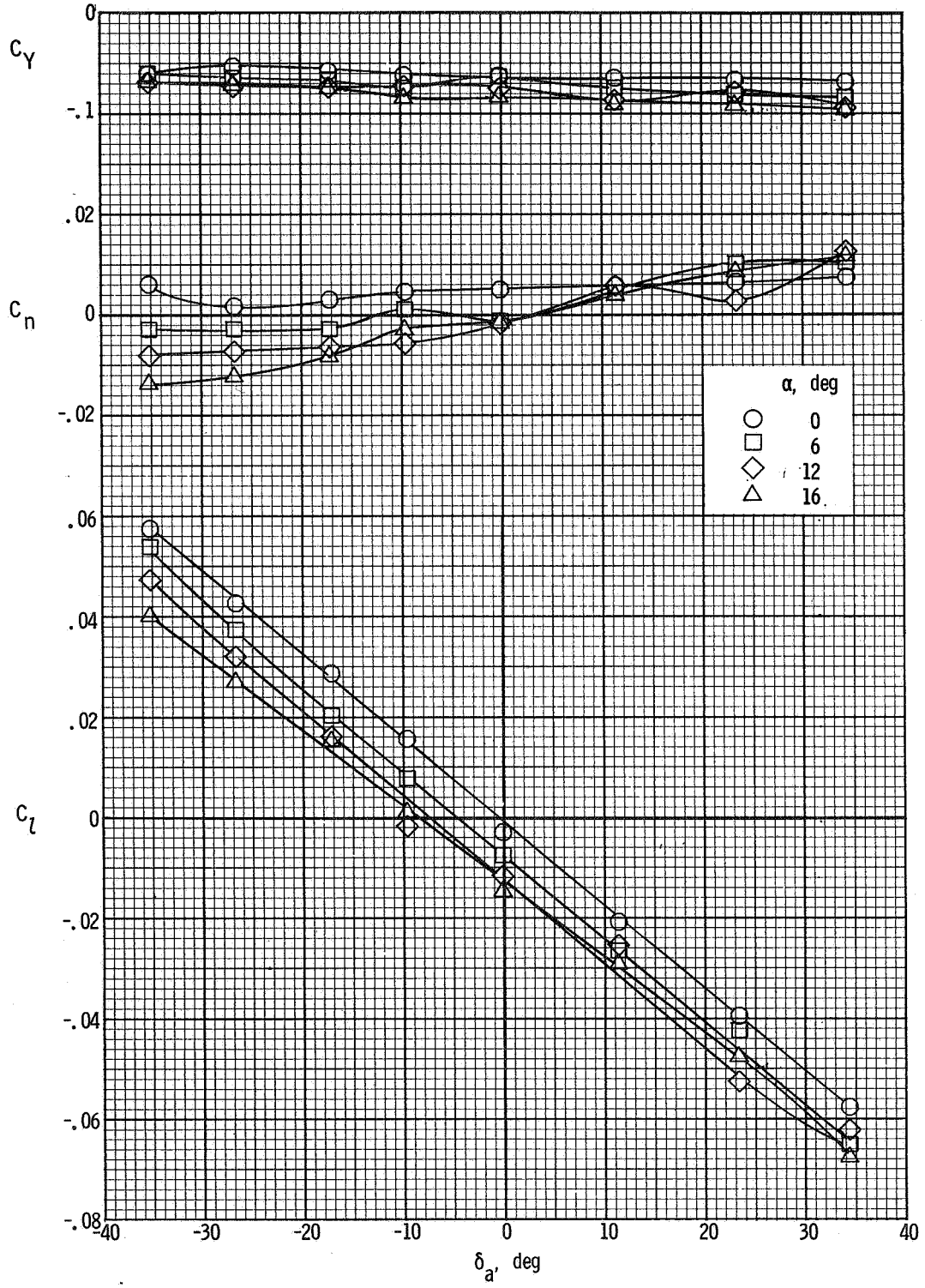

(a) $\beta = 8^o$.

Figure 19.- Variation of the lateral characteristics of the airplane with aileron deflection. $\delta_f = 0^o$; $T_c' = 0.14$.

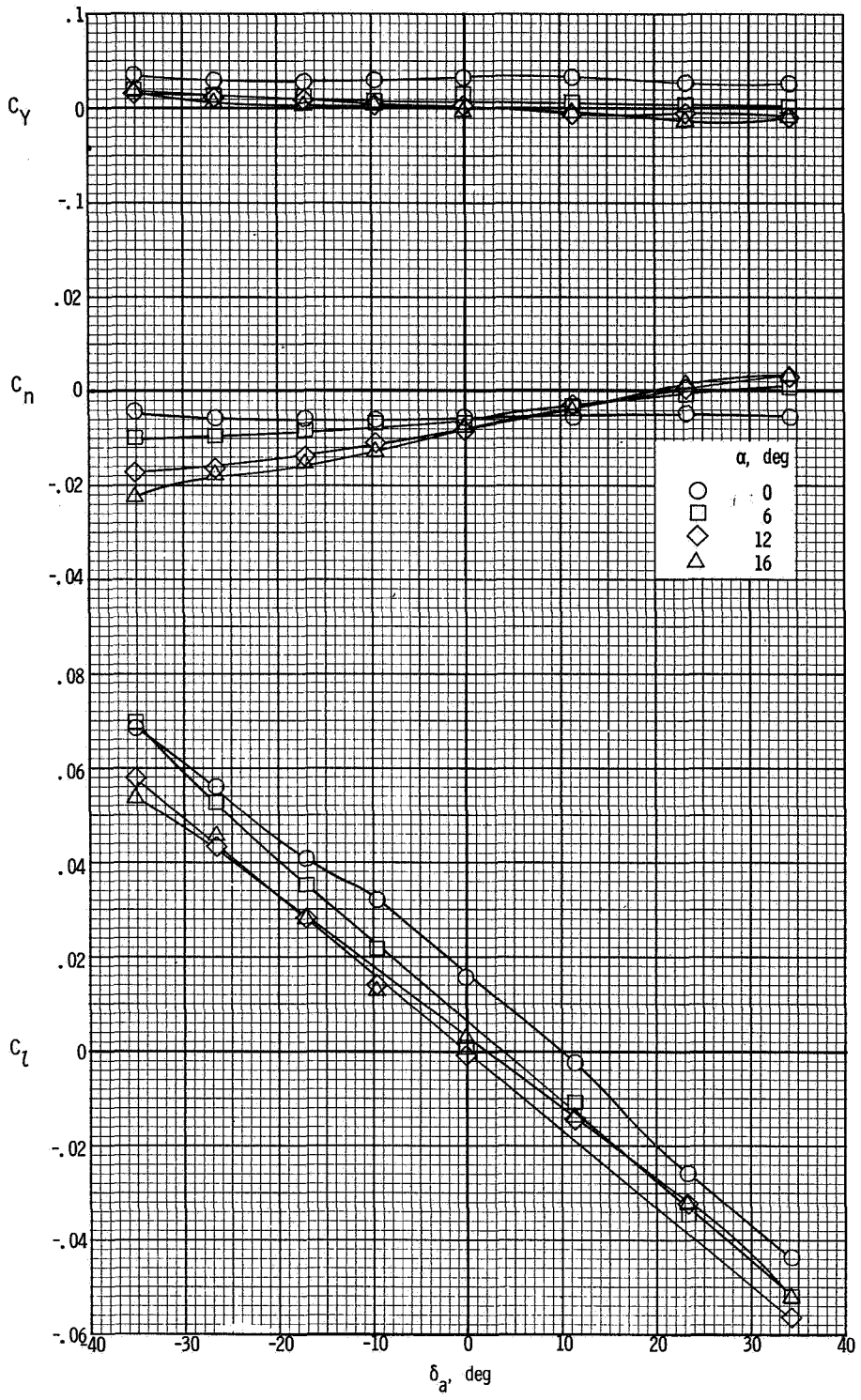

(b) $\beta = 0^o$.

Figure 19.- Continued.

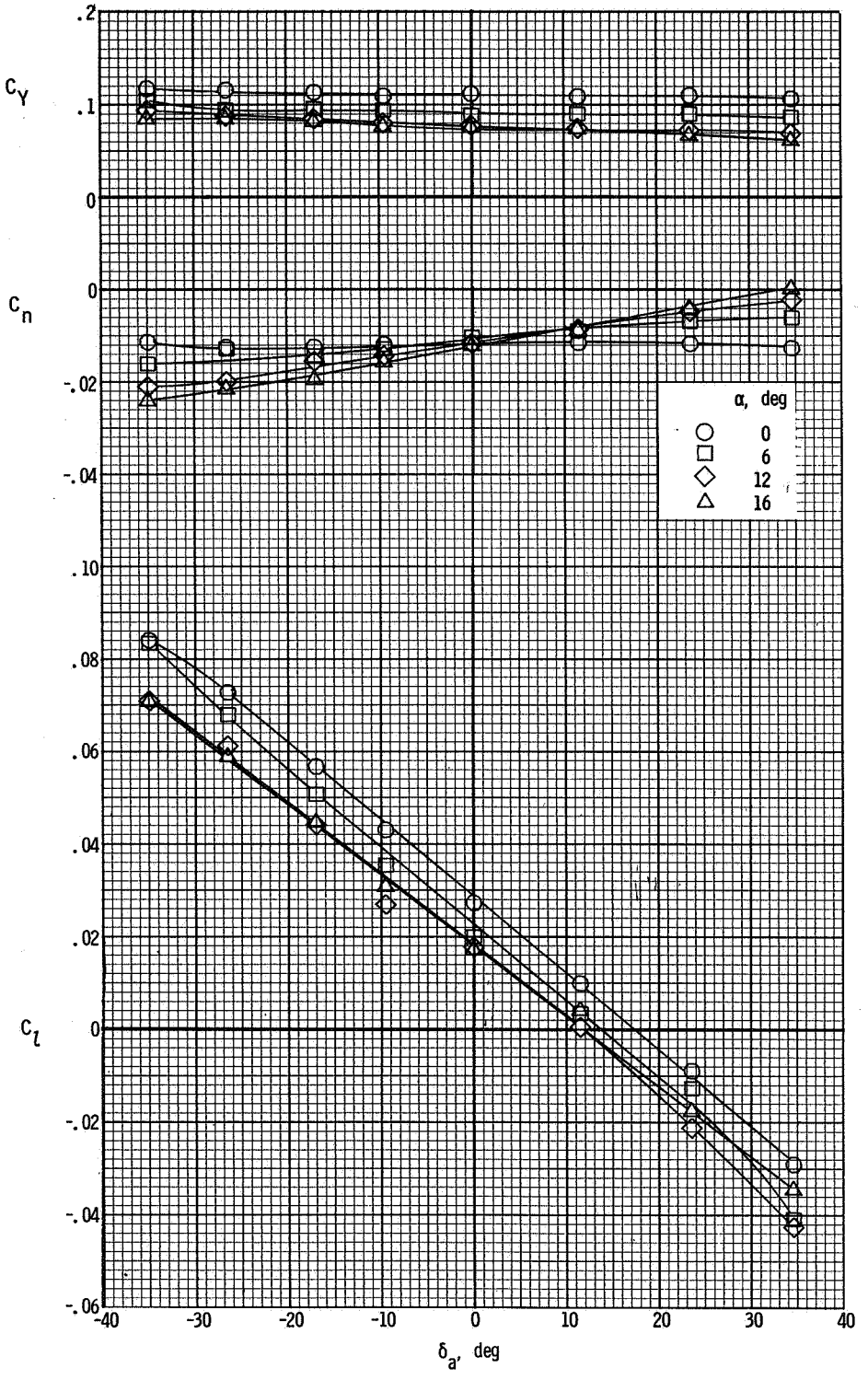

(c) $\beta = -8^{o}$.

Figure 19.- Concluded.

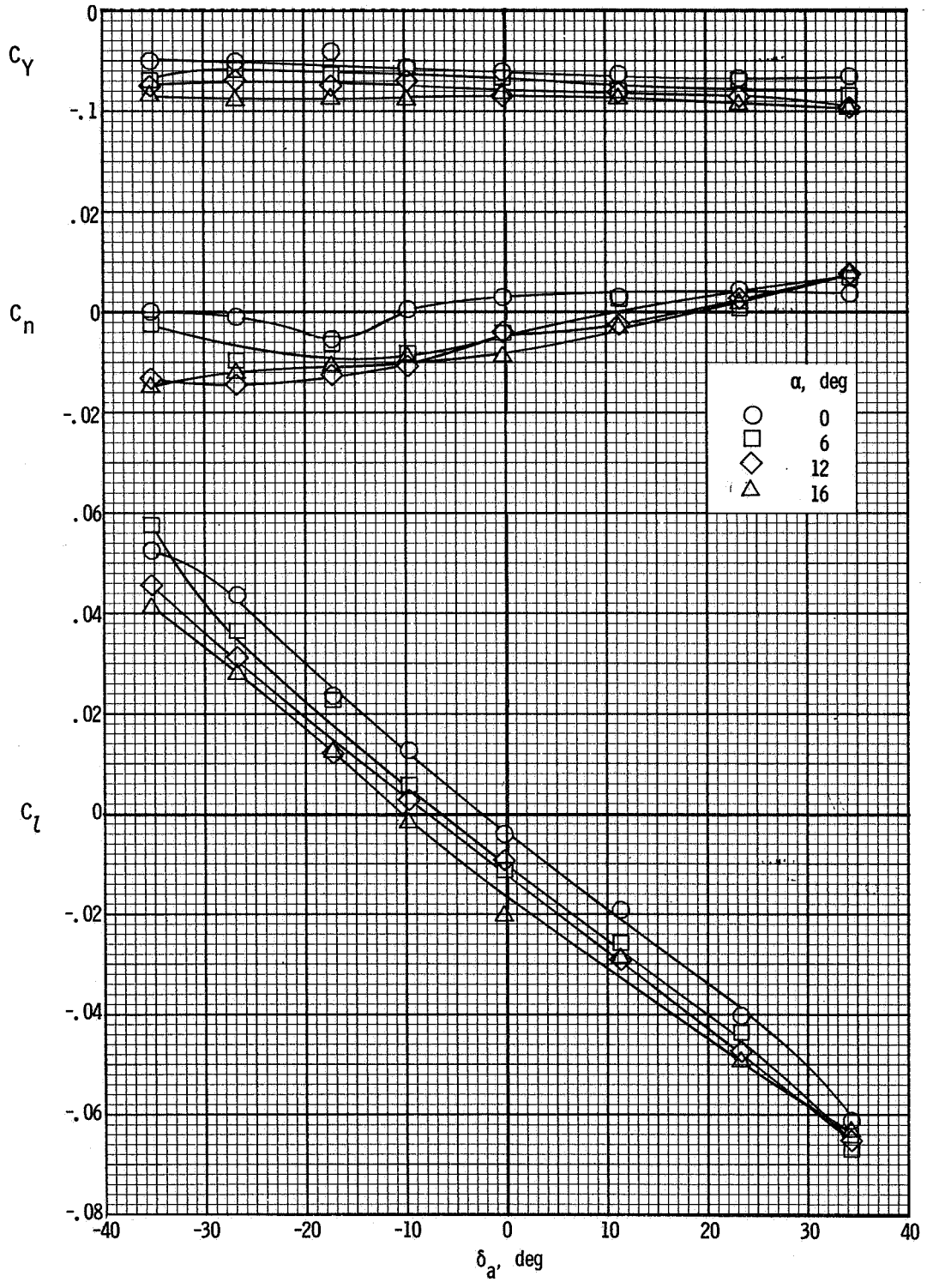

(a) $\beta = 8^{o}$.

Figure 20.- Variation of the lateral characteristics of the airplane with aileron deflection. $\delta_f = 0^{o}$; $T'_c = 0.30$.

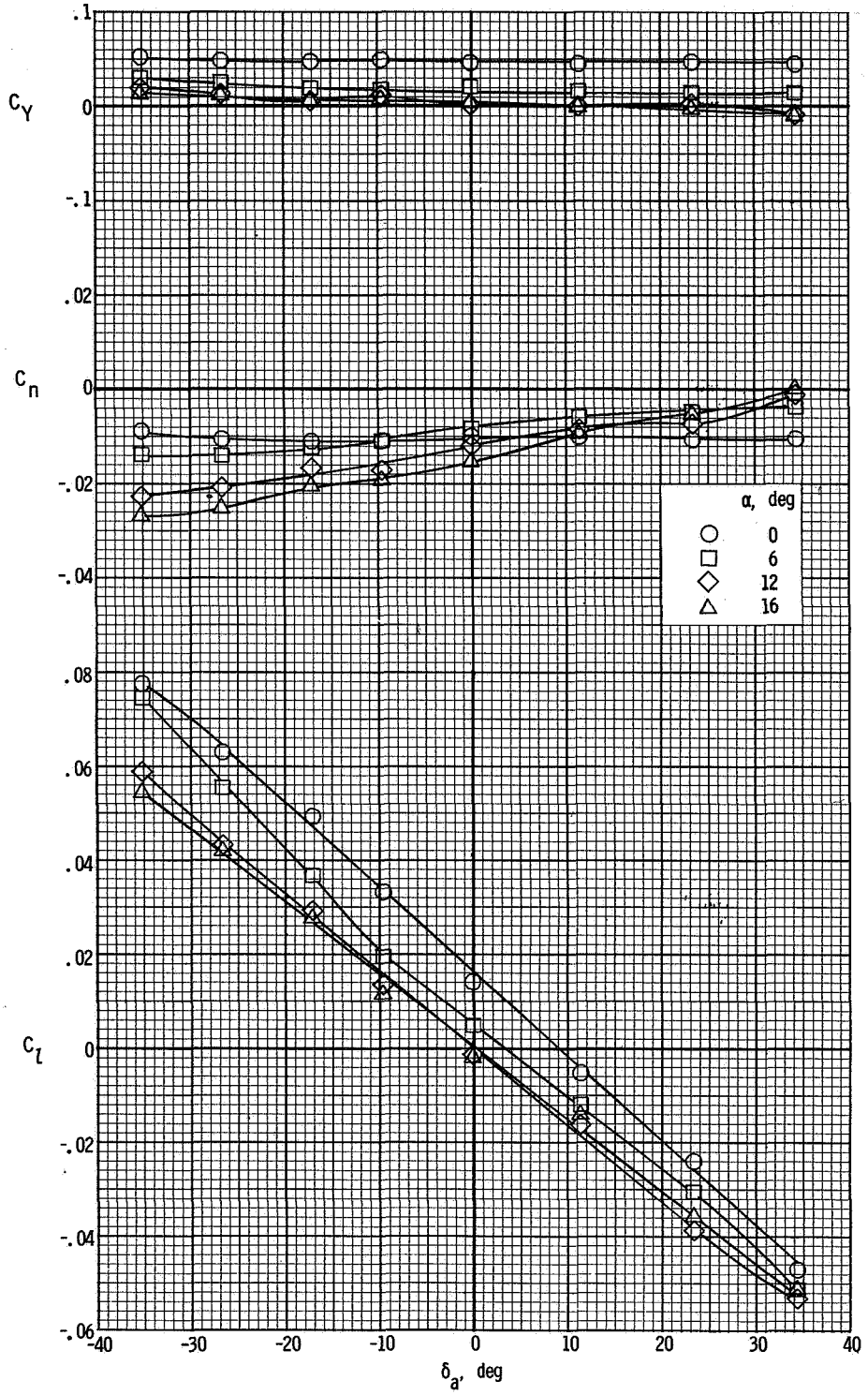

(b) $\beta = 0^{o}$.

Figure 20.- Continued.

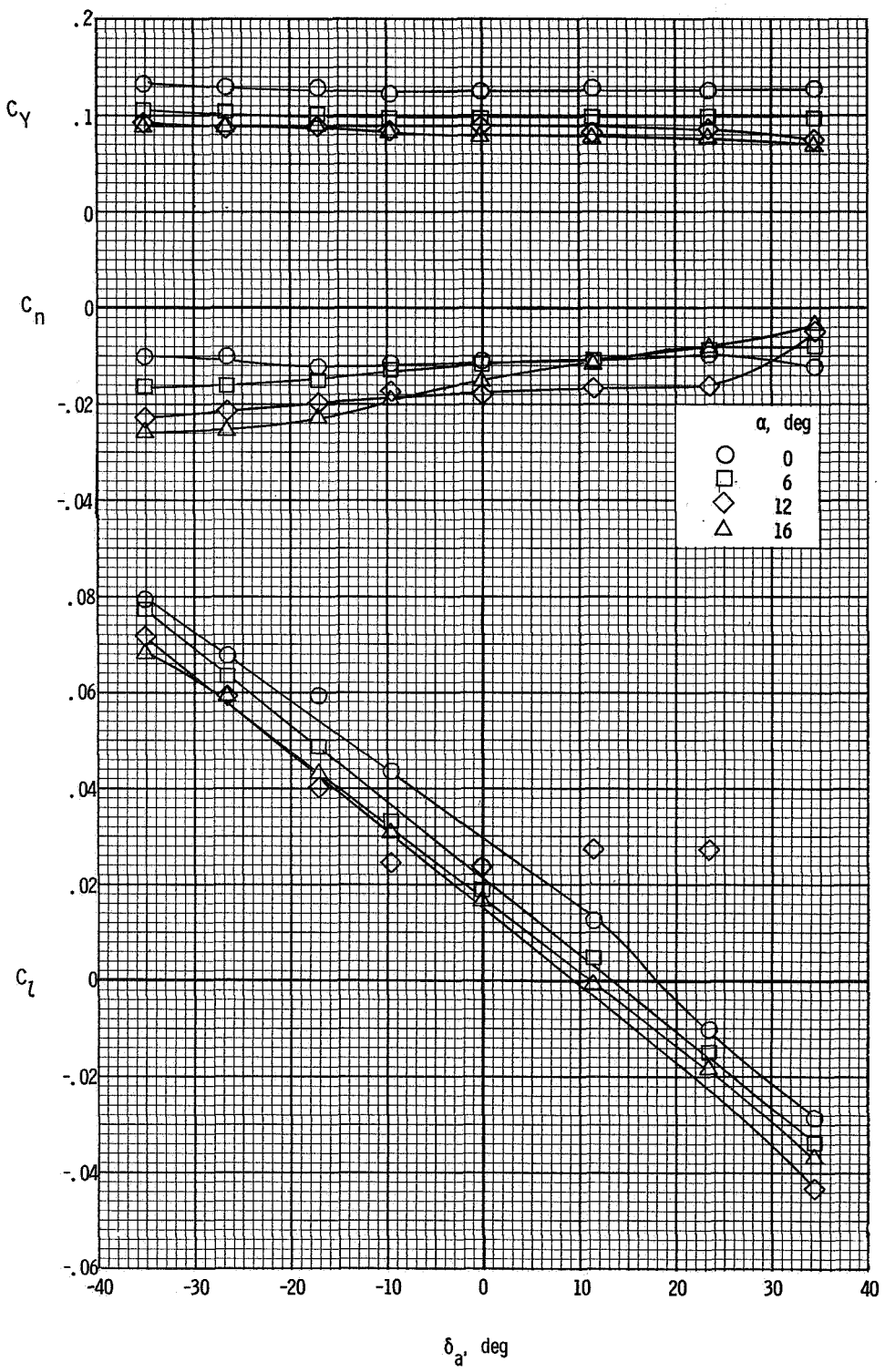

(c) $\beta = -8^{o}$.

Figure 20.- Concluded.

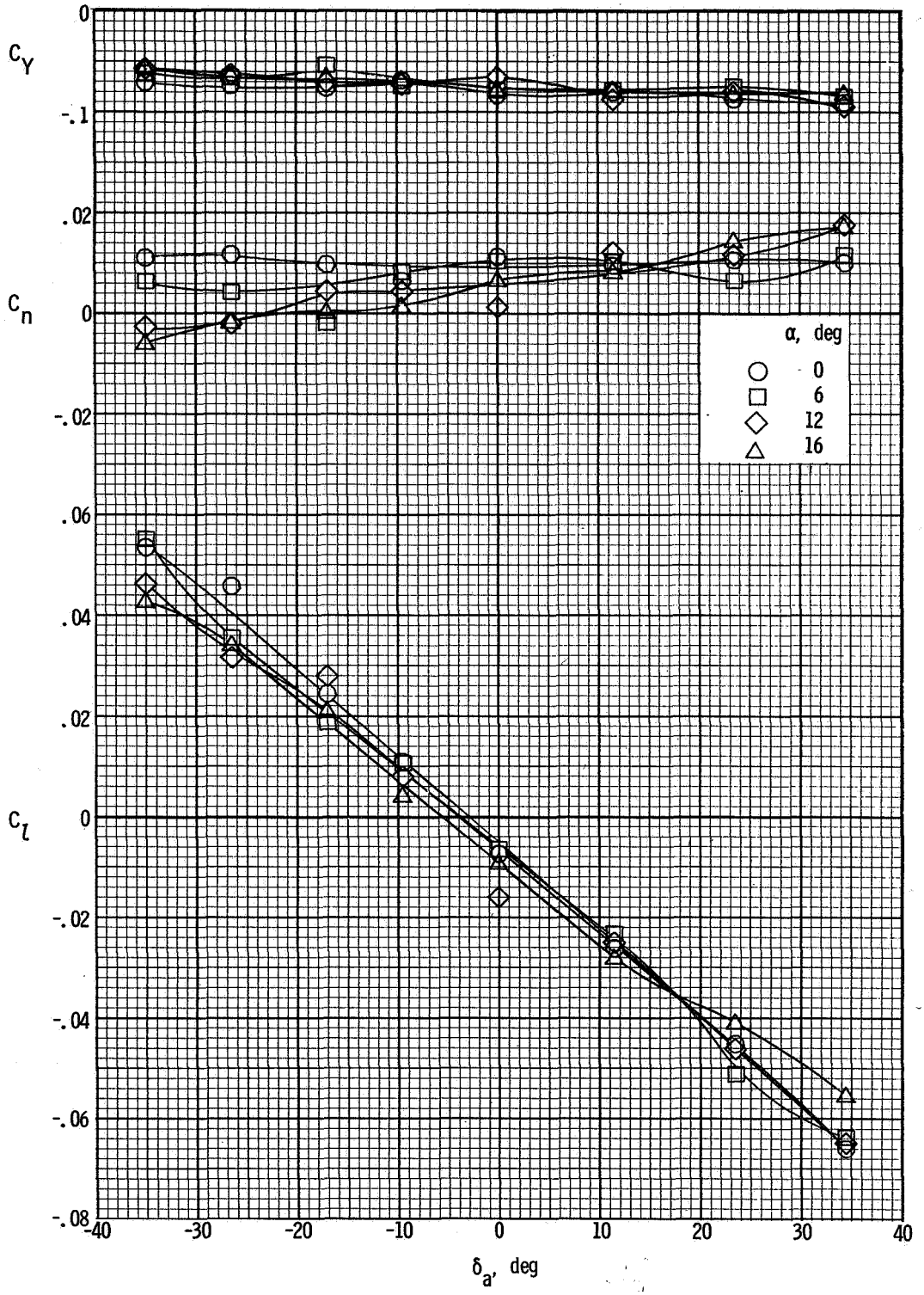

(a) $\beta = 8^{\circ}$.

Figure 21.- Variation of the lateral characteristics of the airplane with aileron deflection. $\delta_f = 30^{\circ}$; $T_c' = 0$.

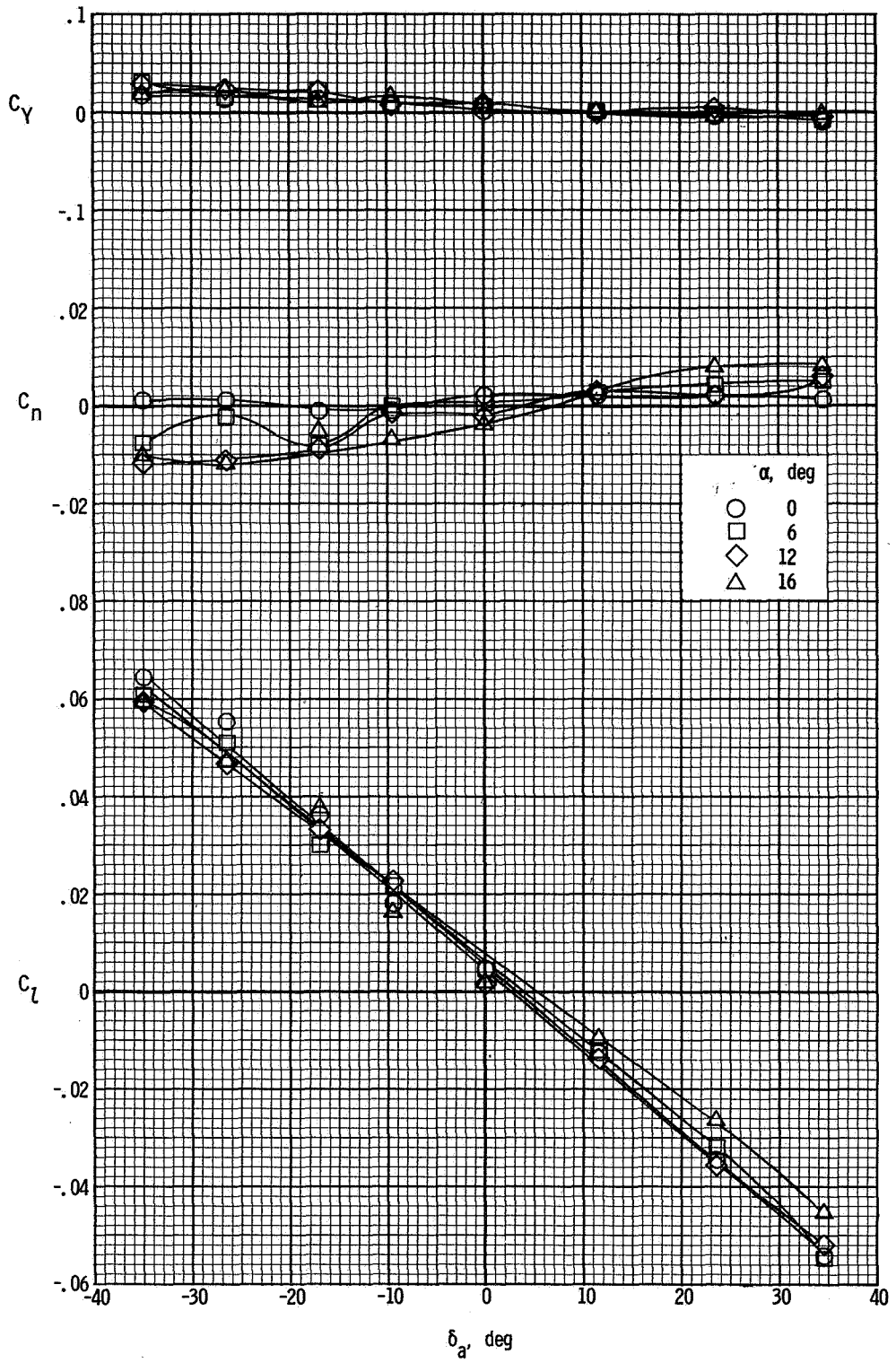

(b) $\beta = 0^o$.

Figure 21.- Continued.

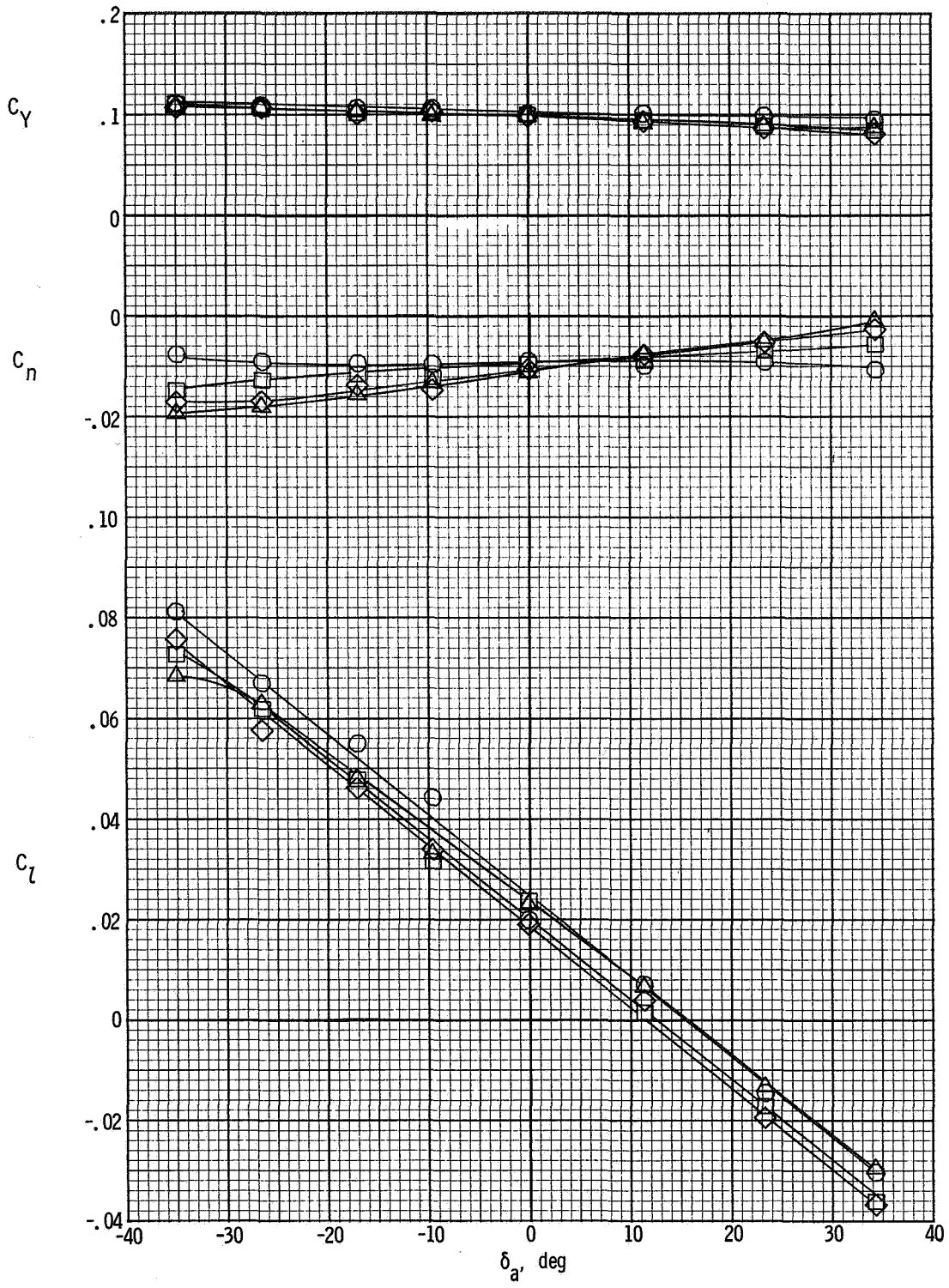

(c) $\beta = -8^o$.

Figure 21.- Concluded.

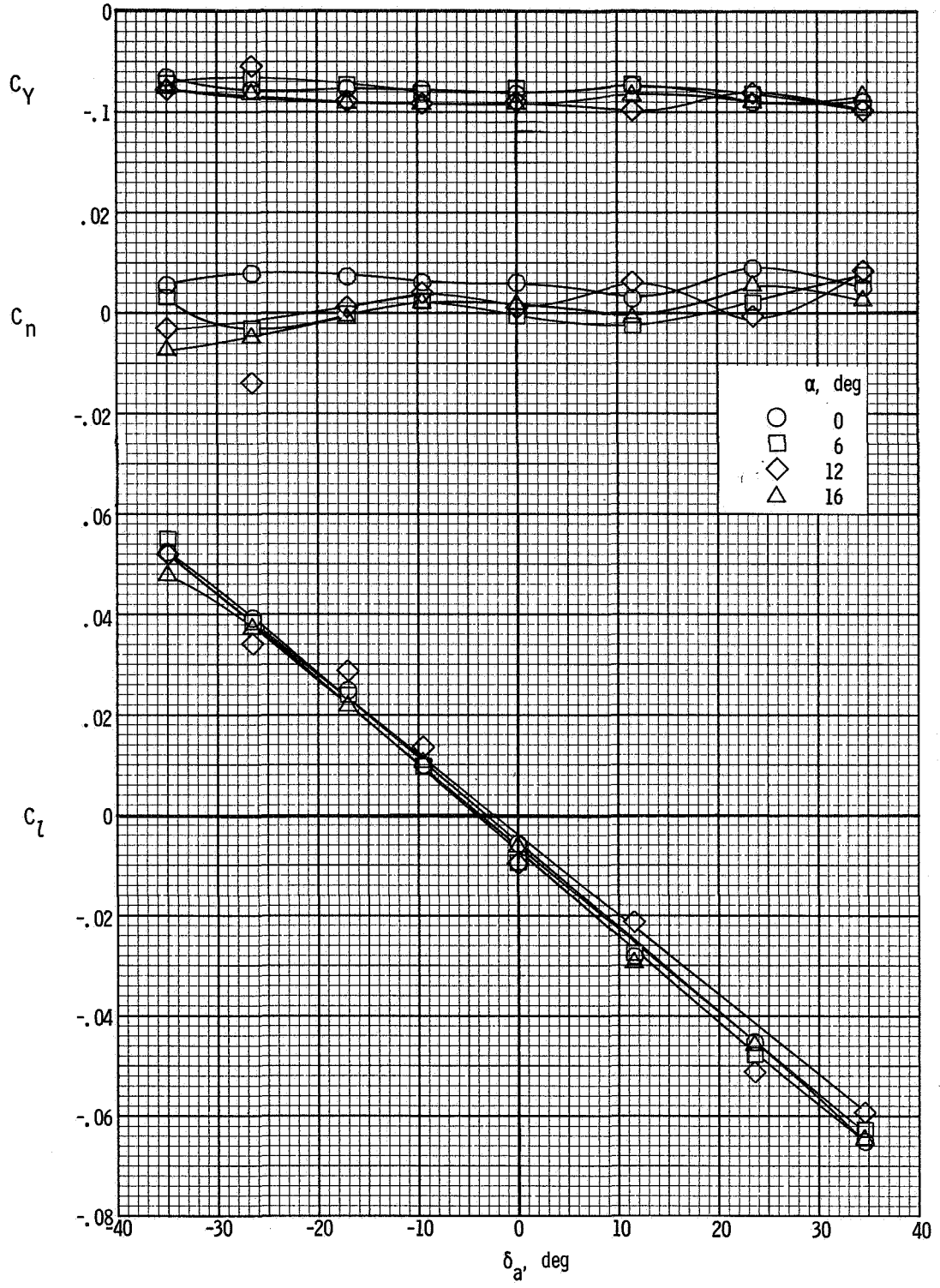

(a) $\beta = 8^{o}$.

Figure 22.- Variation of the lateral characteristics of the airplane with aileron deflection. $\delta_f = 30^{o}$; $T'_c = 0.14$.

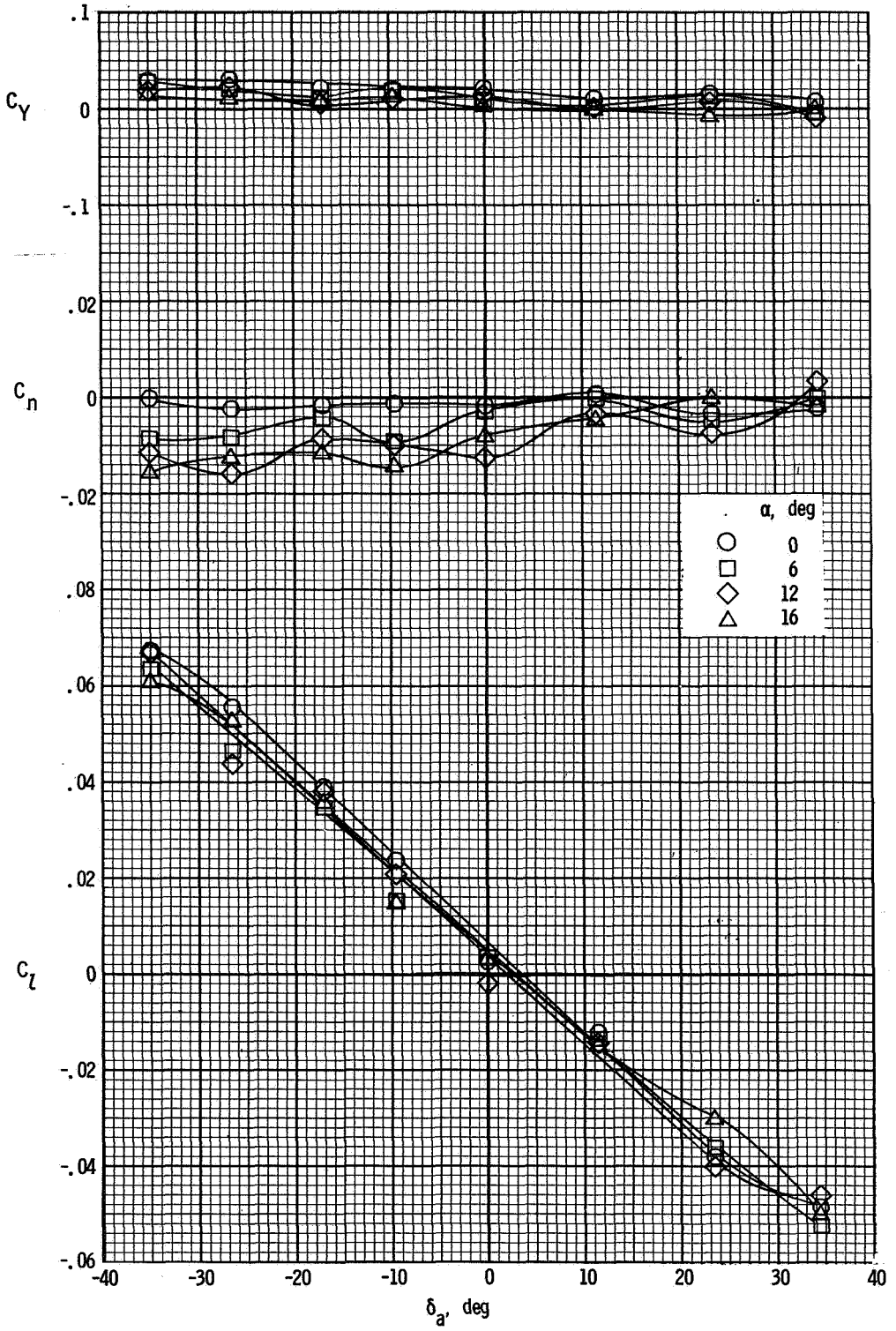

(b) $\beta = 0^o$.

Figure 22.- Continued.

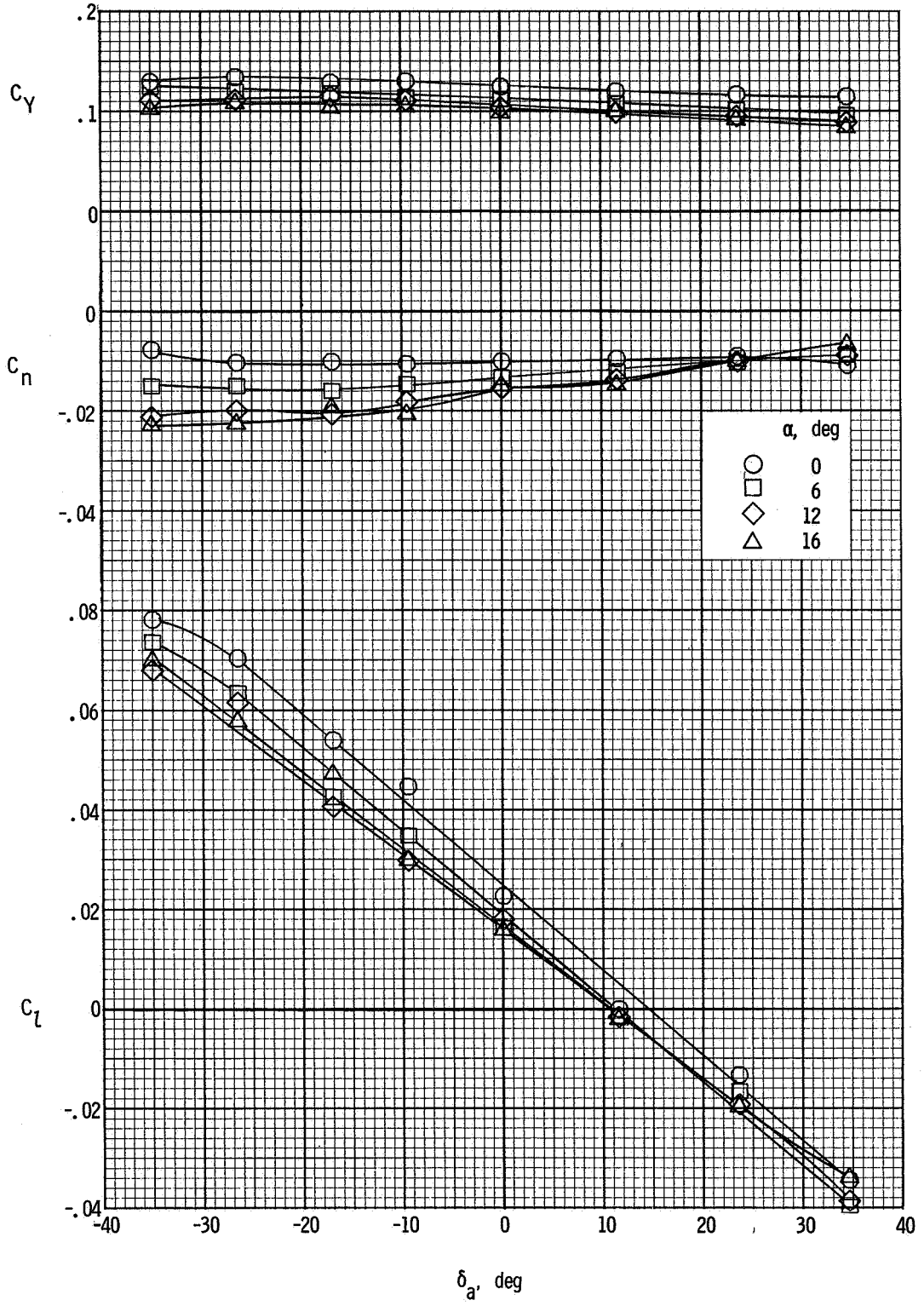

(c) $\beta = -8^{o}$.

Figure 22.- Concluded.

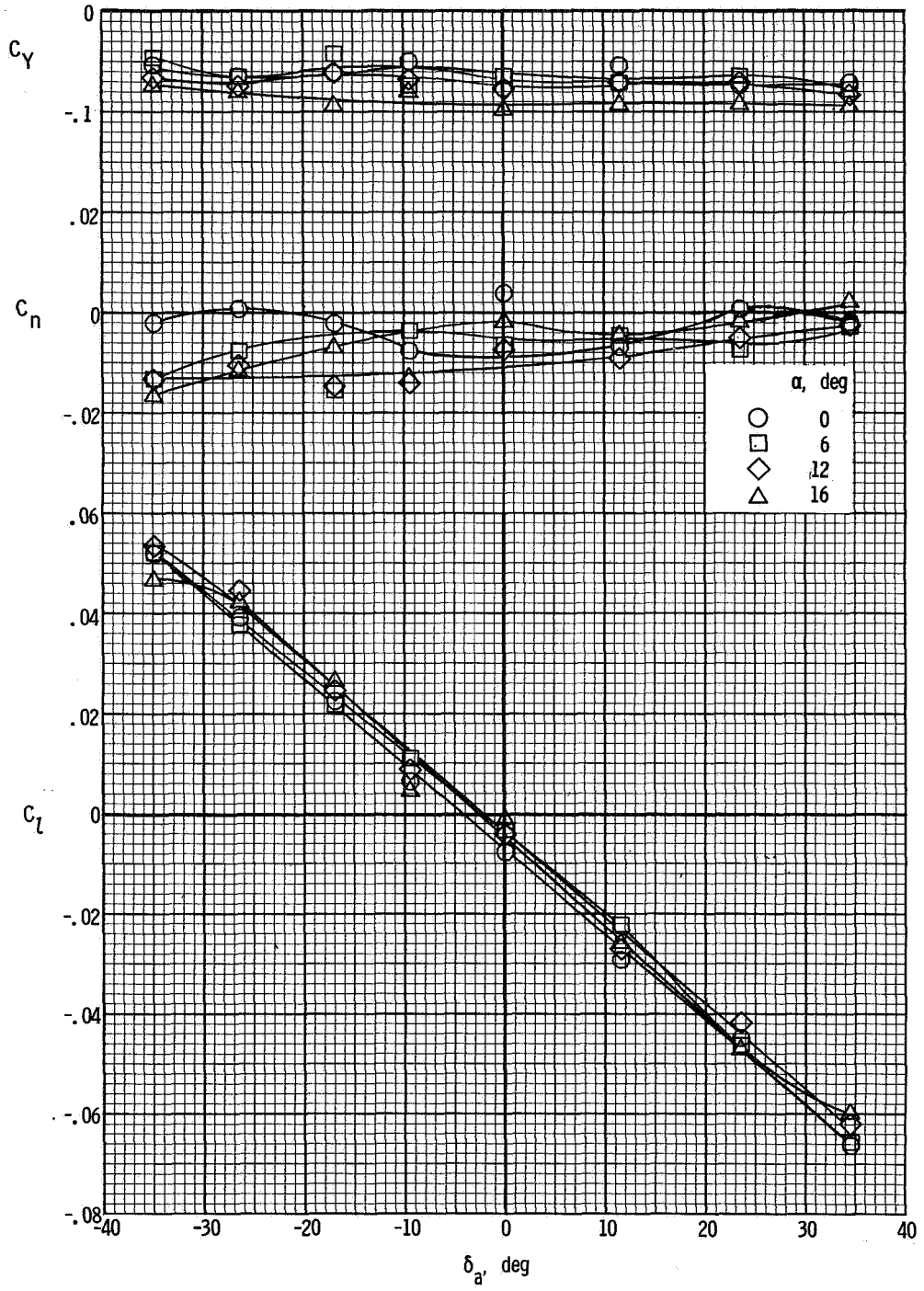

(a) $\beta = 8^{o}$.

Figure 23.- Variation of the lateral characteristics of the airplane with aileron deflection. $\delta_f = 30^{o}$; $T'_c = 0.30$.

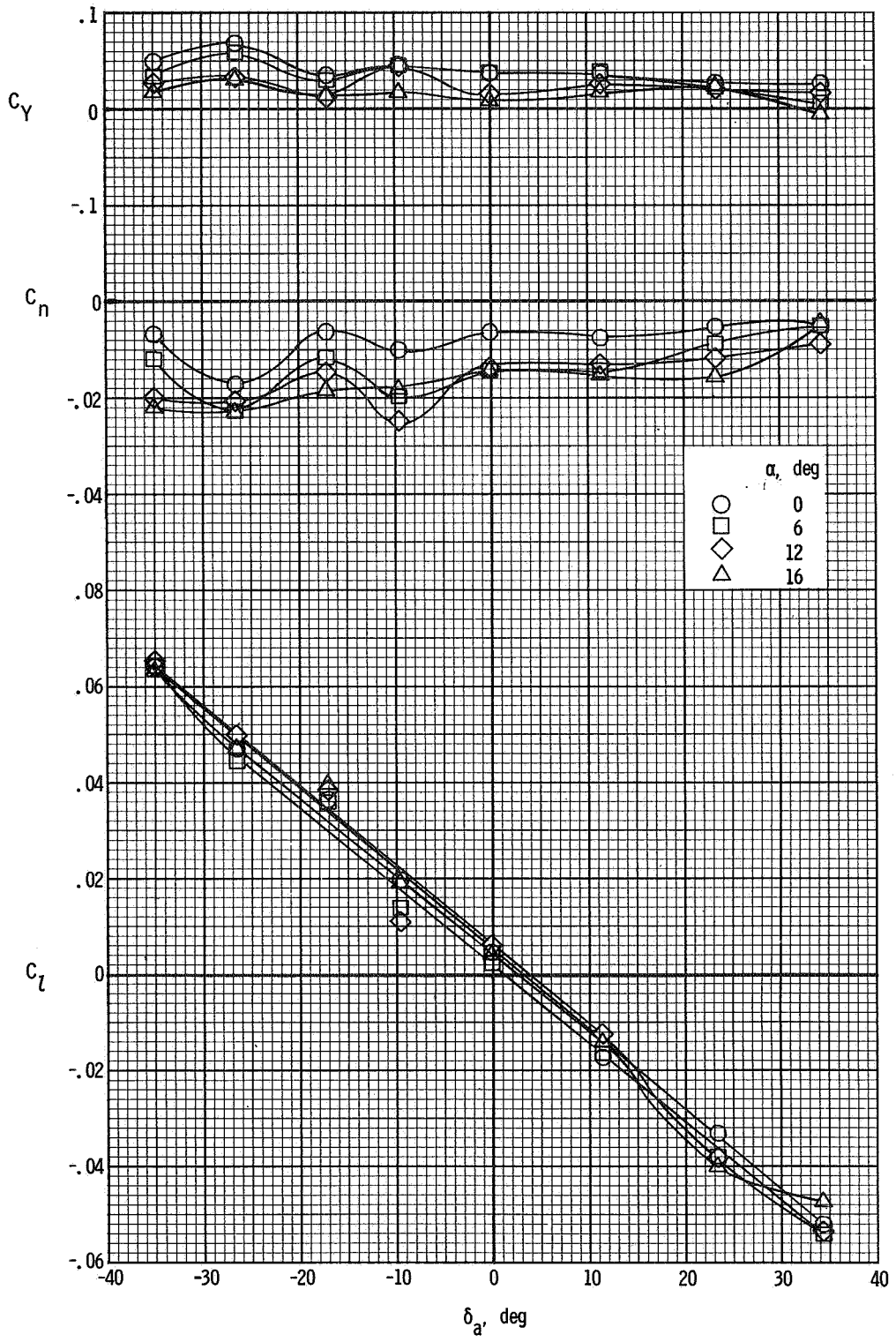

(b) $\beta = 0^{o}$.

Figure 23.- Continued.

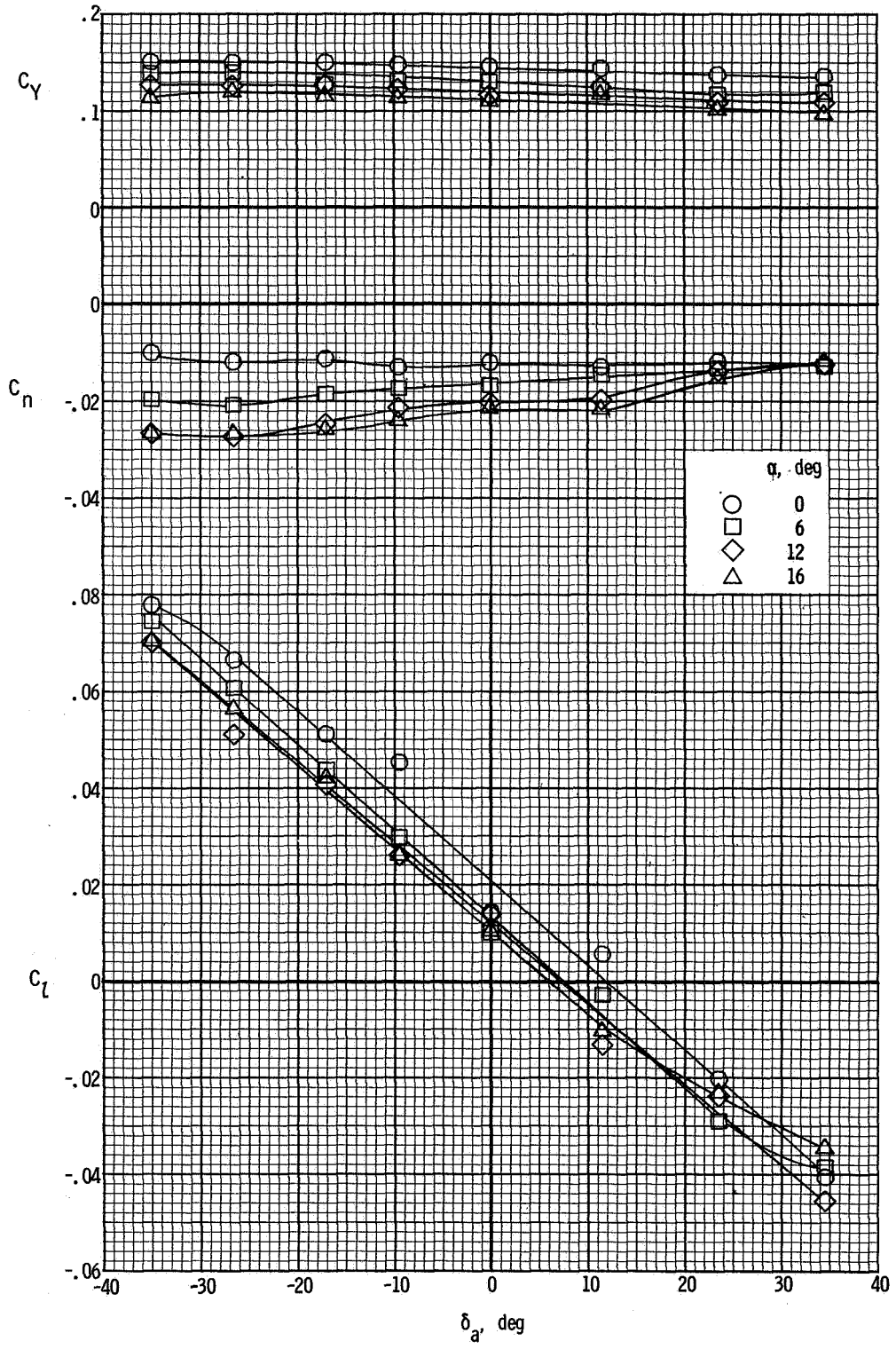

(c) $\beta = -8^{o}$.

Figure 23.- Concluded.

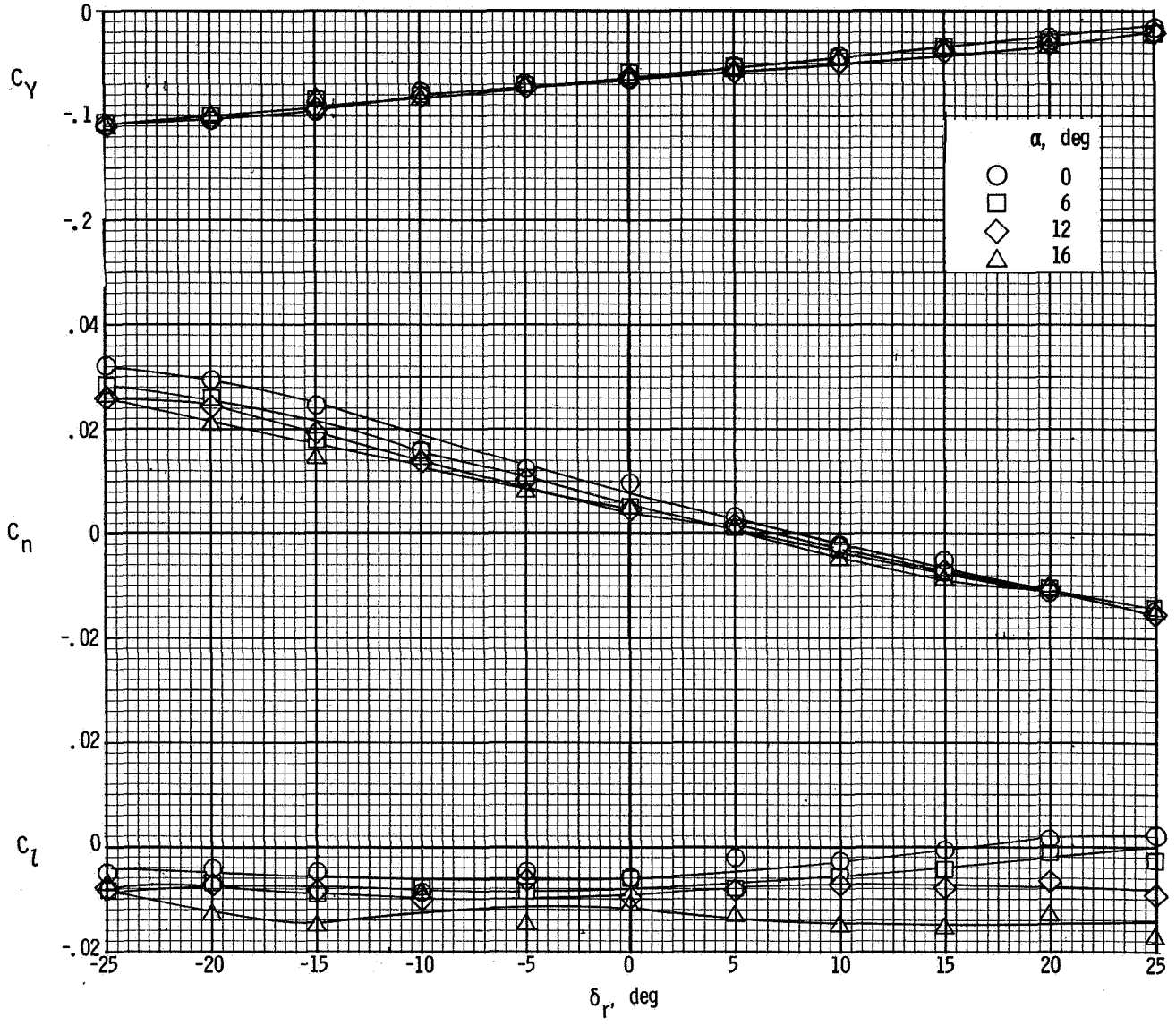

(a) $\beta = 8^{o}$.

Figure 24.- Variation of the lateral characteristics of the airplane with rudder deflection. $\delta_f = 0^{o}$; $T_c' = 0$.

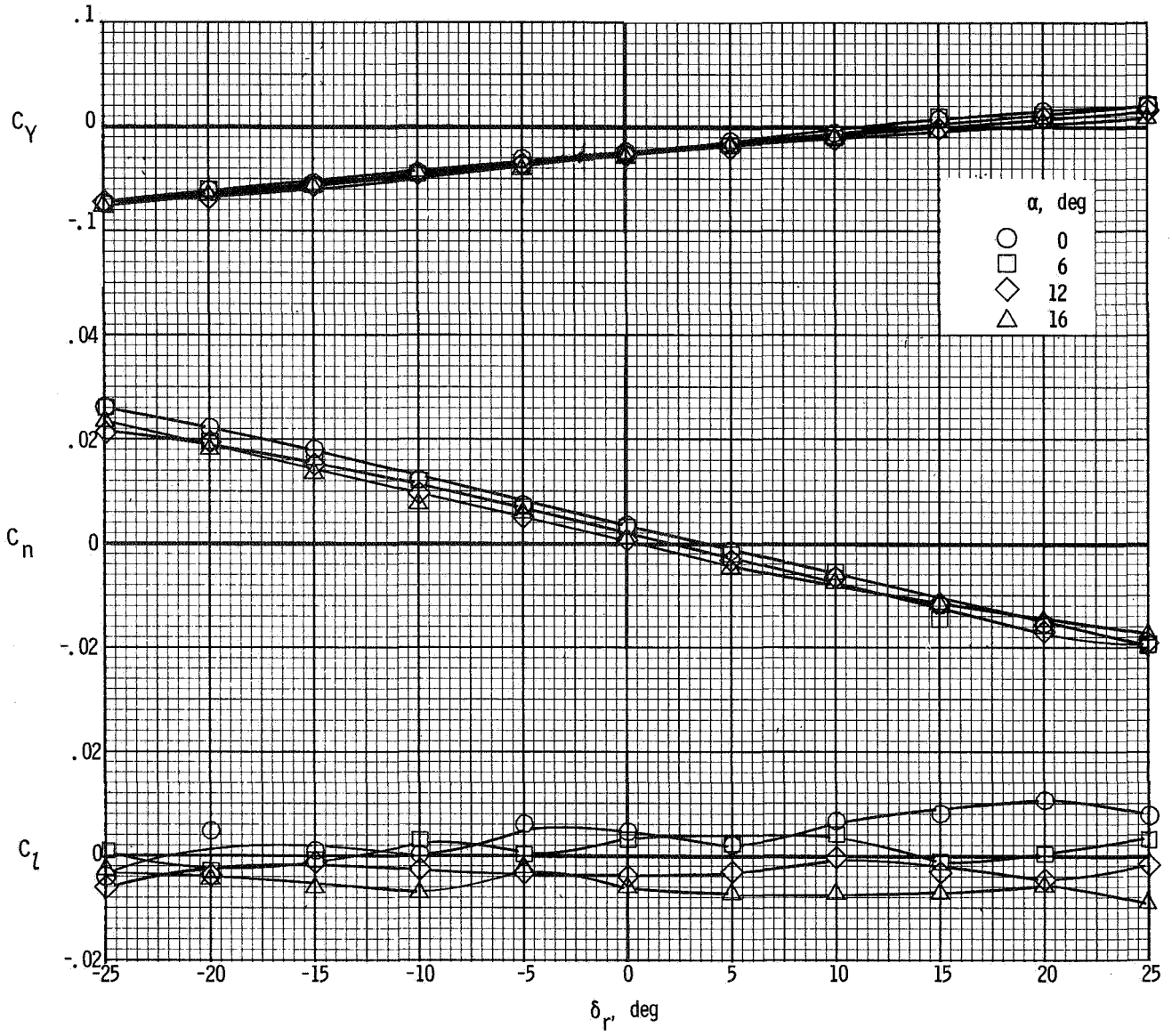

(b) $\beta = 4^{o}$.

Figure 24.- Continued.

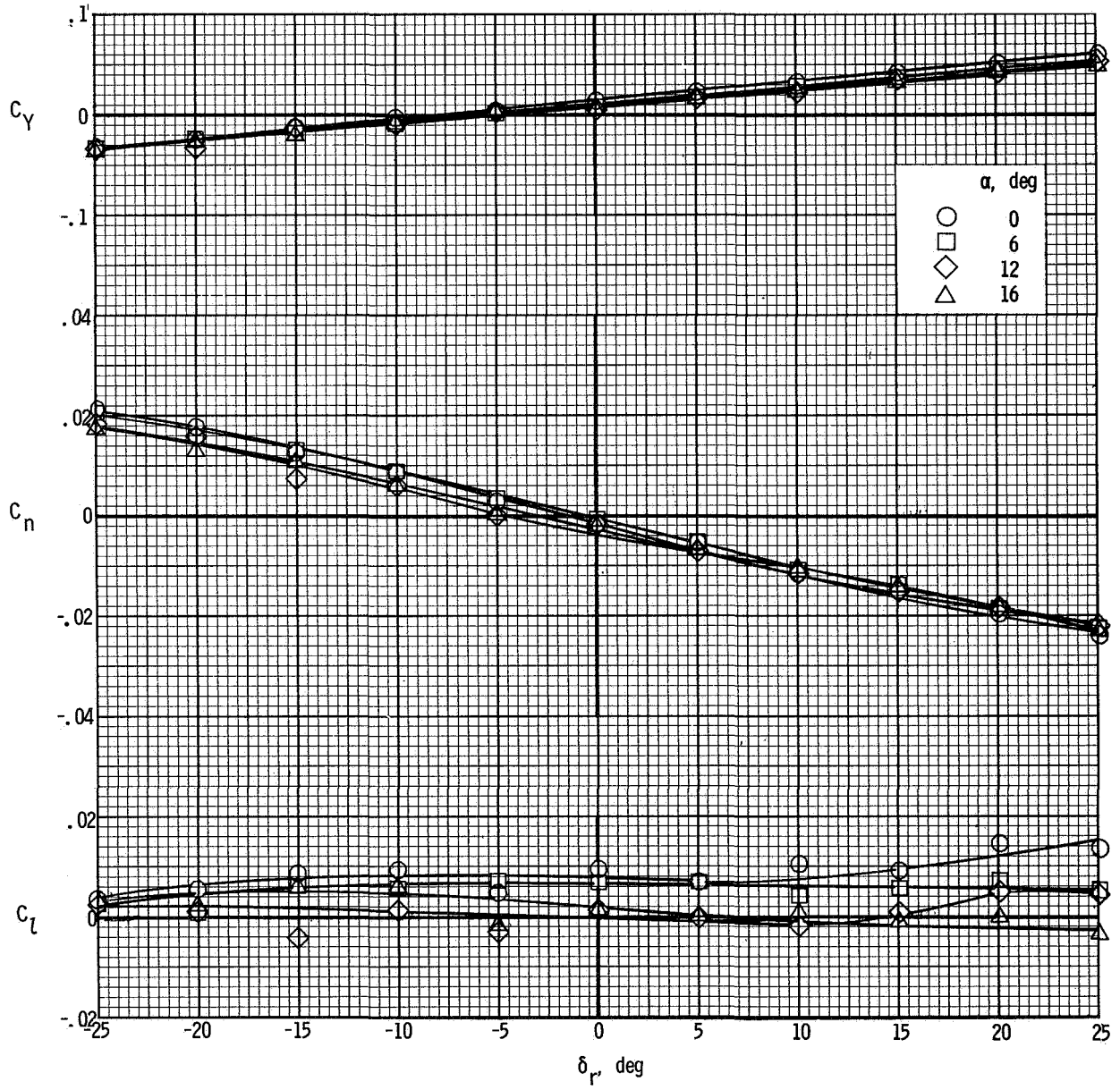

(c) $\beta = 0^o$.

Figure 24.- Continued.

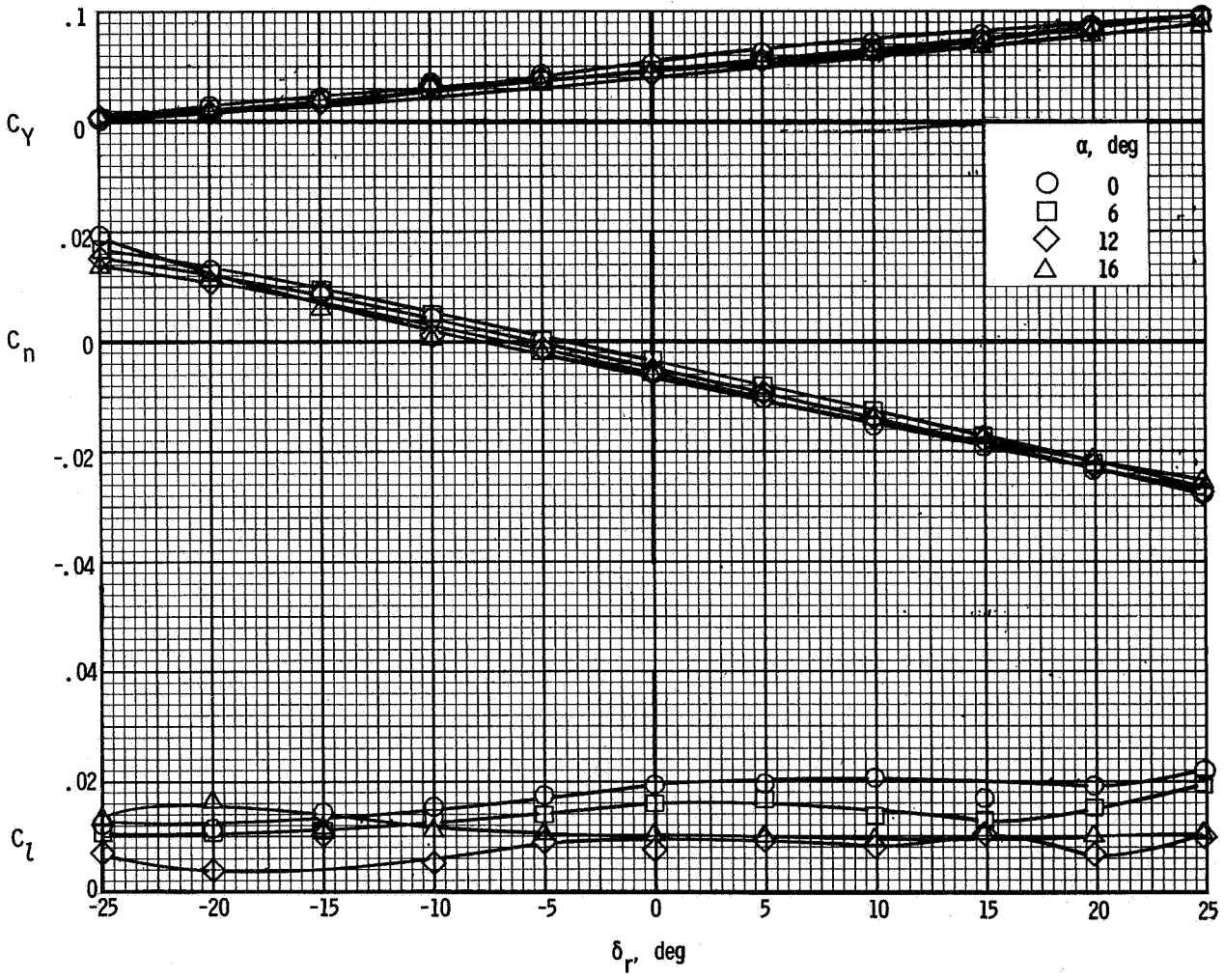

(d) $\beta = -4^{o}$.

Figure 24.- Continued.

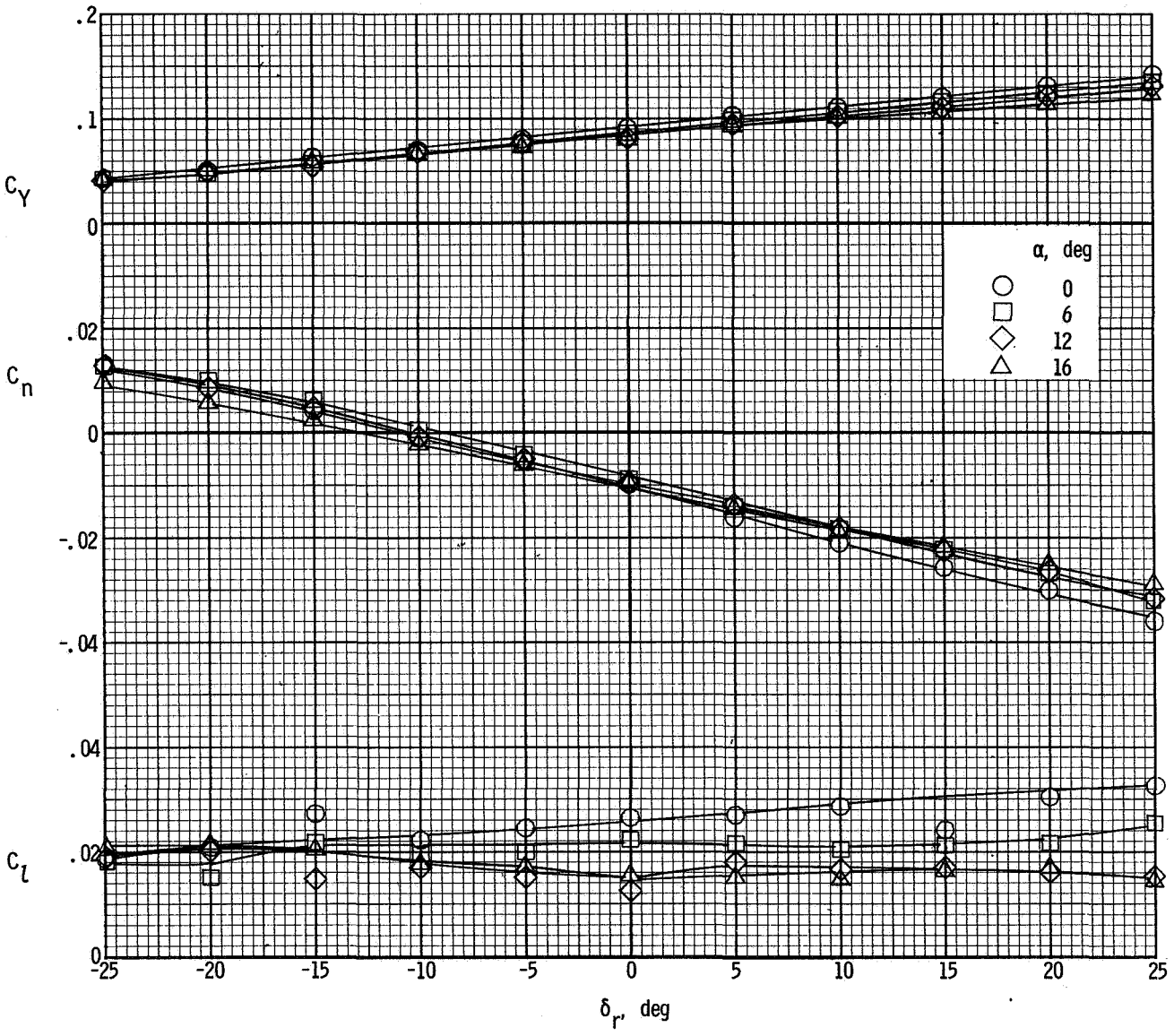

(e) $\beta = -8^{o}$.

Figure 24.- Concluded.

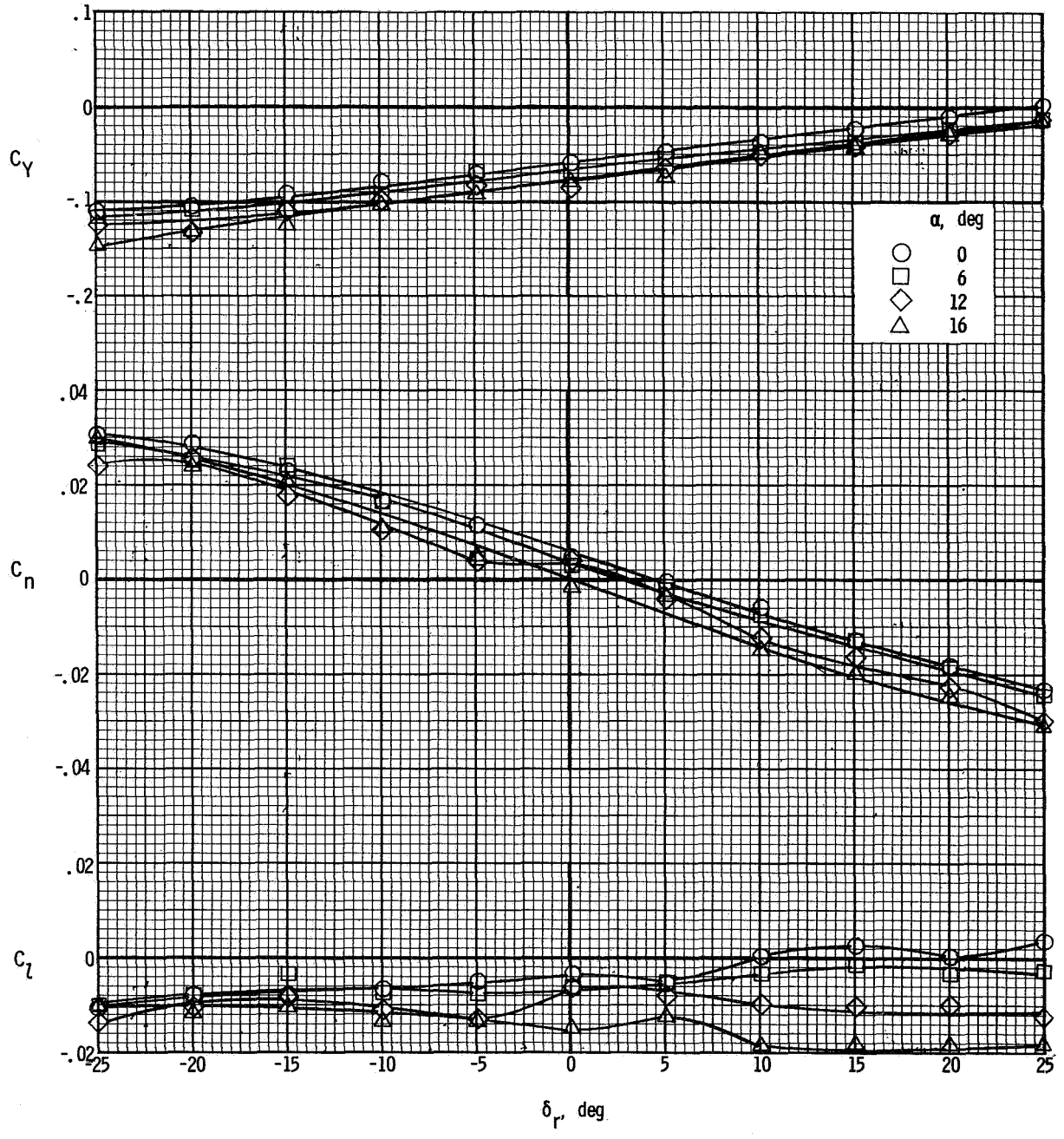

(a) $\beta = 8^{\circ}$.

Figure 25.- Variation of the lateral characteristics of the airplane with rudder deflection. $\delta_f = 0^{\circ}$; $T'_c = 0.14$.

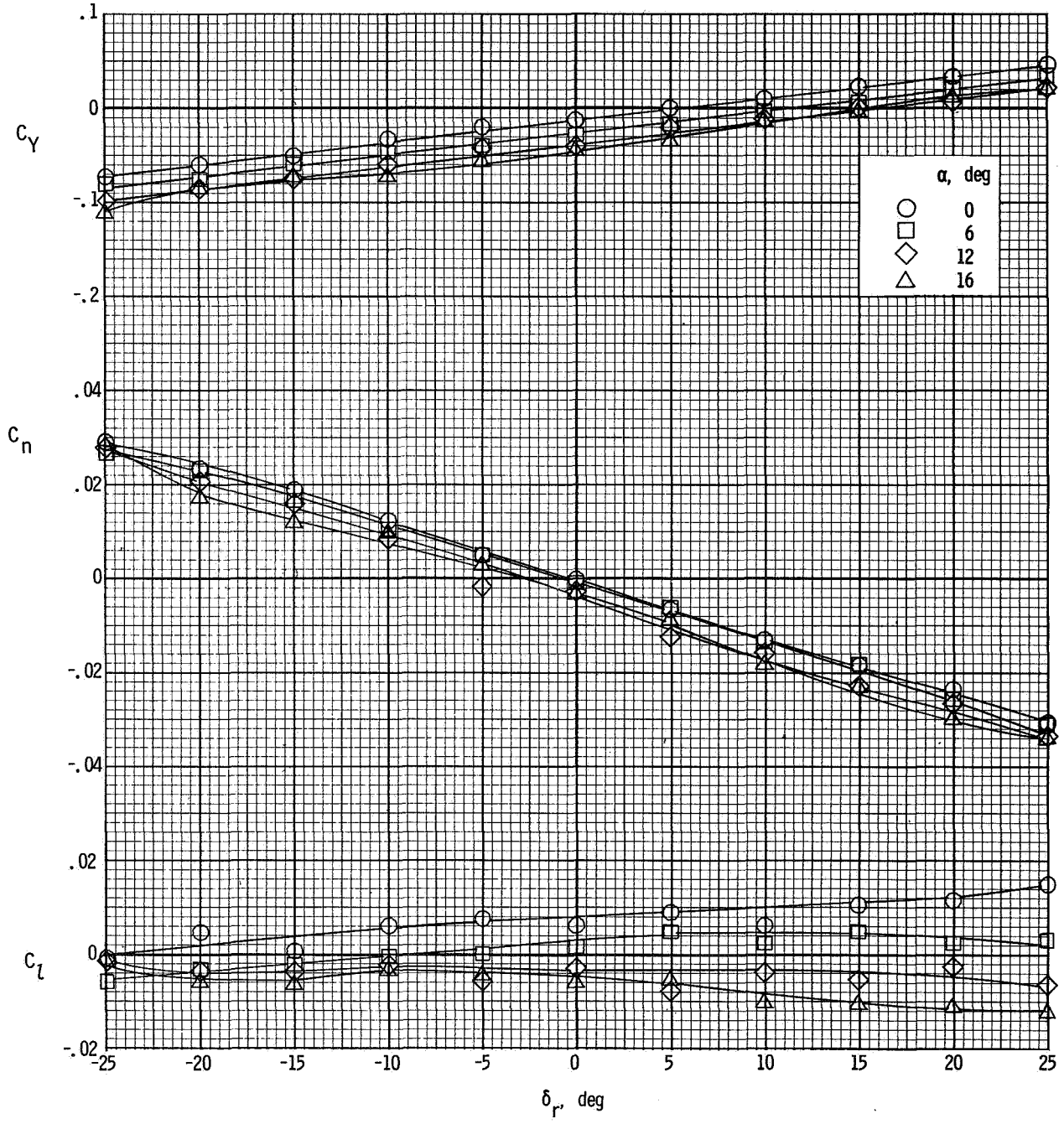

(b) $\beta = 4^{o}$.

Figure 25.- Continued.

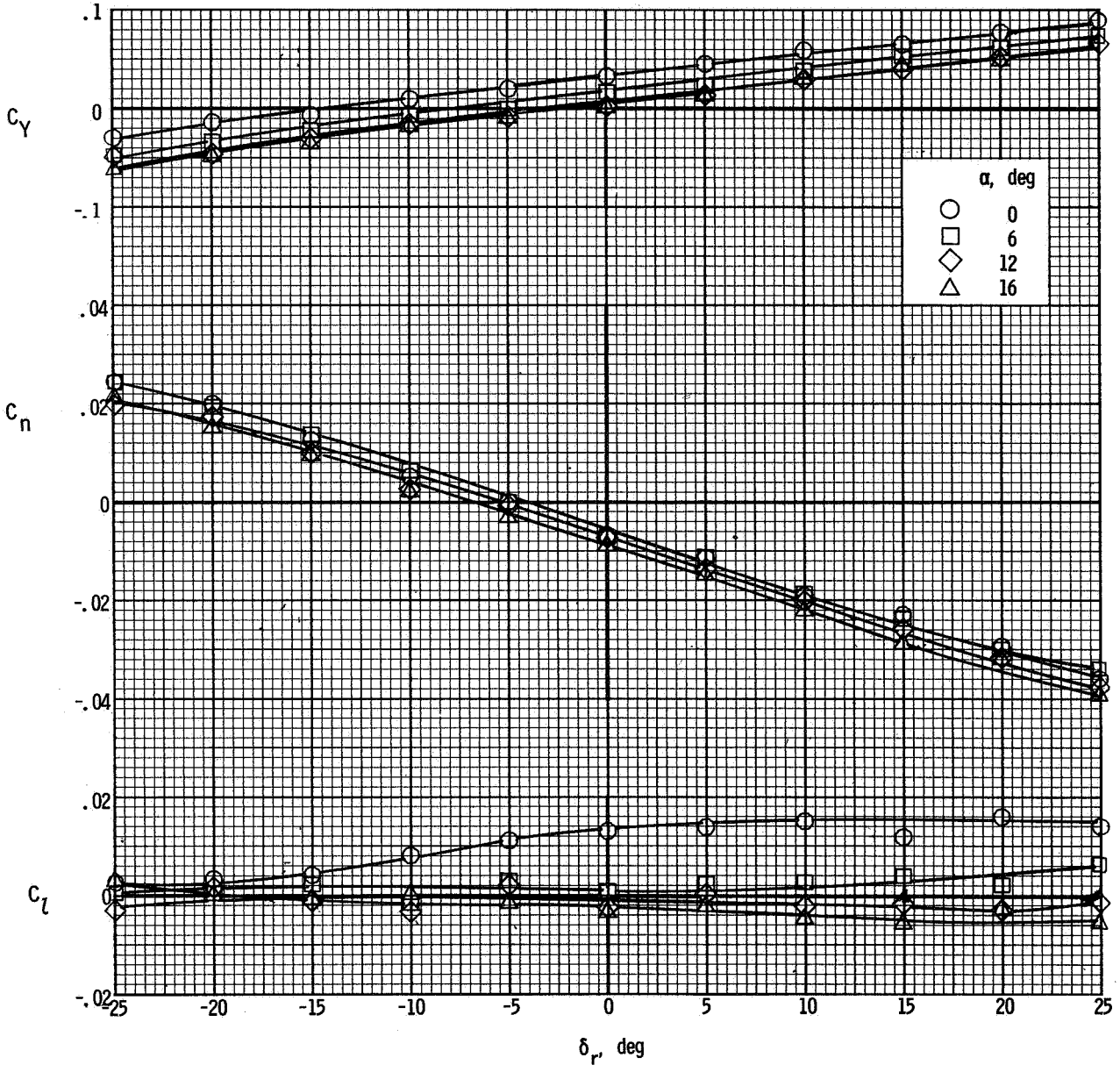

(c) $\beta = 0^o$.

Figure 25.- Continued.

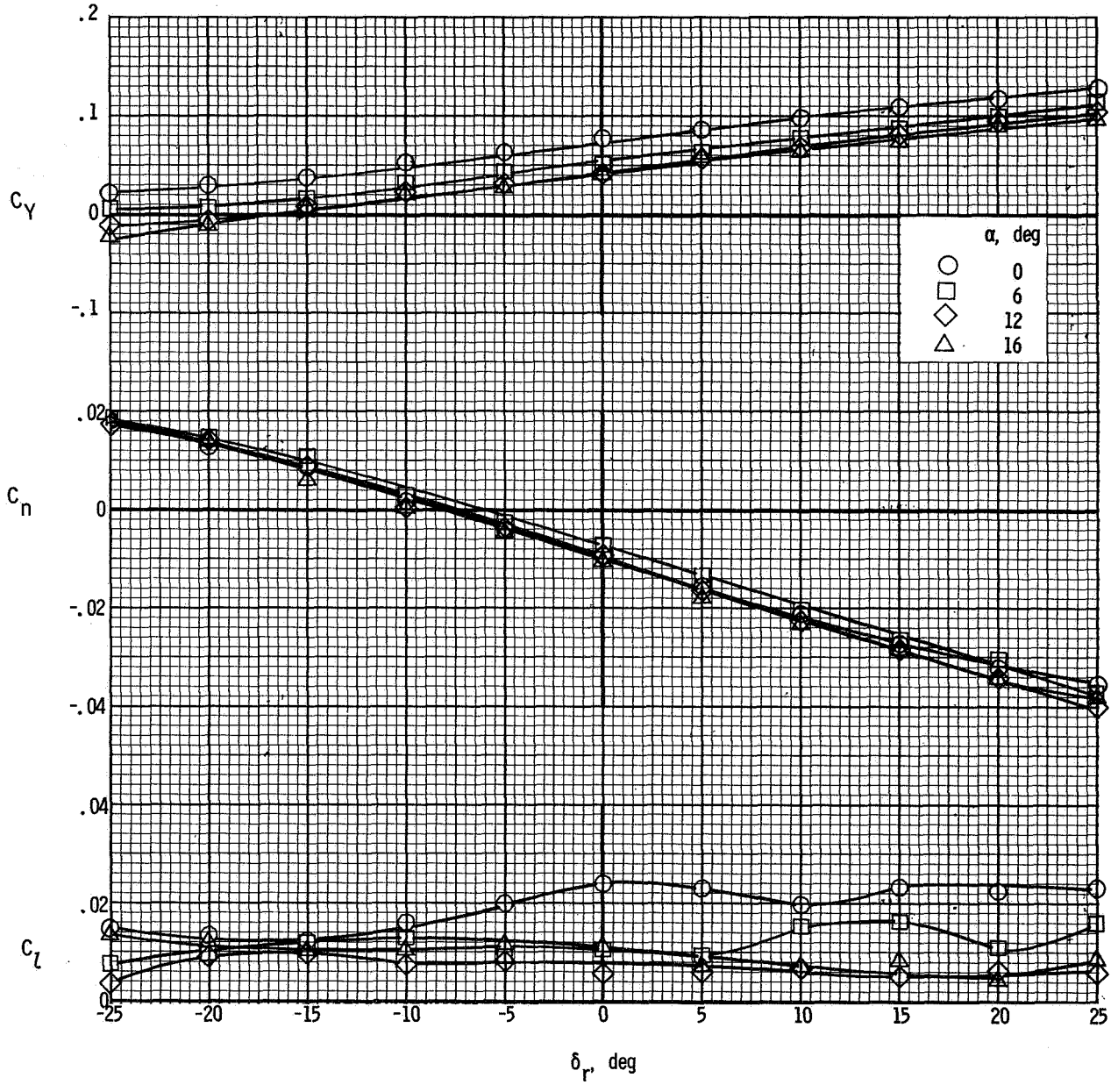

(d) $\beta = -4^{\circ}$.

Figure 25.- Continued.

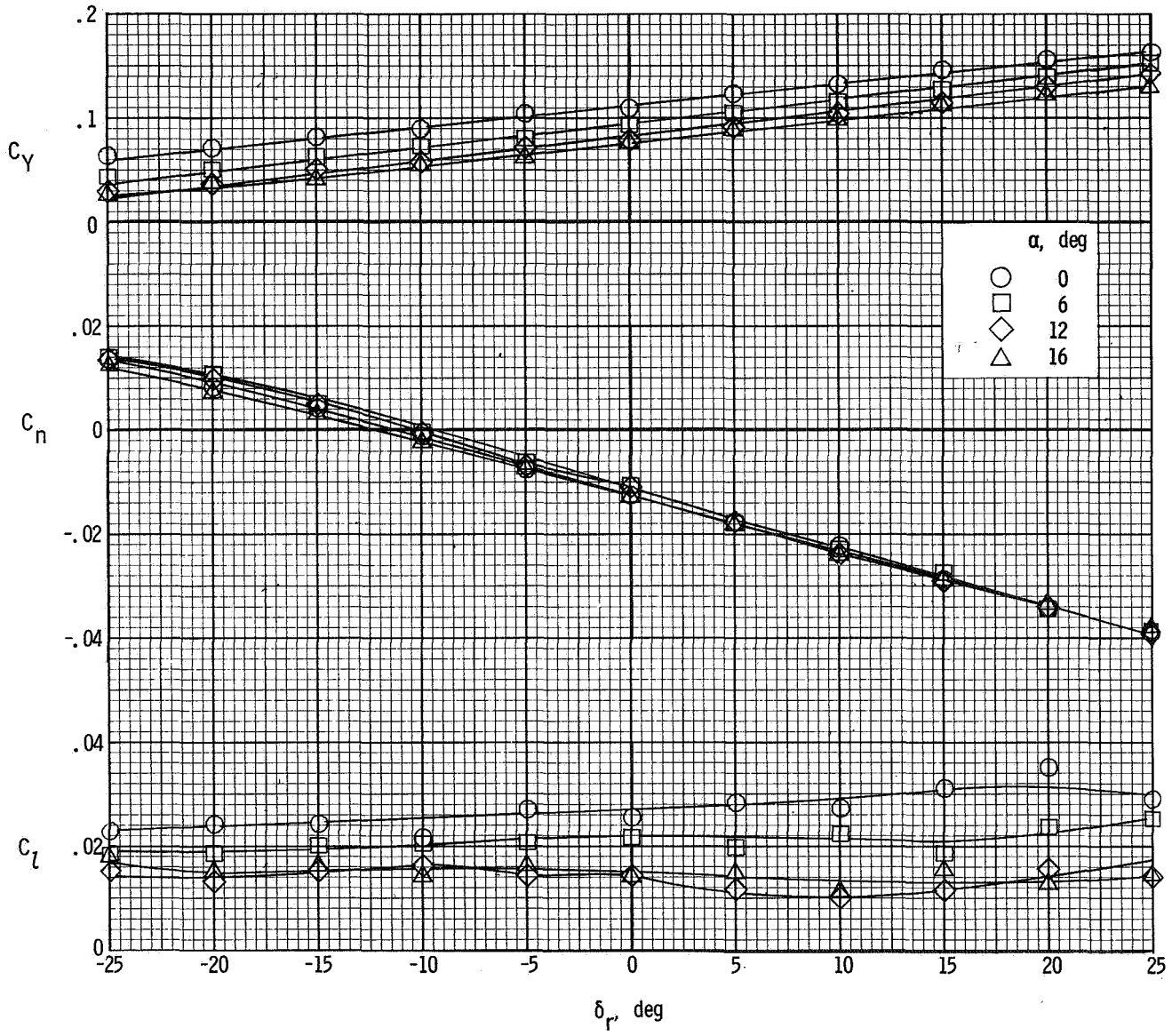

(e) $\beta = -8^{o}$.

Figure 25.- Concluded.

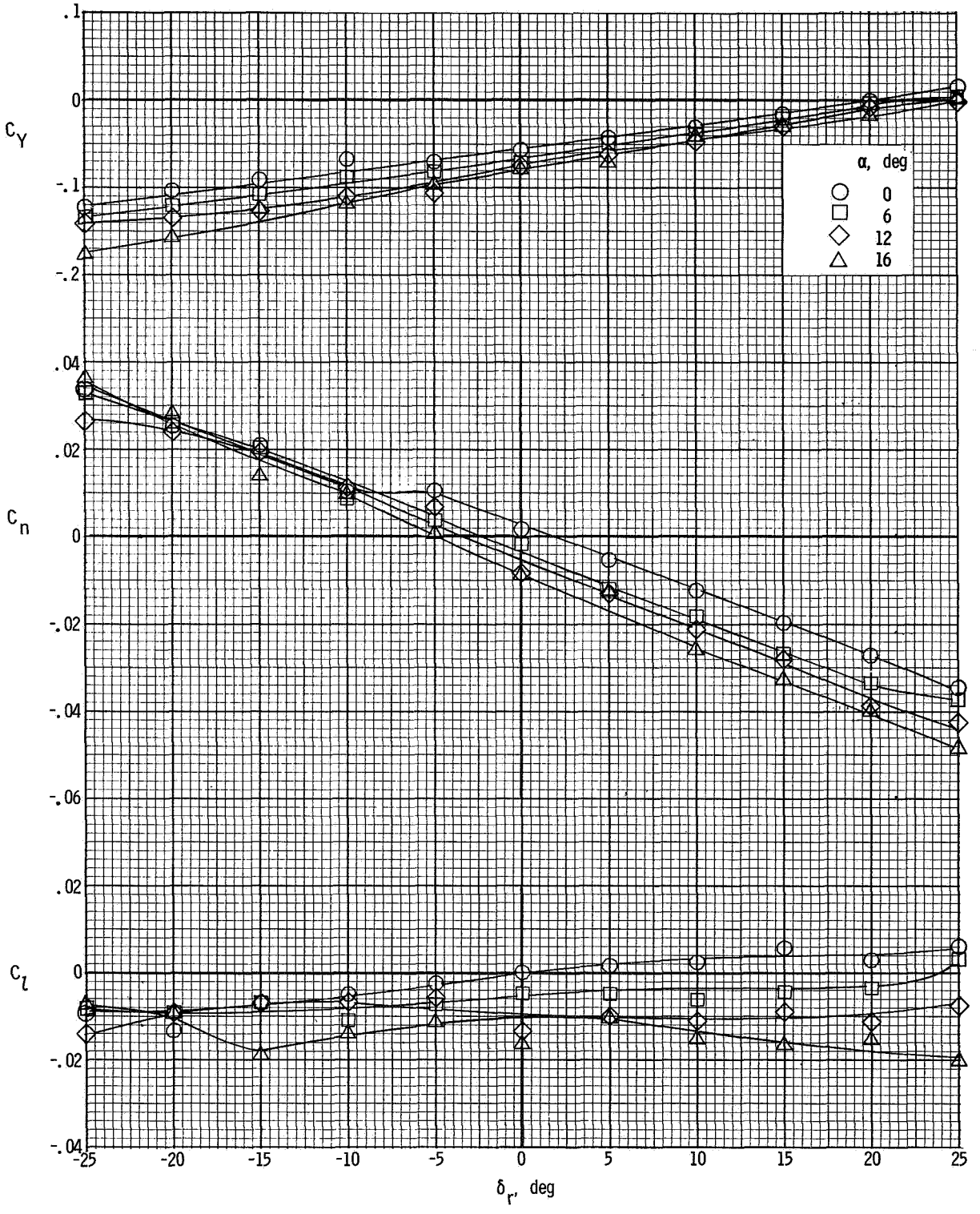

(a) $\beta = 8^{\circ}$.

Figure 26.- Variation of the lateral characteristics of the airplane with rudder deflection. $\delta_f = 0^{\circ}$; $T'_c = 0.30$.

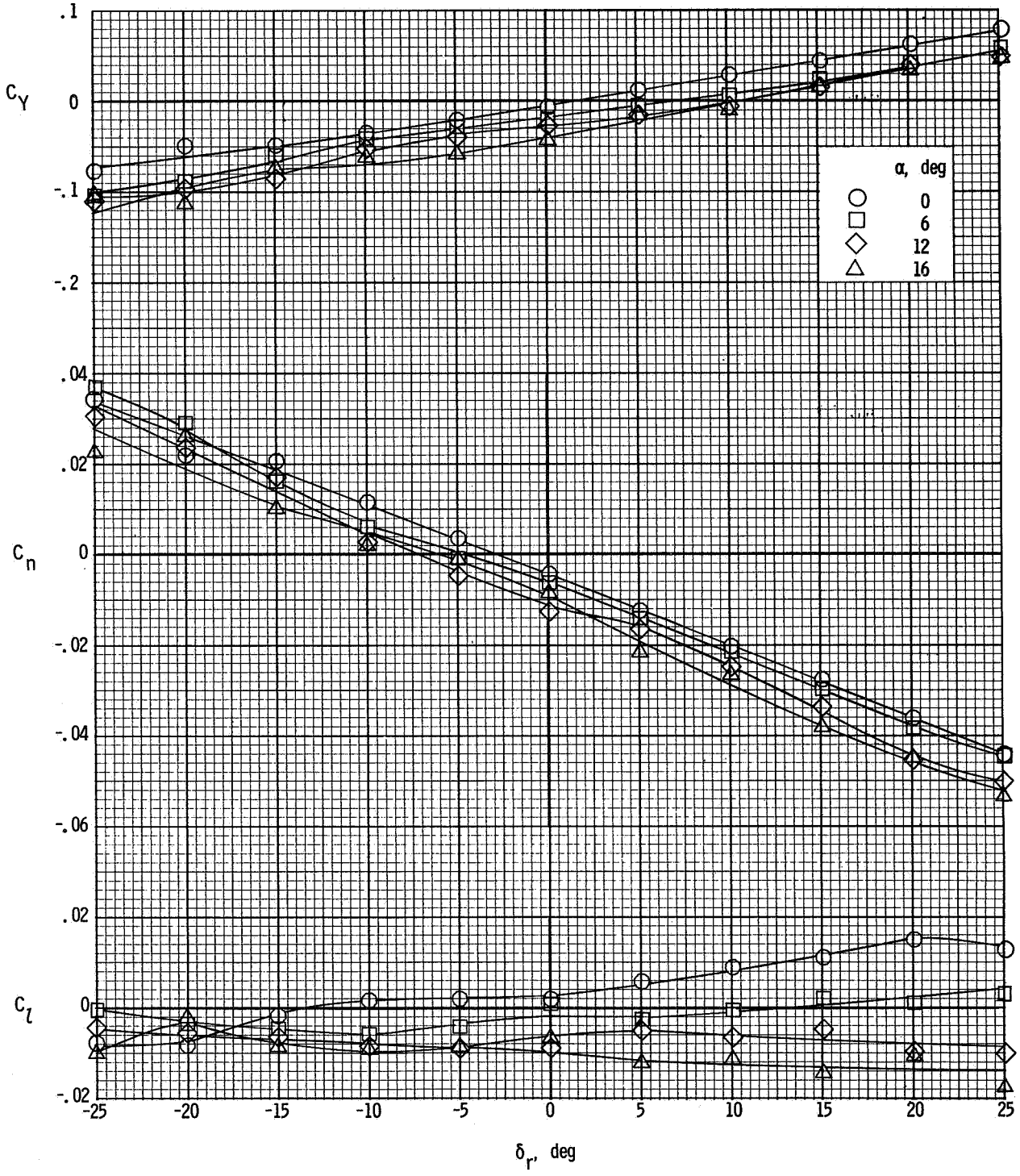

(b) $\beta = 4^{o}$.

Figure 26.- Continued.

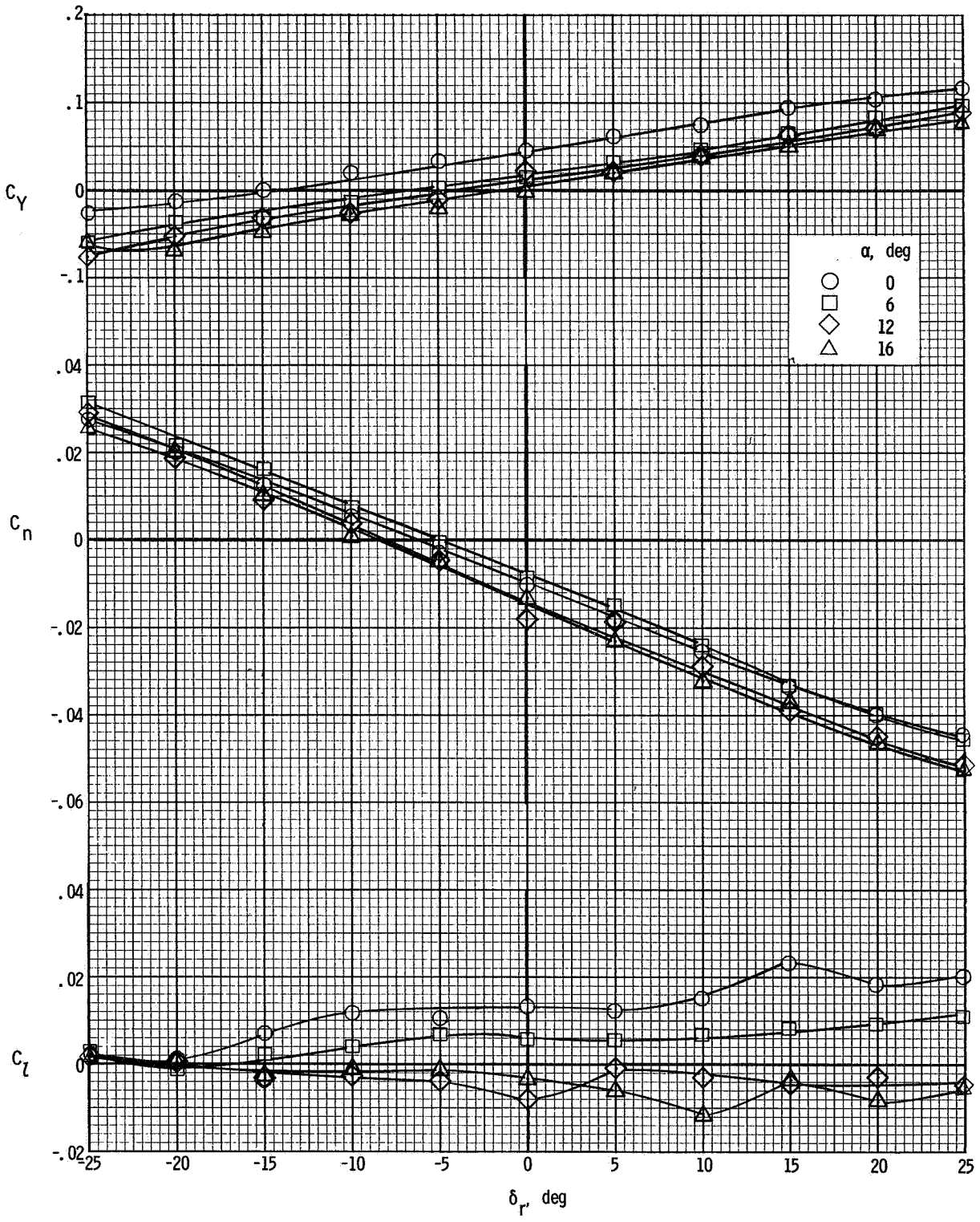

(c) $\beta = 0^{o}$.

Figure 26.- Continued.

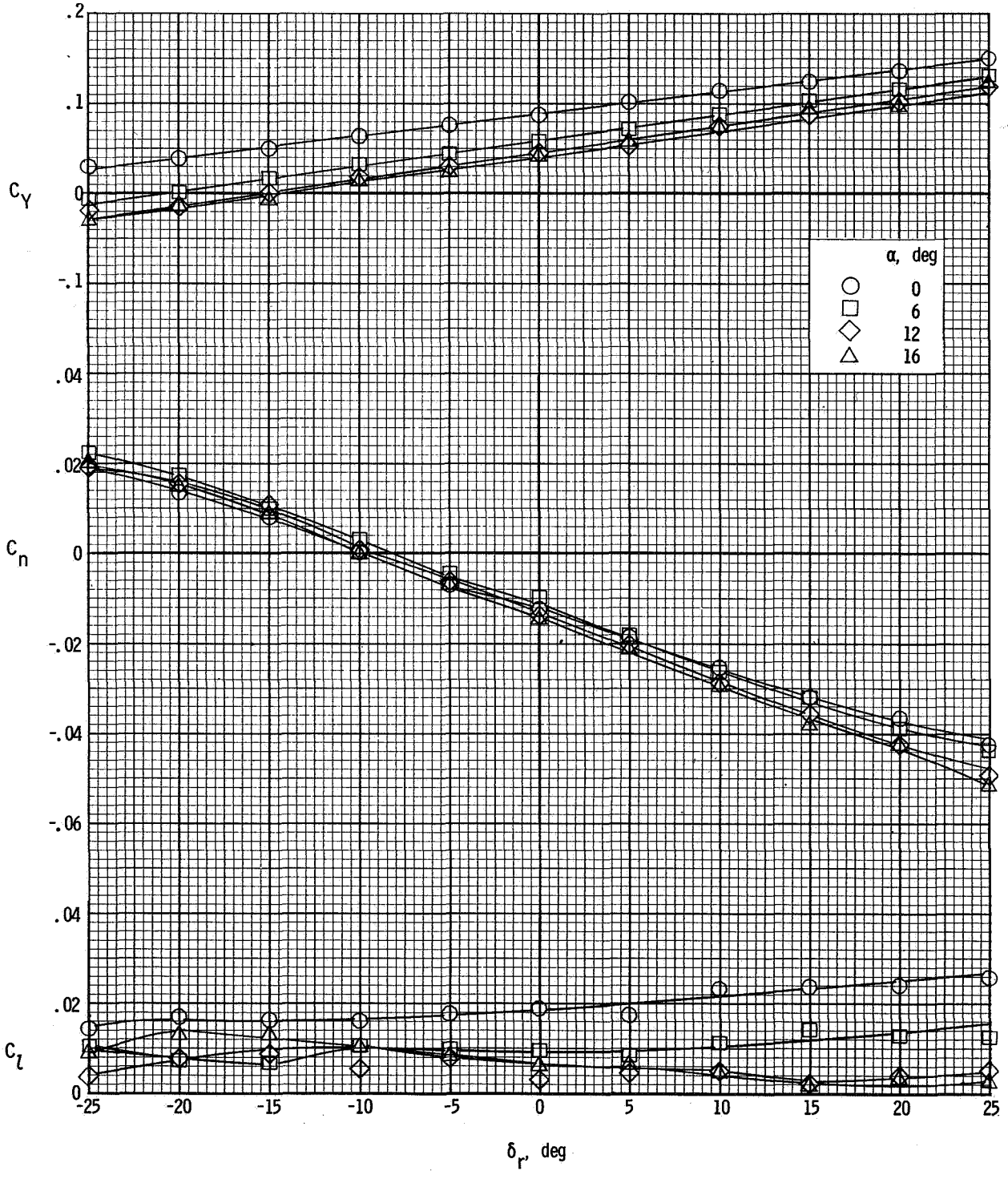

(d) $\beta = -4^{\circ}$.

Figure 26.- Continued.

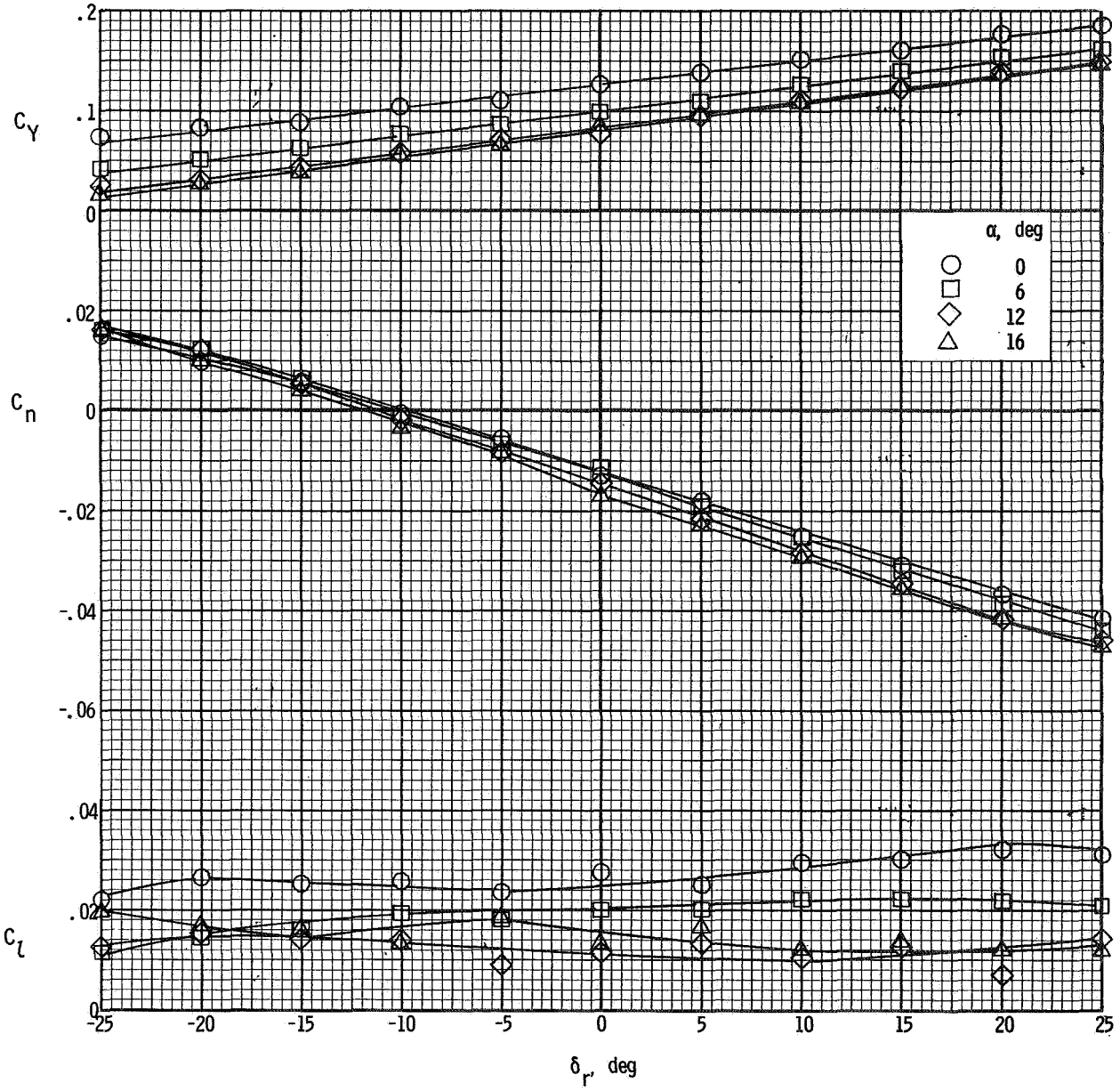

(e) $\beta = -8^{o}$.

Figure 26.- Concluded.

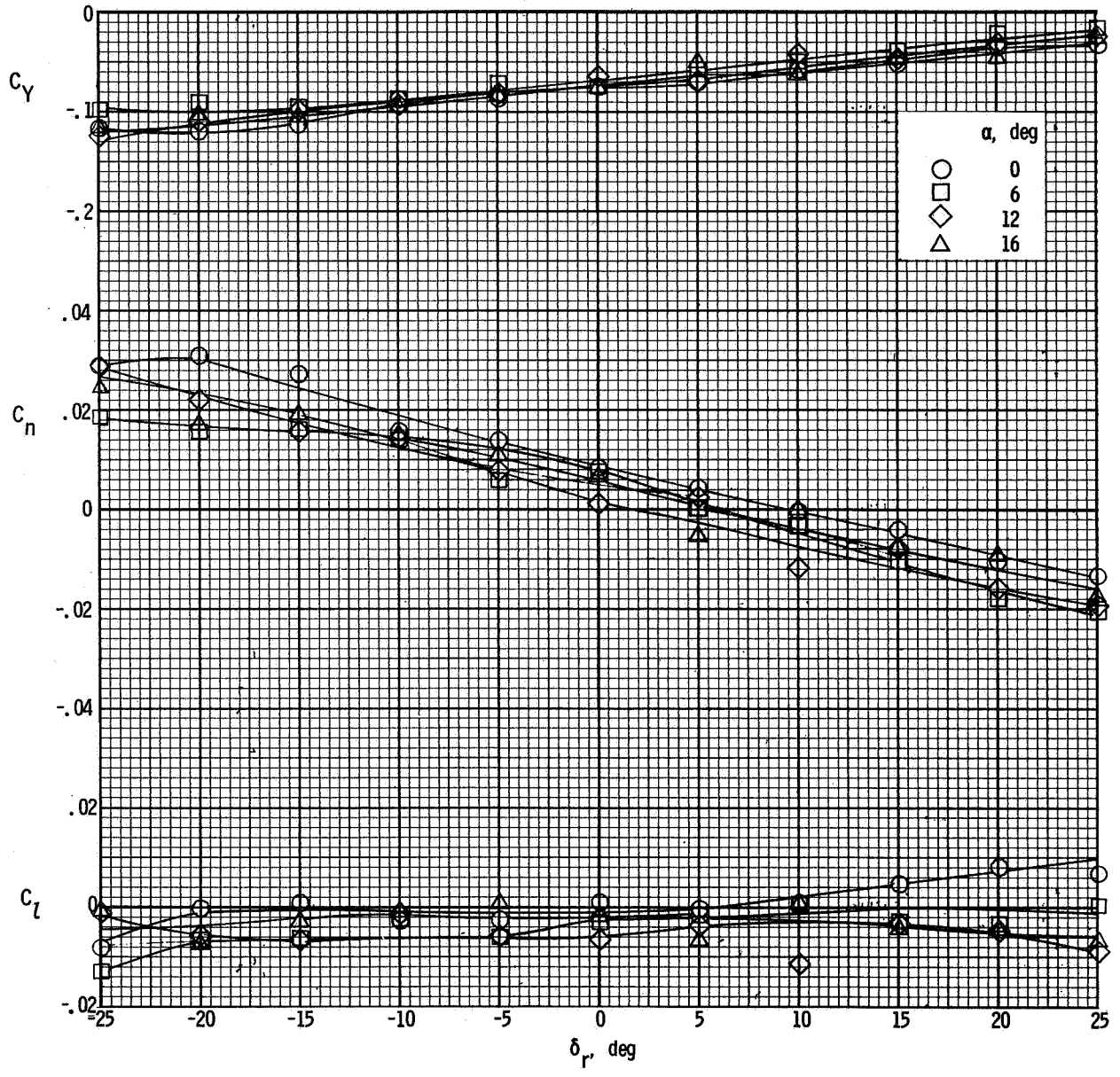

(a) $\beta = 8^{\circ}$.

Figure 27.- Variation of the lateral characteristics of the airplane with rudder deflection. $\delta_f = 30^{\circ}$; $T'_c = 0$.

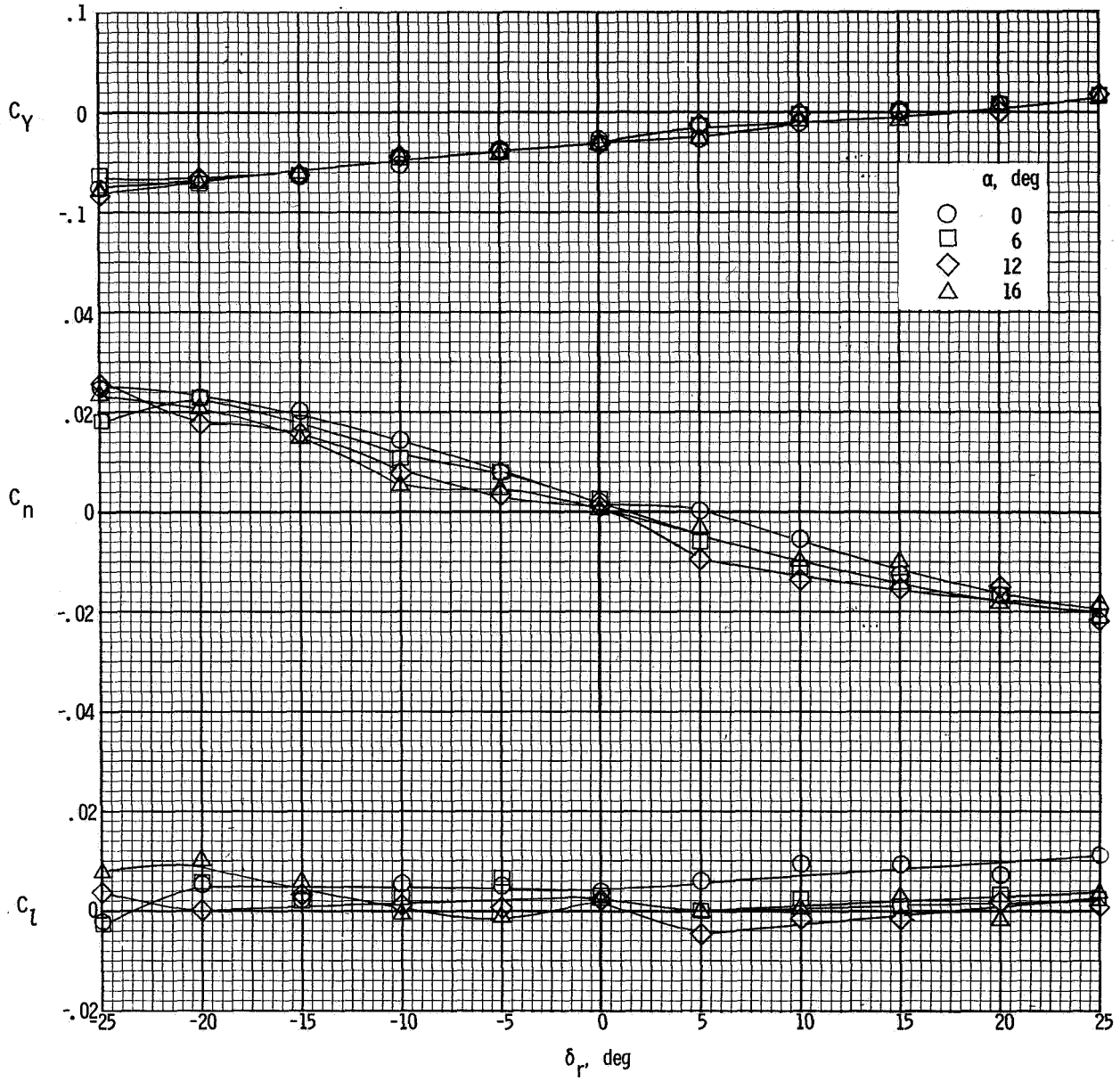

(b) $\beta = 4^{o}$.

Figure 27.- Continued.

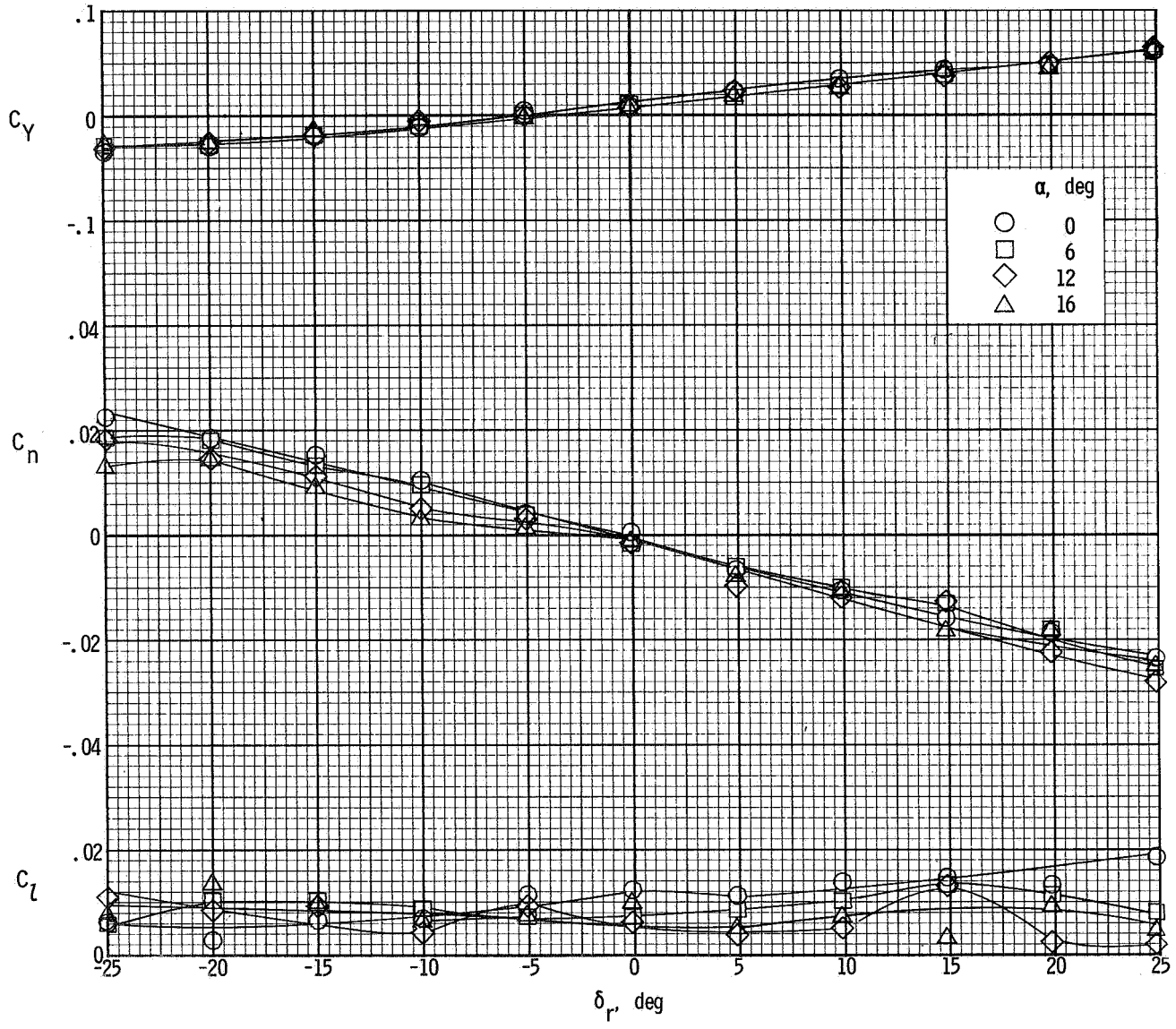

(c) $\beta = 0^{\circ}$.

Figure 27.- Continued.

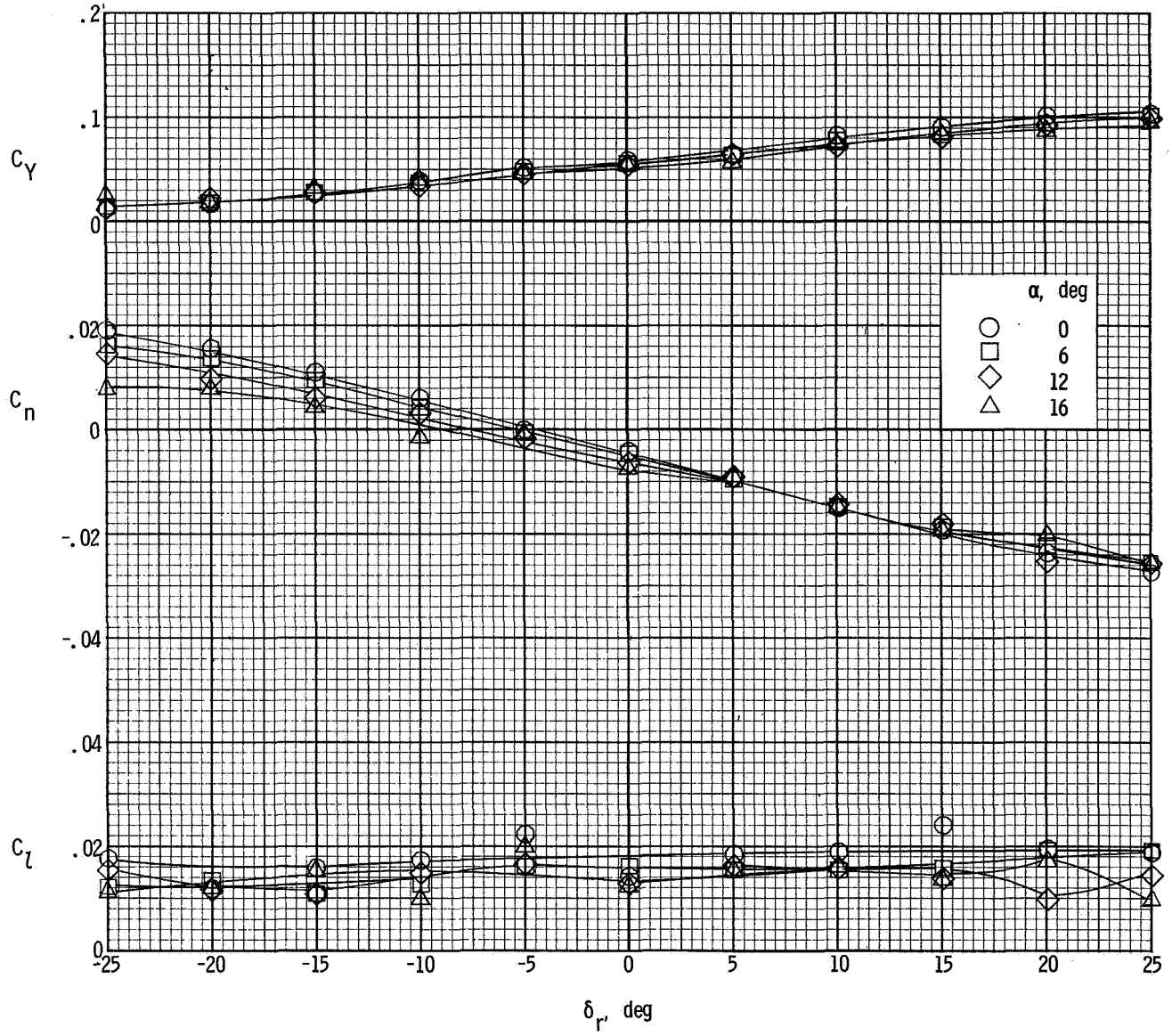

(d) $\beta = -4^{o}$.

Figure 27.- Continued.

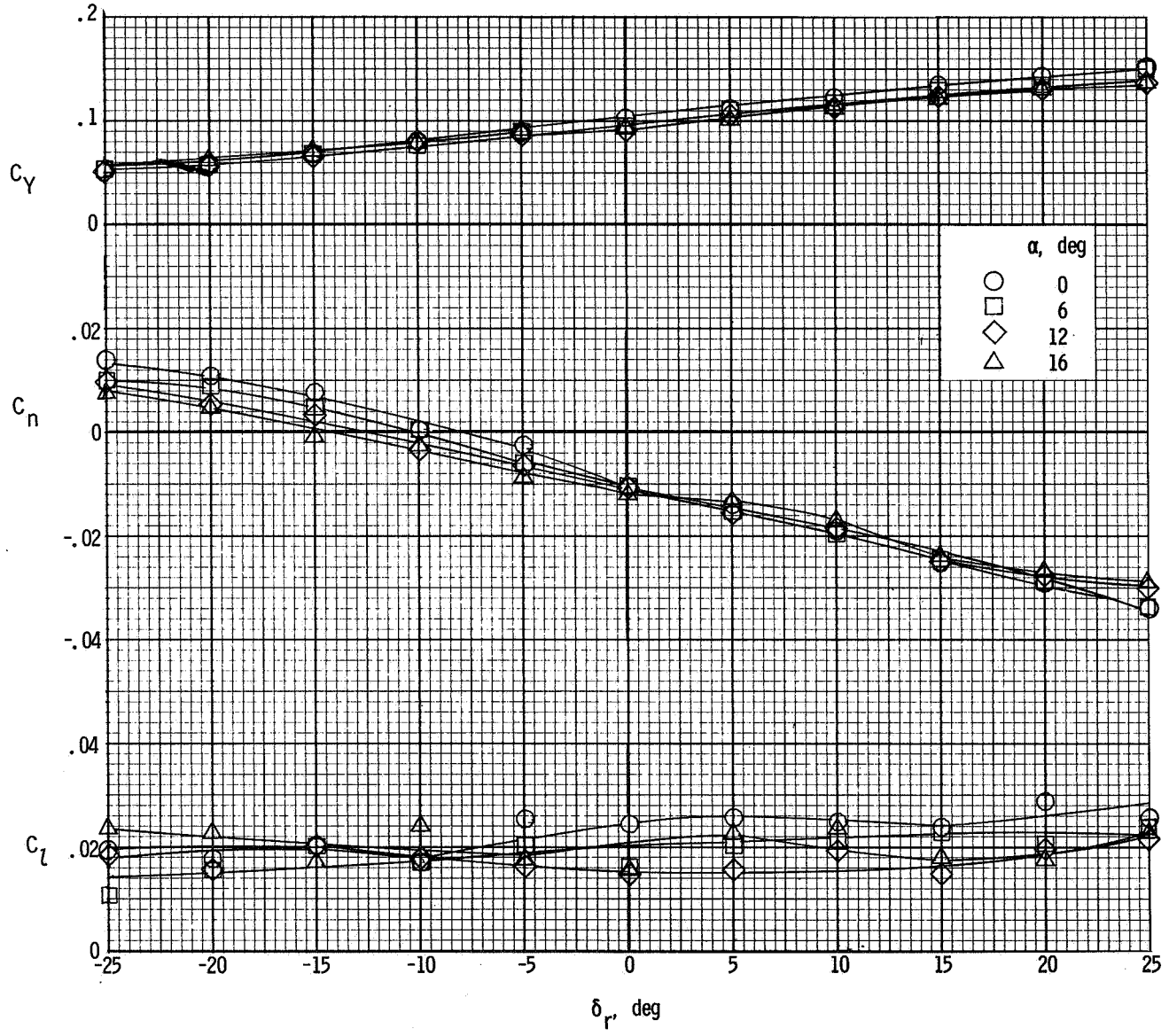

(e) $\beta = -8^{o}$.

Figure 27.- Concluded.

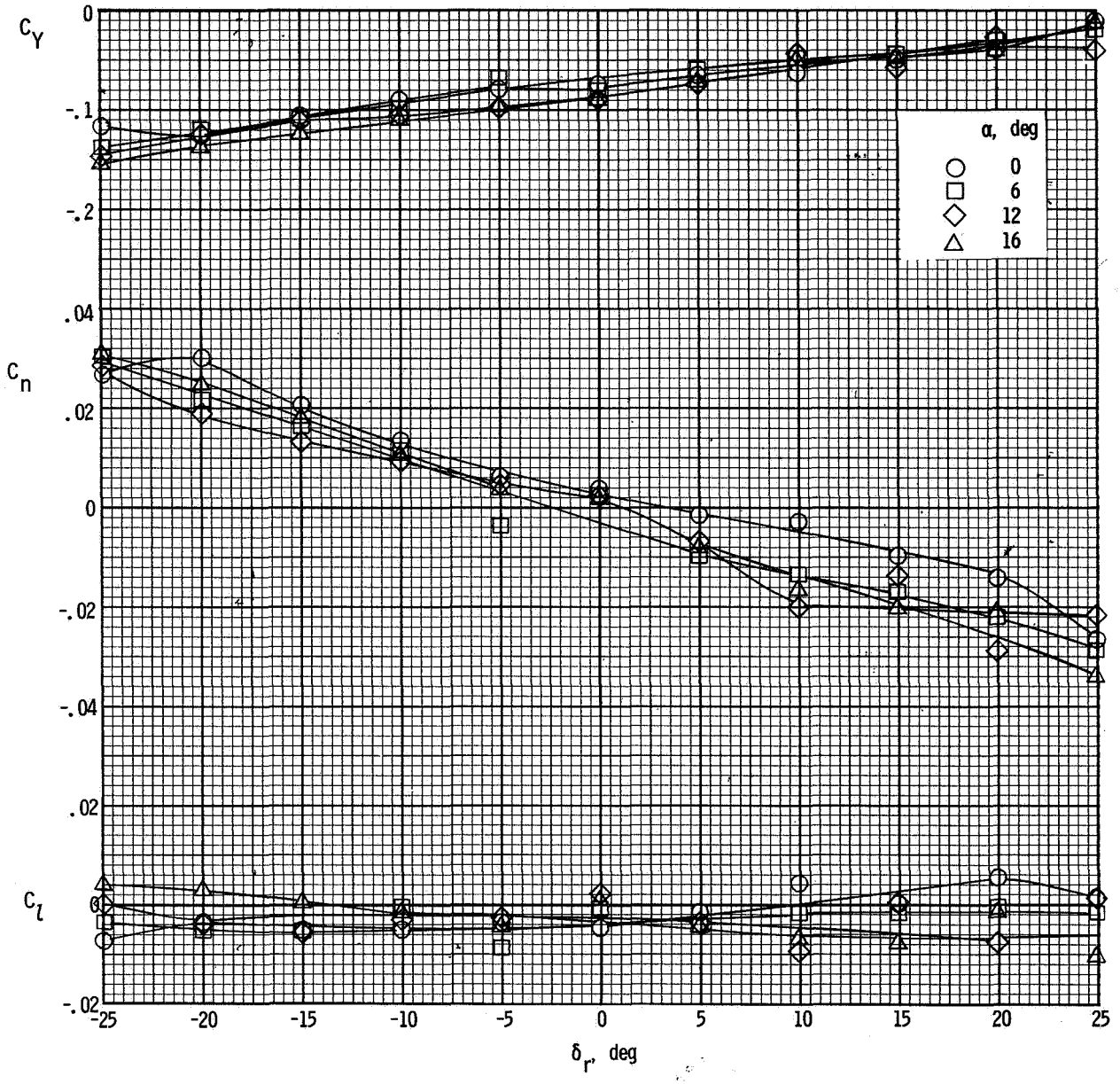

(a) $\beta = 8^{\circ}$.

Figure 28.- Variation of the lateral characteristics of the airplane with rudder deflection. $\delta_f = 30^{\circ}$; $T'_c = 0.14$.

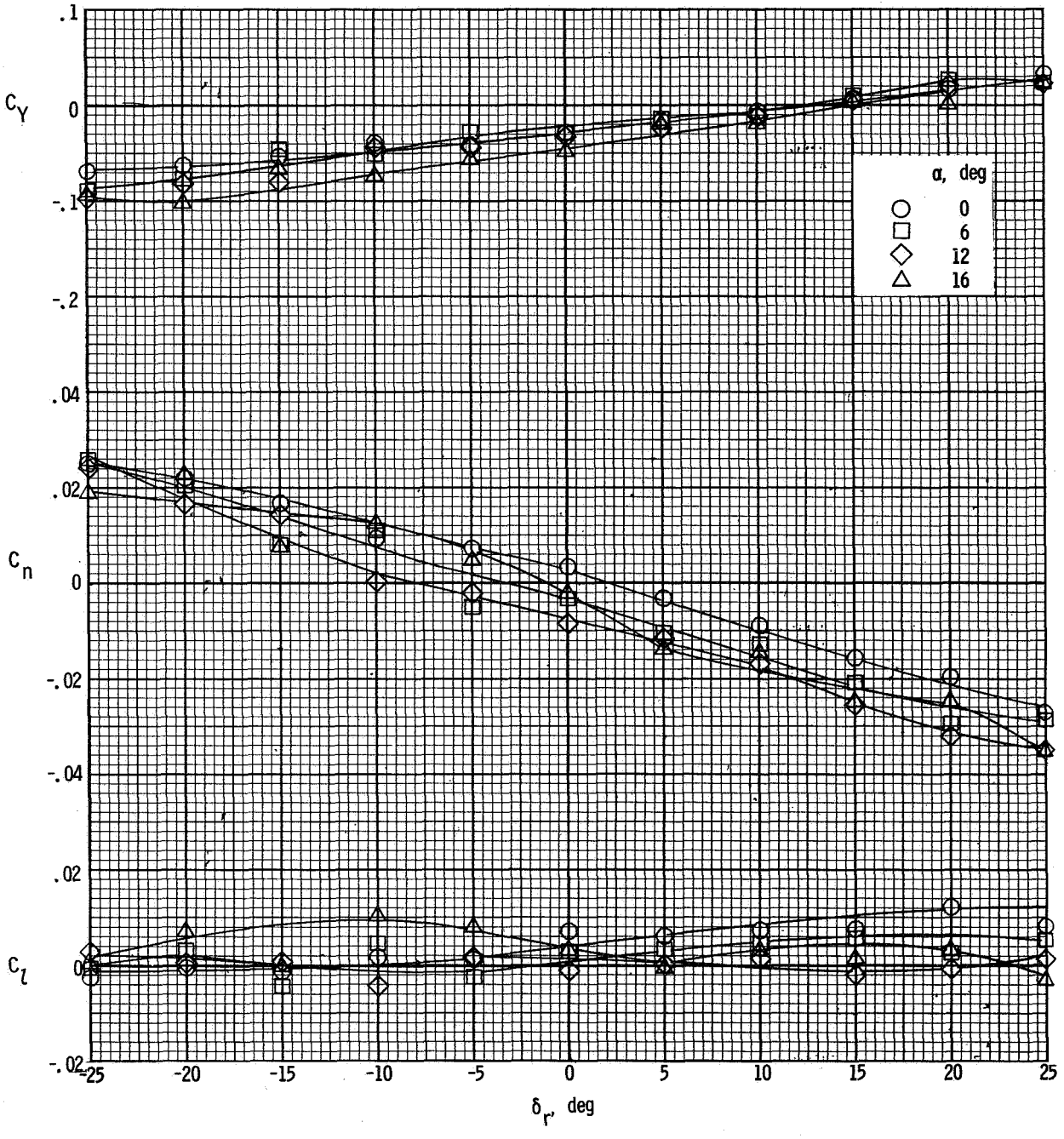

(b) $\beta = 4^{o}$.

Figure 28.- Continued.

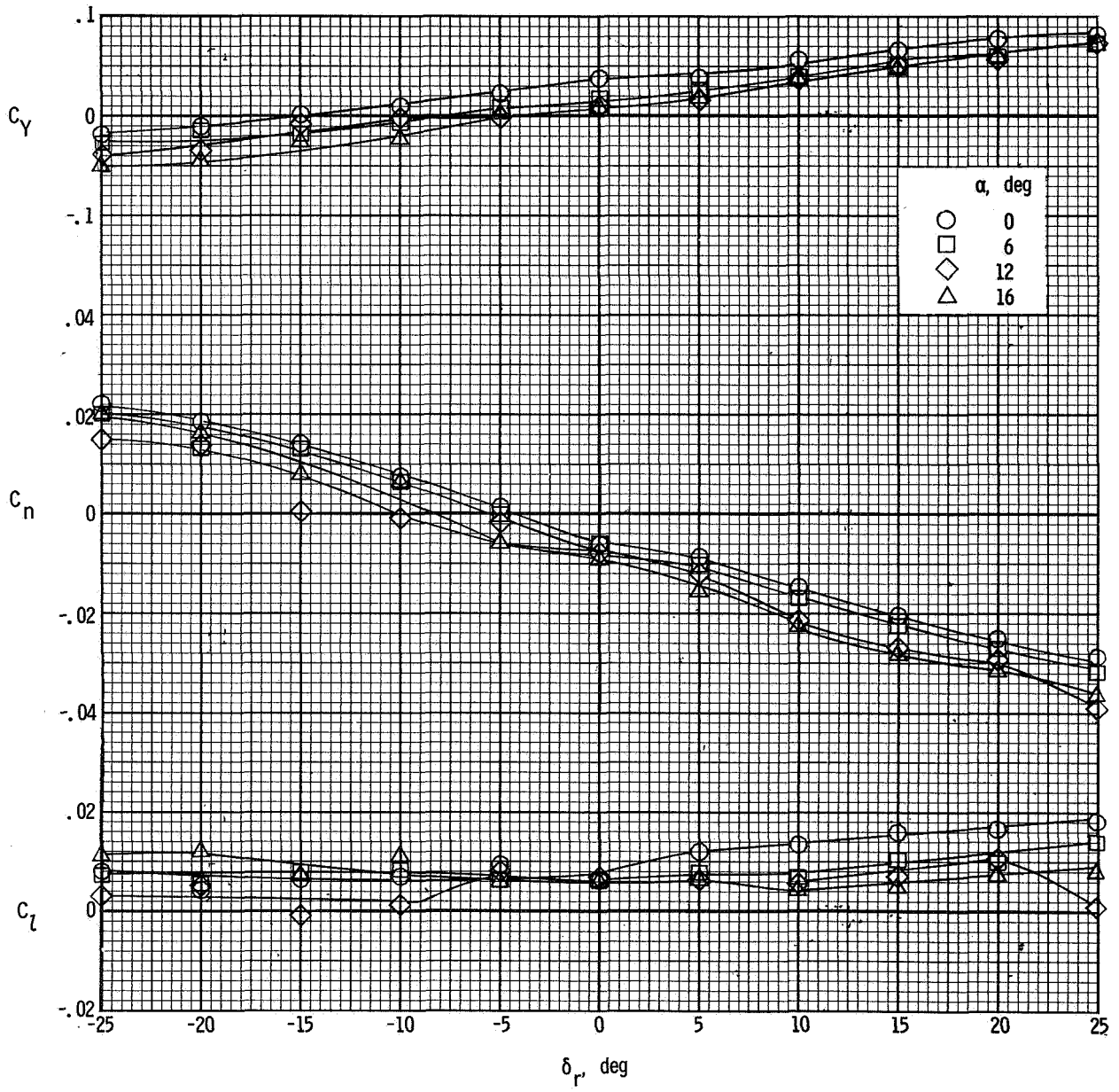

(c) $\beta = 0^o$.

Figure 28.- Continued.

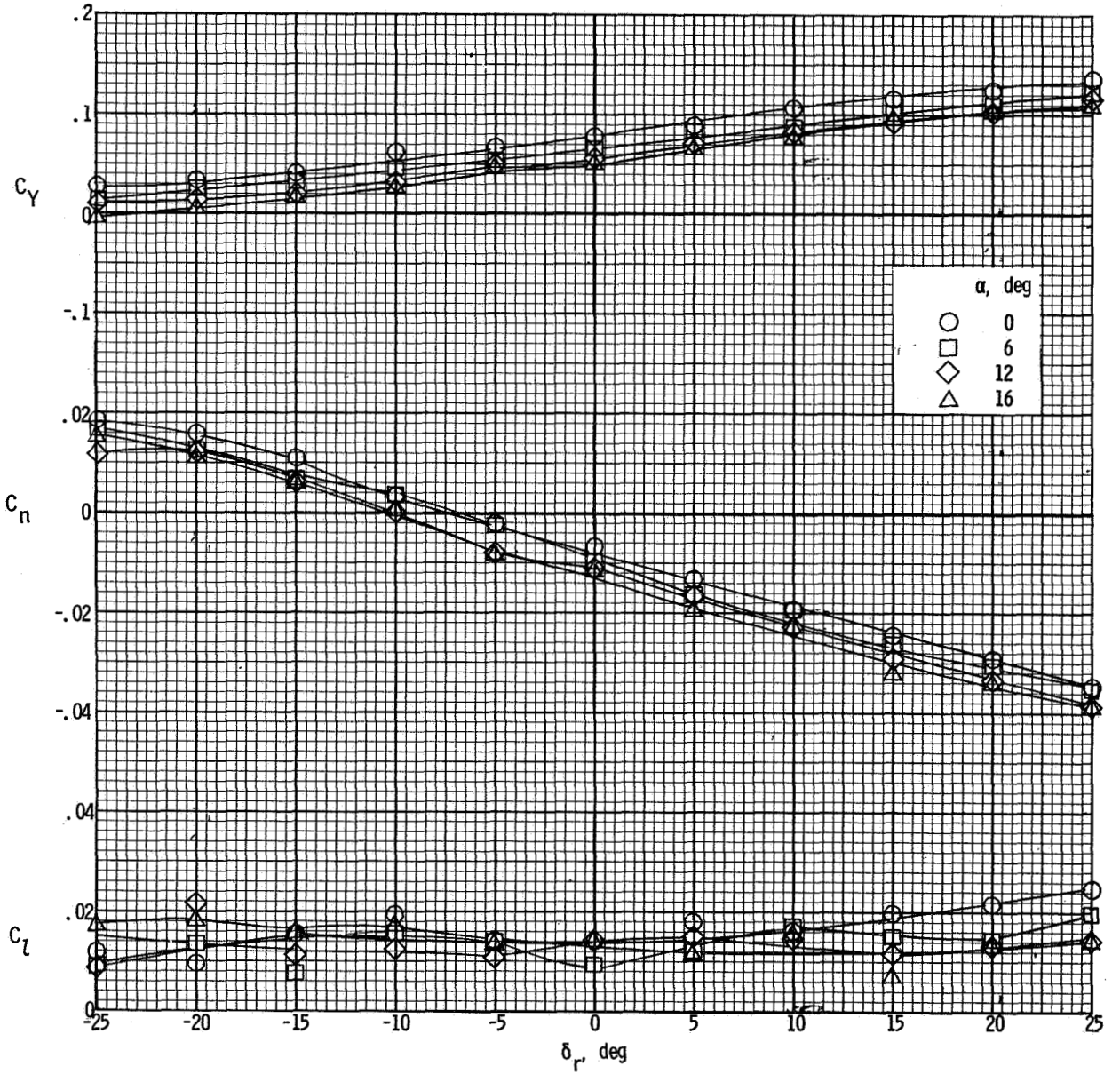

(d) $\beta = -4^{o}$.

Figure 28.- Continued.

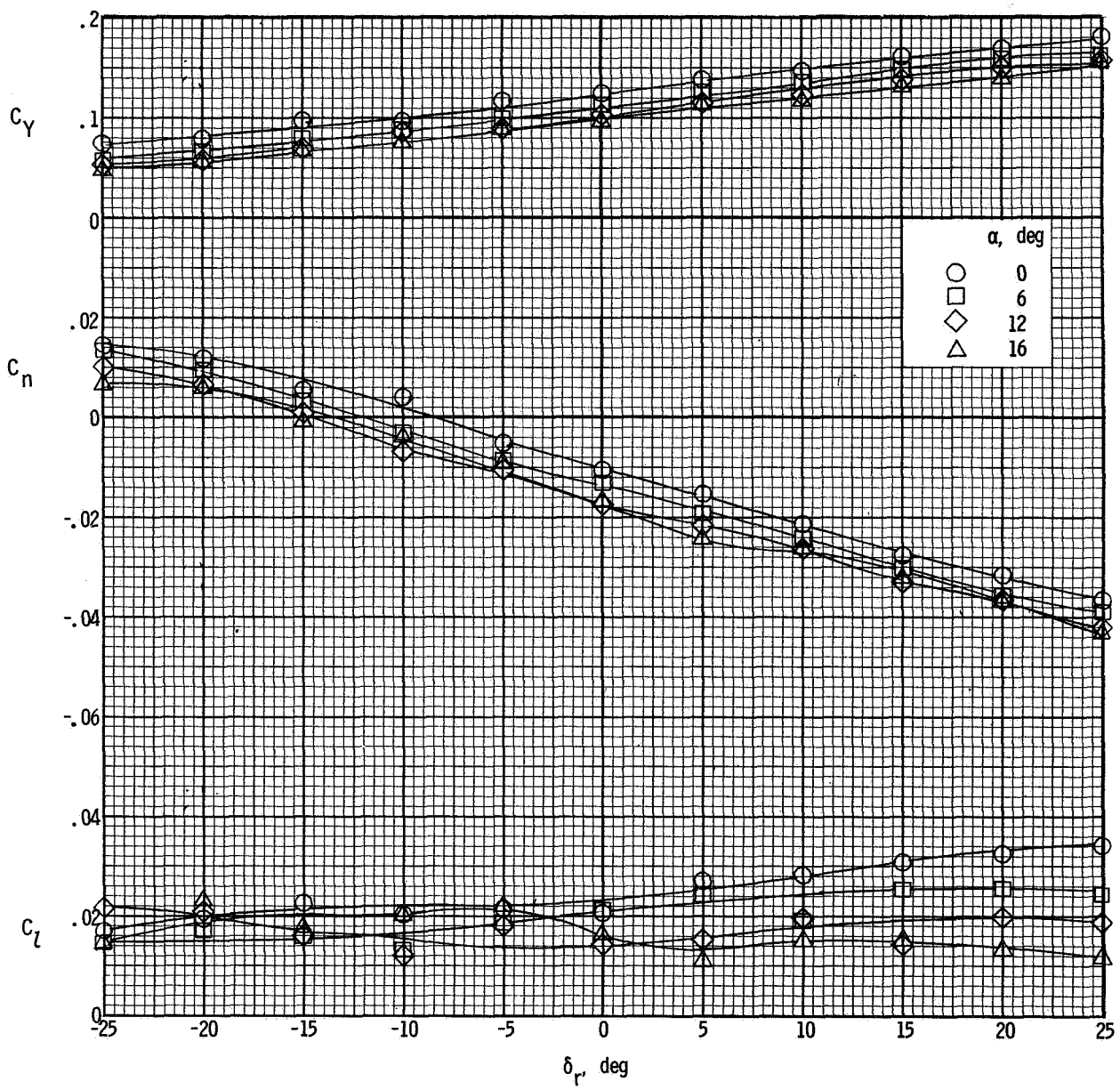

(e) $\beta = -8^{\circ}$.

Figure 28.- Concluded.

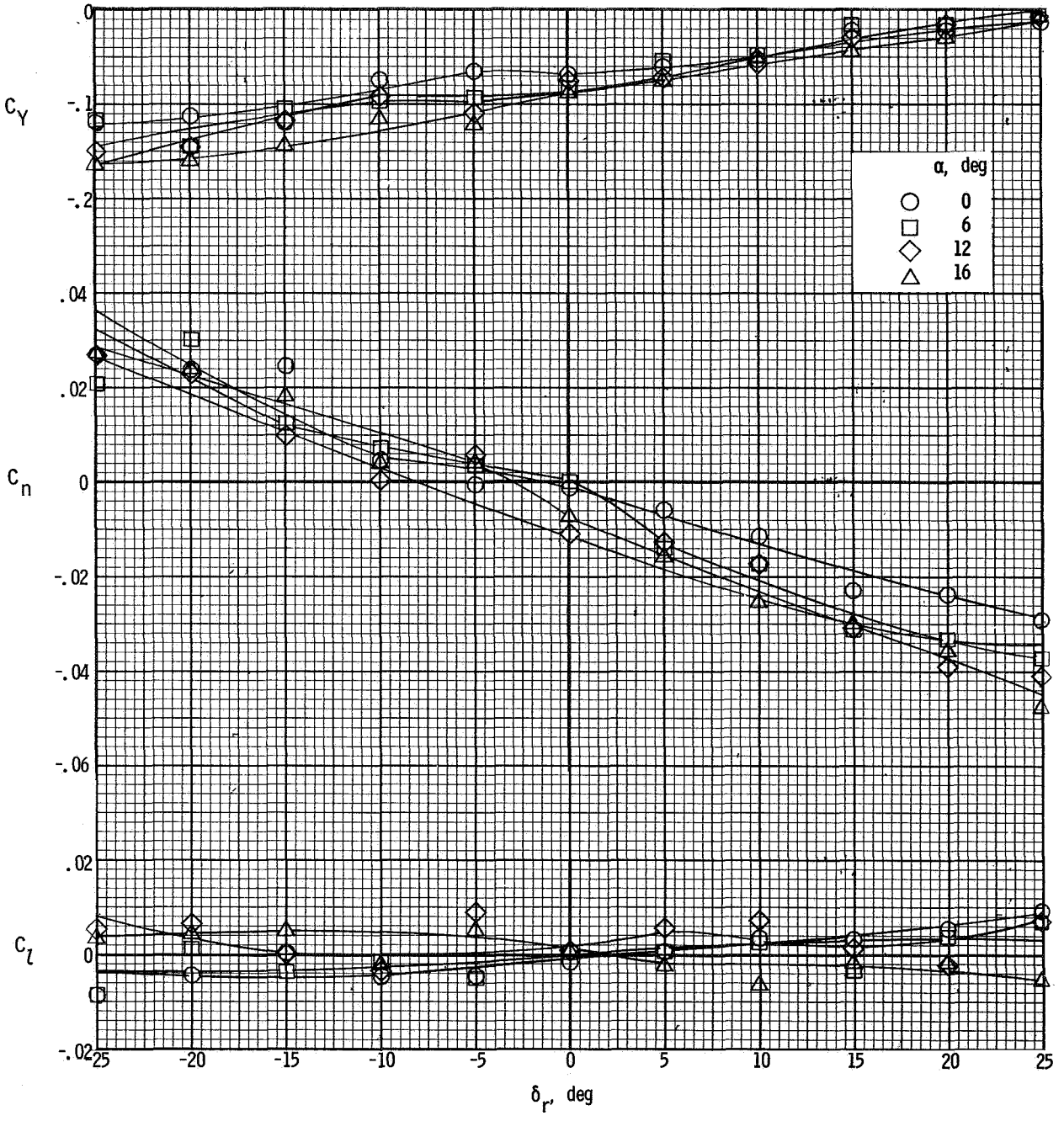

(a) $\beta = 8^{o}$.

Figure 29.- Variation of the lateral characteristics of the airplane with rudder deflection. $\delta_f = 30^{o}$; $T'_c = 0.30$.

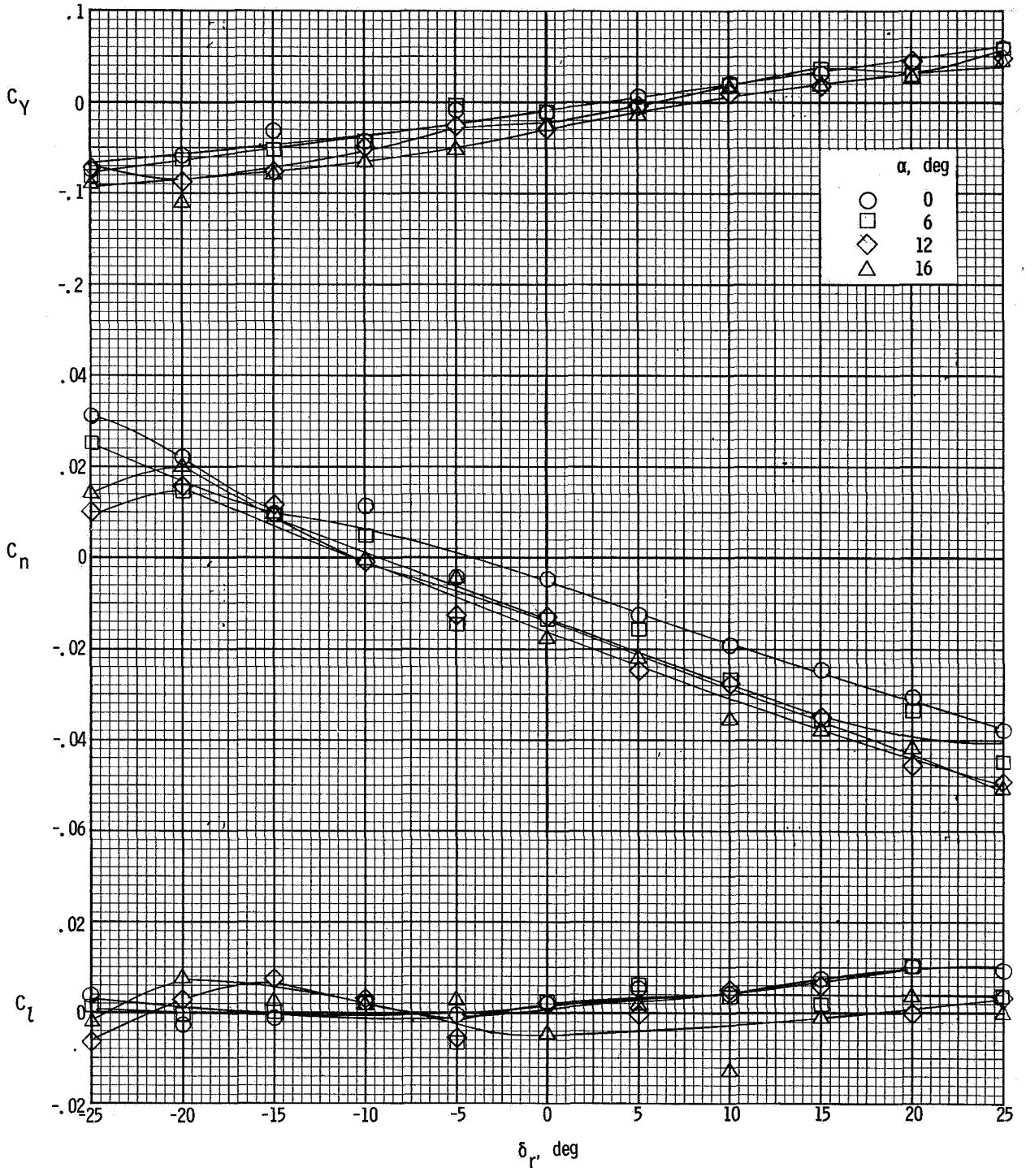

(b) $\beta = 4^o$.

Figure 29.- Continued.

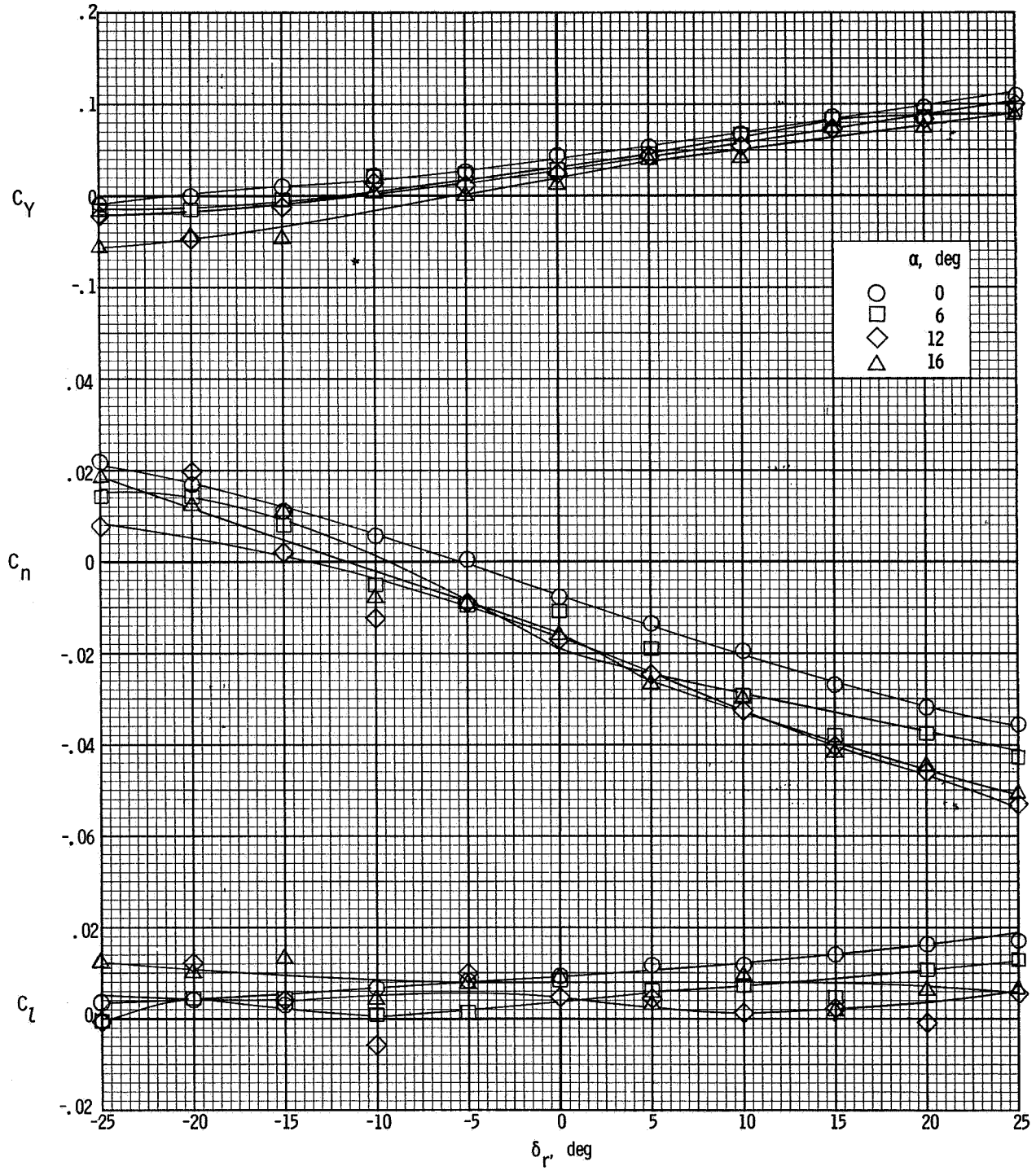

(c) $\beta = 0^o$.

Figure 29.- Continued.

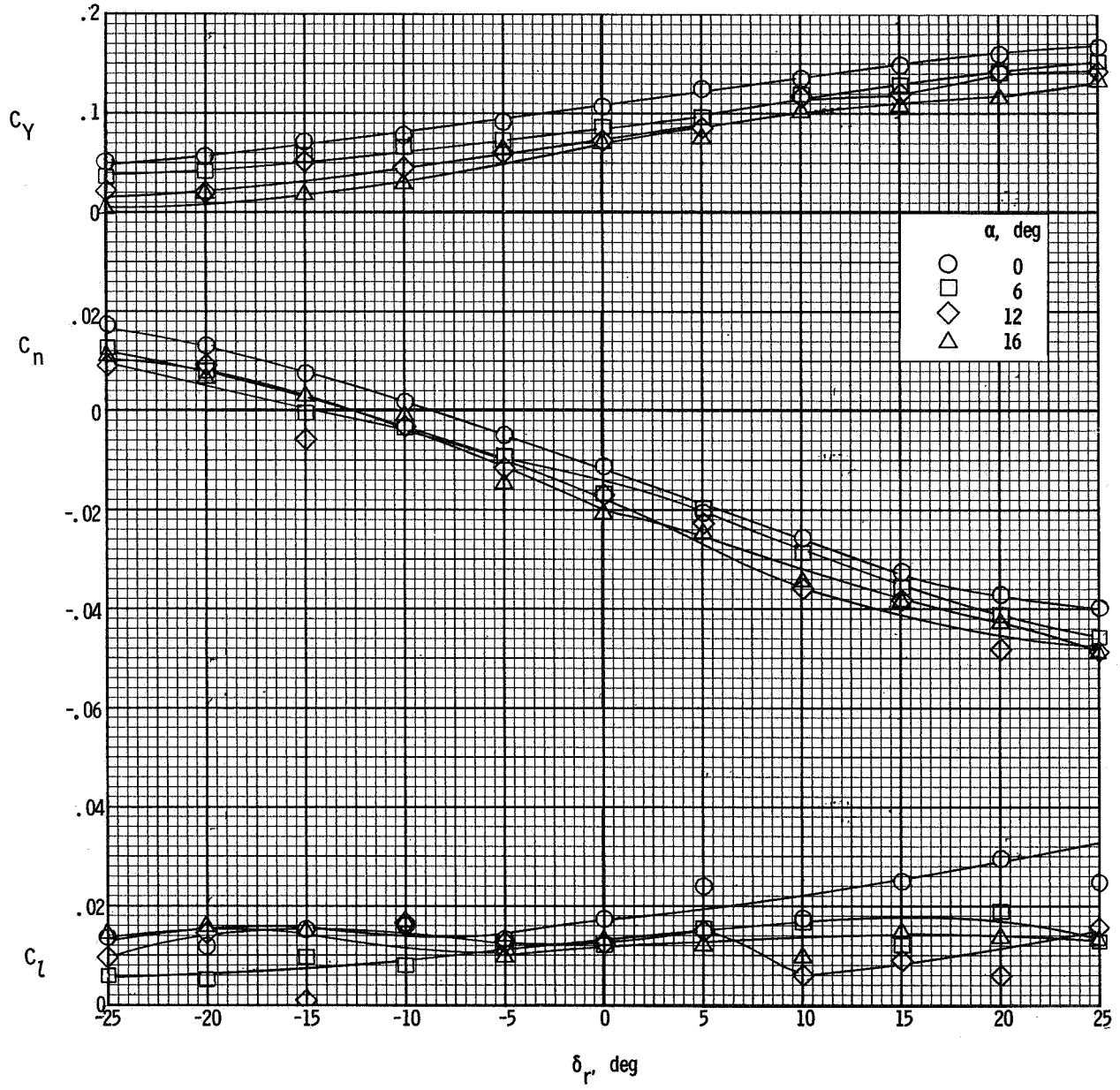

(d) $\beta = -4^{o}$.

Figure 29.- Continued.

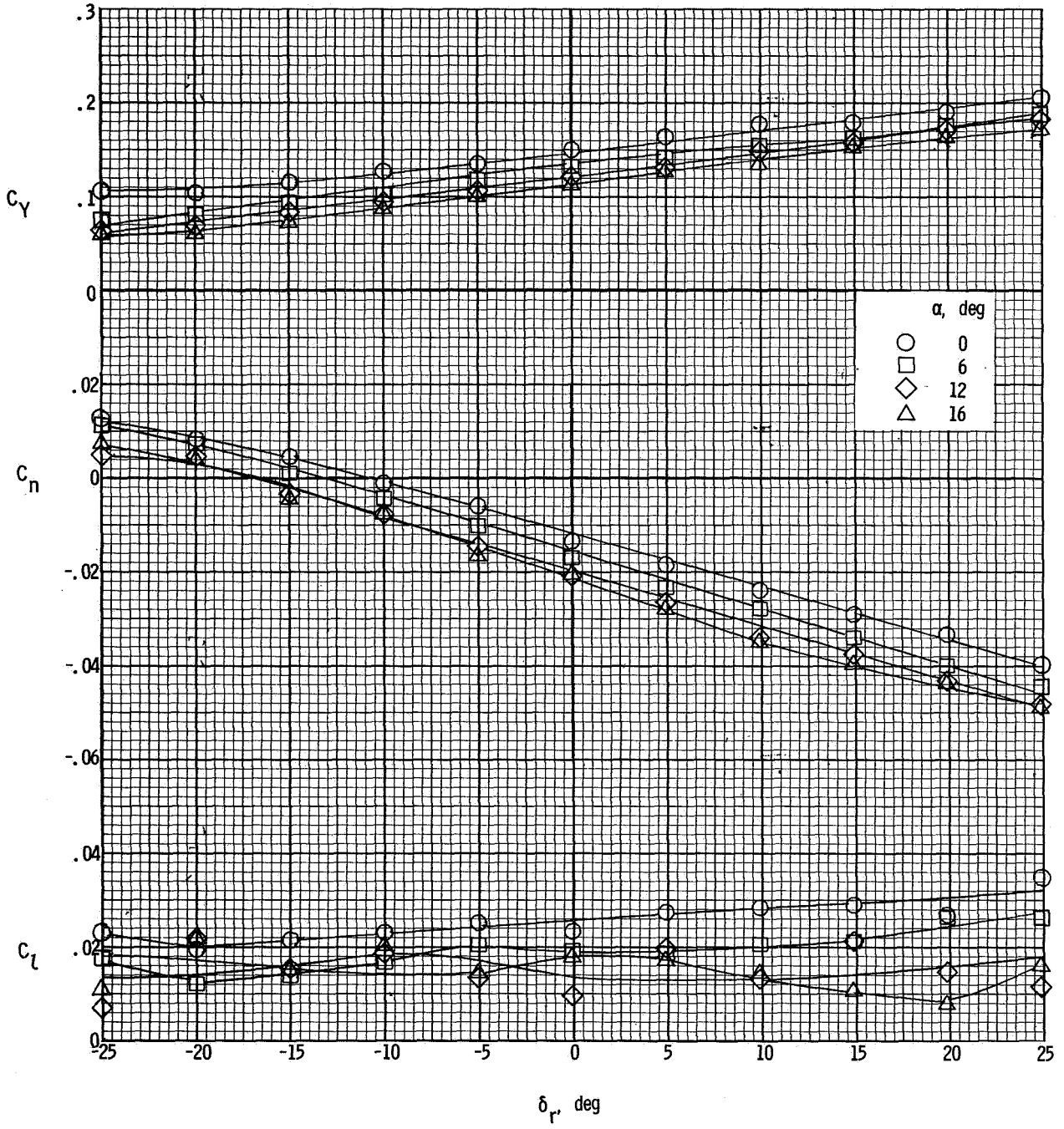

(e) $\beta = -8^{o}$.

Figure 29.- Concluded.

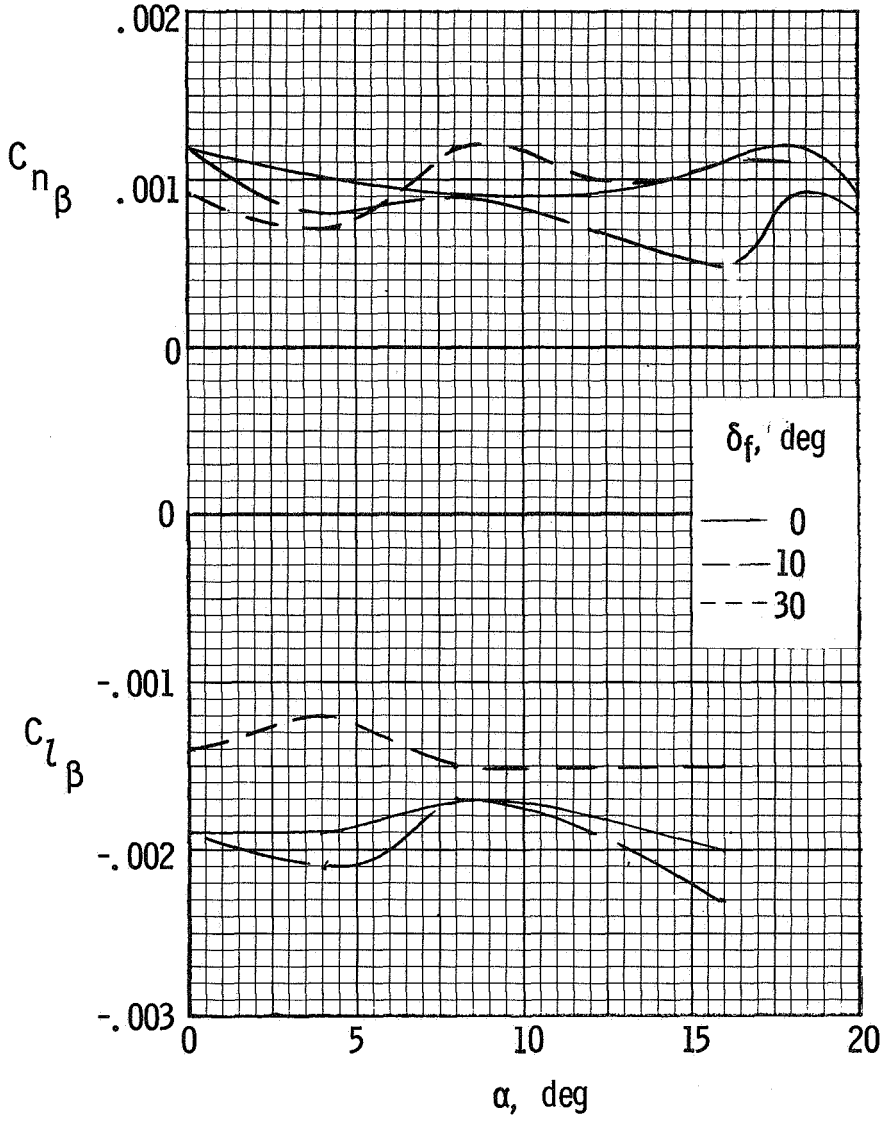

Figure 30.- Variation of effective-dihedral and directional stability parameters with angle of attack. Propeller removed.

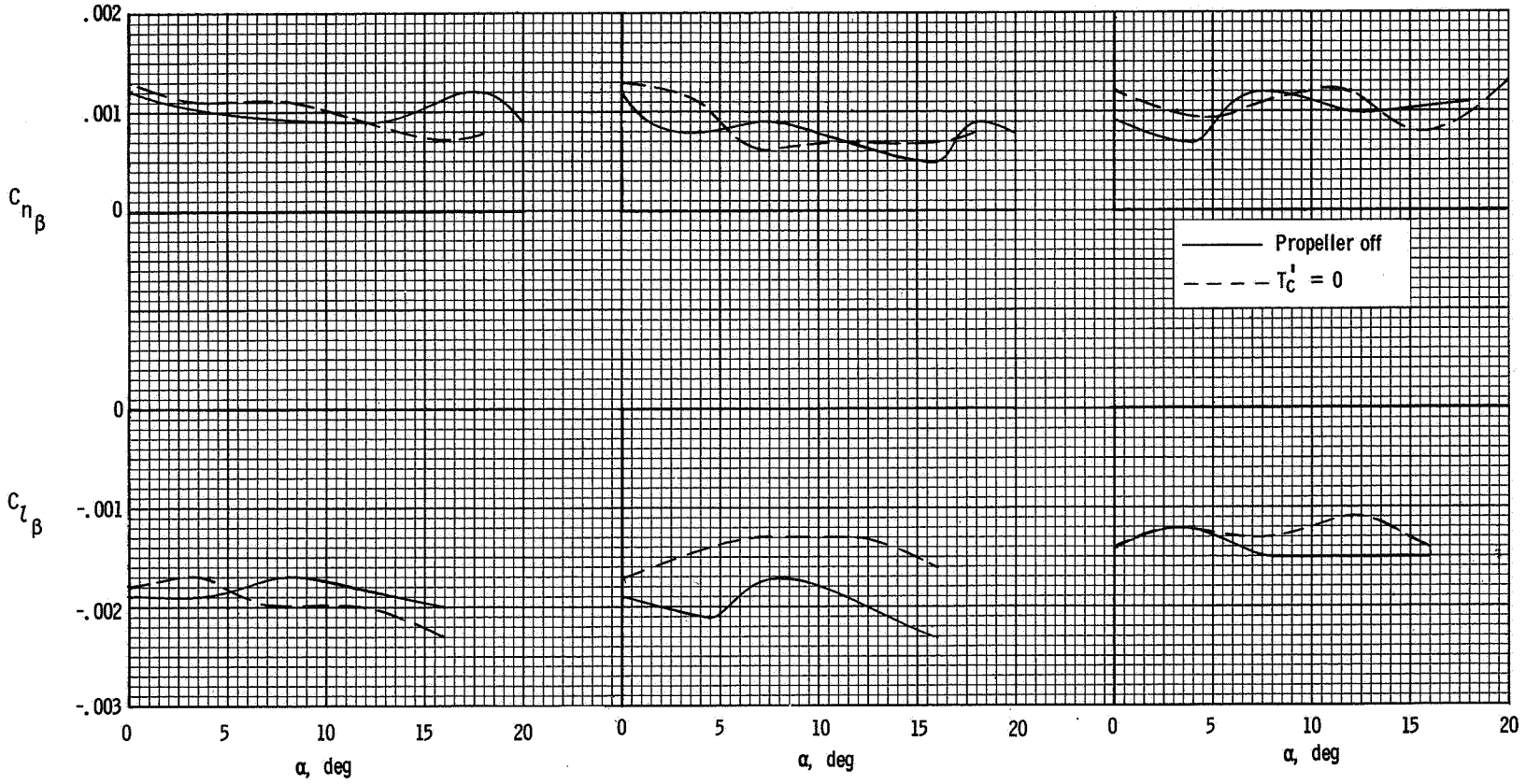

(a) $\delta_f = 0^o$. (b) $\delta_f = 10^o$. (c) $\delta_f = 30^o$.

Figure 31.- The lateral characteristics of the model with the propeller removed and at zero thrust.

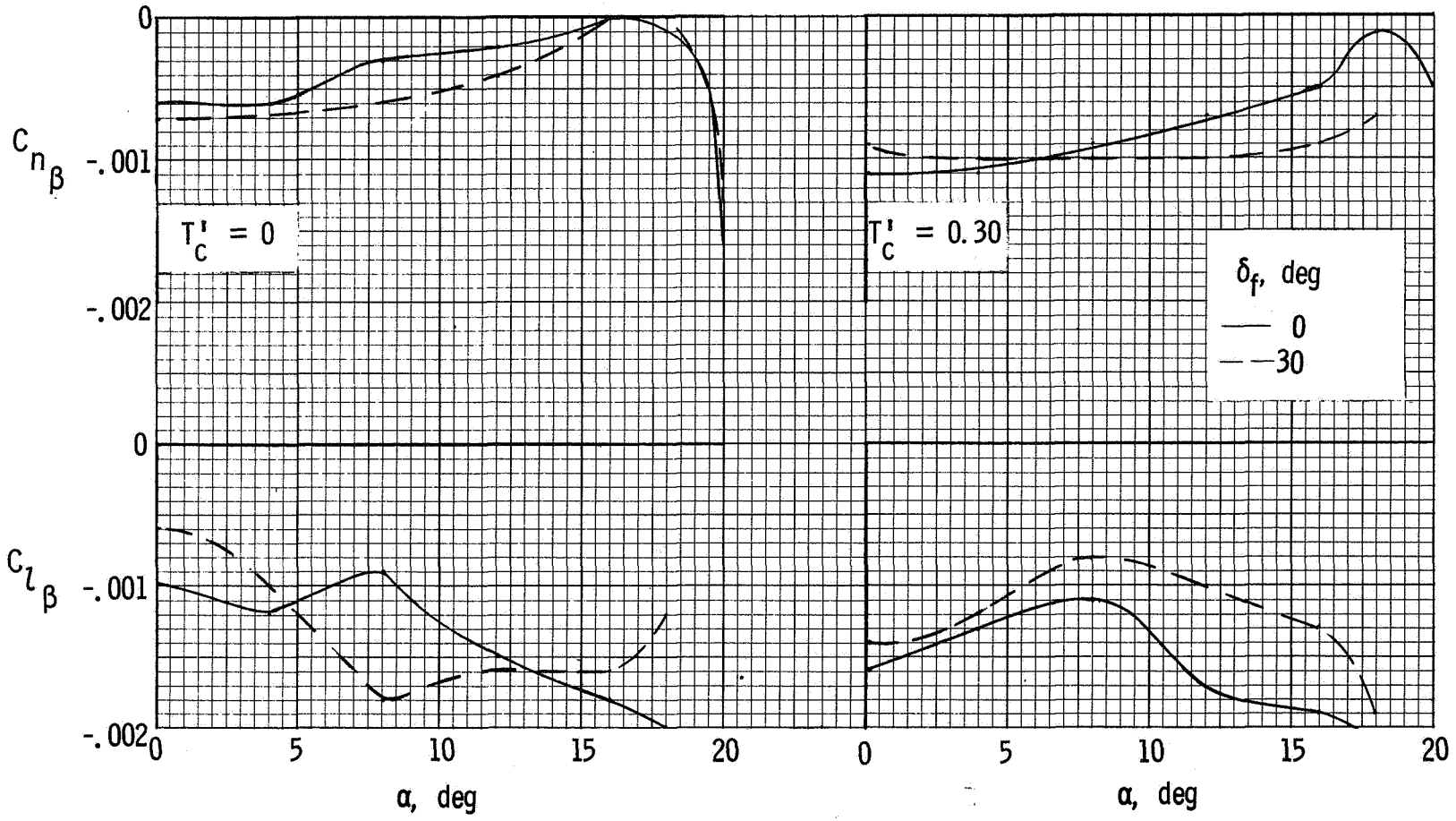

(a) $T_c' = 0$.

(b) $T_c' = 0.30$.

Figure 32.- Variation of effective-dihedral and directional stability parameters with angle of attack with the vertical tail removed.

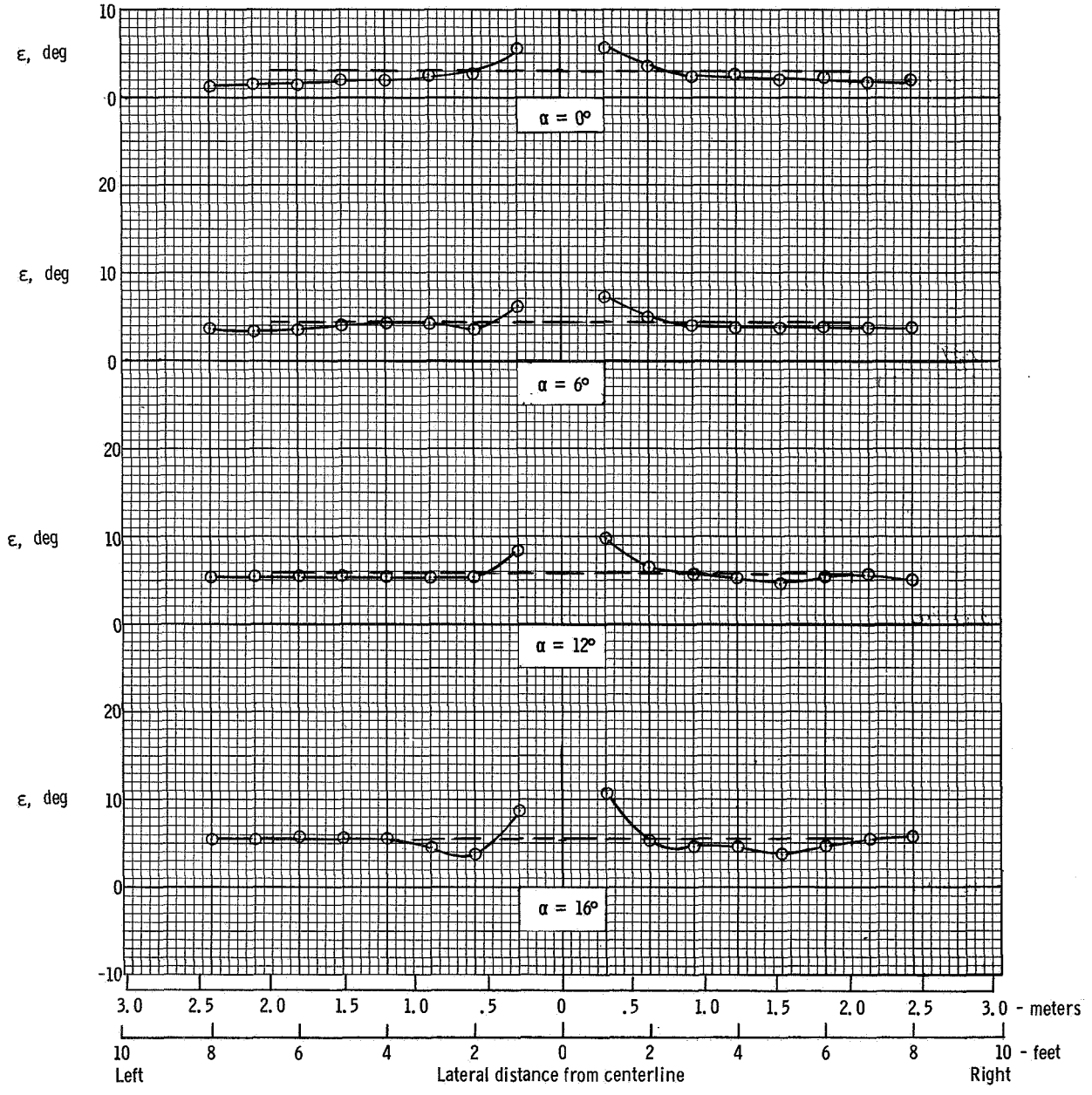

(a) $T_c' = 0$.

Figure 33.- Distribution of downwash across span of horizontal-tail surface. $\delta_f = 0^o$. $\beta = 0^o$. Dashed lines are averages integrated over horizontal-tail span.

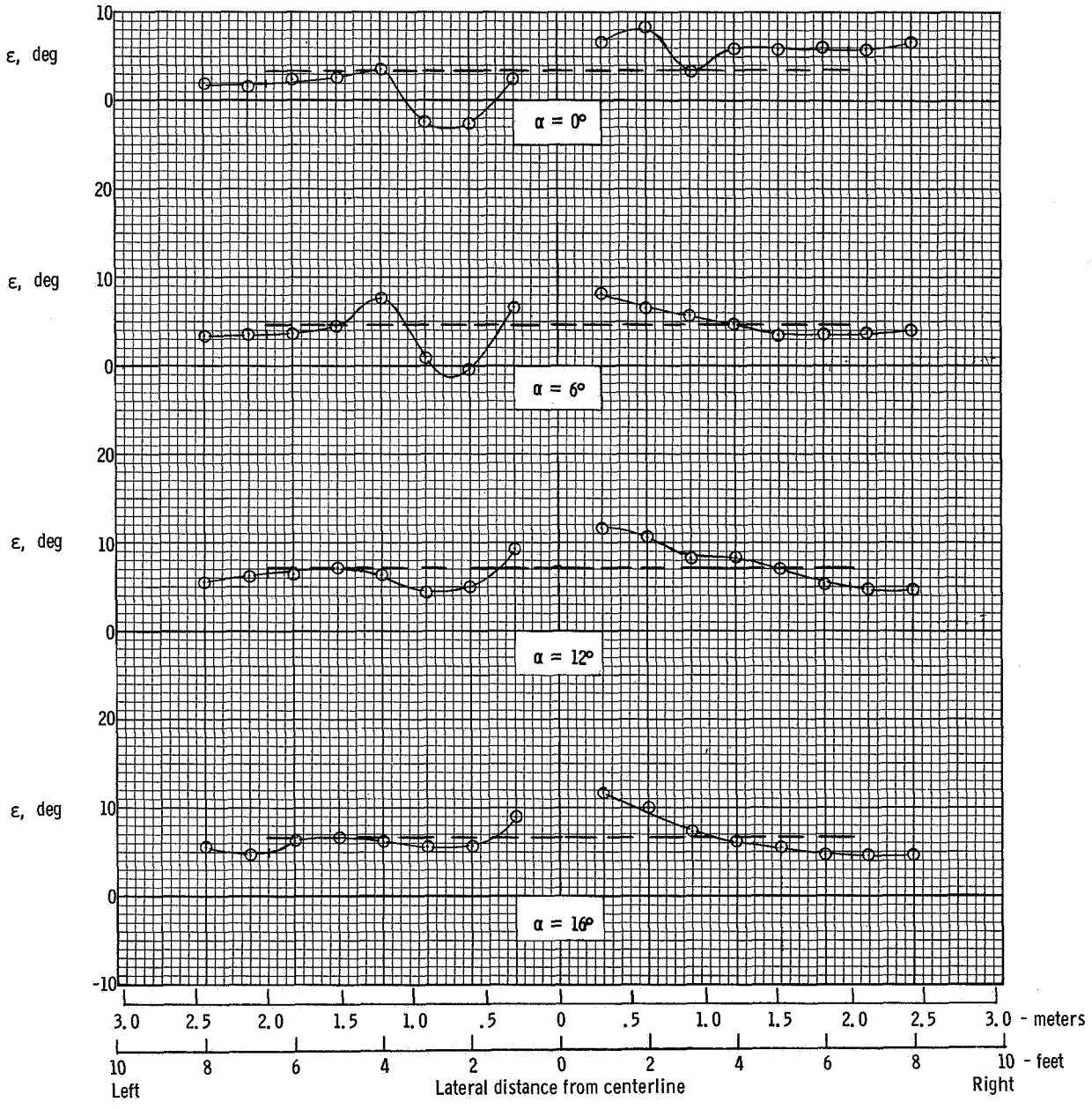

(b) $T'_c = 0.14$.

Figure 33.- Continued.

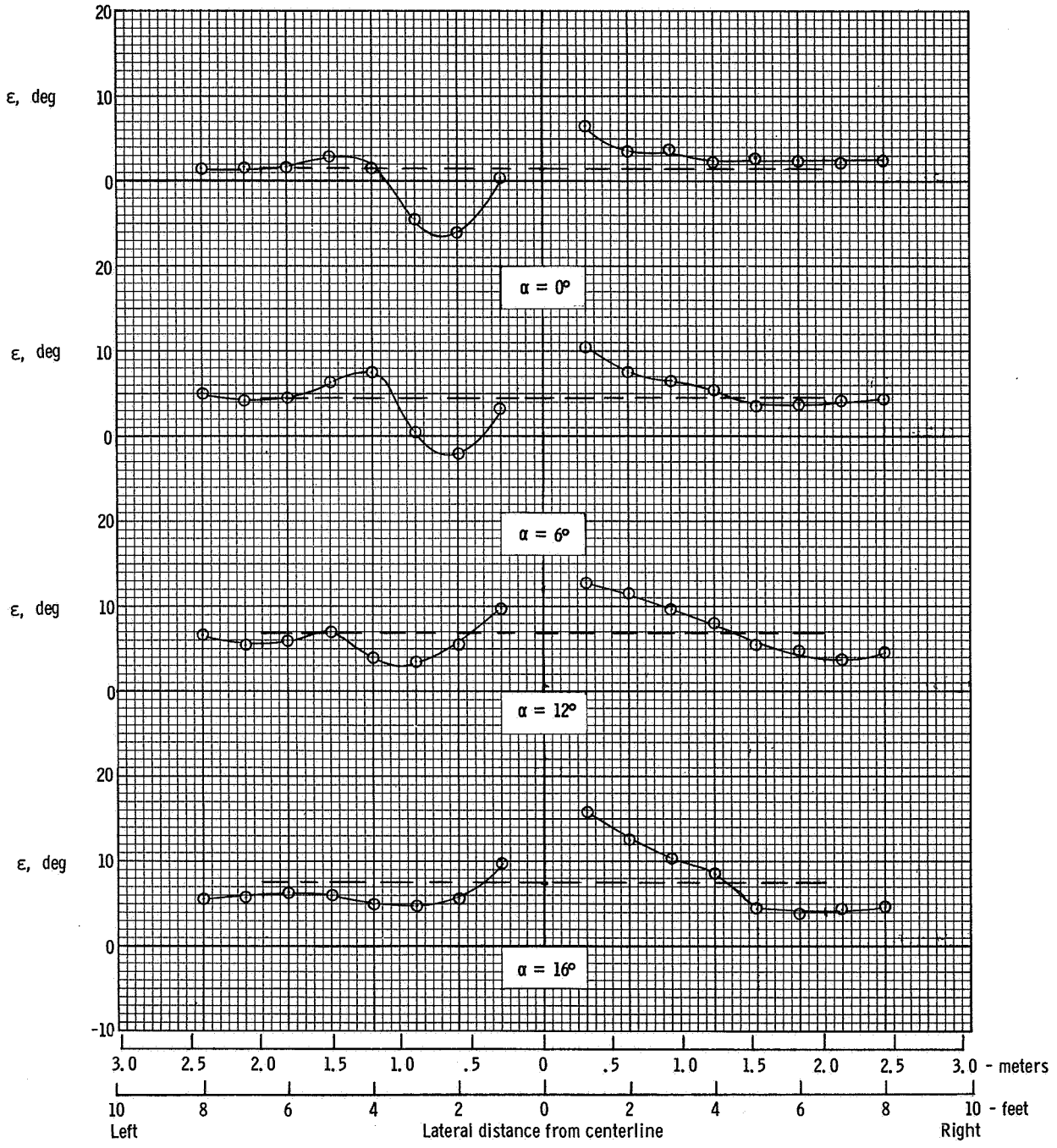

(c) $T'_C = 0.30$.

Figure 33.- Concluded.

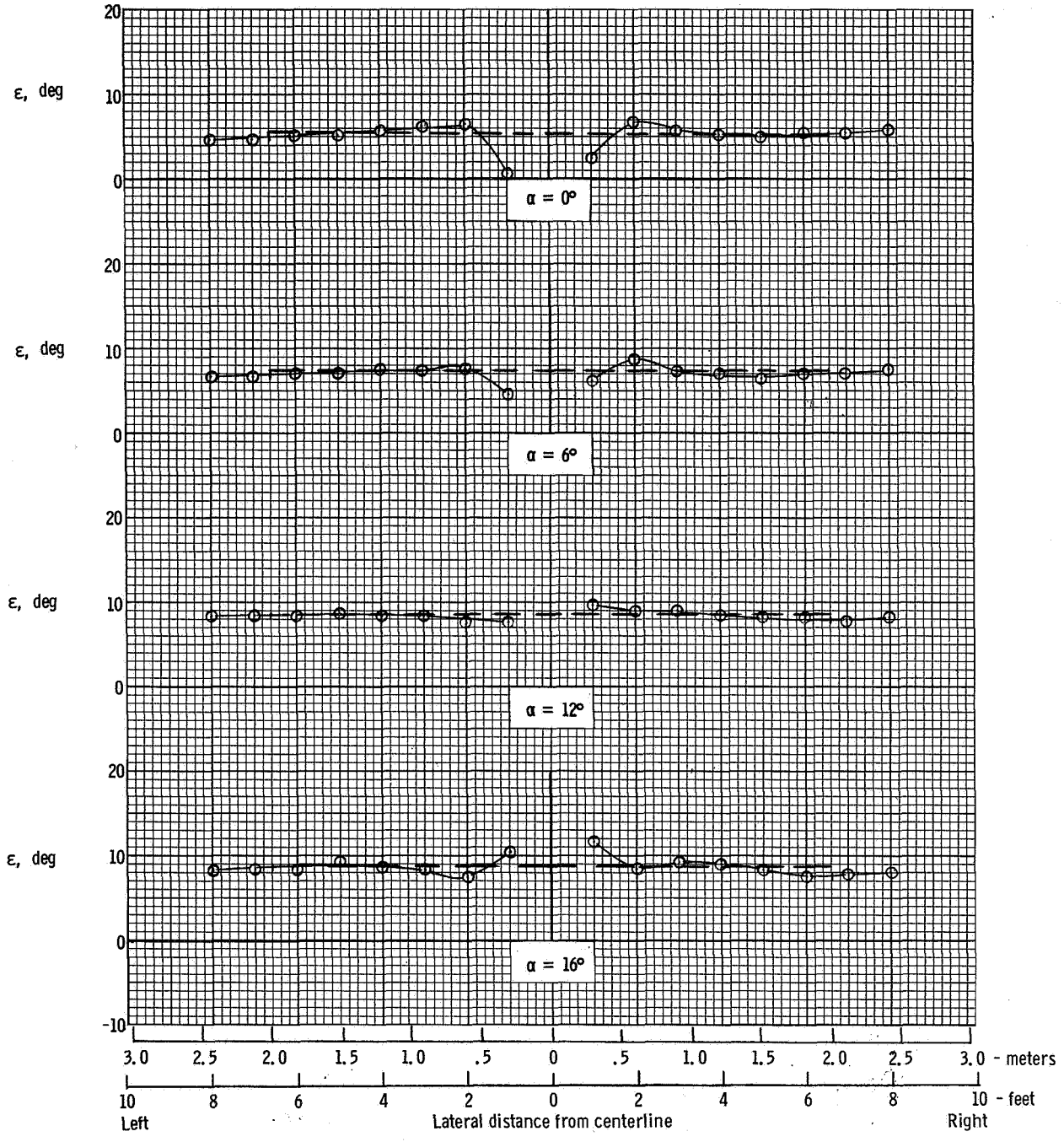

(a) $T'_c = 0$.

Figure 34.- Distribution of downwash across span of horizontal-tail surface. $\delta_f = 10^o$. $\beta = 0^o$. Dashed lines are averages integrated over horizontal-tail span.

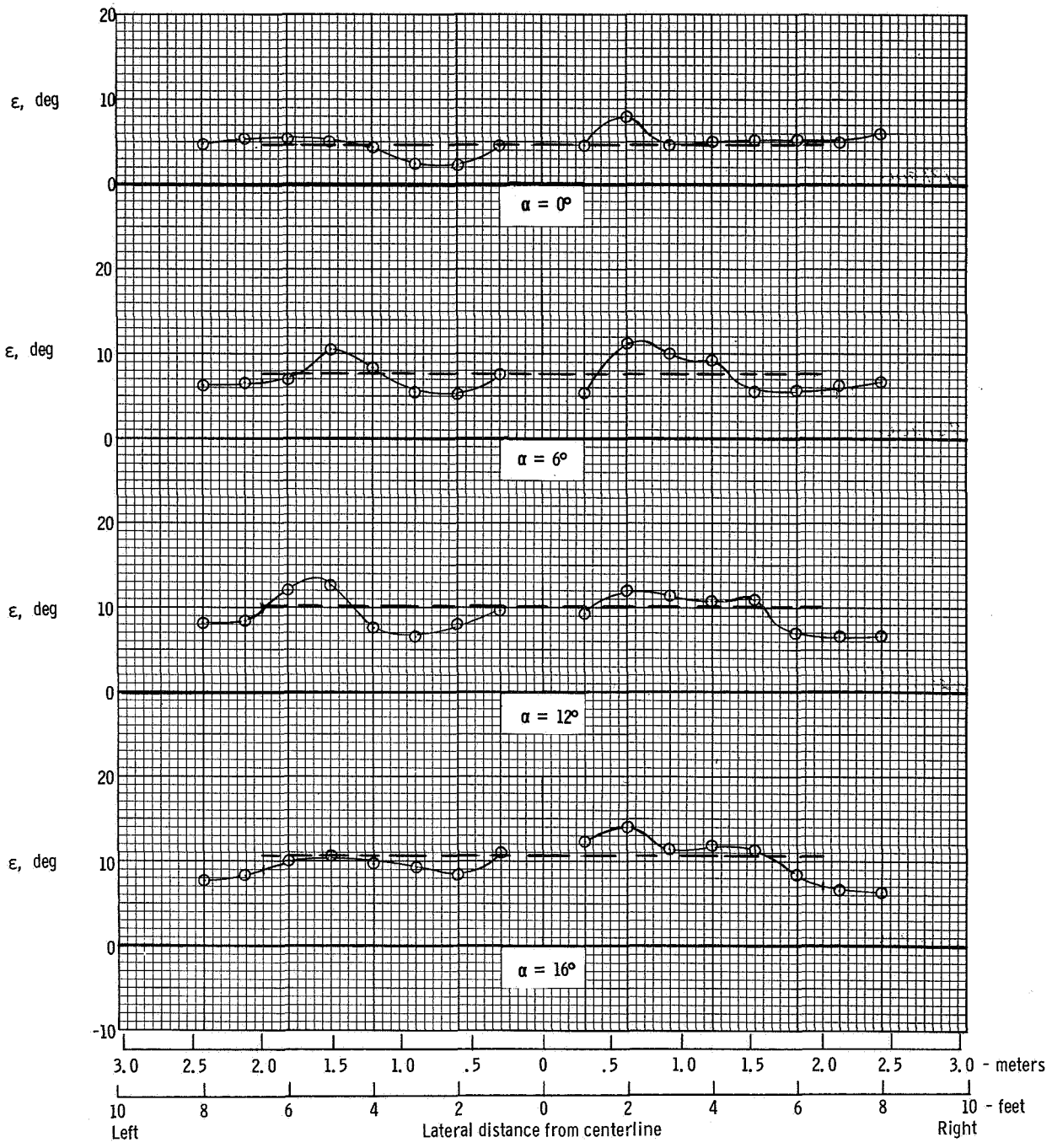

(b) $T'_c = 0.14$.

Figure 34.- Continued.

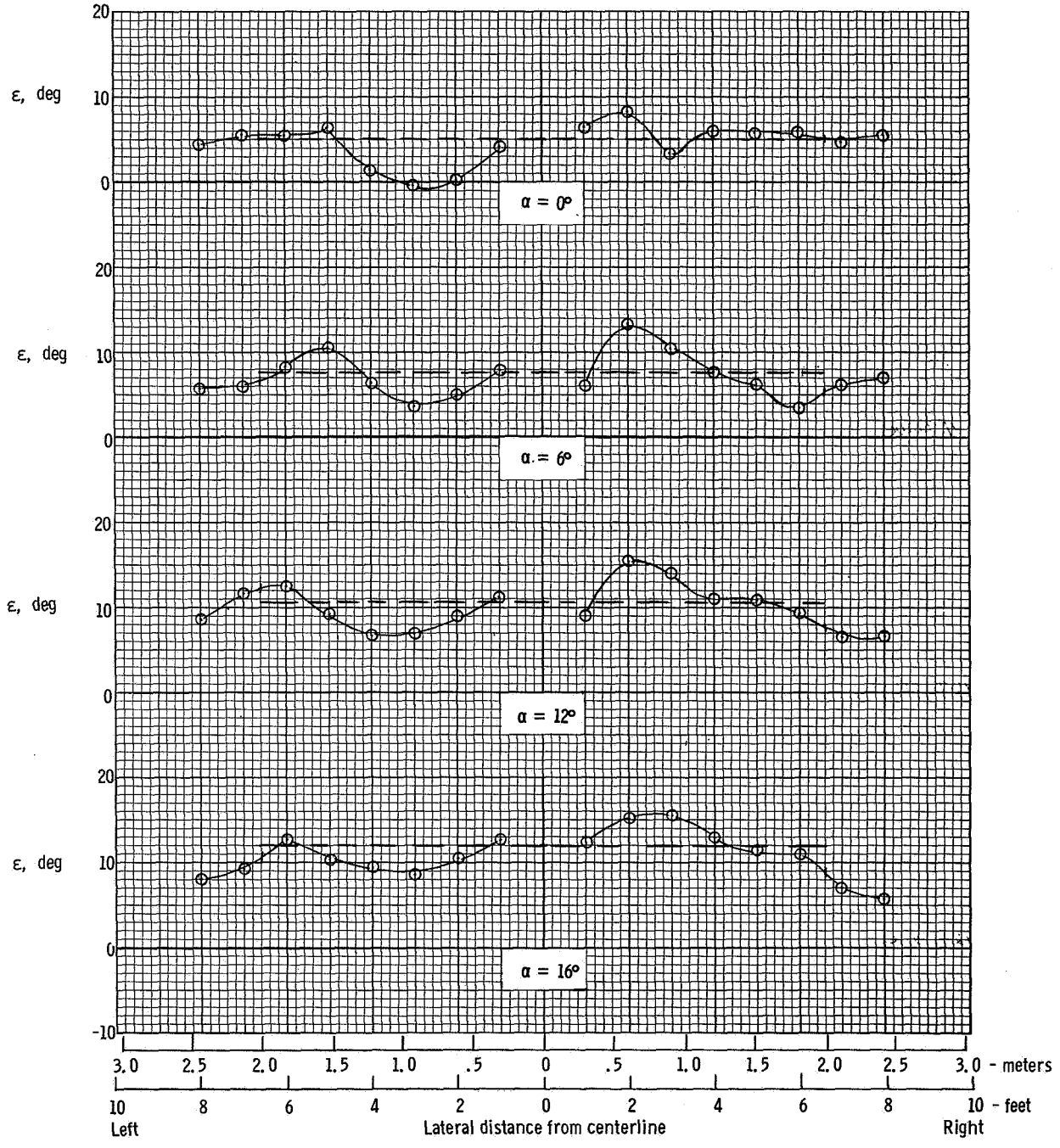

(c) $T'_c = 0.30$.

Figure 34.- Concluded.

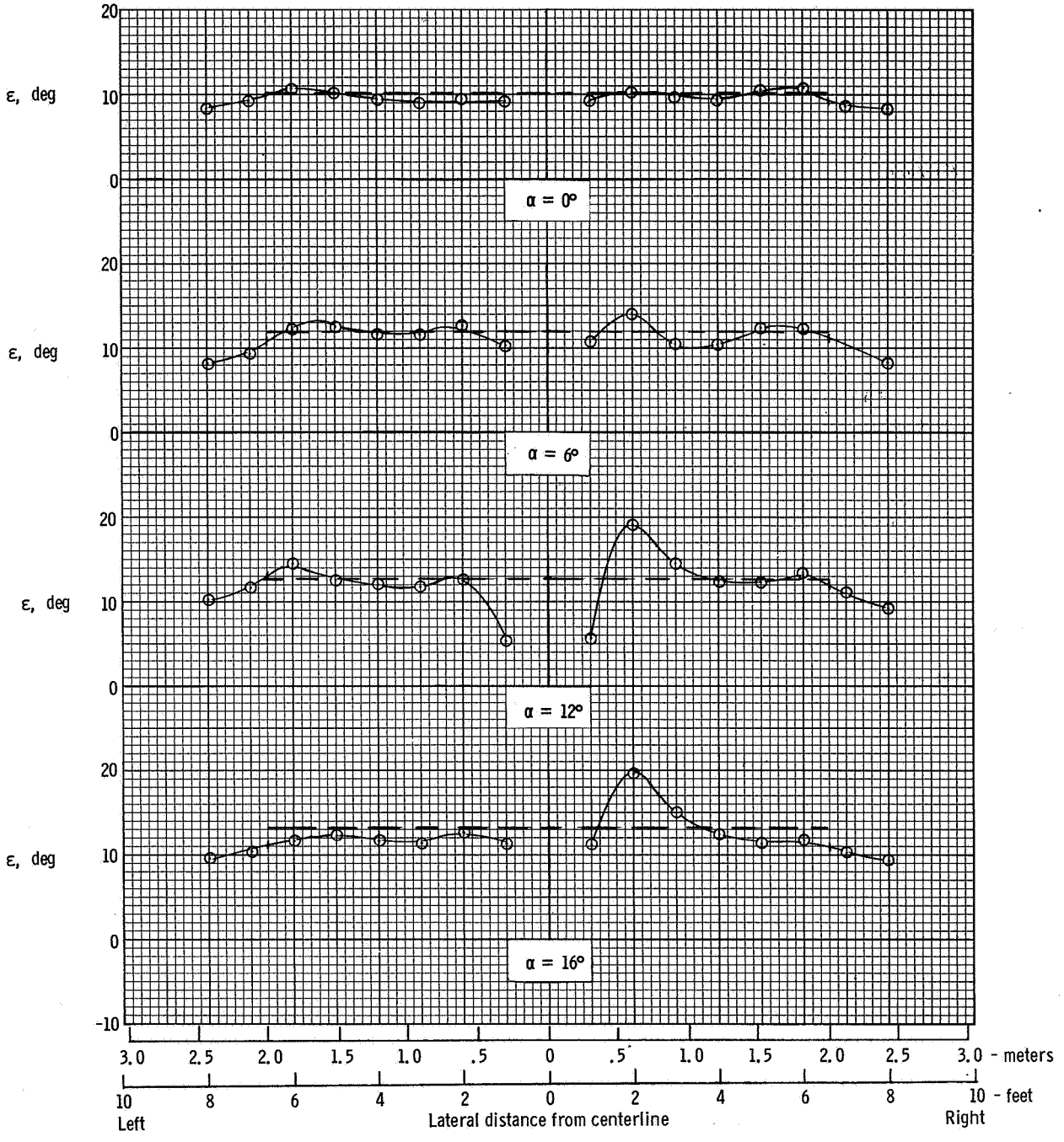

(a) $T_c' = 0$.

Figure 35.- Distribution of downwash across span of horizontal-tail surface. $\delta_f = 30^o$. $\beta = 0^o$. Dashed lines are averages integrated over horizontal-tail span.

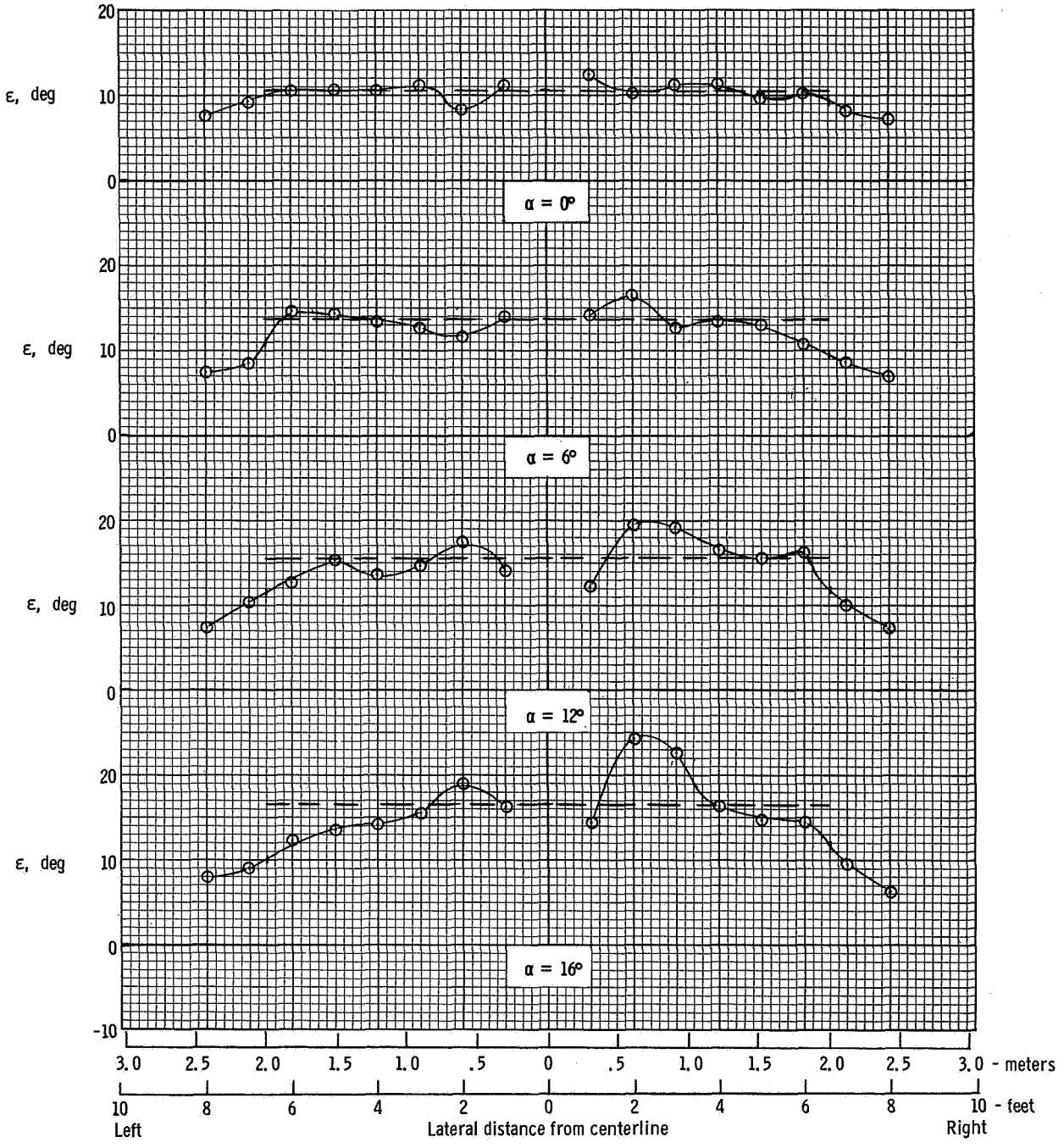

(b) $T_C' = 0.14$.

Figure 35.- Continued.

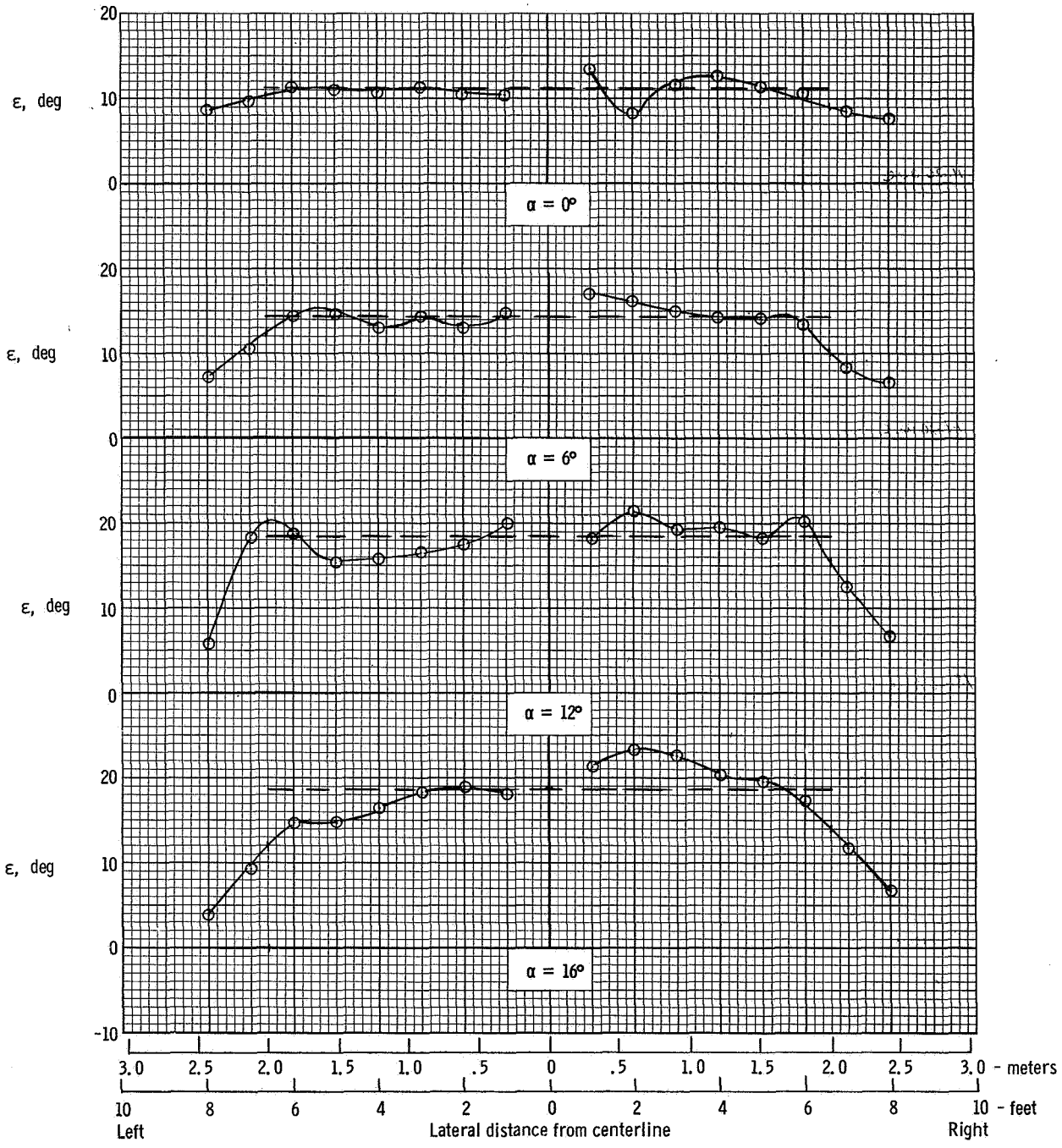

(c) $T_C' = 0.30$.

Figure 35.- Concluded.

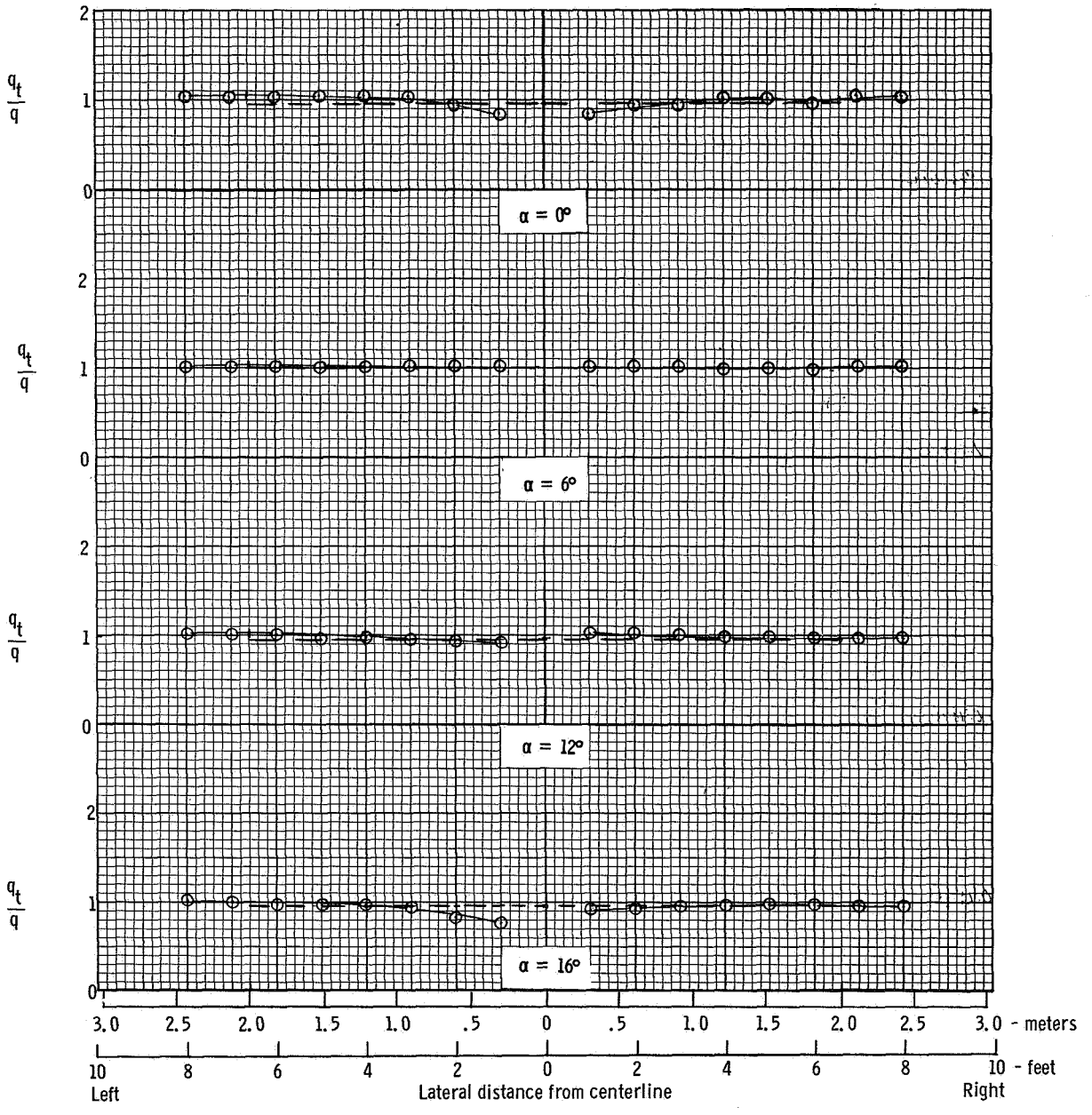

(a) $T'_c = 0$.

Figure 36.- Distribution of dynamic pressure ratio across span of horizontal-tail surface. $\delta_f = 0^o$. $\beta = 0^o$. Dashed lines are averages integrated over horizontal-tail span.

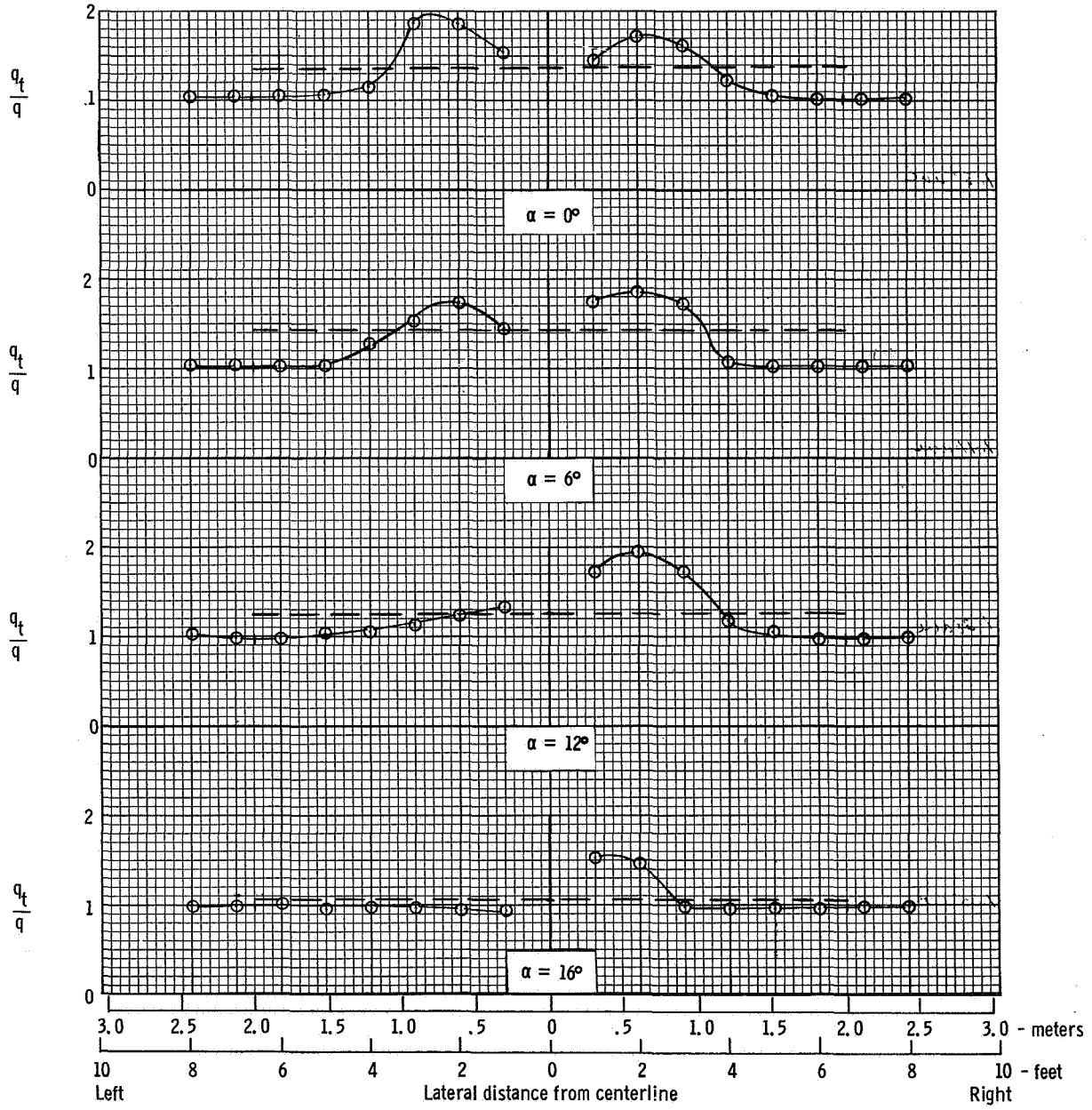

(b) $T'_c = 0.14$.

Figure 36.- Continued.

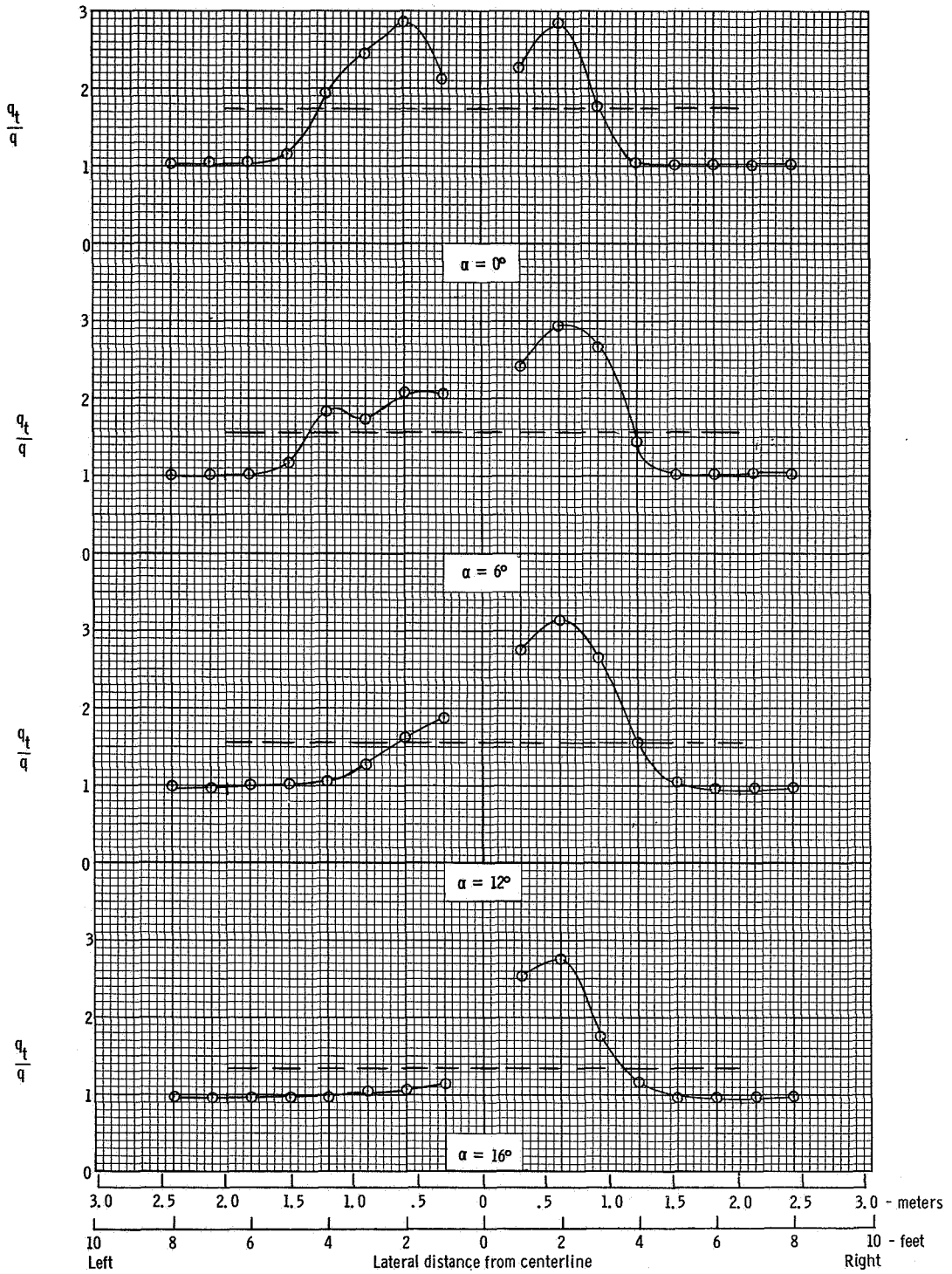

(c) $T'_c = 0.30$.

Figure 36.- Concluded.

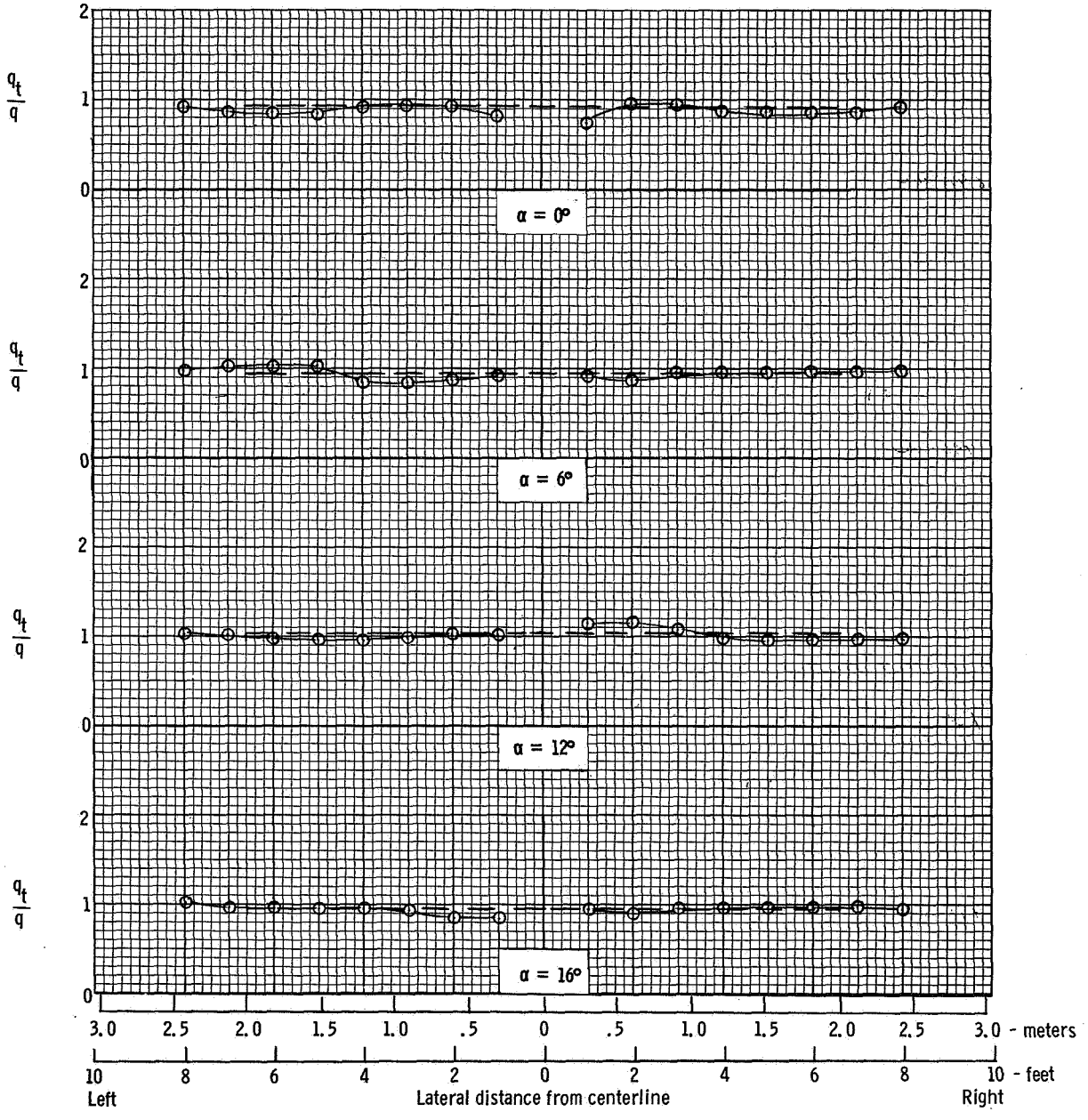

(a) $T'_c = 0$.

Figure 37.- Distribution of dynamic pressure ratio across span of horizontal-tail surface. $\delta_f = 10^o$. $\beta = 0^o$. Dashed lines are averages integrated over horizontal-tail span.

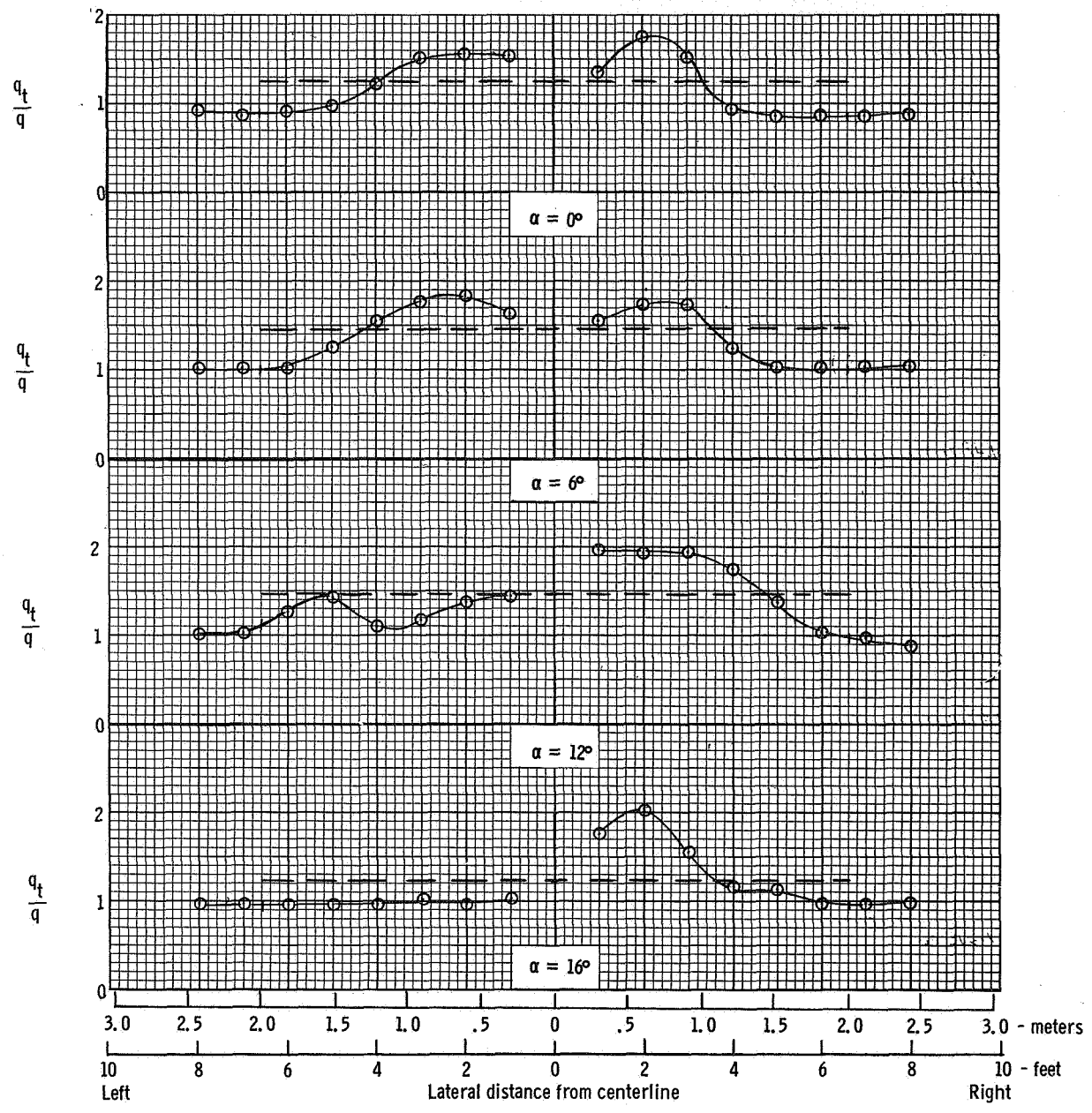

(b) $T_c' = 0.14$.

Figure 37.- Continued.

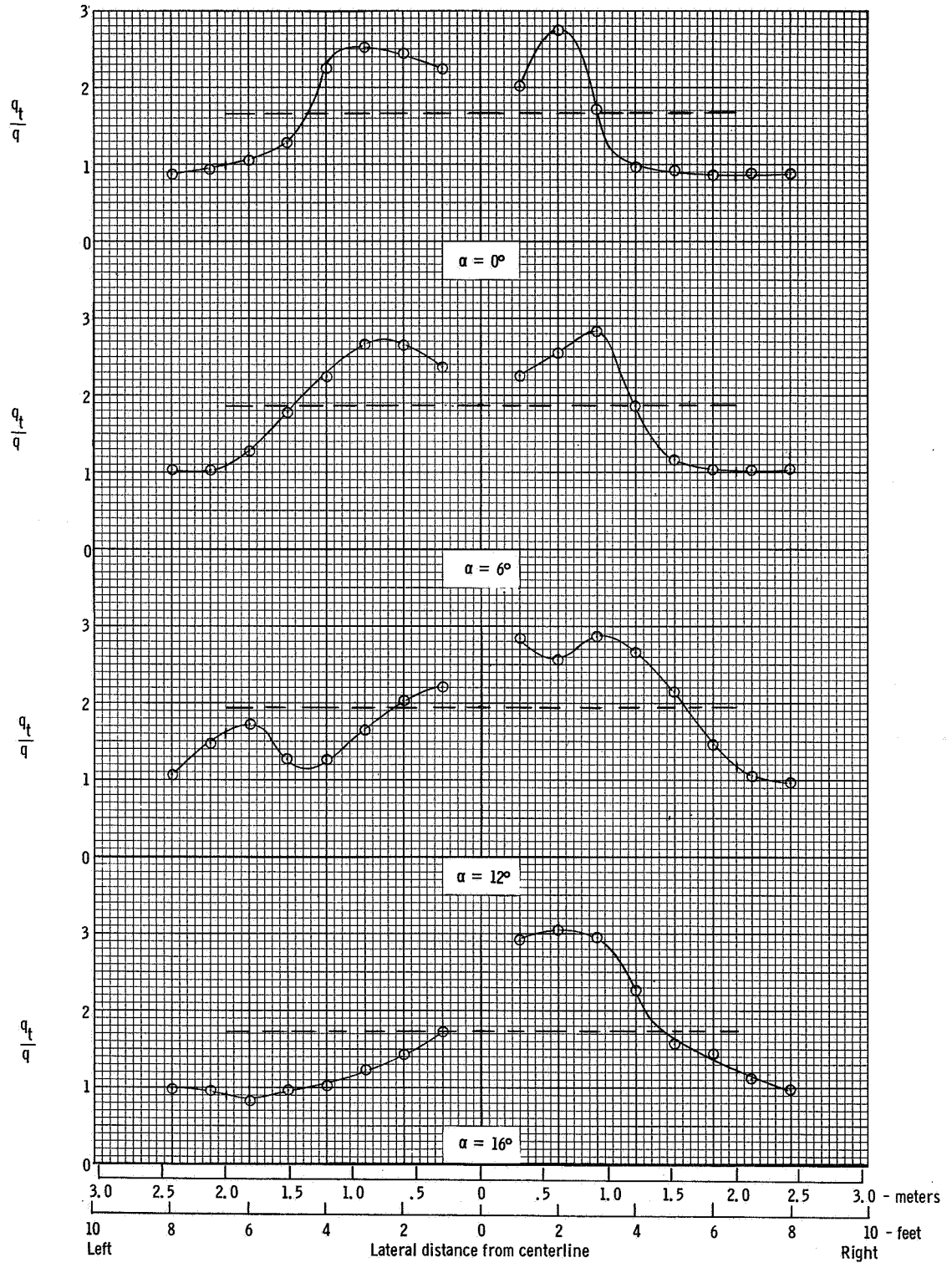

(c) $T'_c = 0.30$.

Figure 37.- Concluded.

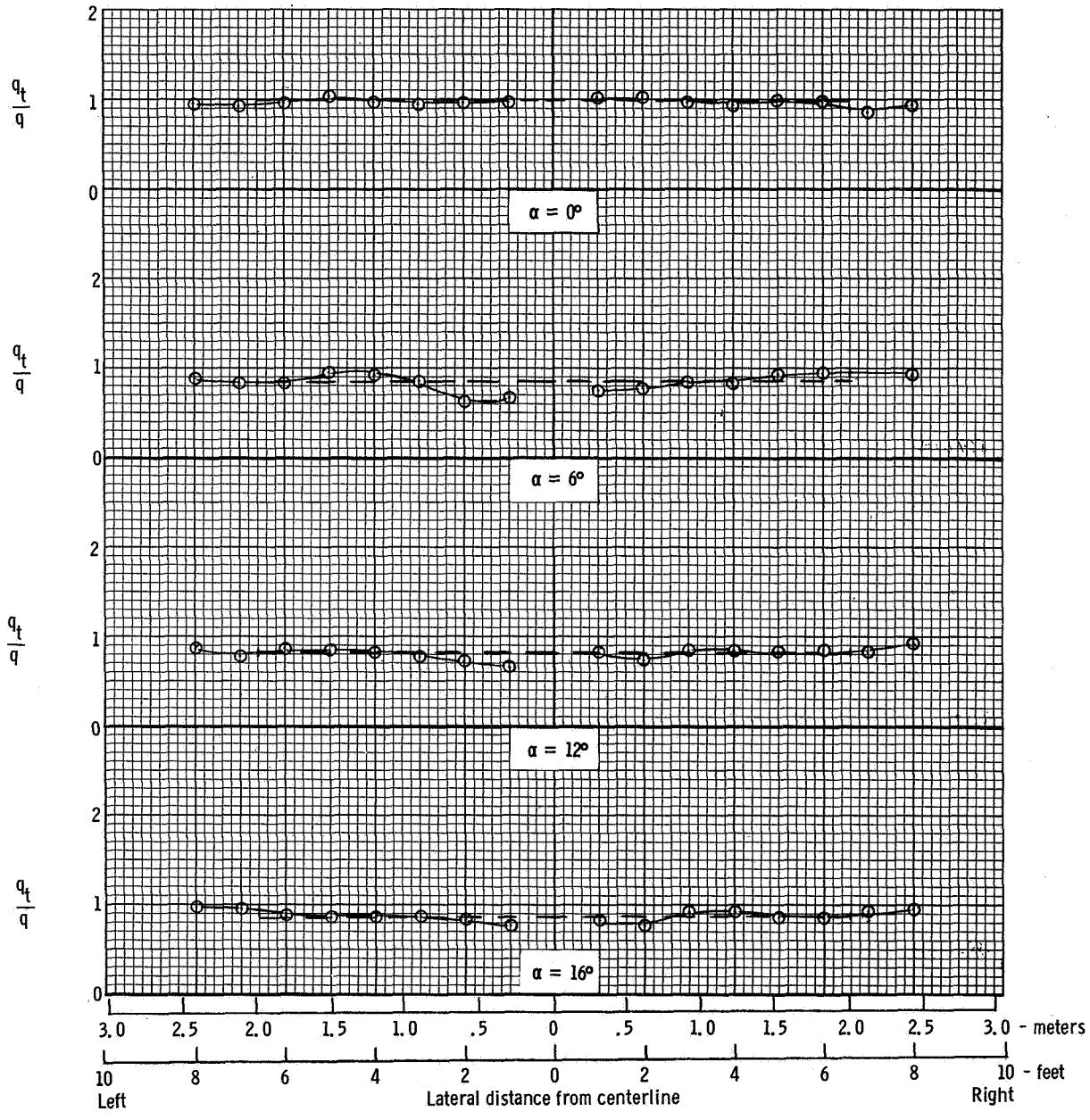

(a) $T'_c = 0$.

Figure 38.- Distribution of dynamic pressure ratio across span of horizontal-tail surface. $\delta_f = 30^o$. $\beta = 0^o$. Dashed lines are averages integrated over horizontal-tail span.

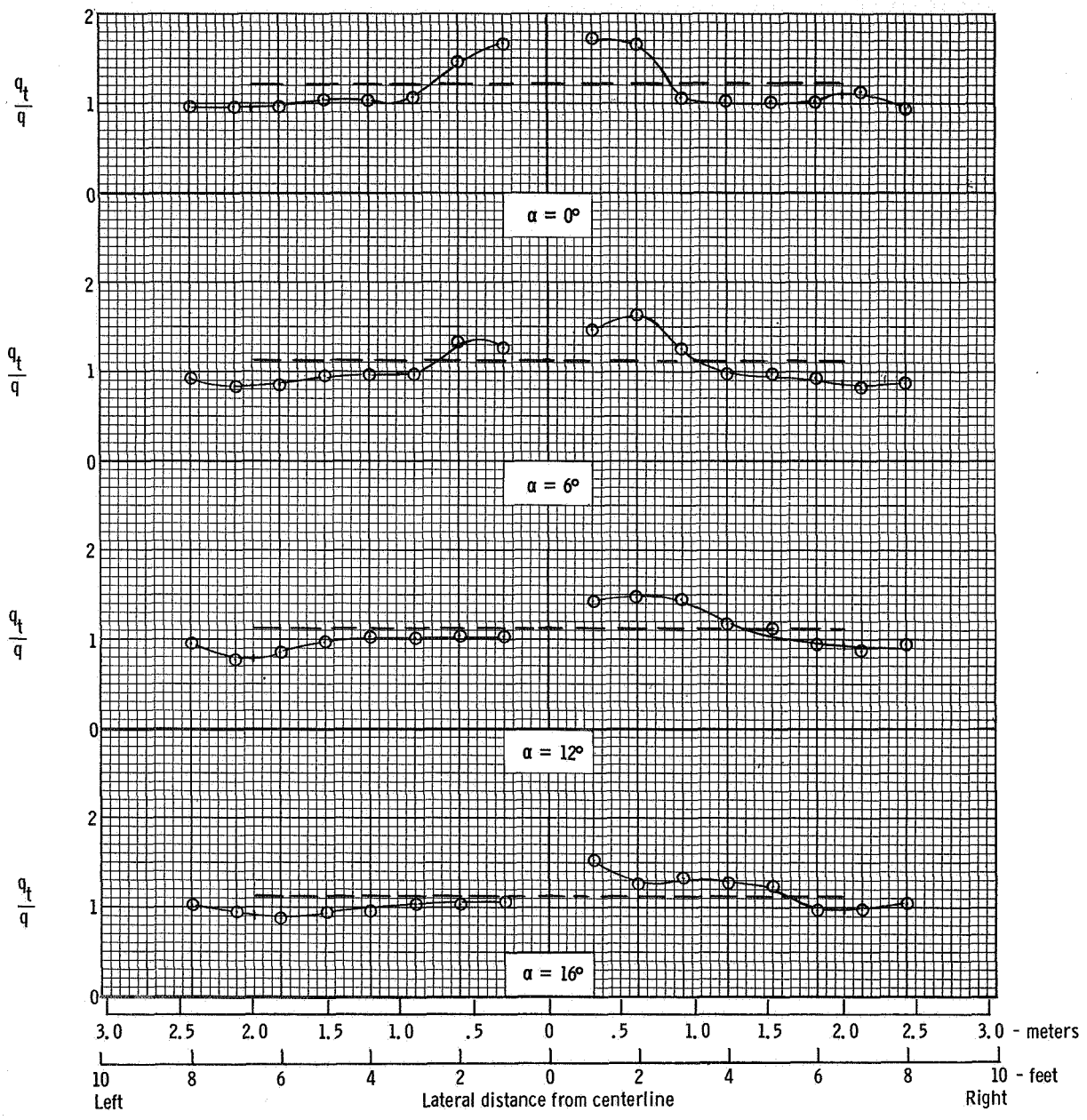

(b) $T'_c = 0.14$.

Figure 38.- Continued.

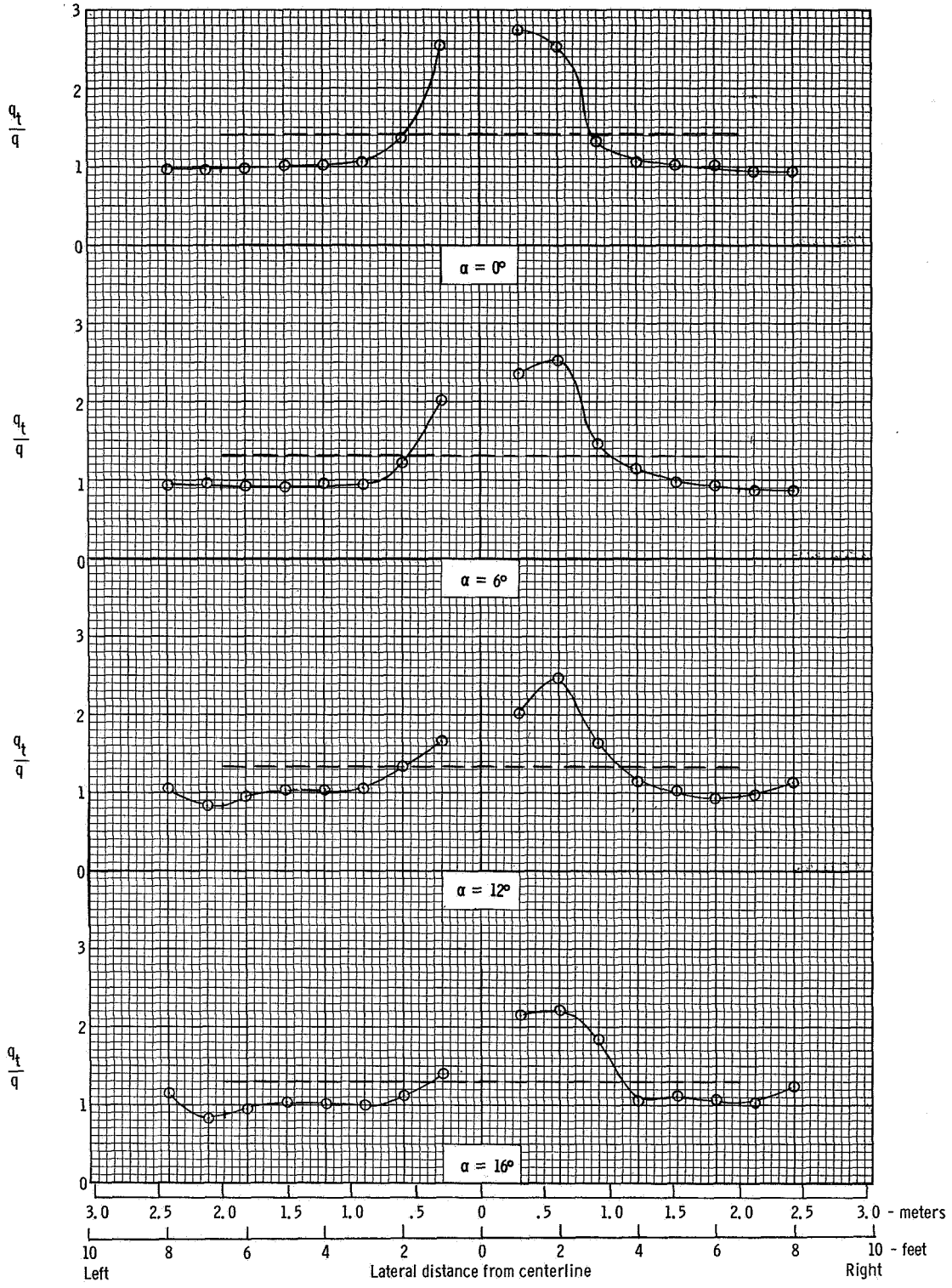

(c) $T'_c = 0.30$.

Figure 38.- Concluded.

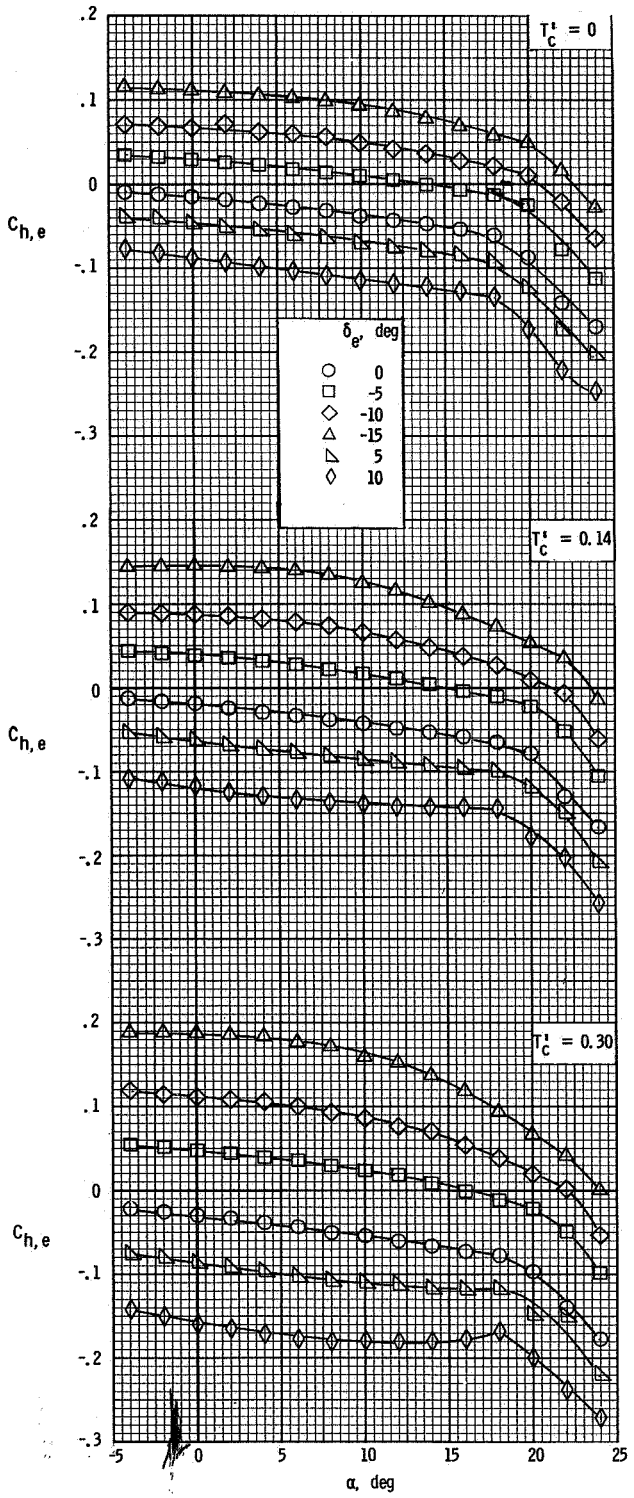

(a) $\delta_f = 0^o$.

Figure 39.- Variation of elevator hinge-moment coefficient with angle of attack for several power and flap settings.

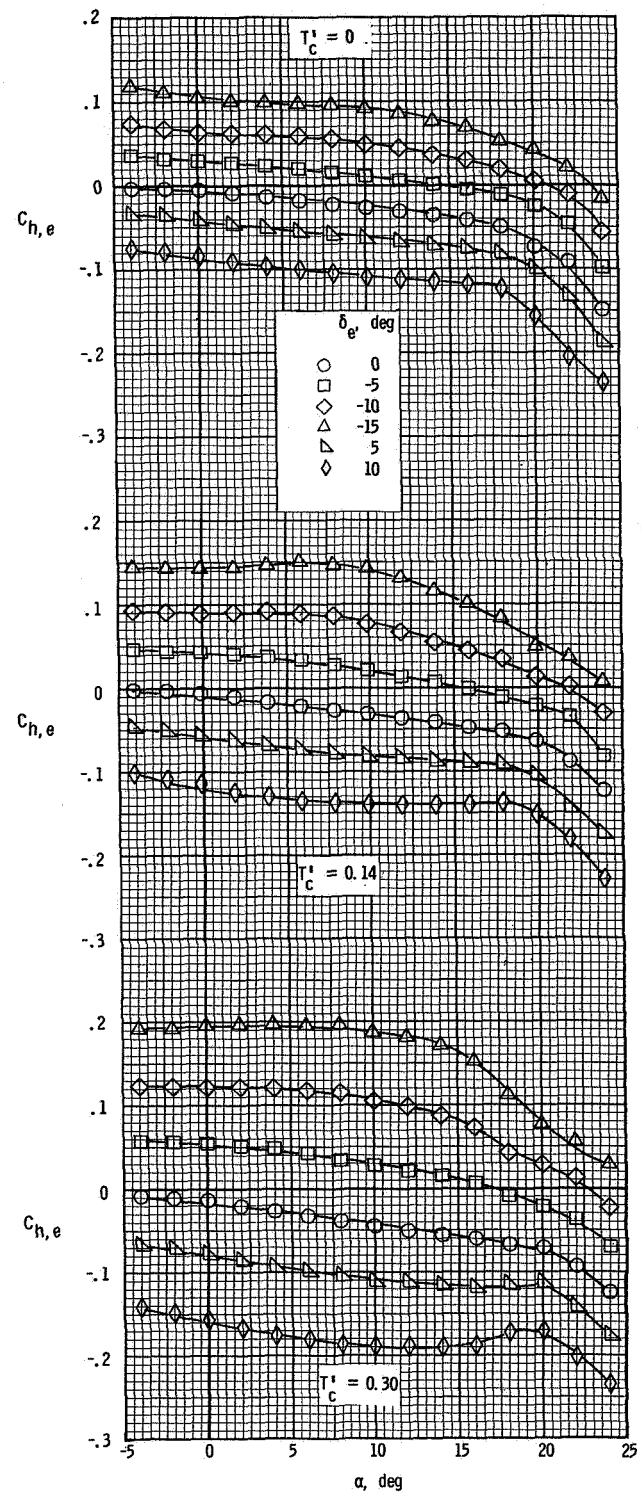

(b) $\delta_f = 10^o$.

Figure 39.- Continued.

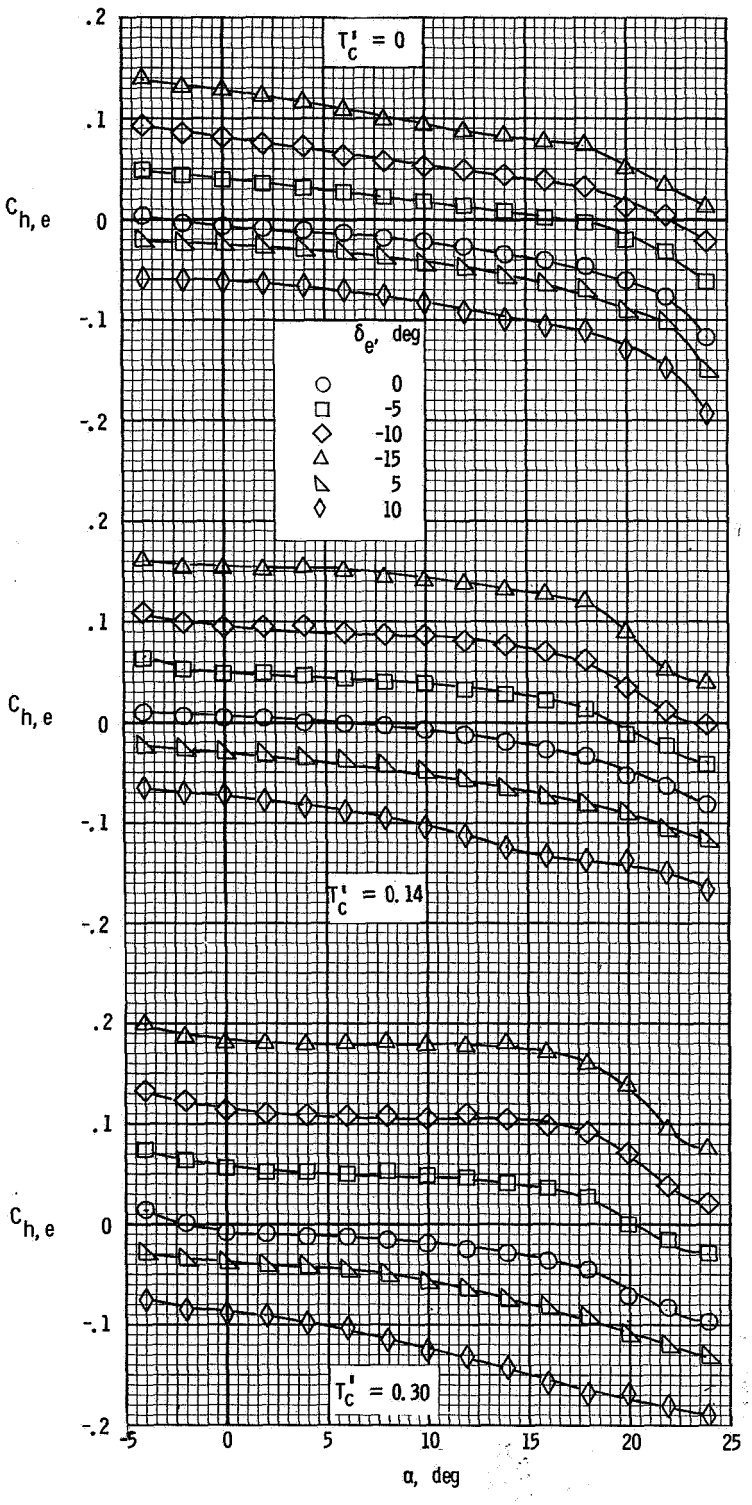

(c) $\delta_f = 30^o$.

Figure 39.- Concluded.

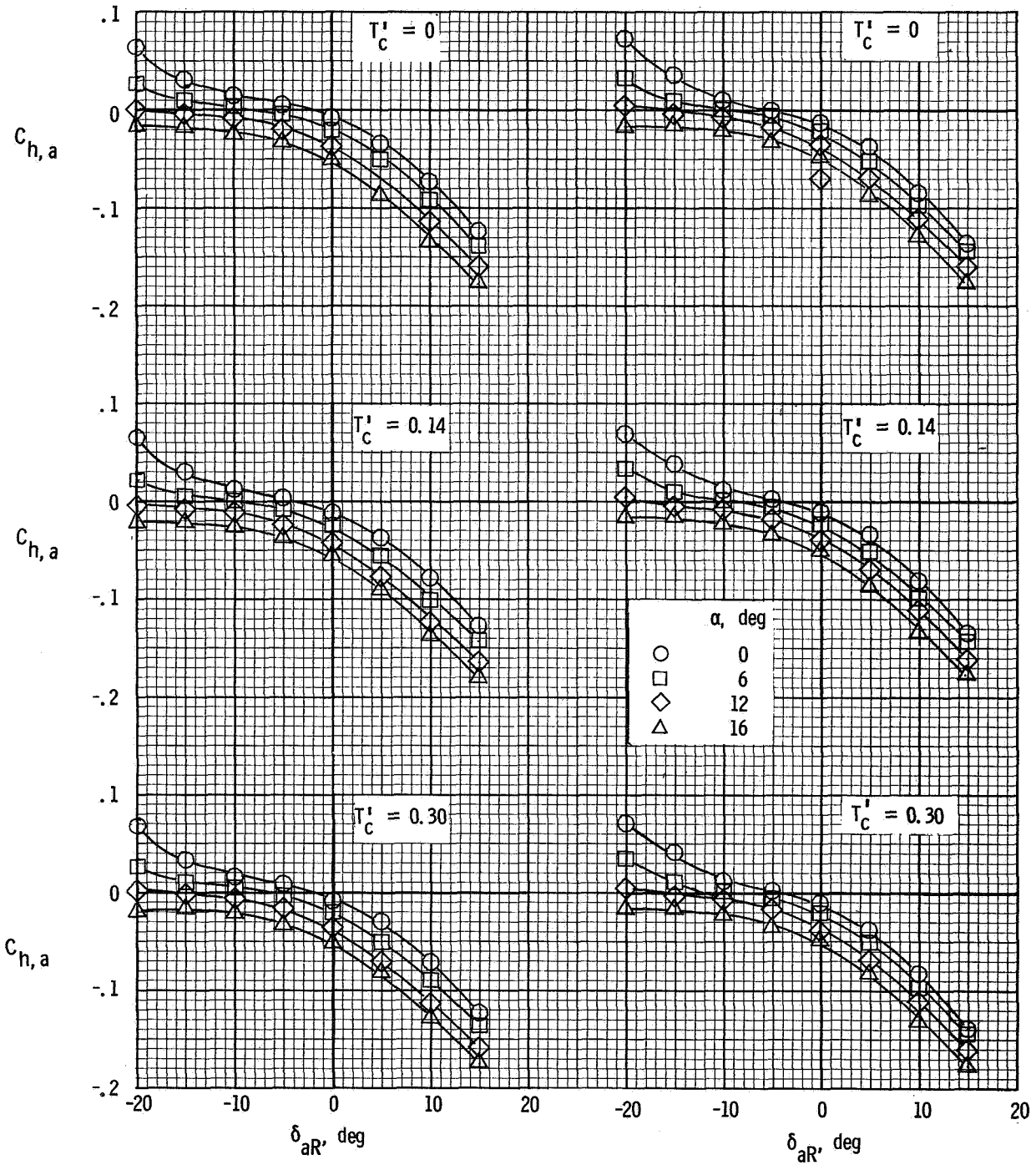

(a) $\beta = 8^{o}$. (b) $\beta = 0^{o}$.

Figure 40.- Variation of right aileron hinge-moment coefficient with control deflection. $\delta_f = 0^{o}$.

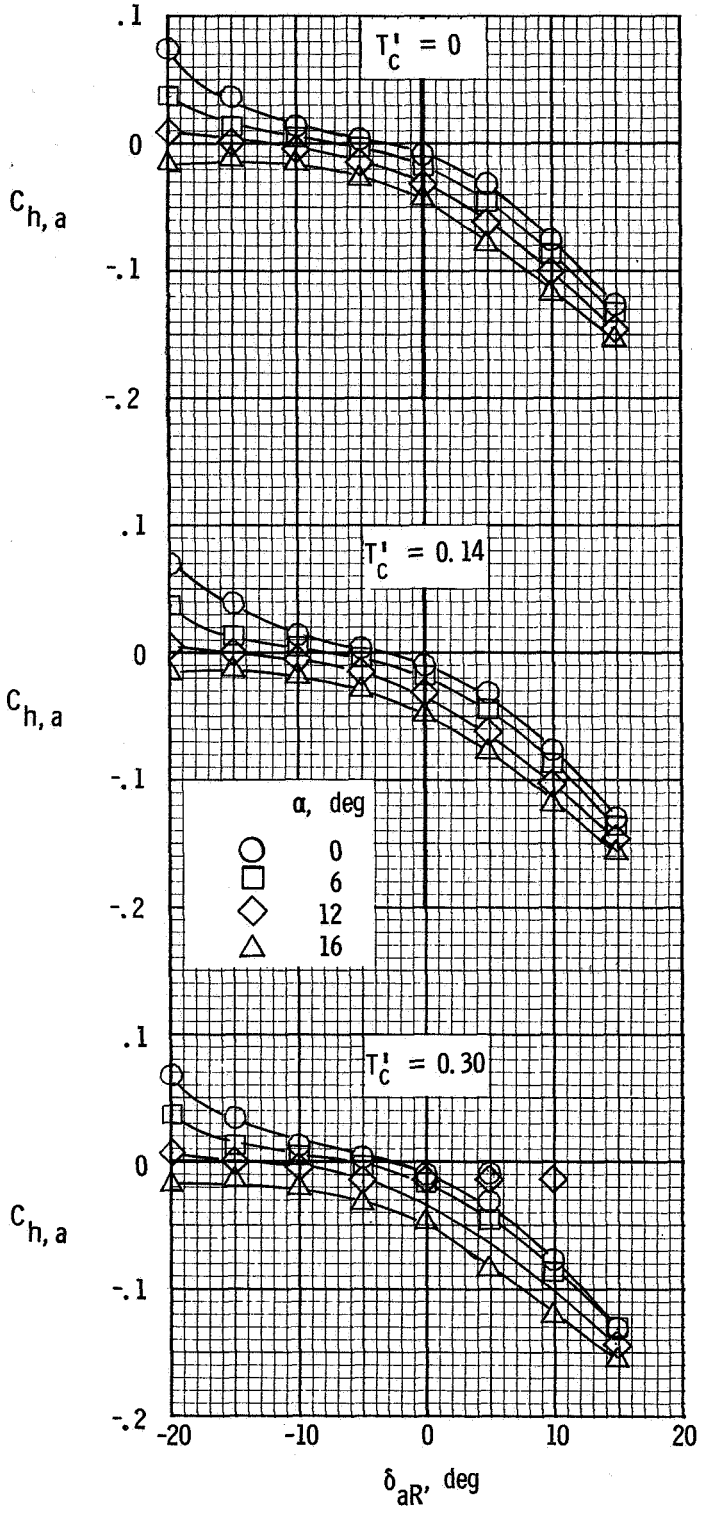

(c) $\beta = -8^{o}$.

Figure 40.- Concluded.

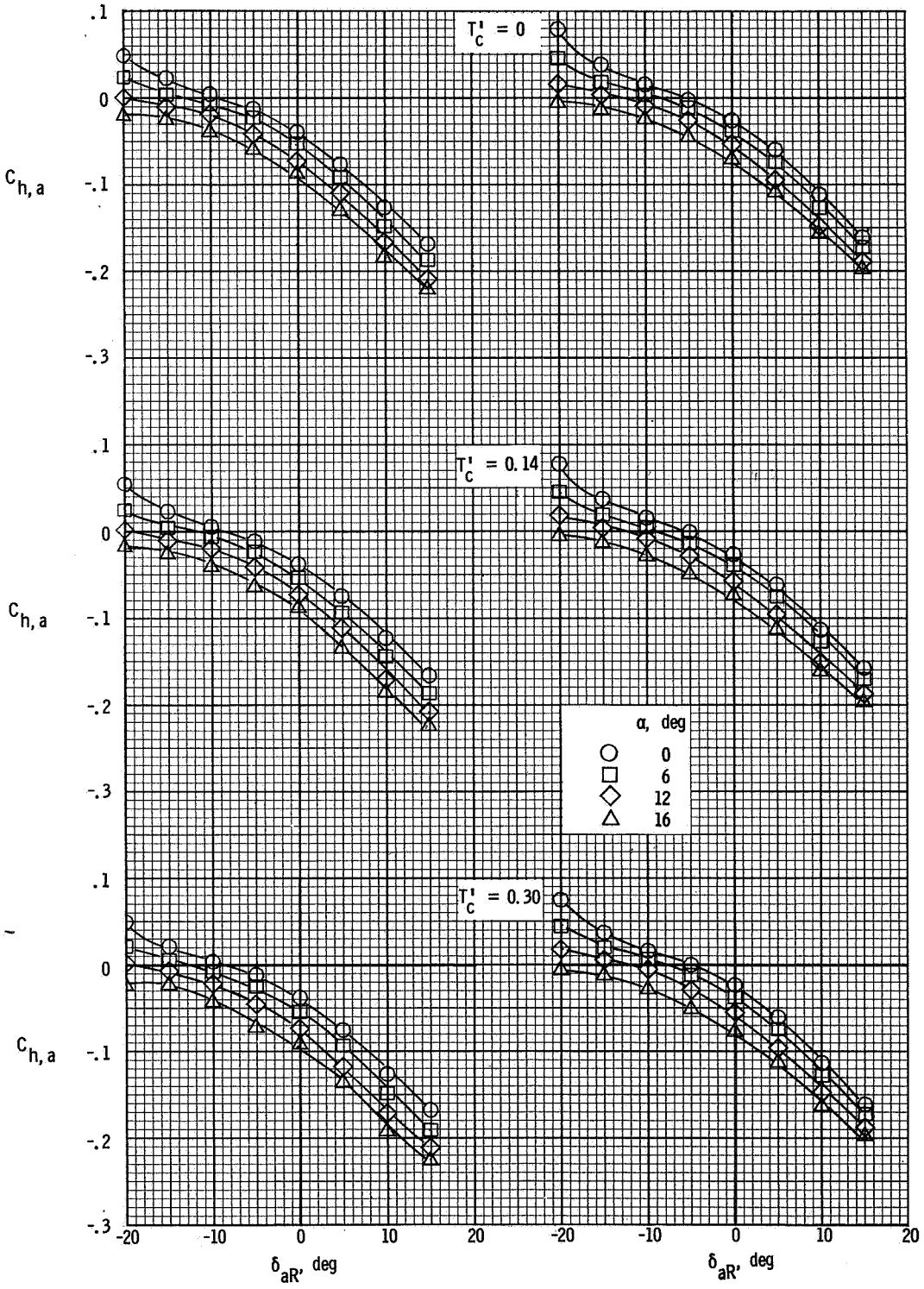

(a) $\beta = 8^{o}$.

(b) $\beta = 0^{o}$.

Figure 41.- Variation of right aileron hinge-moment coefficient with control deflection. $\delta_f = 30^{o}$.

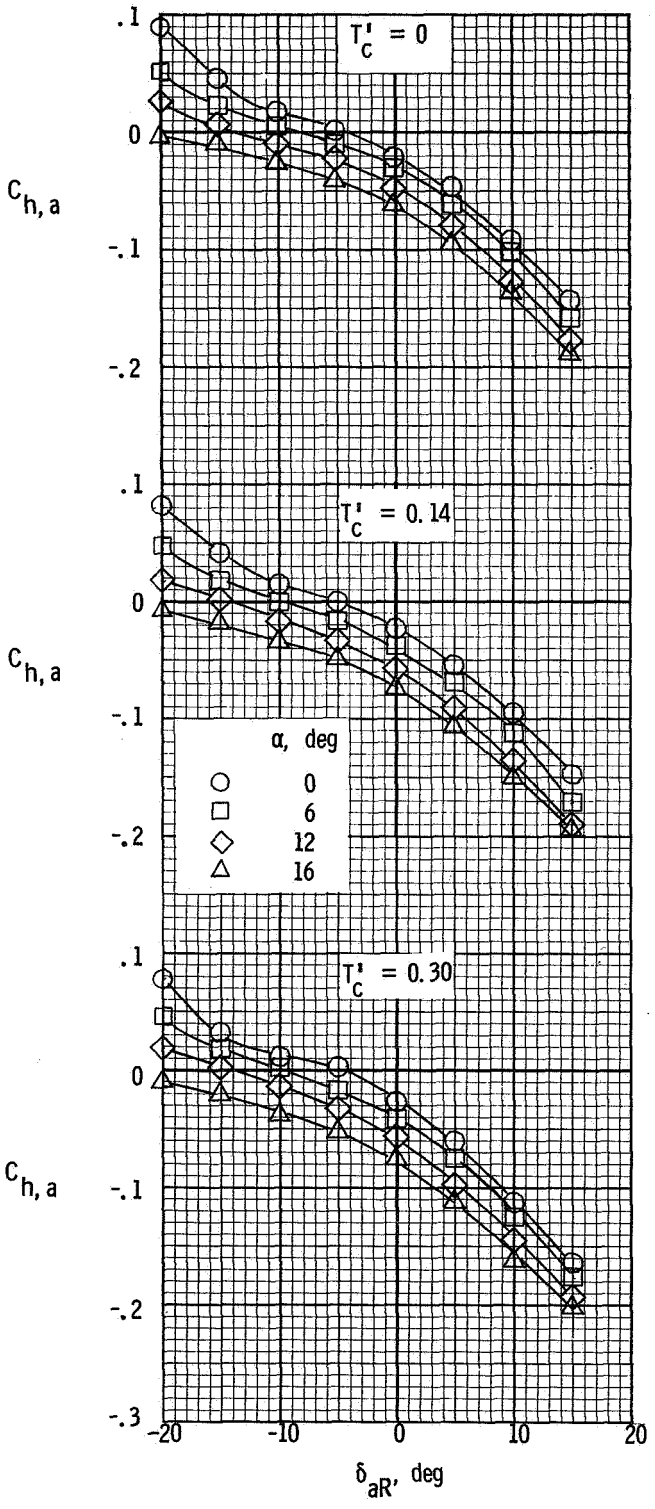

(c) $\beta = -8^{o}$.

Figure 41.- Concluded.

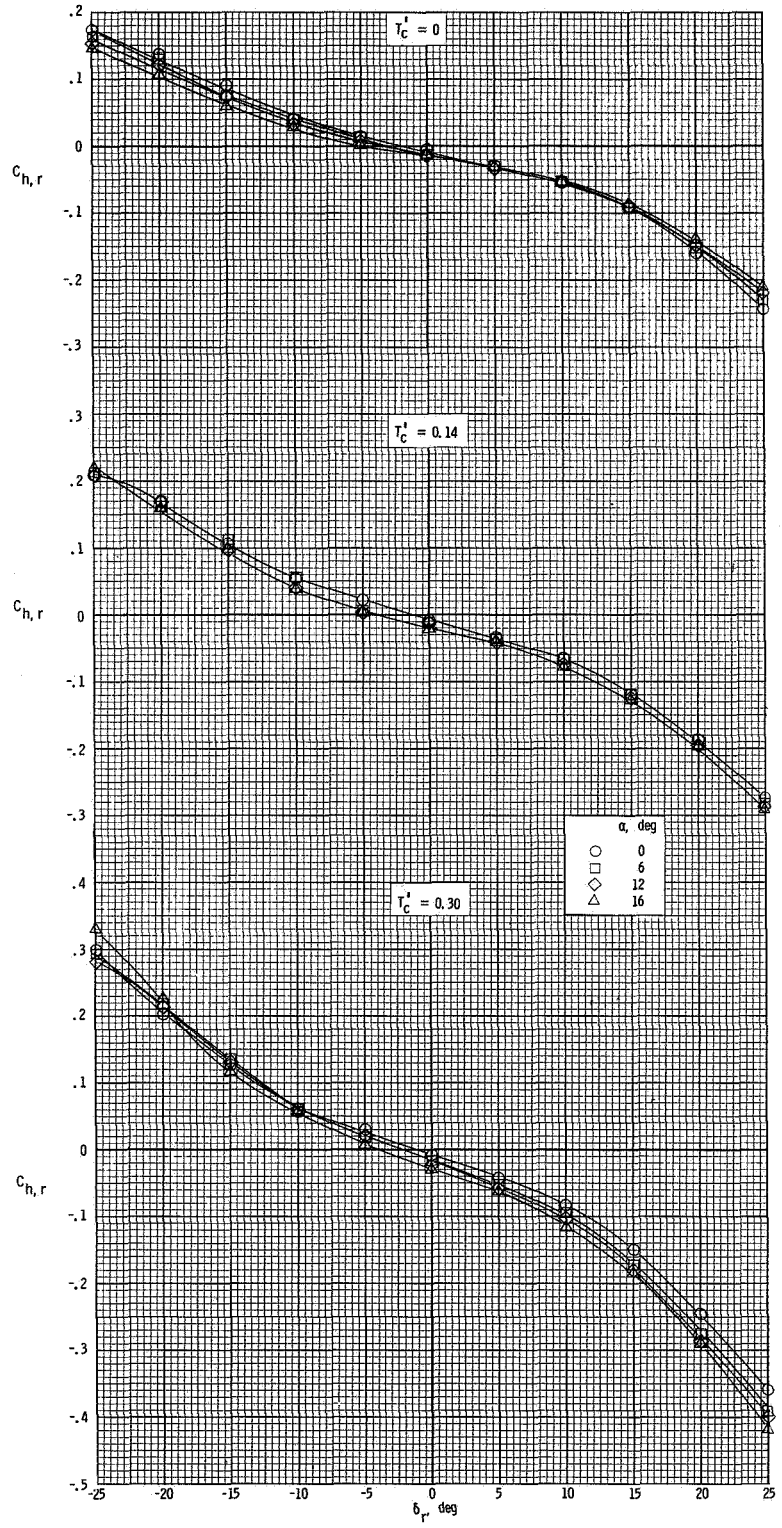

(a) $\beta = 8^{o}$.

Figure 42.- Variation of rudder hinge-moment coefficient with control deflection. $\delta_f = 0^{o}$.

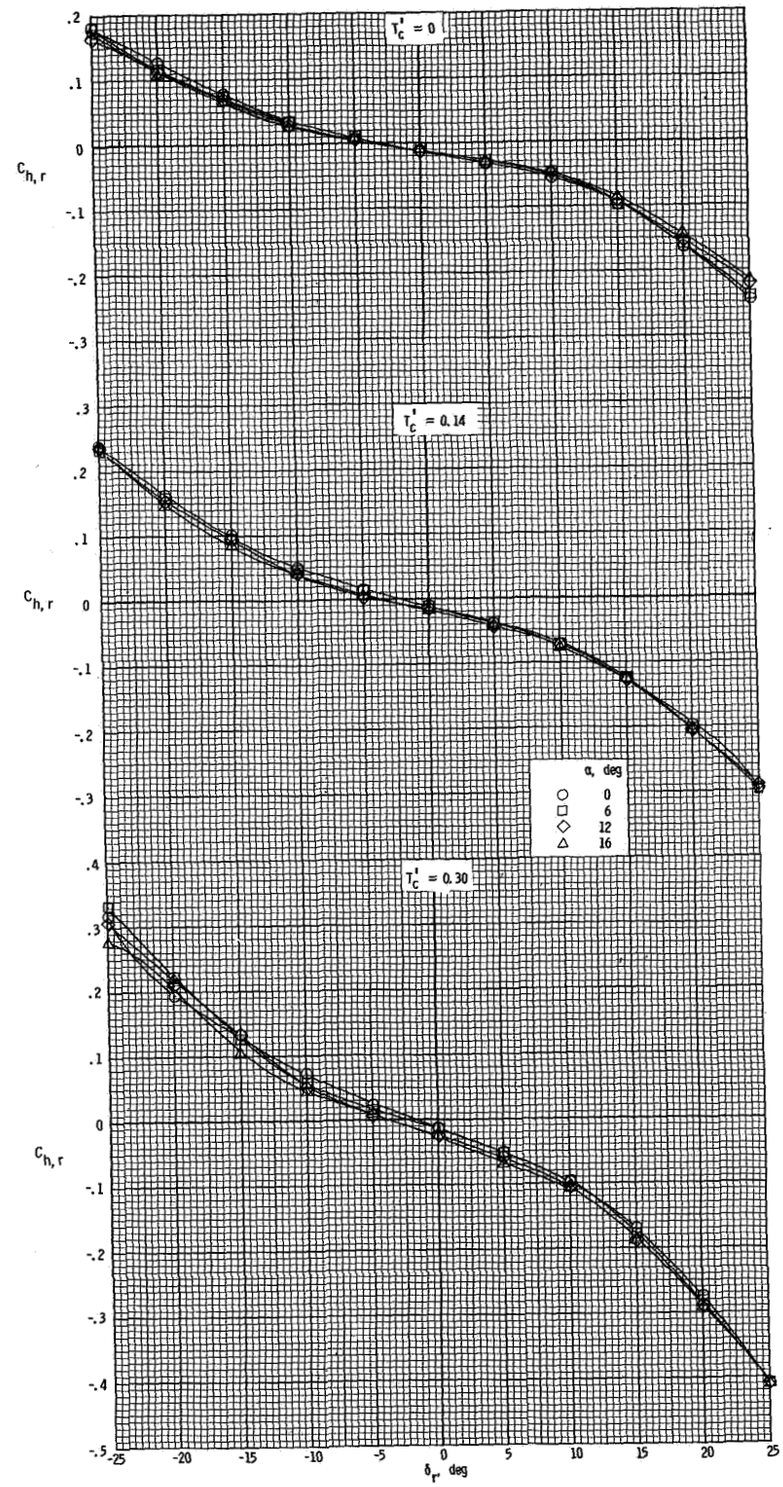

(b) $\beta = 4^{o}$.

Figure 42.- Continued.

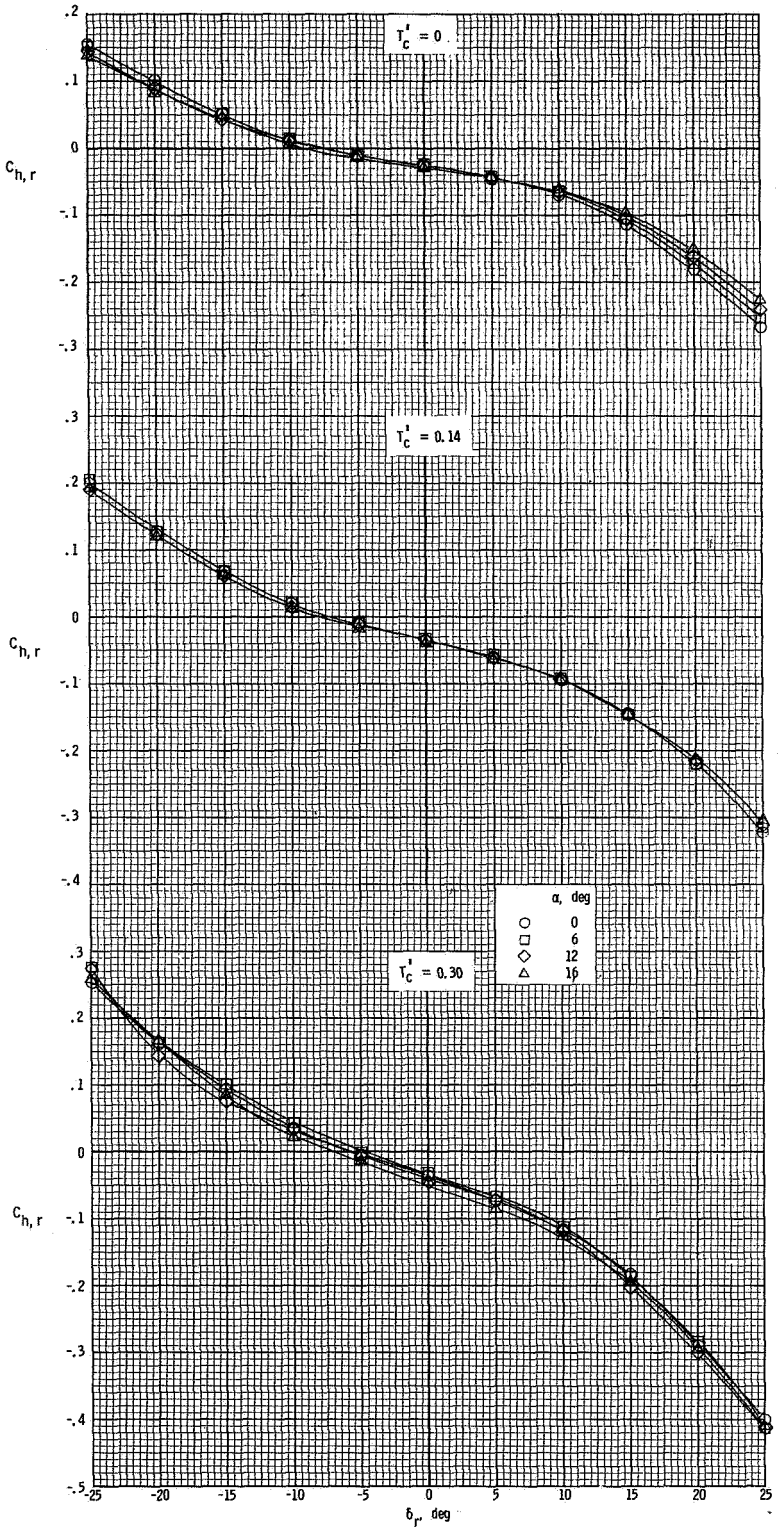

(c) $\beta = 0^o$.

Figure 42.- Continued.

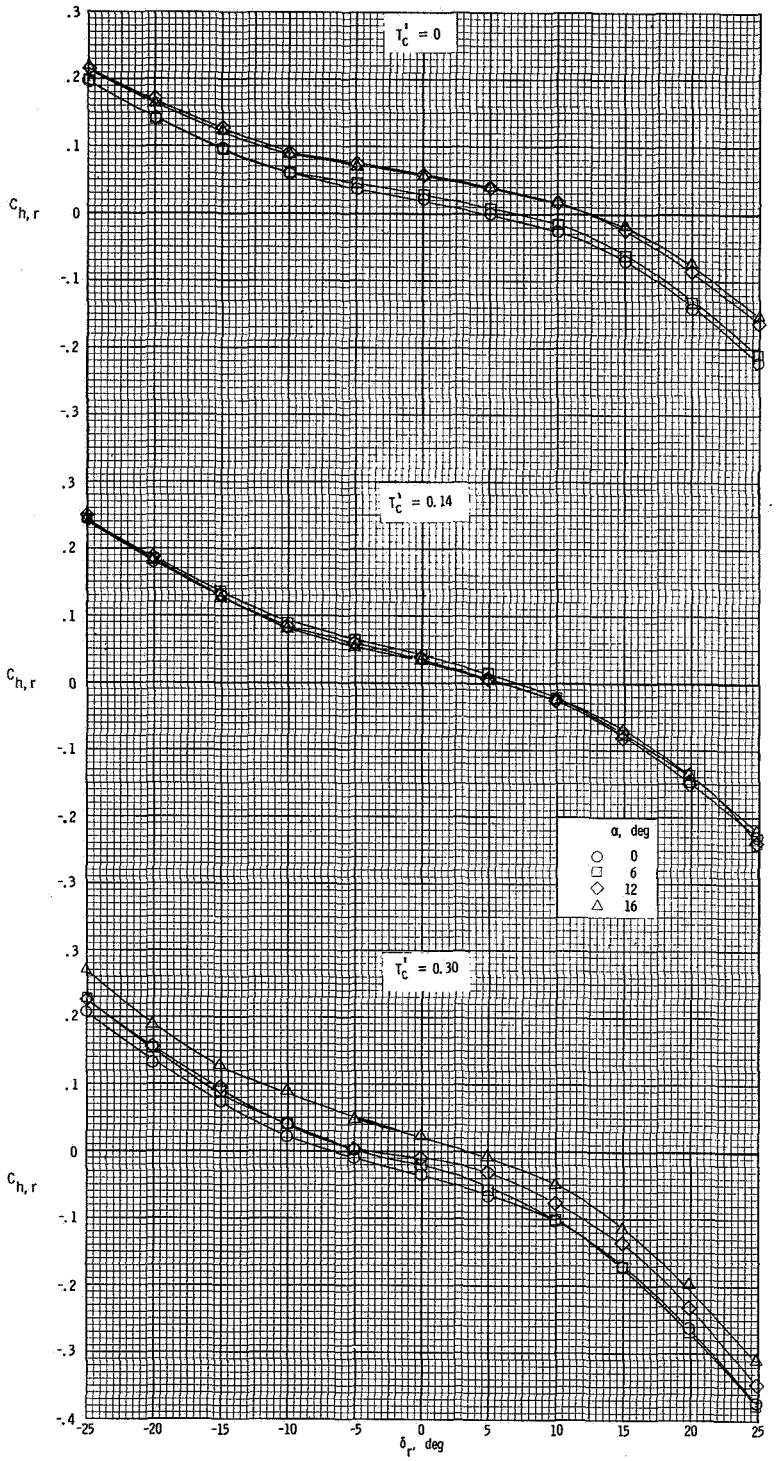

(d) $\beta = -4^{o}$.

Figure 42.- Continued.

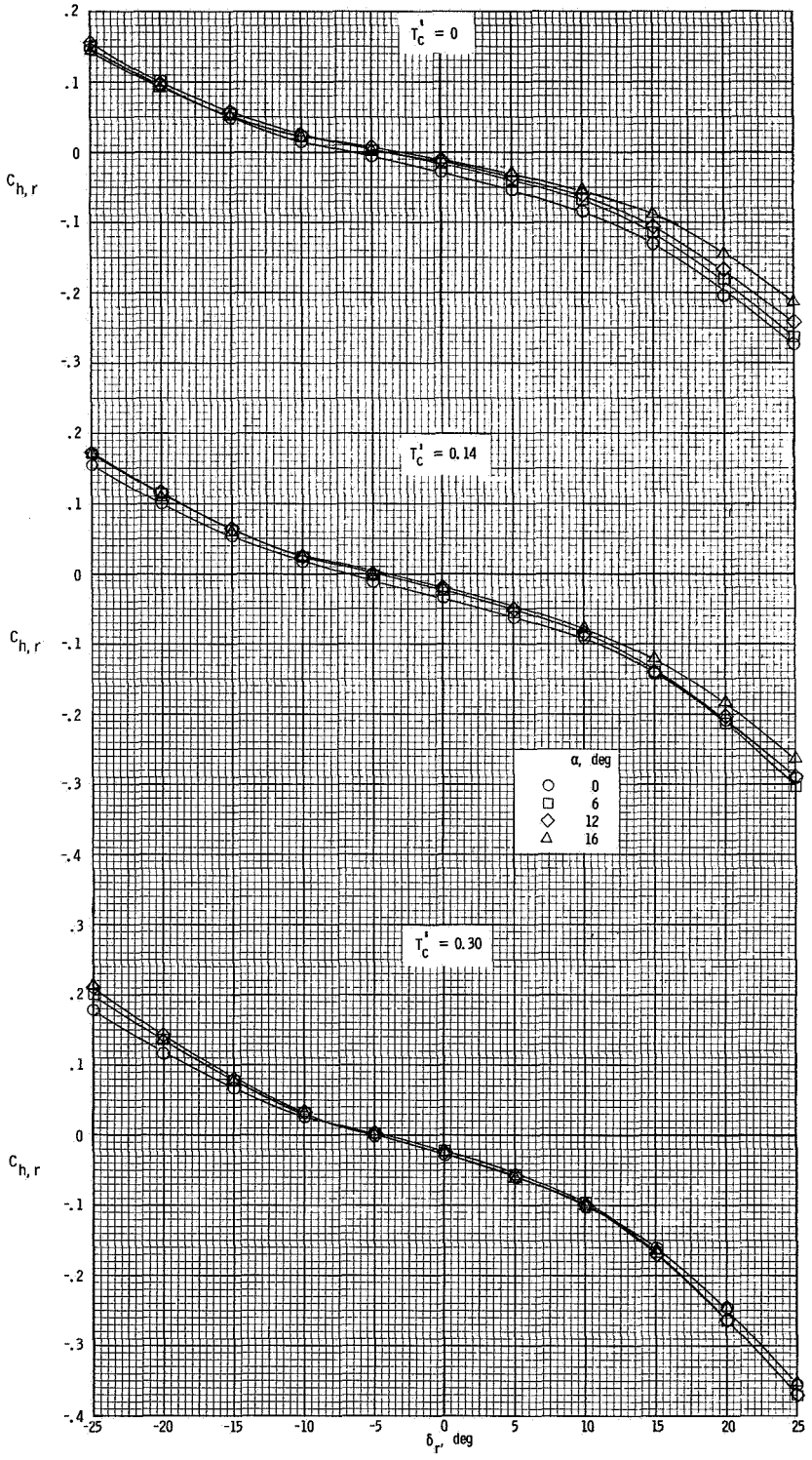

(e) $\beta = -8^{o}$.

Figure 42.- Concluded.

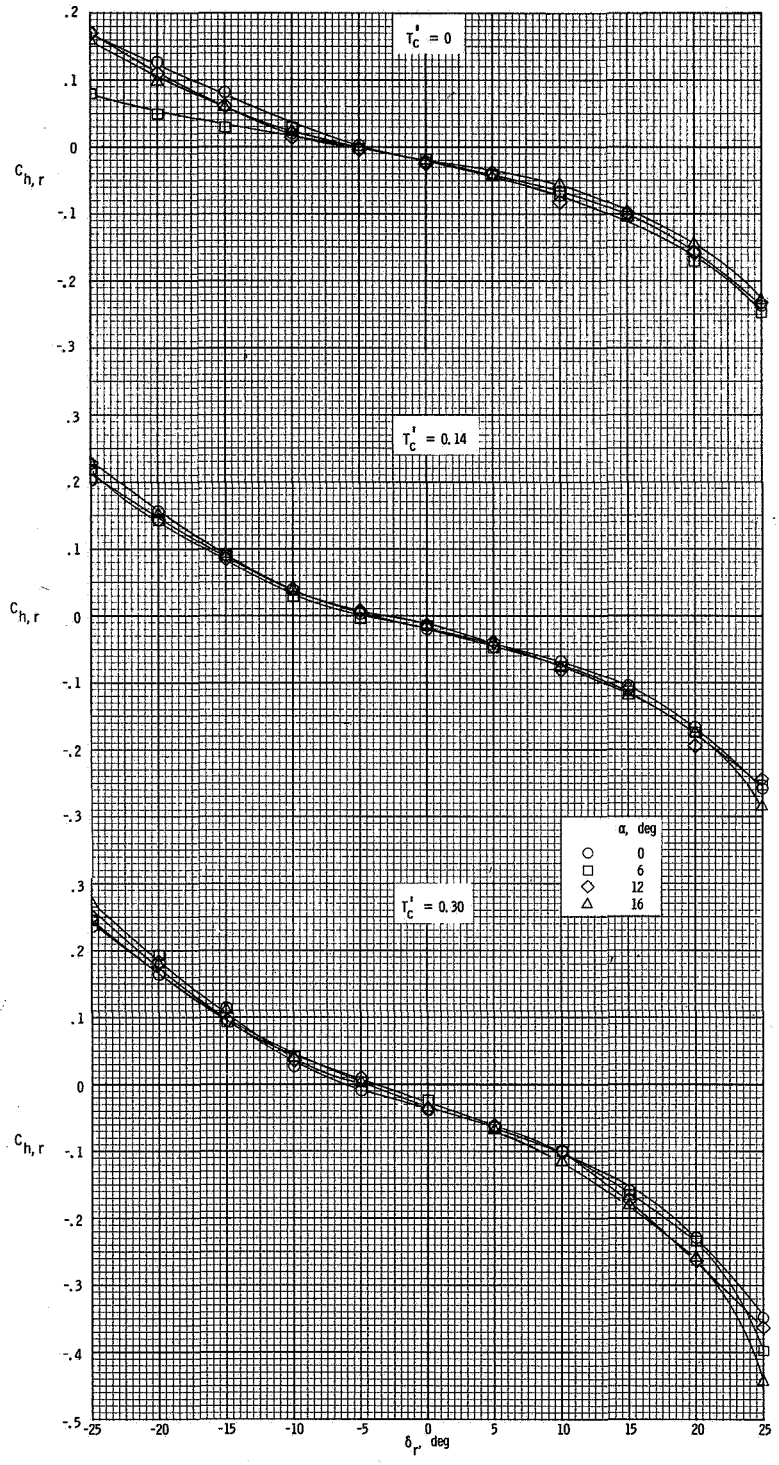

(a) $\beta = 8^{o}$.

Figure 43.- Variation of rudder hinge-moment coefficient with control deflection. $\delta_f = 30^{o}$.

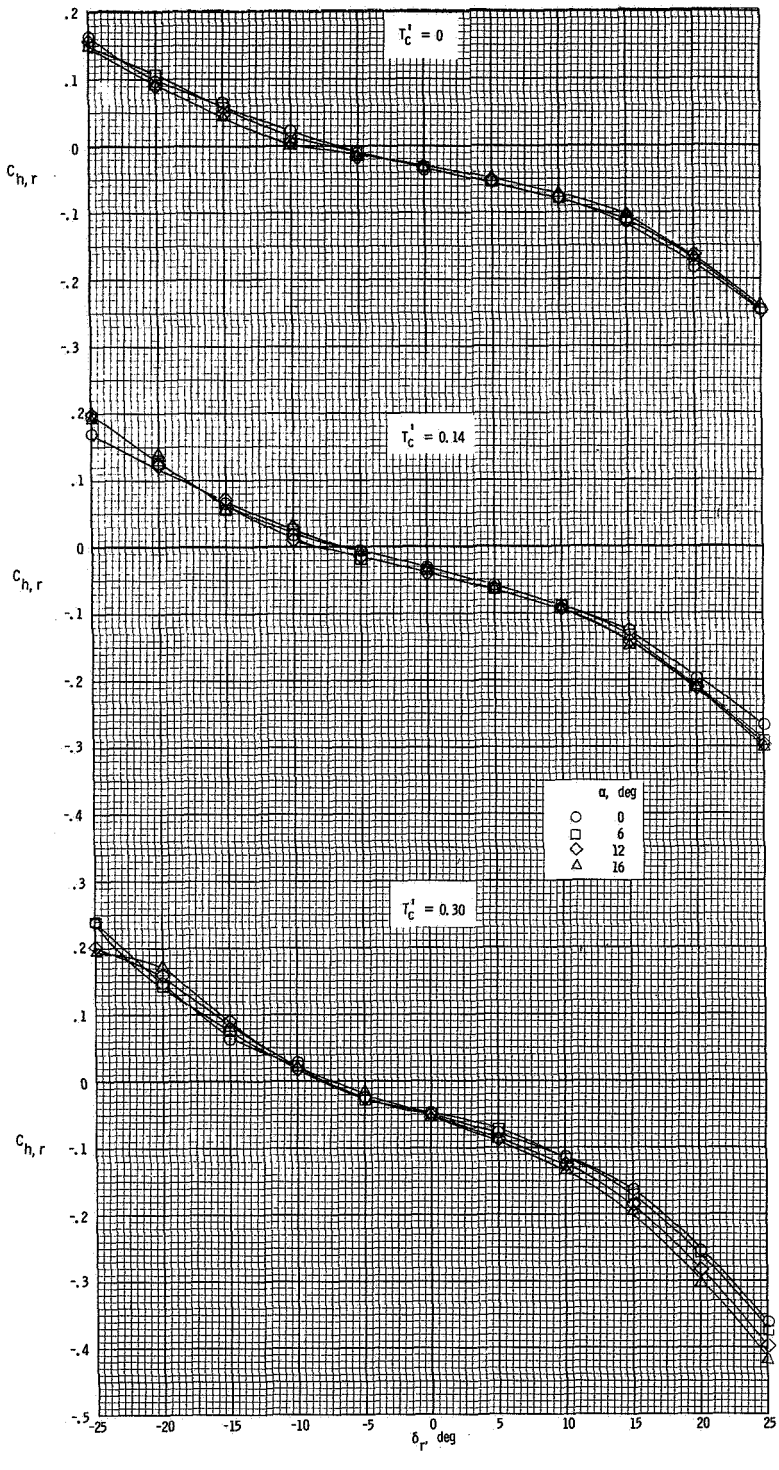

(b) $\beta = 4^{o}$.

Figure 43.- Continued.

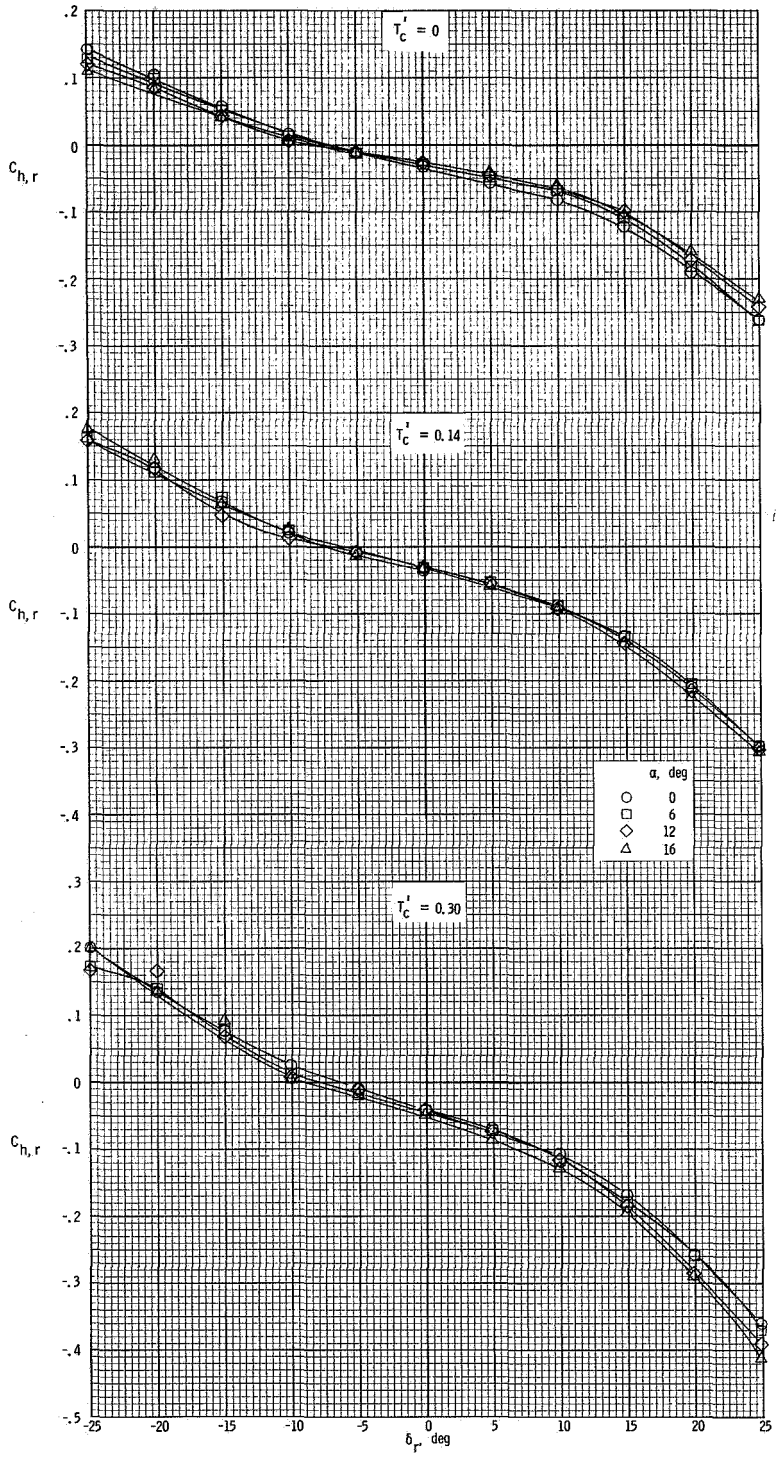

(c) $\beta = 0^o$.

Figure 43.- Continued.

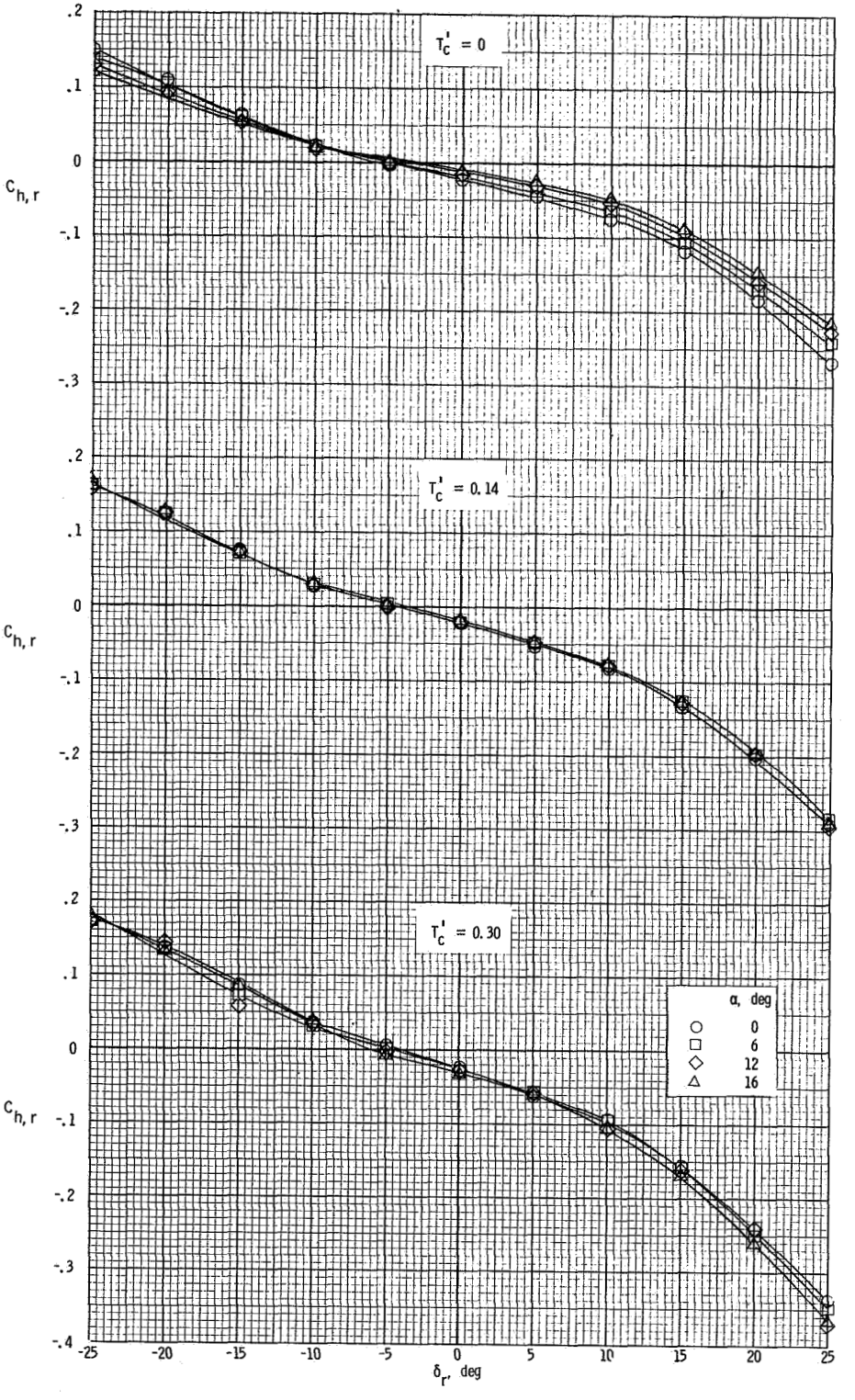

(d) $\beta = -4^{o}$.

Figure 43.- Continued.

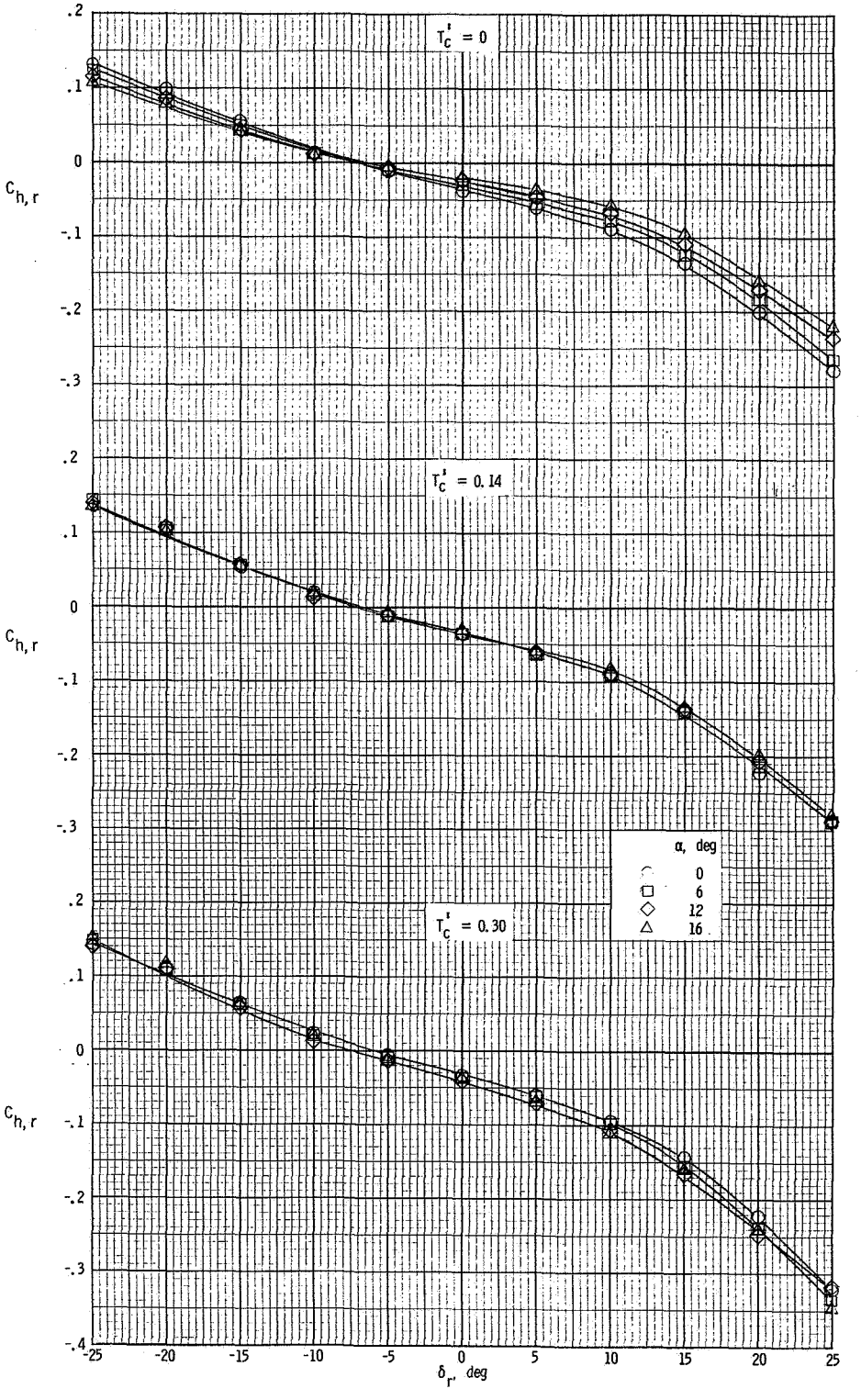

(e) $\beta = -8^{o}$.

Figure 43.- Concluded.

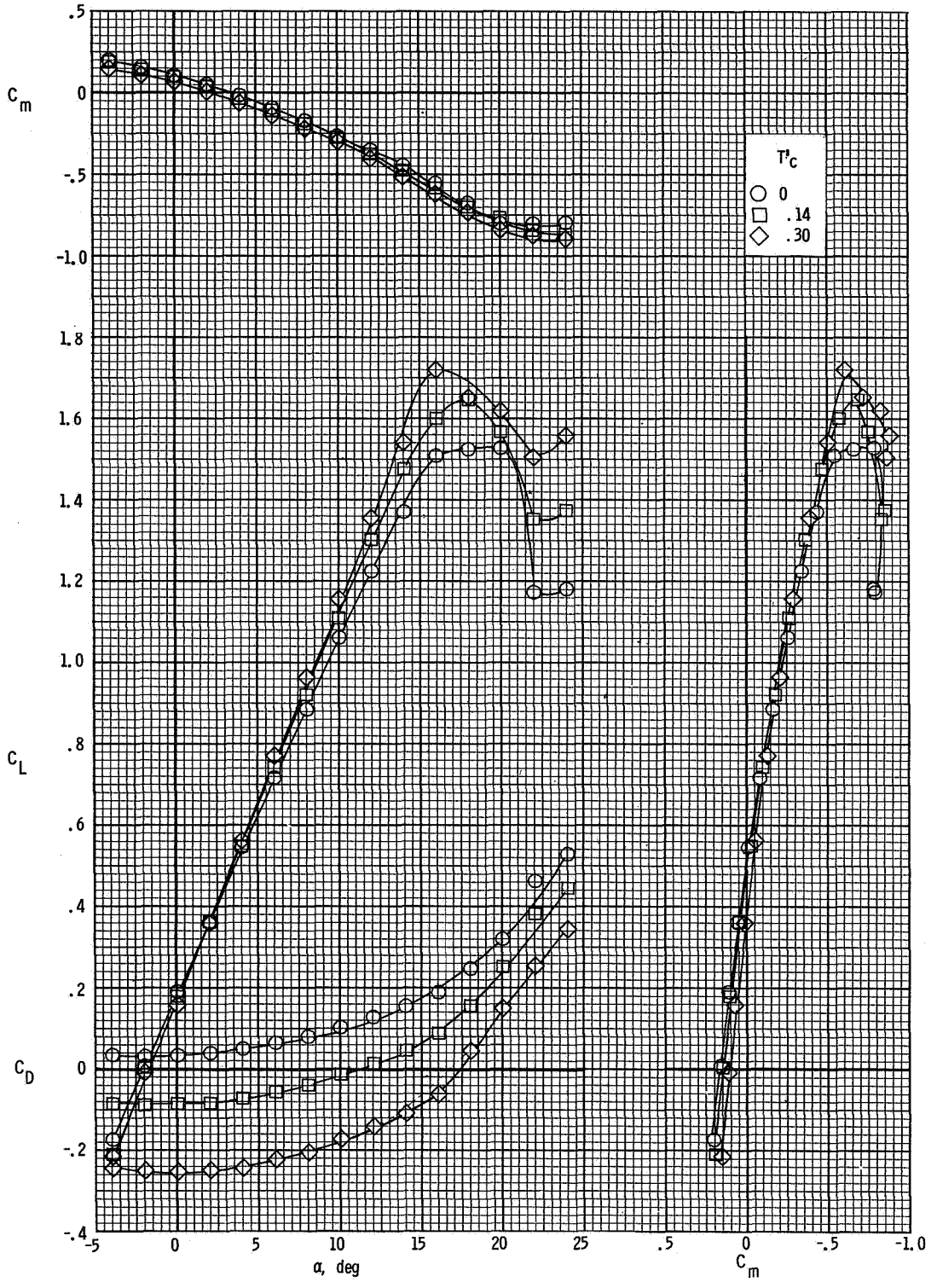

(a) $\delta_f = 0^o$.

Figure 44.- Effect of power on longitudinal aerodynamic characteristics. $\beta = 0^o$; $\delta_e = 0^o$.

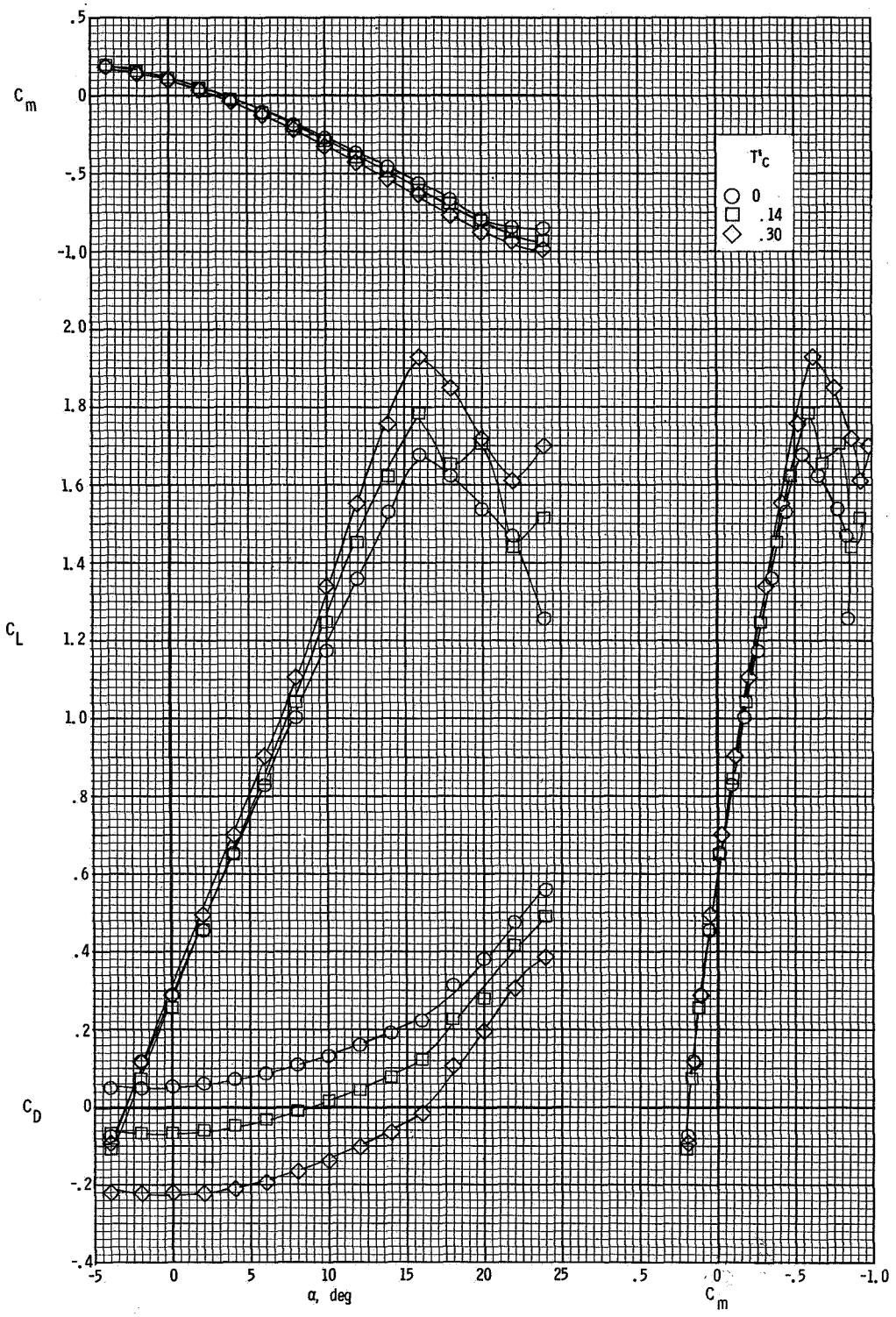

(b) $\delta_f = 10^o$.

Figure 44.- Continued.

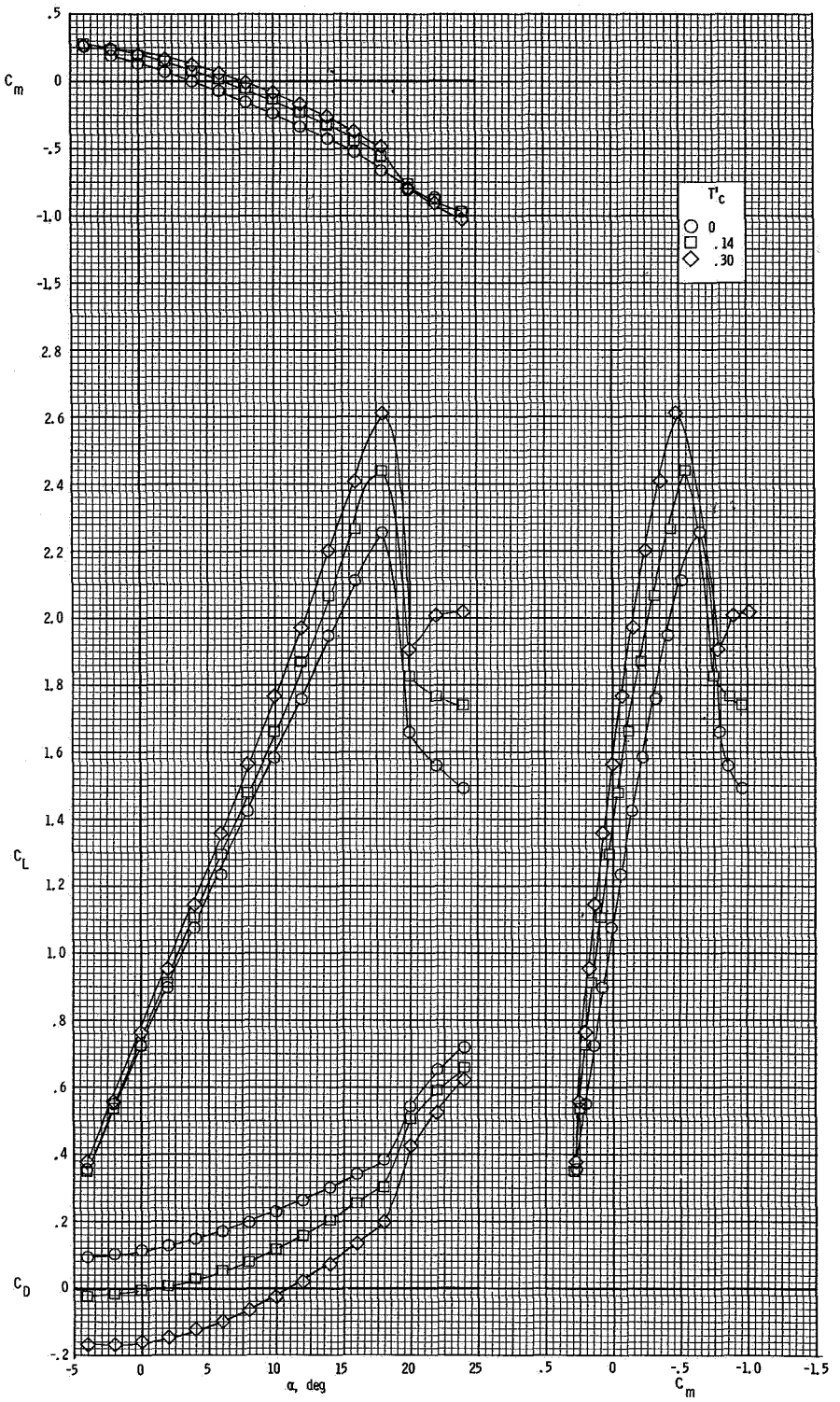

(c) $\delta_f = 30^o$.

Figure 44.- Concluded.

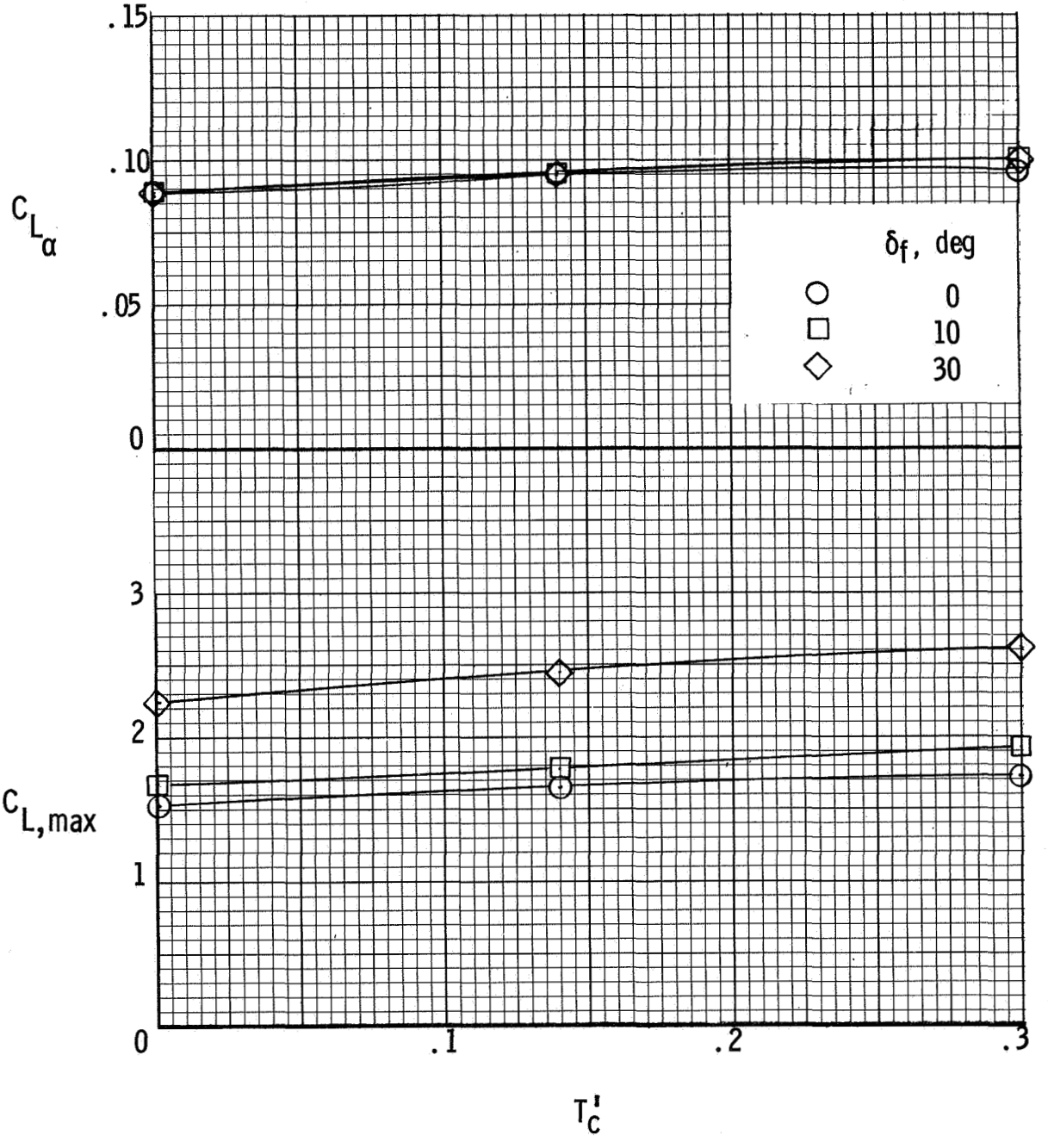

Figure 45.- Effect of power on lift-curve slope and maximum lift coefficient.

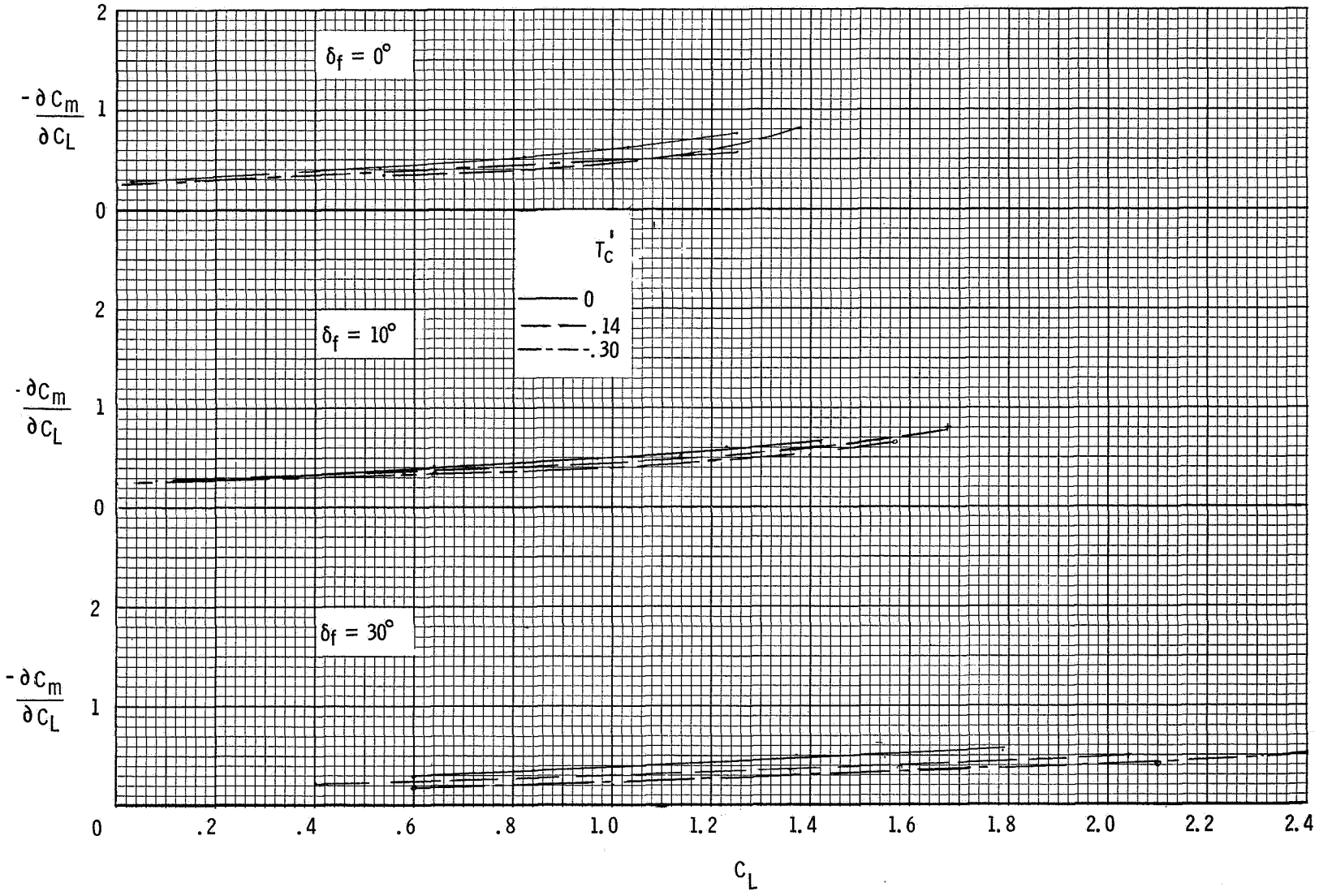

Figure 46.- Variation of stick-fixed power-on longitudinal stability characteristics with lift coefficient for $0.14\bar{c}$ center-of-gravity location.

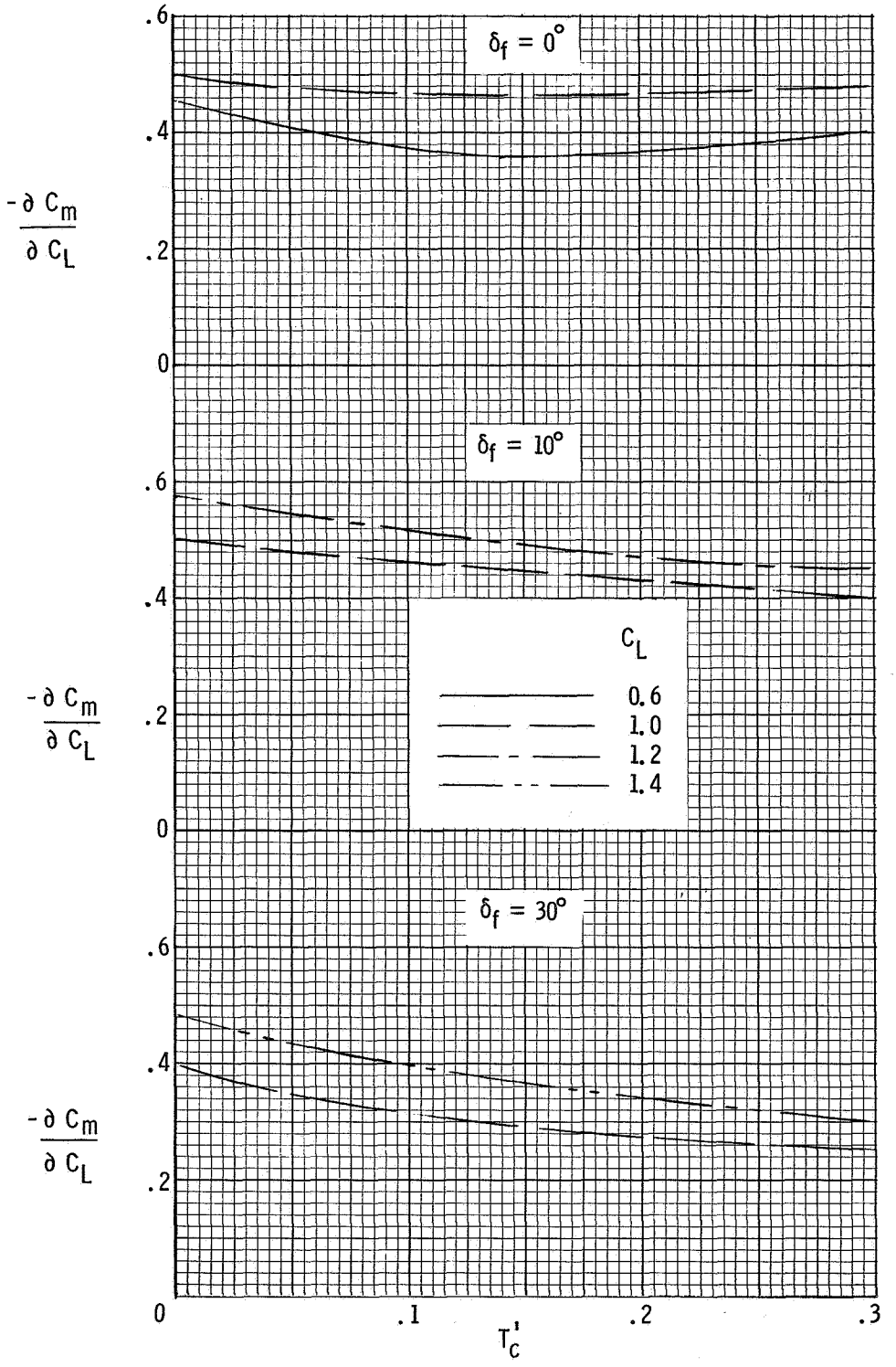

Figure 47.- Variation of stick-fixed power-on longitudinal stability characteristics with thrust coefficient for $0.14\bar{c}$ center-of-gravity location.

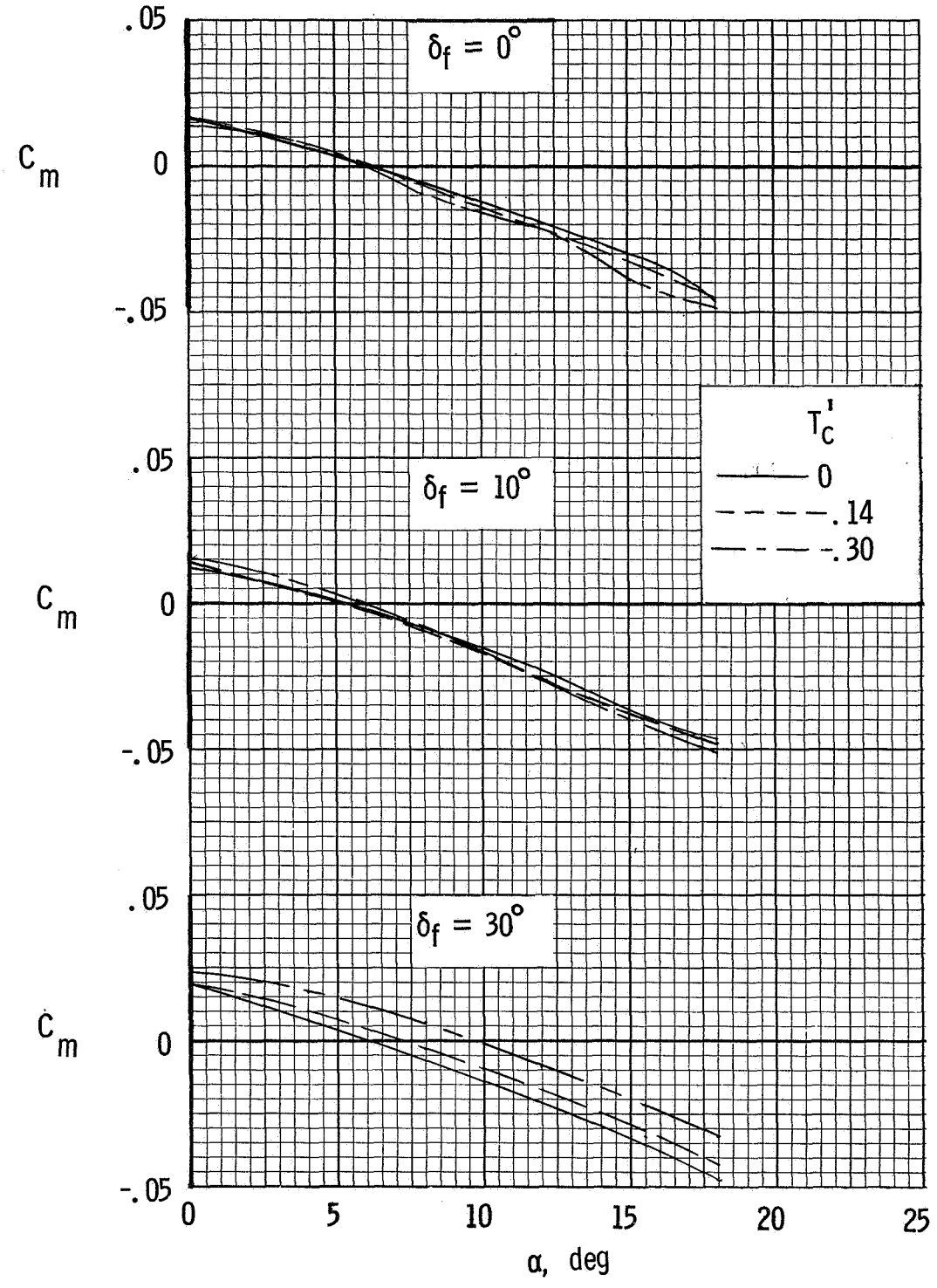

(a) Variation of stick-free pitching moment with angle of attack.

Figure 48.- Stick-free static longitudinal stability characteristics.

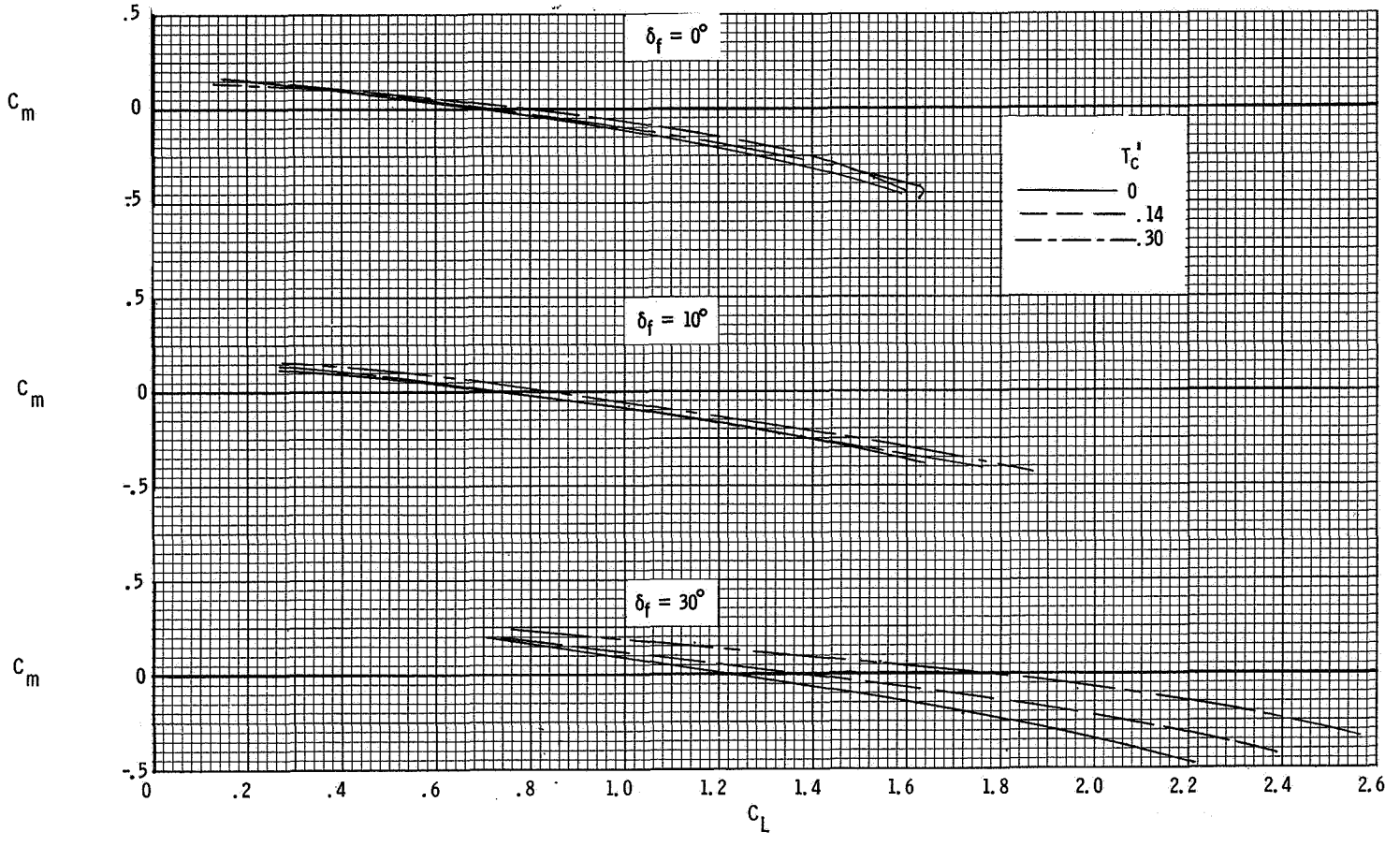

(b) Variation of stick-free pitching moment with lift coefficient.

Figure 48.- Concluded.

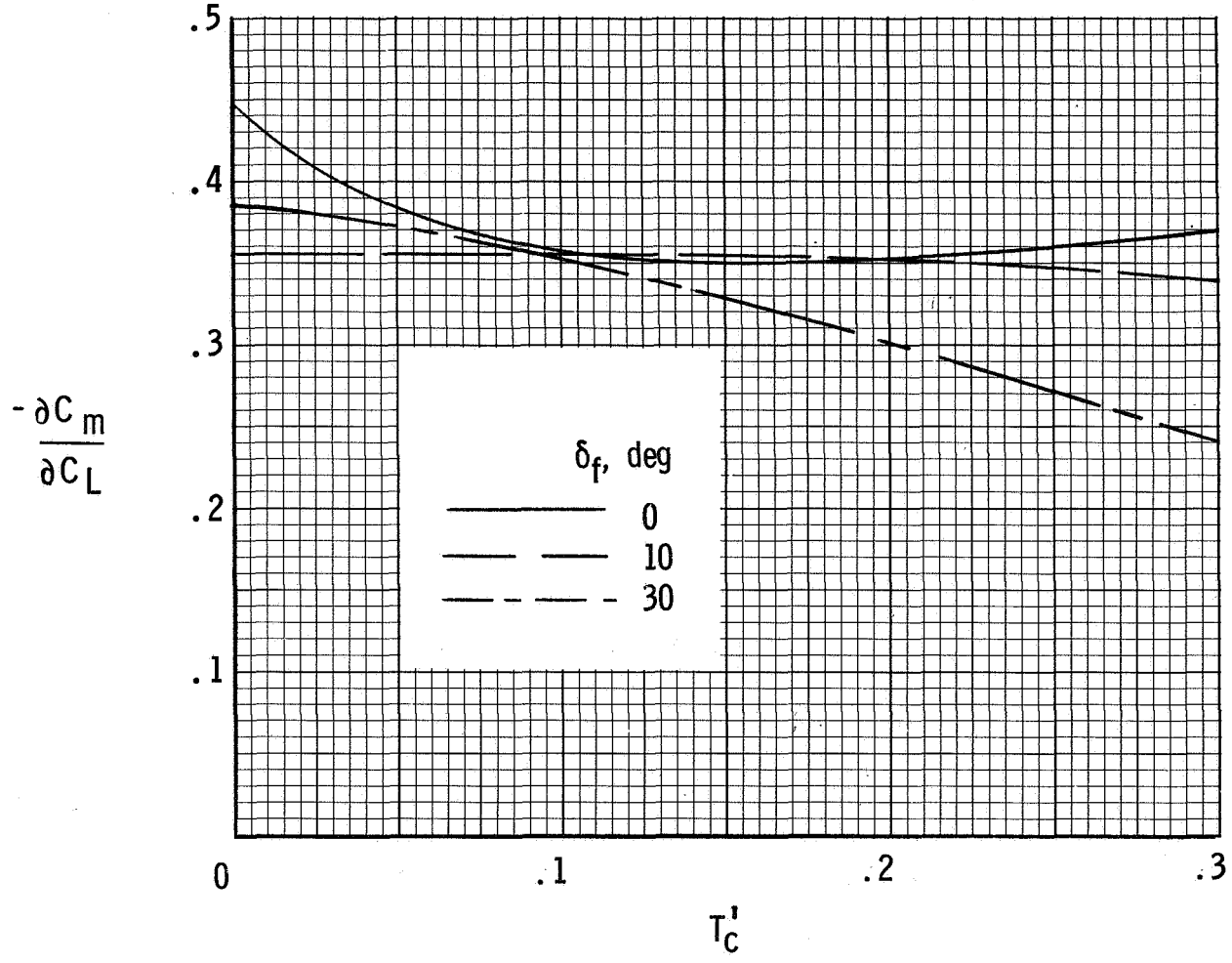

Figure 49.- Effect of power on stick-free stability. $C_L = 1.0$.

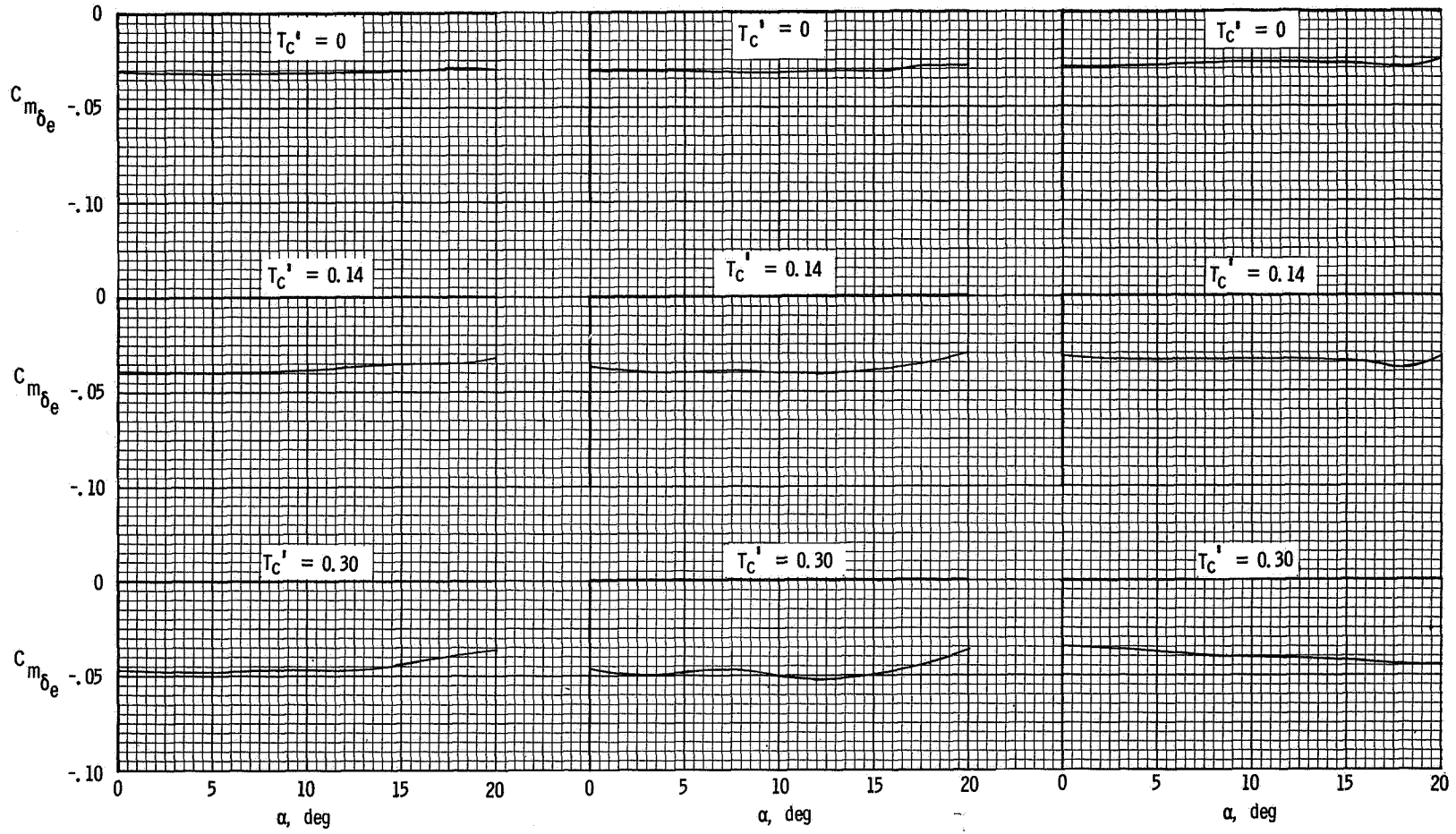

(a) $\delta_f = 0^o$. (b) $\delta_f = 10^o$. (c) $\delta_f = 30^o$.

Figure 50.- Variation of elevator effectiveness with angle of attack.

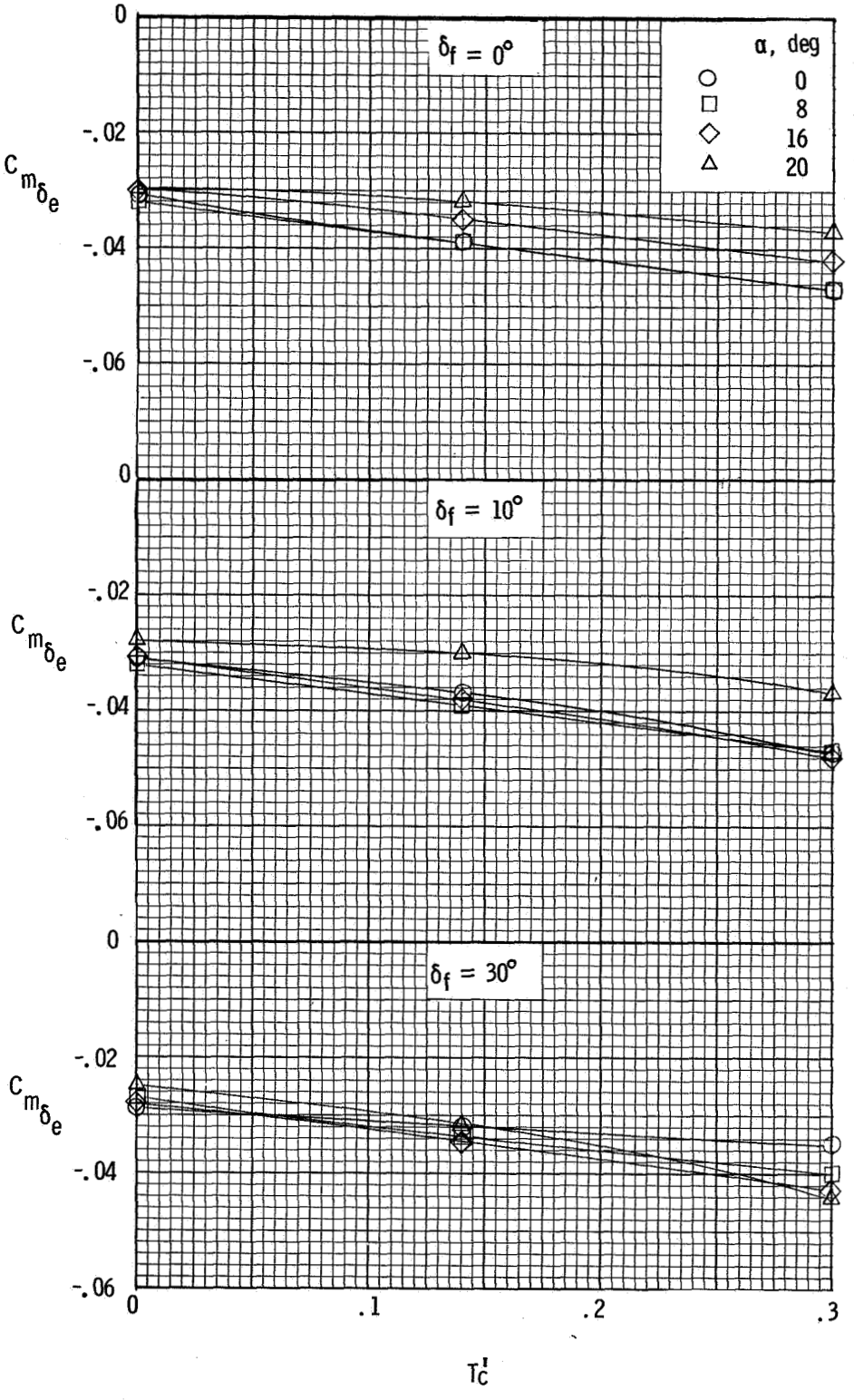

Figure 51.- Effect of power on elevator effectiveness.

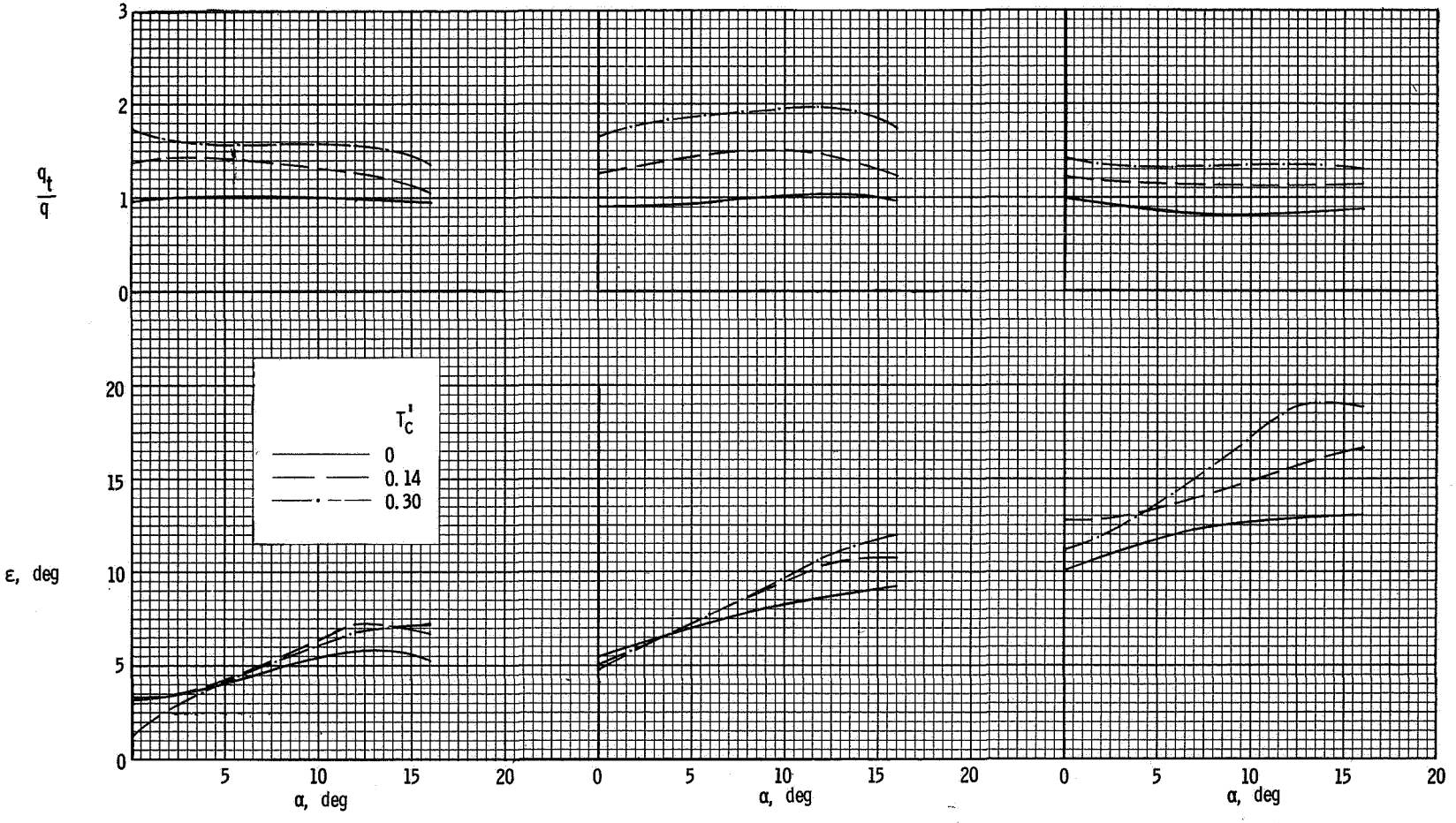

(a) $\delta_f = 0^o$. (b) $\delta_f = 10^o$. (c) $\delta_f = 30^o$.

Figure 52.- Variation of average downwash angle and dynamic pressure ratio at the elevator hinge line with angle of attack for several power and flap settings.

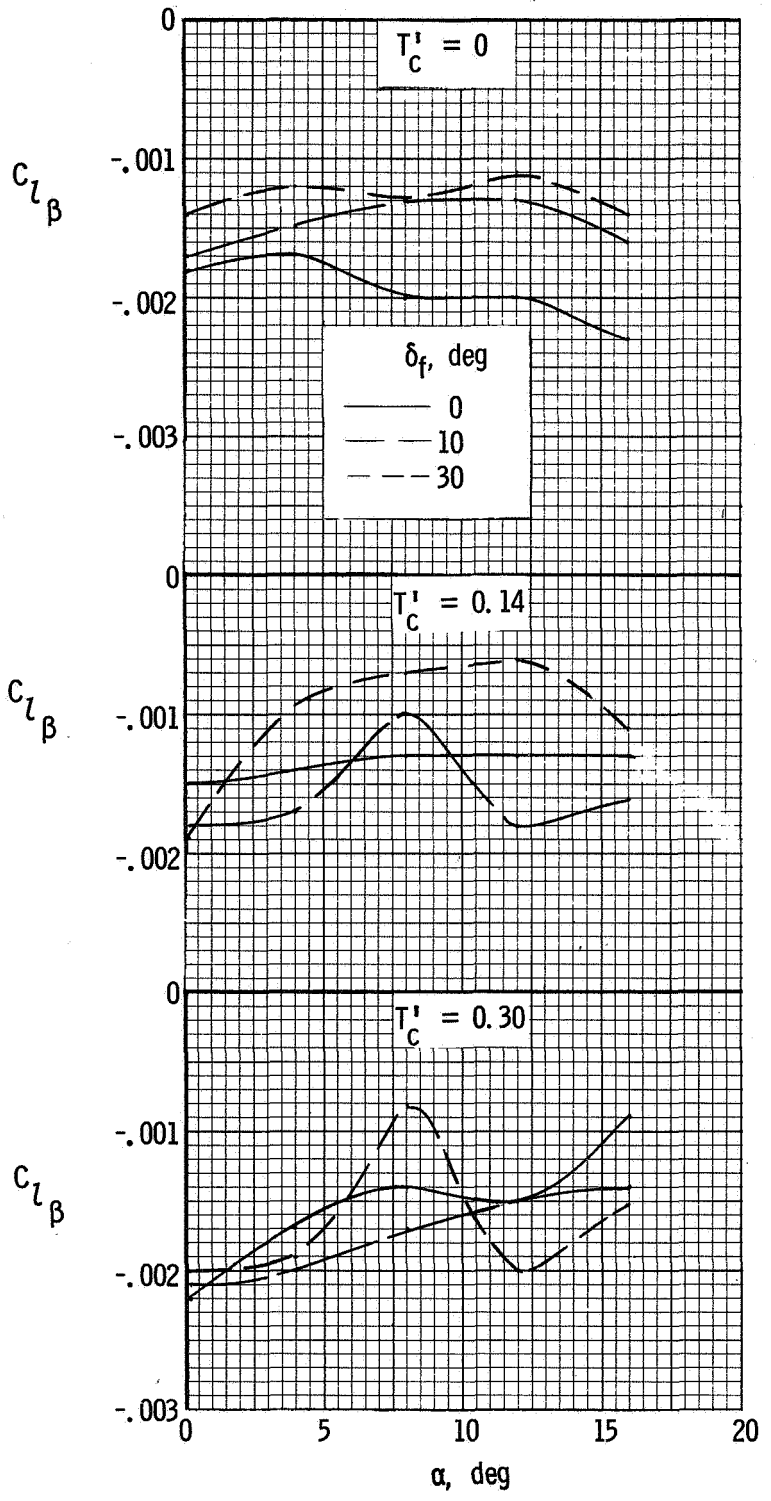

Figure 53.- Effective-dihedral characteristics.

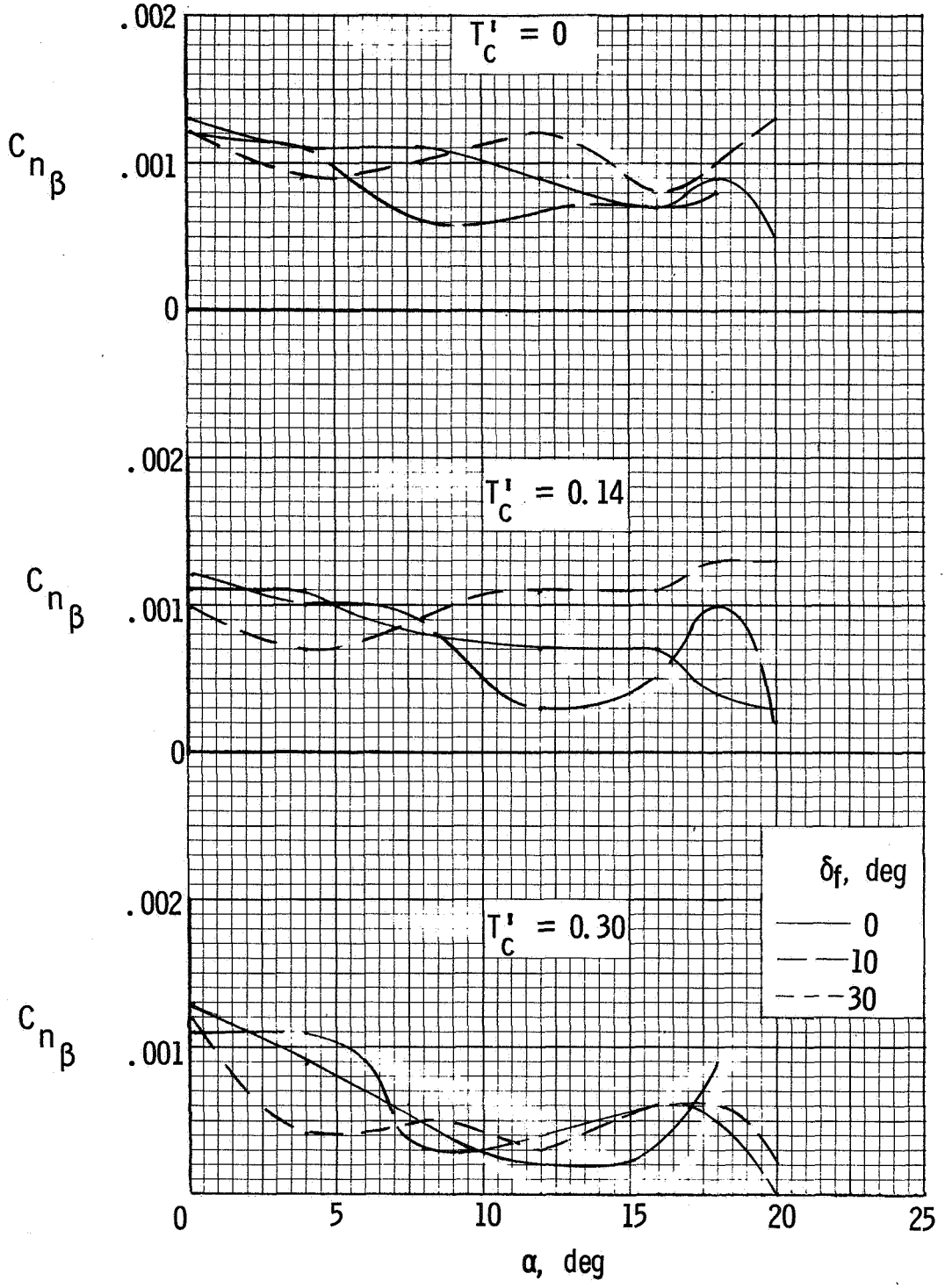

Figure 54.- Directional stability characteristics.

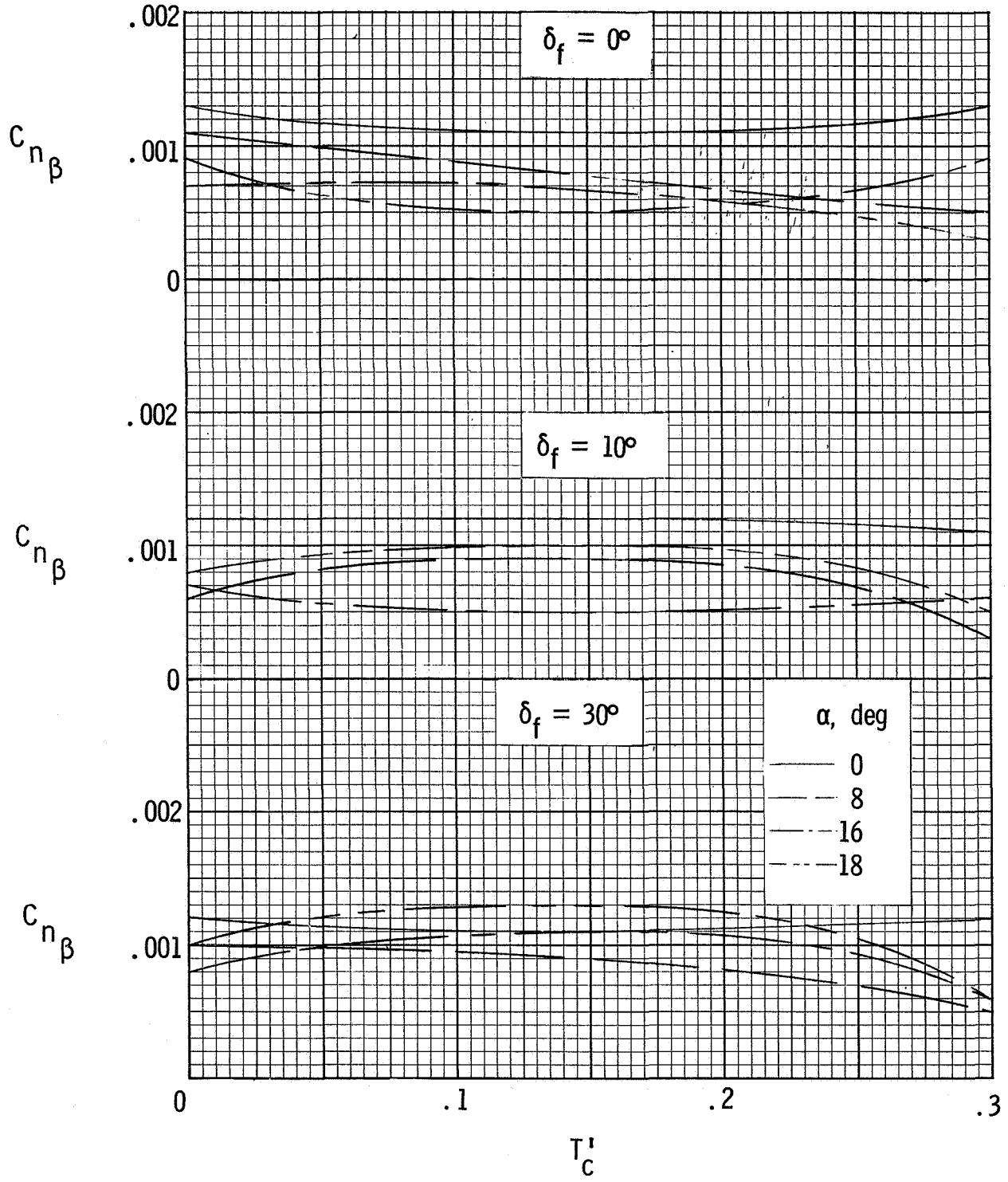

Figure 55.- Effect of power on directional stability parameters.

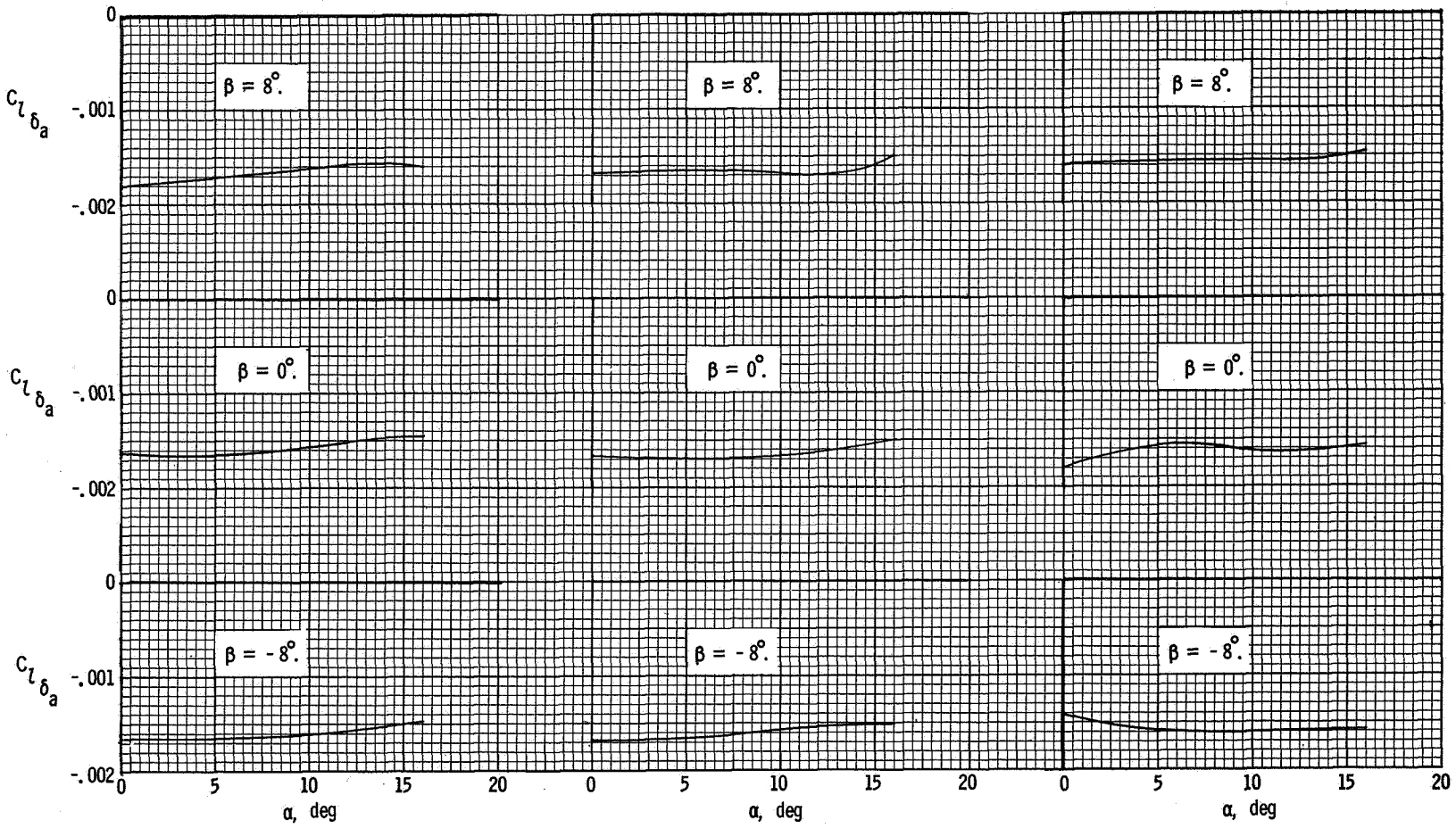

(a) $T'_c = 0$; $\delta_f = 0^o$. (b) $T'_c = 0.14$; $\delta_f = 0^o$. (c) $T'_c = 0.30$; $\delta_f = 0^o$.

Figure 56.- Variation of aileron effectiveness with angle of attack for several sideslip angles and flap deflections.

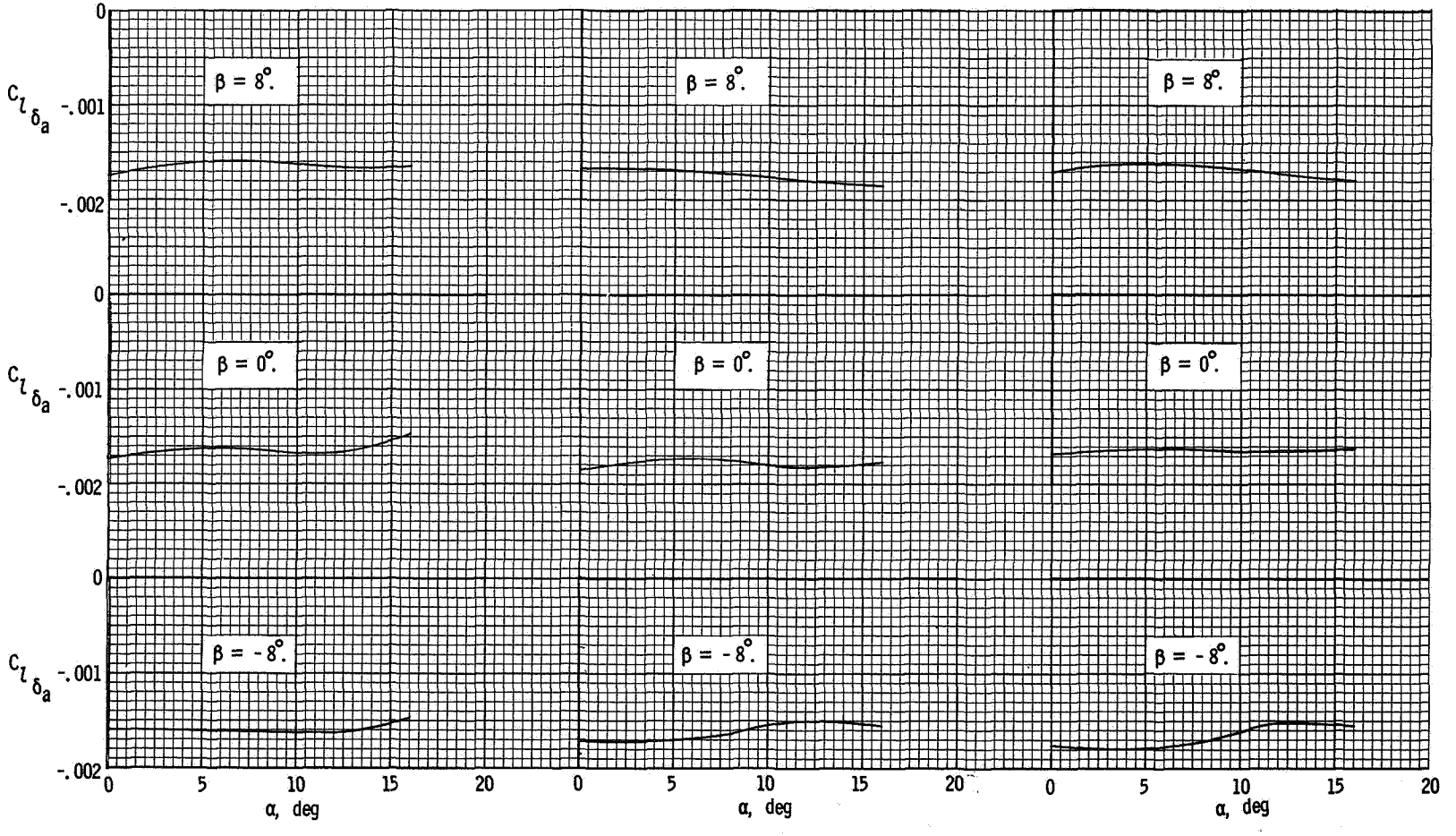

(d) $T'_c = 0$; $\delta_f = 30^o$.

(e) $T'_c = 0.14$; $\delta_f = 30^o$.

(f) $T'_c = 0.30$; $\delta_f = 30^o$.

Figure 56.- Concluded.

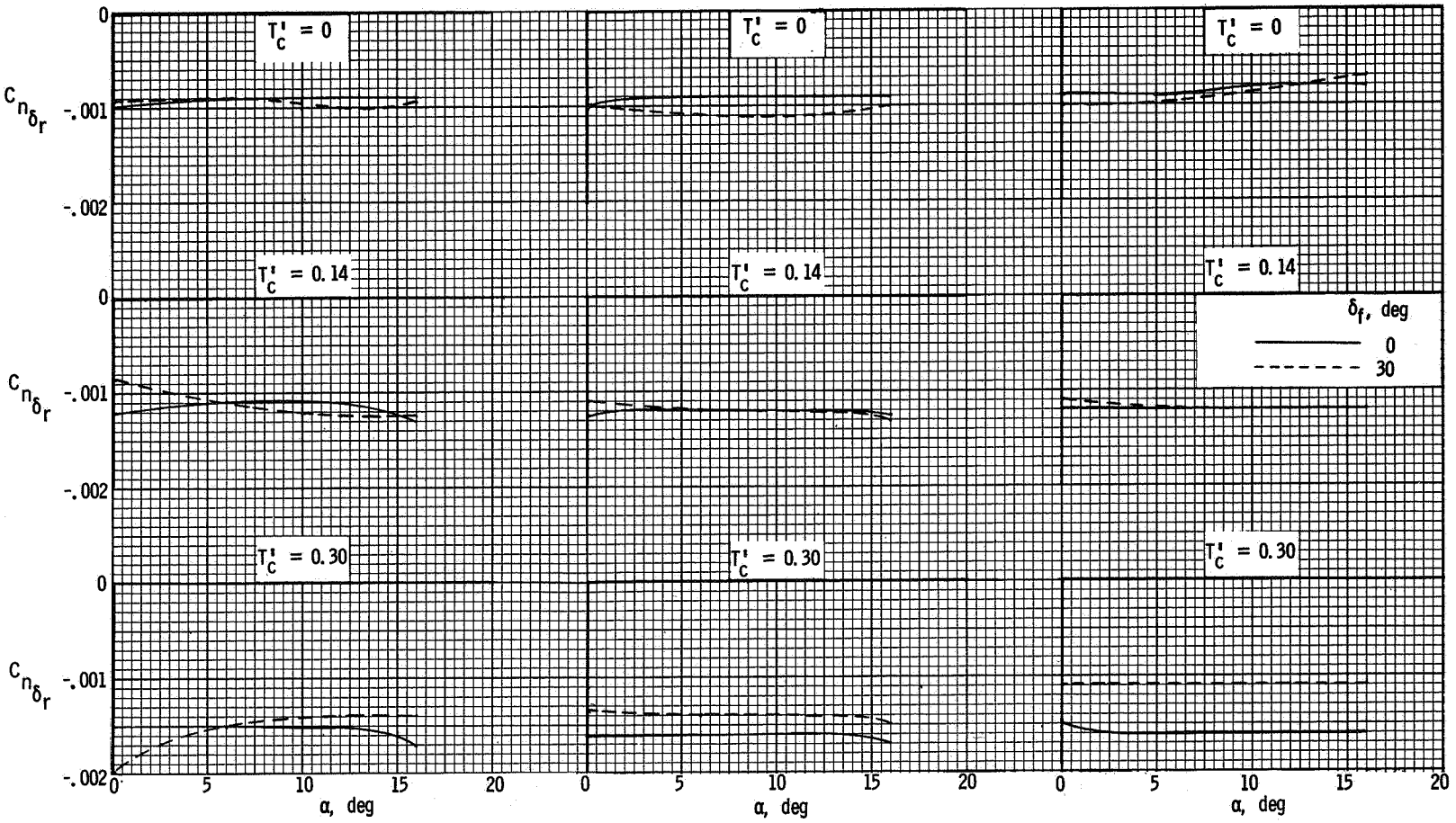

(a) $\beta = 8^o$. (b) $\beta = 4^o$. (c) $\beta = 0^o$.

Figure 57.- Variation of rudder effectiveness with angle of attack for several slideslip angles and flap deflections.

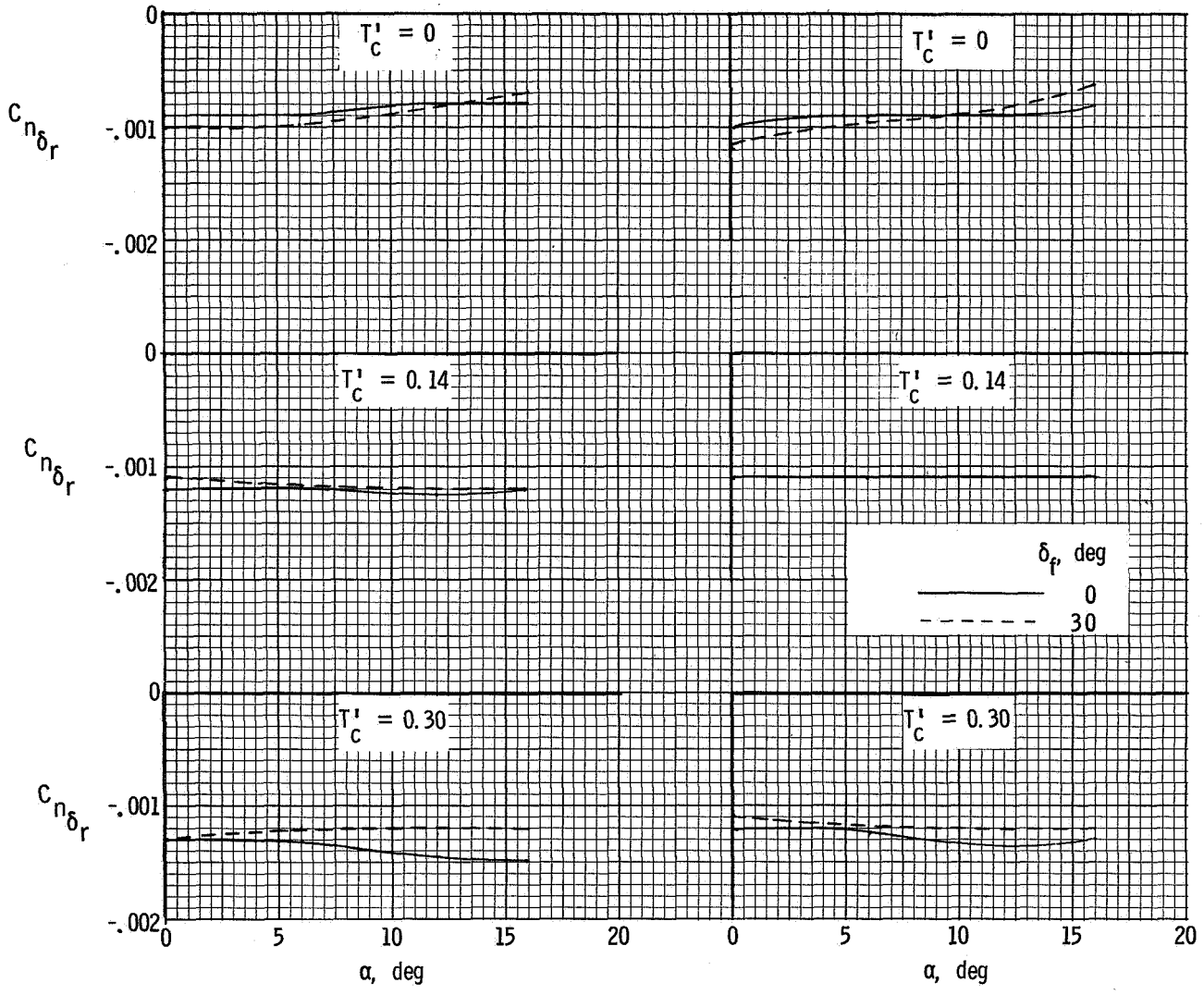

(d) $\beta = -4^{o}$.

(e) $\beta = -8^{o}$.

Figure 57.- Concluded.

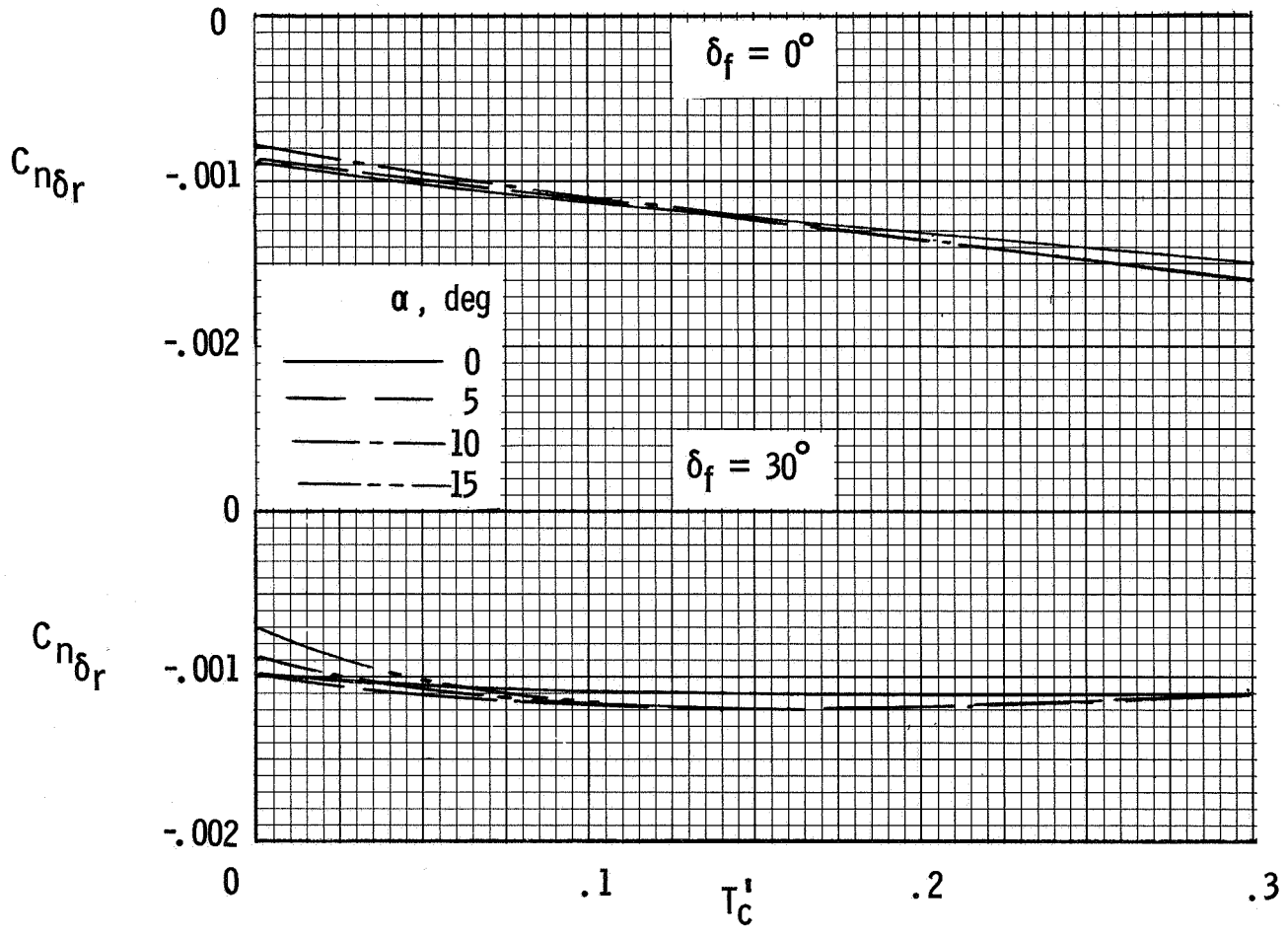

Figure 58.- Effect of power on rudder effectiveness. $\beta = 0^o$.

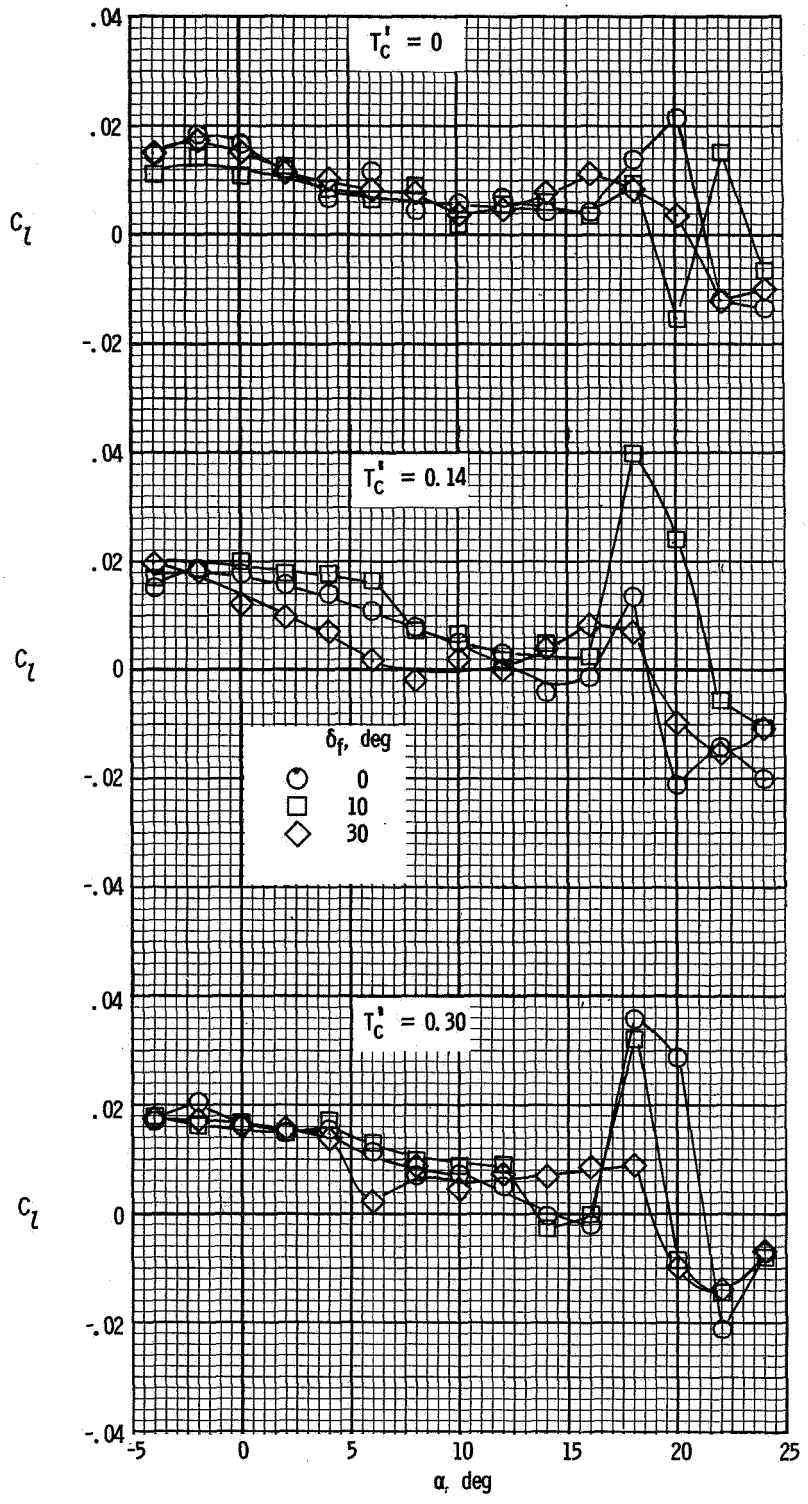

(a) Rolling-moment coefficients.

Figure 59.- Rolling- and yawing-moment coefficients for various power settings and flap deflections for $\beta = 0^{o}$.

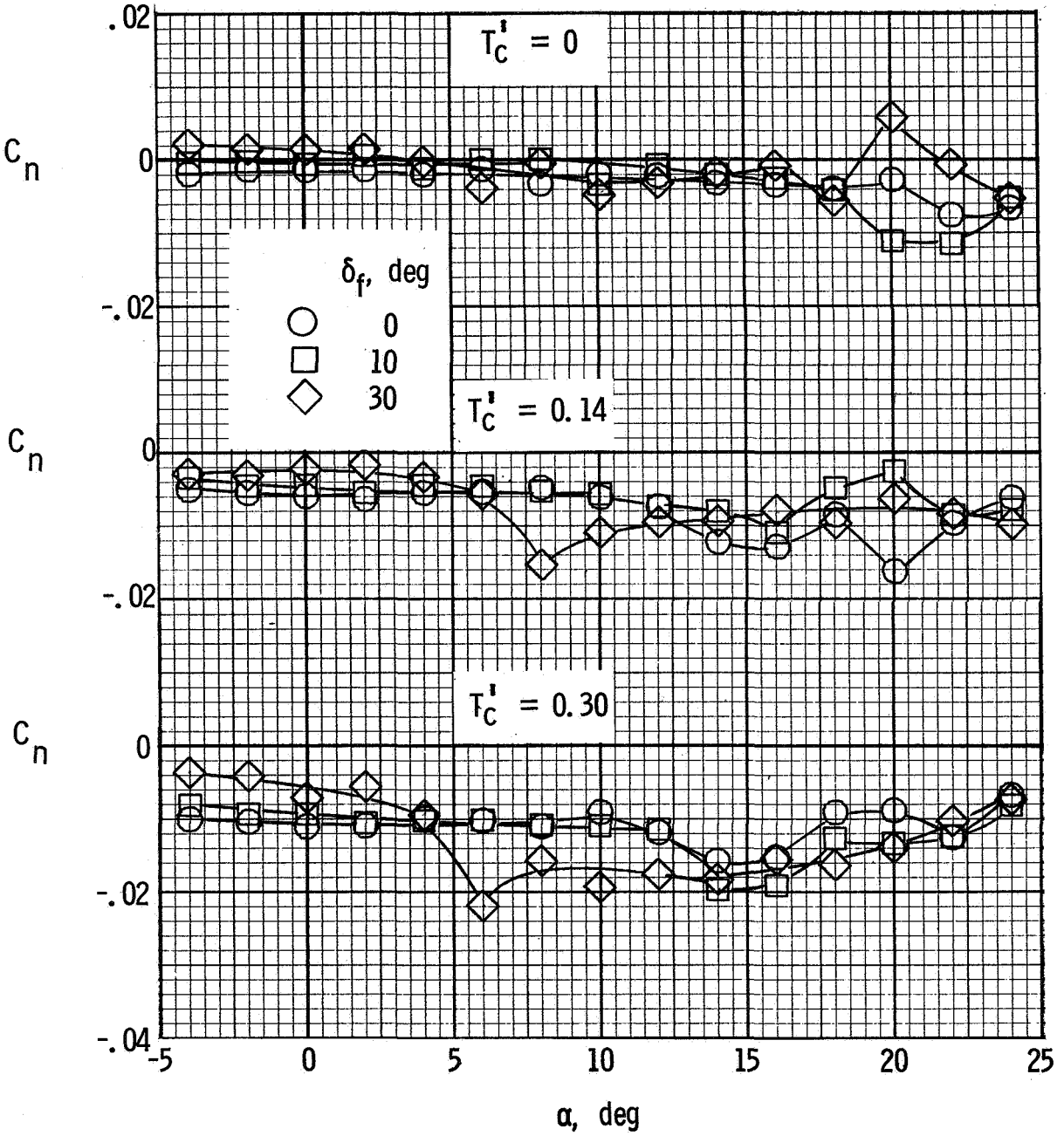

(b) Yawing-moment coefficients.

Figure 59.- Concluded.

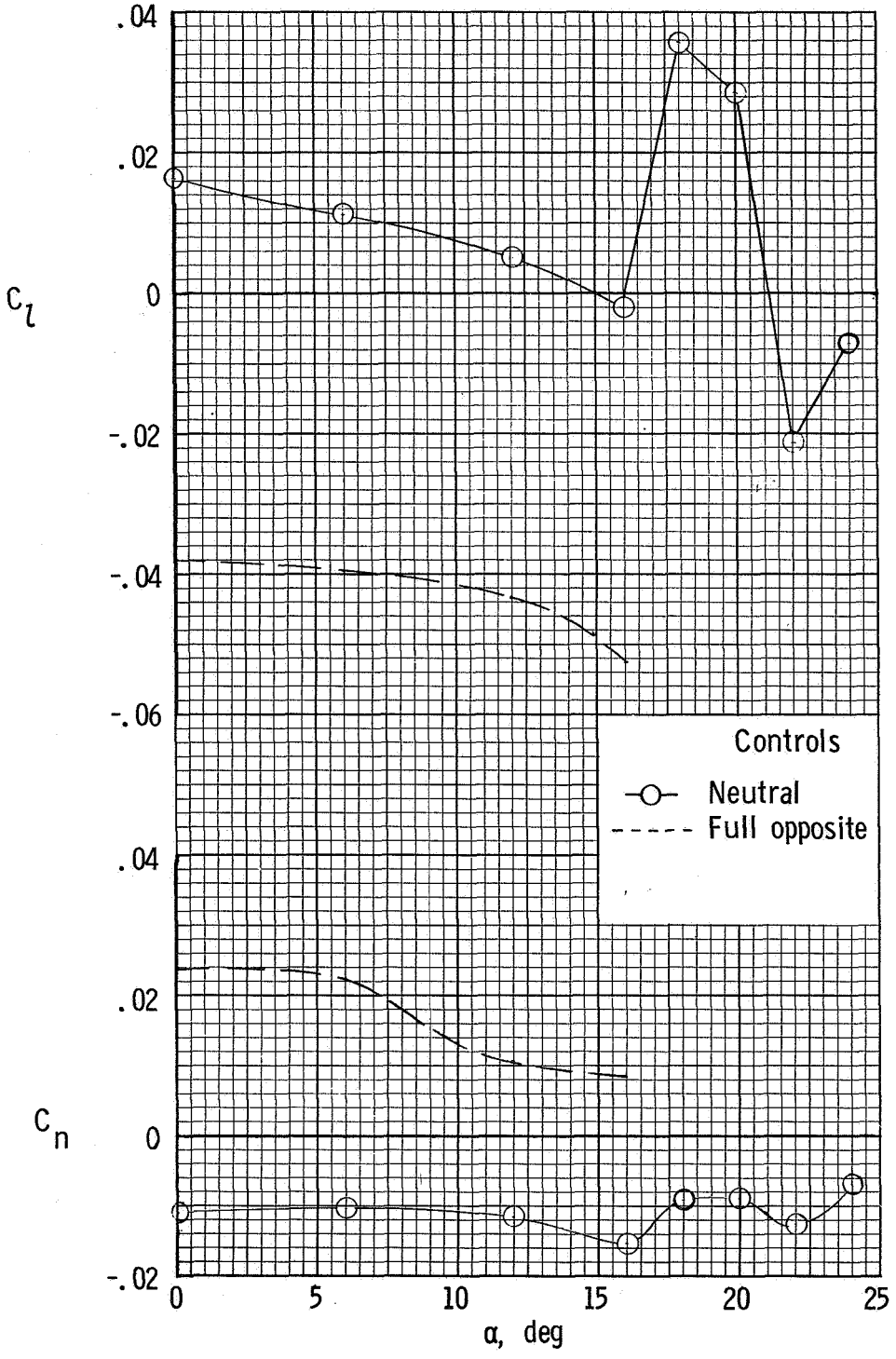

Figure 60.- Control capability for overcoming lateral moments. $\delta_f = 0^o$; $T'_c = 0.30$; $\beta = 0^o$.

*U.S. GOVERNMENT PRINTING OFFICE: 1973-739-027/30

NATIONAL AERONAUTICS AND SPACE ADMINISTRATION
WASHINGTON, D.C. 20546

OFFICIAL BUSINESS
PENALTY FOR PRIVATE USE $300

SPECIAL FOURTH-CLASS RATE BOOK

POSTAGE AND FEES PAID
NATIONAL AERONAUTICS AND SPACE ADMINISTRATION
451

U.S.MAIL

POSTMASTER: If Undeliverable (Section 158 Postal Manual) Do Not Return

"The aeronautical and space activities of the United States shall be conducted so as to contribute . . . to the expansion of human knowledge of phenomena in the atmosphere and space. The Administration shall provide for the widest practicable and appropriate dissemination of information concerning its activities and the results thereof."

—NATIONAL AERONAUTICS AND SPACE ACT OF 1958

NASA SCIENTIFIC AND TECHNICAL PUBLICATIONS

TECHNICAL REPORTS: Scientific and technical information considered important, complete, and a lasting contribution to existing knowledge.

TECHNICAL NOTES: Information less broad in scope but nevertheless of importance as a contribution to existing knowledge.

TECHNICAL MEMORANDUMS: Information receiving limited distribution because of preliminary data, security classification, or other reasons. Also includes conference proceedings with either limited or unlimited distribution.

CONTRACTOR REPORTS: Scientific and technical information generated under a NASA contract or grant and considered an important contribution to existing knowledge.

TECHNICAL TRANSLATIONS: Information published in a foreign language considered to merit NASA distribution in English.

SPECIAL PUBLICATIONS: Information derived from or of value to NASA activities. Publications include final reports of major projects, monographs, data compilations, handbooks, sourcebooks, and special bibliographies.

TECHNOLOGY UTILIZATION PUBLICATIONS: Information on technology used by NASA that may be of particular interest in commercial and other non-aerospace applications. Publications include Tech Briefs, Technology Utilization Reports and Technology Surveys.

Details on the availability of these publications may be obtained from:

SCIENTIFIC AND TECHNICAL INFORMATION OFFICE

NATIONAL AERONAUTICS AND SPACE ADMINISTRATION

Washington, D.C. 20546